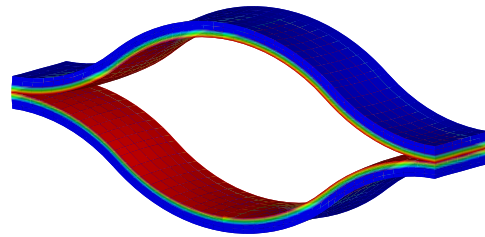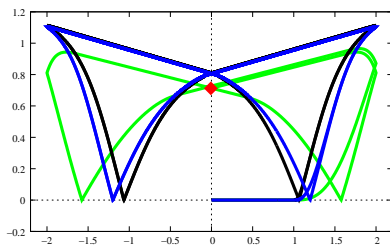# On the Formulation and Numerical Implementation of Dissipative Electro–Mechanics at Large Strains

Daniele Rosato

$$W(\mathfrak{F}) = \inf_{\dot{\mathfrak{Q}}} \left\{ \int\limits_{t_n}^{t_{n+1}} \left[\frac{d}{dt}\rho_0\psi'(\mathfrak{F},\mathfrak{Q}) + \rho_0\phi(\dot{\mathfrak{Q}}) \right] d\tau \right\}$$

On the Formulation and Numerical Implementation of Dissipative Electro–Mechanics at Large Strains

Von der Fakultät Bau- und Umweltingenieurwissenschaften
der Universität Stuttgart zur Erlangung der Würde
eines Doktor-Ingenieurs (Dr.-Ing.)
genehmigte Abhandlung

von

Daniele Rosato

aus Mesagne (Italien)

Hauptberichter : Prof. Dr.-Ing. C. Miehe
Mitberichter : Prof. Dr.-Ing. A. Menzel
Tag der mündlichen Prüfung: 7. Dezember 2009

Institut für Mechanik (Bauwesen) der Universität Stuttgart

2010

Abstract

In recent years an increasing interest in functional materials such as ferroelectric polymers and ceramics has been shown. For those materials, viscous effects or electric polarizations cause hysteresis phenomena accompanied with possibly large remanent strains and rotations. In this work aspects of the formulation and numerical implementation of dissipative electro-mechanics at large strains are outlined. In particular continuous and discrete variational formulations for the treatment of the non-linear dissipative response of electro-mechanical solids are developed and these formulations are adapted to the modeling of the hysteretic material response of piezoceramics and ferroelectric polymers under electrical loading. The point of departure is a general internal variable formulation that determines the hysteretic response of the material as a generalized standard medium in terms of an energy storage and a rate-dependent dissipation function. Consistent with this type of standard dissipative continua, an incremental variational formulation of the coupled electro-mechanical boundary-value-problem is developed. The variational formulation for a setting based on a smooth rate-dependent dissipation function which governs the hysteretic response is specified. Further, the geometric nature of dissipative electro-mechanics is underlined. An important aspect is the numerical implementation of the coupled problem. The discretization of the two-field problem appears, as a consequence of the proposed incremental variational principle, in a symmetric and very compact format. Further, constitutive assumptions which account for specific problems arising in the geometric nonlinear setting are discussed. With regard to the choice of the internal variables entering the constitutive functions, a critical point are the kinematic assumptions. Here, the multiplicative decomposition of the local deformation gradient into reversible and remanent parts as well as the introduction of a remanent metric are discussed. Such a formulation allows us to reproduce the dielectric and butterfly hysteresis responses characteristic of the ferroelectric materials together with their rate-dependency and to account for macroscopically non-uniform distribution of the polarization in the specimen together with large attained deformations. The performance of the proposed methods is demonstrated by means of a spectrum of benchmark problems which eventually show large deformations.

Zusammenfassung

Im Laufe der letzten Jahre ist ein zunehmendes Interesse an Funktionsmaterialien wie ferroelektischen Polymeren und Keramiken aufgetreten. Viskose Effekte oder elektrische Polarisierung verursachen bei diesen Materialien Hysteresephänomene, die oft mit großen und remenenten Verzerrungen und Rotationen verbunden sind. Die vorliegende Arbeit beschäftigt sich in diesem Kontext mit Aspekten der Formulierung und numerischen Implementierung dissipativer Elektromechanik bei finiten Deformationen. Dazu wird eine kontinuierliche und diskrete Variationsformulierung für das nichtlineare dissipative Verhalten elektromechanischer Festkörper entwickelt und an das Hystereseverhalten von Piezokeramiken und Ferroelektrischen Polymeren unter elektrischer Belastung angepasst. Ausgangspunkt ist dabei eine allgemeinen Formulierung mit internen Variablen, die die Hystereseantwort als generalisiertes standard-dissipatives Kontinuum mittels Energiespeicherung und ratenabhängiger Dissipation beschreibt. Konsistent dazu wird eine inkrementelle Variationsformulierung des gekoppelten elektromechanischen Randwertproblems entwickelt. Diese Variationsformulierung wird für den Fall der Beschreibung der Hysterese durch eine glatte, ratenabhängige Dissipationsfunktion spezifiziert, wobei die geometrischen Aspekte der dissipativen Elektromechanik besonders hervorgehoben werden. Ein wichtiger Gesichtspunkt ist die numerische Umsetzung des gekoppelten Zweifeld-Problems, dessen Diskretisierung aufgrund des vorgestellten inkrementellen Variationsprinzips auf eine symmetrische und kompakte Form führt. Weiterhin werden konstitutive Annahmen für die speziell im geometrisch nichtlinearen Rahmen auftretenden Probleme diskutiert. Bei der Wahl der internen Variablen in den konstitutiven Funktionen sind kinematische Annahmen entscheidend. In der vorliegenden Arbeit untersuchen wir die multiplikative Zerlegung des lokalen Deformationsgradienten in einen reversiblen und einen remanenten Anteil sowie die Einführung einer remanenten Metrik. Eine solche Formulierung ermöglicht die Vorhersage von dielektrischen Hysteresen und Schmetterlingshysteresen, die für ferroelektrische Materialien zusammen mit der Ratenabhängigkeit charakteristisch sind. Ausserdem kann die makroskopisch ungleichmäßige Verteilung der Polarisation im Probekörper im Rahmen großer Deformationen reproduziert werden. Die Effizienz der vorgestellten Methoden wird anhand einer Auswahl an Benchmark-Problemen aufgezeigt, die auch grosse Deformationen beinhalten.

Acknowledgements

Stuttgart, March 2010   Daniele Rosato

Contents

1. Introduction

Increased demands for high performance control design in combination with recent advances in material science have produced a class of systems termed smart, intelligent, or adaptive systems, SMITH [138]. Smart systems trace their origin to a field of research that envisioned devices and materials which could mimic human muscular and nervous systems. The essential idea is to produce non-biological systems that will achieve the optimum functionality observed in biological systems through emulation of their adaptive capabilities and integrated design. By definition smart systems consist of ensembles of sensors and actuators that are embedded or attached to the system to form an integral part of it. The system and its related components form an entity that will act and react in a predicted manner, and ultimately behave in a pattern that emulates a biological function. The human body is the ideal or ultimate system.

For aeronautical and aerospace systems, control transducers must be lightweight and should typically have minimal effect on the passive system dynamics. Furthermore, actuator must provide the required strain or force inputs using the available power supplies. Restriction on size and weight also dictate that transducers in some regimes must be capable of multiple roles. The limitations on the mass and size of transducers are often relaxed in industrial applications but output requirements may be more stringent.

Actuators and sensors comprised of smart or active materials can meet many of these criteria. Smart or intelligent materials are materials that have the intrinsic or extrinsic capabilities, first, to respond to stimuli and environmental changes and, second, to achieve their functions according to these changes. The stimuli could originate internally or externally. Thus, we define actuator materials as those which convert electrical, magnetic or thermal energy to mechanical energy whereas sensor effects are provided by the opposite conversion of energy.

The most popular smart materials are piezoelectric materials, magnetostrictive materials, shape-memory alloys, electro rheological fluids, electrostrictive materials, and optical fibers. Magnetostrictives, electrostrictives, shape-memory alloys, and electro rheological fluids are used as actuators; optical fibers are used primarily as sensors.

Among these active materials, piezoelectric materials are most widely used because of their bandwidth, fast electro-mechanical response, relatively low power requirements, and high generative forces. A classical definition of piezoelectricity, a Greek term for "pressure electricity", is the generation of electrical polarization in a material in response to mechanical stress. This phenomenon is known as the *direct effect*. Piezoelectric materials also display the *converse effect*: mechanical deformation upon the application of an electrical charge or signal. Piezoelectricity is the property of many non-centrosymmetric ceramics, polymers, and other biological systems. Pyroelectricity is a subset of piezoelectricity, whereby the polarization is a function of the temperature. Some pyroelectric materials are also ferroelectric, although not all ferroelectrics are pyroelectric. Ferroelectricity is the property of certain dielectrics that exhibit spontaneous electric polarization (separation of the center of positive and negative electric charges that makes one side of the crystal positive and the opposite side negative) that can be reversed in direction by applying an appropriate electric field. Traditionally, ferroelectricity is defined for crystalline materials, or at least in the crystalline region of semicrystalline materials. In the last couple of years, however, a number of researchers have explored the possibility of ferroelectricity in
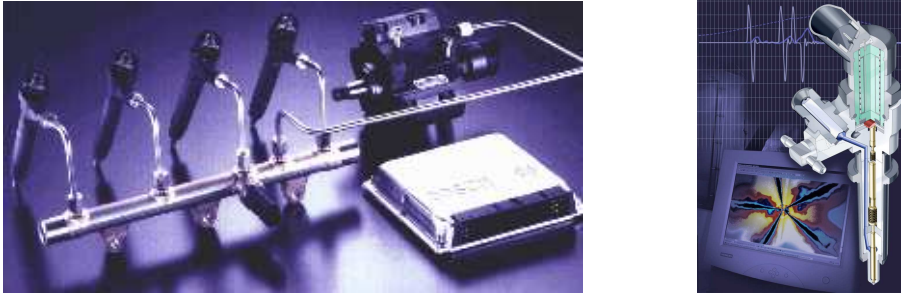
Figure 1.1: Bosch piezo inline injector (www.bosch.com).

amorphous polymers, that is, ferroelectricity without a crystal structure.

The design of smart systems which are based on smart materials requires both the characterization of their constitutive properties and the development of coupled structural models in order to give an accurate prediction of the system dynamics and response. Thus the development of linear, non-linear and hysteretic constitutive relations and their incorporation in coupled structural models which should eventually be able to account for large strains and rotations is of primary importance.

Piezoceramics belong to the group of materials which are most commonly used for electromechanical coupling applications. They are exploited in industrial application as sensors and actuators. Detection of pressure in the form of sound is one of the most common sensor application. In a piezoelectric microphone sound waves bend the material creating a changing voltage. They are especially used with high frequencies in ultrasonic transducers for medical imaging. Further, they can be used in acoustic-electrical applications as noise analysis or acoustic emission spectroscopes. In addition, they are well known in mechanic-electrical application as igniters or acceleratometers. The inverse piezoelectric effect is used in actuators, or piezoelectric motors for micro- and nano-positioning, laser tuning, active vibration damping et cetera. Everyday life applications are ink jet printers where piezoelectric crystals are used to control the flow of ink from the ink jet head to the paper. In automotive engineering, for instance, piezoceramics are utilized in new generation of common-rail piezo inline injectors in recent years. This system reduces not just exhaust emission from the diesel engine but also its operating noise and fuel consumption. Figure 1.1 shows the inline piezo injector used in Bosch's Common Rail System. In comparison with solenoidal valves, piezo injectors can be controlled much more precisely so they can inject fuel during an engine cycle with much more accuracy.

Concerning precise micro- and nano-deformation of sensors and actuators piezoceramic materials are particularly suitable. However, these rigid and fragile piezoelectric ceramics are not suited for applications where large deformations are required. For several decades, it has been known that certain types of polymers can change shape in response to electrical stimulation. Polymers have many attractive characteristics: they are generally lightweight, inexpensive, fracture tolerant, and pliable. Further they can be configured into almost any conceivable shape and their properties can be tailored to suit a broad range of requirements. Since the beginning of the 1990s, a series of new electroactive polymer (EAP in the following) materials has been developed that can induce large strains. Since these polymers behave very similarly to biological muscles, EAPs have acquired the byname "artificial muscles". In 1999 the worldwide research and engineering com-
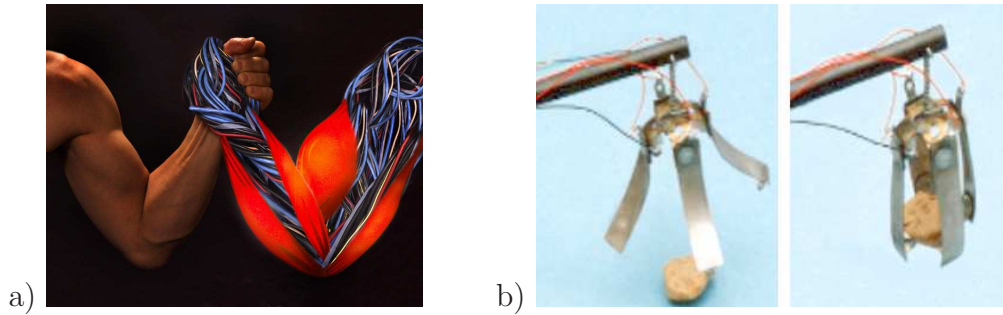
Figure 1.2: a) armwrestling match between an EAP actuated robotic arm and a human (http://jpl.nasa.gov); b) Robotic arm with 4-finger EAP gripper (http://ndeaa.jpl.nasa.gov).

munity was challenged to develop a robotic arm that is actuated by artificial muscles to win a wrestling match against a human opponent (Figure 1.2a). On Figure 1.2b a further application of EAP is shown, i.e. a robotic arm with 4-finger EAP gripper. The strain performances of these materials demand a material models which consider the large deformations, especially in terms of bending motions.

1.1. State of the Art

We are concerned with aspects of the formulation and numerical implementation of dissipative electromechanics at large strains. We would like to focus in particular on the geometric nature of dissipative electro-mechanics, the constitutive updates as well as the finite element formulation, both on the basis of compact variational principles. Furthermore, we would like to concentrate on the constitutive assumptions to model time-dependent hysteretic phenomena for piezoceramics and ferroelectric polymers.

The theoretical foundations for the analysis of electro-mechanical interactions in solids were developed in part during the 1950s and 1960s, and a detailed summary may be found, for example, in TRUESDELL & TOUPIN [144], LANDAU & LIFSCHITZ [89], in the lecture notes by PAO [122], HUTTER, VAN DE VEN AND URESCU [67] (enlarged version of lecture notes appeared in 1978). The more recent books by MAUGIN [99] and ERINGEN & MAUGIN [48, 49] provide a more comprehensive overview of the electrodynamics of solids. The book by KOVETZ [87] has a nice account of the merging of the mechanics, thermomechanics and electromagnetics of continua. Other recent developments in this area are described in the publications by JAMES & KINDERLEHRER [72], DESIMONE & PODIO-GUIDUGLI [36], DESIMONE & JAMES [35] JAMES [71], BRIGADNOV & DORFMANN [13, 14], DORFMANN & OGDEN [37, 39, 38, 40, 41], DORFMANN, OGDEN, AND SACCOMANDI [42, 43], BUSTAMANTE, DORFMANN AND OGDEN [17, 18, 20, 19], BUSTAMANTE & OGDEN [21], STEIGMANN [139], and KANKANALA AND TRIANTAFYLLIDIS [78]. In particular in BRIGADNOV & DORFMANN [13, 14], DORFMANN & OGDEN [37, 39, 38, 40, 41], DORFMANN, OGDEN, AND SACCOMANDI [42, 43], BUSTAMANTE, DORFMANN AND OGDEN [17, 18, 20, 19], BUSTAMANTE & OGDEN [21], the authors have the main intent to set up universal relations for the electro-magneto-mechanical material response. A universal relation for a particular deformation or class of deformations is an equation relating the stress and strain components that holds independently of the specific choice of constitutive law for the considered class of materials. They have developed forms of the quasi-static theories for nonlinear magnetoelasticity and electroelasticity

that are applicable to magneto-sensitive and electro-sensitive elastomers, respectively. In each of the theories developed is made up use of a total stress tensor and an associated total energy density function. These theories have relatively simple mathematical structures and do not require the notion of Maxwell stress within the material. Between the recent developments we need also to mention the papers of MCMEEKING & LANDIS [103] and MCMEEKING, LANDIS AND JIMENEZ [104]. In [103] an isothermal energy balance is formulated for a system consisting of deformable dielectric bodies, electrodes, and the surrounding space. The formulation is obtained in the electrostatic limit but with the possibility of arbitrarily large deformations of polarizable material. In [104] the equations governing mechanics and electrostatics are formulated for a system in which the material deformations and electrostatic polarizations are arbitrary. A mechanical-electrostatic energy balance is formulated for this situation in terms of the electric enthalpy, in which the electric potential and the electric field are the independent variables, and charge and electric displacement are the conjugate thermodynamic forces. This energy statement is presented in the form of a principle of virtual work and is the basis for a rigorous formulation of a finite element method.

Although the basic equations and some analytic analysis of non-linear electroelasticity were established in the above cited works, very few numerical studies are known in this field. Recent studies in this respect can be found in VU & STEINMANN [147, 148], VU, AND STEINMANN AND POSSART [149], BUTZ & KLINKEL [23], KLINKEL [84] and KLINKEL [86]. In VU & STEINMANN [147, 148] and VU, AND STEINMANN AND POSSART [149] a variational formulation is built and the finite element method is employed to solve the non-linear electro-mechanical and magneto-mechanical coupling problem. In [23] a finite element formulation for a three-dimensional piezoelectric beam which includes geometrical and material nonlinearities is presented while in [86] a piezoelectric solid shell finite element formulation within a geometrically nonlinear based on a variational principle of the Hu-Washizu type is proposed.

On the other hand the numerical studies for the geometrically linear electroelasticity are well established. Typical electro-mechanical finite element models use displacements and the electric potential as nodal degrees of freedom, see GAUDENZI & BATHE [55], BEN-JEDDOU [11] and KLINKEL & WAGNER [85] and the references therein. Accordingly the electric field and the strains are calculated from the gradients of the nodal degrees of freedom. GHANDI & HAGOOD [81], suggested a hybrid finite element formulation, which incorporates electric displacement degrees of freedom as well as the conventional displacement and electric potential degrees of freedom. In KAMLAH & BÖHLE [74] the finite element analysis is carried out in a two-step scheme. In the first step a purely dielectric boundary problem is solved to obtain the electric potential. Secondly, the electro-mechanical problem for the mechanical boundary conditions is analyzed with the prescribed electric potential. In LANDIS [90] a new finite-element formulation for the solution of electro-mechanical boundary value problems is presented. As opposed to the standard formulation that uses scalar electric potential as nodal variables, this new formulation implements a vector potential from which components of electric displacement are derived. For linear piezoelectric materials with positive definite material moduli, the resulting finite-element stiffness matrix from the vector potential formulation is also positive definite. In SEMENOV ET AL. [136] a vector potential for the electric induction is applied to static three-dimensional fully coupled electro-mechanical problems. A Coulomb gauge condition imposed on the electric vector potential improves the convergence behav-

ior of nonlinear problems. The work of MIEHE [109] gives an overview and an overall understanding of these different approaches.

As we mentioned above, in this work we will propose a model able to reproduce the macroscopic dissipative response of a ferroelectric ceramic and polymer. The existing models are geometrically linear models and could be divided into two main categories: microscopically motivated and phenomenological models. A review in this regard is given by the papers of KAMLAH [73], LANDIS [92] and HUBER [65].

Microscopically motivated material models are presented by e.g. CHEN & LYNCH [30], HUBER ET AL. [66] and HUBER & FLECK [64]. These models are concerned with the constitutive behavior of single crystals and employ an energy argument as switching criterion. An other type of microscopically motivated models are the one based on a phase field type of modeling, see ZHANG & BHATTACHARYA [154, 155], SU & LANDIS [141], SCHRADE, MÜLLER, AND GROSS [133], XU ET AL. [152] and references therein.

The over all material behavior of a ceramic polycrystal is obtained by averaging over a large number of oriented crystallites. The consideration of switching for each crystal leads to a large number of internal variables.

The reduction of the number of internal variables motivates phenomenological macroscopical models. Typically the phenomenological constitutive models are used for the analysis of the inhomogeneous electro-mechanical fields occurring in devices and structures fabricated from ferroelectric ceramics and polymers. A very simple model to capture arbitrary hysteresis effects is the so-called Preisach-model, introduced in PREISACH [128]. It requires only a few material parameters and was originally developed to describe effects arising in magnetization processes. In recent years the model is being successfully adopted to model ferroelectric ceramics, see e.g. HWANG ET AL. [68]. HWANG ET AL. [68] employed the Preisach model to predict the remanent polarization and the remanent strain from an imposed electric field and stress. They introduced a simple fully coupled one-dimensional model with uni-axial loading. Another approach for a phenomenological model based on a macroscopic theory is suggested in CHEN & MONTGOMERY [28], CHEN [27] and CHEN & TUCKER [29]. The key idea is that the remanent polarization is a function of aligned dipoles. The number of the aligned dipoles is used as an internal state variable. The model is able to represent the uni-axial dielectric and the butterfly hysteresis. Similarly to Preisach this model is not thermodynamically motivated.

Based on the analogies existing between non-linear ferroelectric response and metal plasticity, the phenomenological models are usually akin to J2 flow plasticity theory and thus are rate-independent models. In BASSIOUNY ET AL. [6, 7] and BASSIOUNY & MAUGIN [8, 9] we find a thermodynamically consistent formulation of the electro-mechanical hysteresis. There the concepts of the phenomenological plasticity theory are used. A free energy function per unit volume depending on temperature, strain and the polarization is introduced. The polarization is additively decomposed into a reversible and an irreversible part, which serves as internal state variable. According to thermodynamic arguments the constitutive relations are derived within the Clausius-Duhem-Inequality. For rate independent effects an electric loading function (switching criterion) is suggested to determine the evolution of the internal state variable. On the basis of this concept several models for domain switching effects have been developed. One of the first applications of these notions into an algorithmic model can be found in COCKS & MCMEEKING [31] where a phenomenological constitutive law for piezoceramics is formulated in analogy to incremen-

tal plasticity. The model is based on an additive decomposition of polarization and strain. A convex yield surface (commonly referred as switching surface) is introduced and the evolution equations for the remanent polarization and strain are derived from this yield function by the normality rule and consistency condition. Another one dimensional model can be found in KAMLAH & TSAKMAKIS [76] and KAMLAH [73]. Here the irreversible strain is additively decomposed into two parts. One irreversible strain appears due to the alignment of the domains in a certain direction by applying an electrical loading. For this strain a one-to-one relationship to the irreversible polarization is assumed. The other irreversible strain arises due to mechanical stresses and is determined by an evolution equation. Here yield surfaces for the ferroelectric and ferroelastic switching surfaces are introduced together with saturation surfaces. The flow rules for the remanent polarization and strain are specified in terms of them. This model is extended to the three dimensional case in KAMLAH & BÖHLE [74], and is capable to simulate all hysteresis and butterfly loops including mechanical depolarization effects, which arise in ferroelectric ceramics. In KAMLAH & WANG [77] a constitutive model based on microscopically internal variables is sketched. A multiaxial thermodynamically consistent description is given by LANDIS [91]. The author's consideration of switching surfaces and associated flow rules guarantee a positive dissipation during switching. In this paper as well as in HUBER & FLECK [64] a cross–coupling into the switching function is introduced in order to account for the generation of remanent strain by the application of electric field, and remanent polarization by stress. This model is simplified in MCMEEKING & LANDIS [102] where the remanent strain is obtained in terms of the remanent polarization and thus the number of internal variables is reduced. A model which makes use of only one switching criterium is suggested by SCHRÖDER & ROMANOWSKI [135]. The co-ordinate invariant thermodynamic consistent model is based on the work of SCHRÖDER & GROSS [134] and accounts for two hysteresis effects: the ferroelectric hysteresis and the butterfly hysteresis. In the uni-axial model the polarization direction is assumed to be constant. Furthermore, the model makes use of the simplifying one-to-one relation discussed above. The uni-axial model of EL-HADROUZ ET AL. [46, 45] considers the additive split of the irreversible strains proposed by KAMLAH & TSAKMAKIS [76]. For one part the discussed one-to-one relationship is assumed. Furthermore, ELHADROUZ ET AL. [46, 45] introduced an additive decomposition of the irreversible depolarization, where it is distinguished between a polarization caused by an electric field and a polarization caused by stress. Two switching criteria are used to control the different ferroelastic and ferroelectric hysteresis and butterfly loops. The model is also able to predict mechanical depolarization. MIELKE & TIMOFTE [112, 111] show that the phenomenological models mentioned above can be formulated in an energetic framework which is based on the elastic and the electric displacements as reversible variables and irreversible variables like the remanent polarization. Instead of splitting the electric displacement into a reversible and irreversible part KLINKEL [83] introduces an irreversible electric field, which serves, instead of the remanent polarization, as internal variable. The irreversible electric field has only theoretical meaning, but makes the formulation very suitable for a finite element implementation, where displacements and the electric potential are the nodal degrees of freedom. BUTZ [22] is one of the few works were a geometrically non-linear approach is combined with a dissipative material response which results to be based on simple additive kinematic assumptions. All the other works cited above deal with a geometrically linear type of dissipative material response.

The above phenomenological models are rate-independent models. On the other hand, it

is experimentally observed (see ZHOU, KAMLAH AND MUNZ [156], VIEHLAND & CHEN [145]) that the dissipative ferroelectric response is rate-dependent as illustrated in Figure 2.5. Based on this observation, we would like to model the ferroelectric material response by using a smooth rate-dependent viscous approach within the framework of an incremental variational formulation (MIEHE [108], MIEHE ET AL. [110]) which ensures a canonical symmetrical structure. In contrast to the rate–independent type of models, only few proposed rate–dependent types of models exist. Among the others we would like to cite BELOV & KREHER [10] where non-linear hysteretic phenomena in polycrystalline ferroelectric ceramics are simulated using viscoplastic (rate-dependent) models without a switching condition within a microscopical framework, and AROCKIARAJAN ET AL. [4] which focuses on modeling of rate-dependent behavior of piezoelectric materials within a three-dimensional finite element setting and uses the reduction in free energy of a grain as a criterion for the onset of the domain switching process. ROSATO & MIEHE [131] proposed continuous and discrete variational formulations for the treatment of the non-linear response of piezoceramics under electrical loading and specified the variational formulation for a setting based on a smooth rate-dependent dissipation function governing the hysteretic response.

The set up of a general incremental variational formulation of inelasticity has been developed in the recent works MIEHE [108], MIEHE, SCHOTTE AND LABRECHT [110] which were conceptually in line with the papers of ORTIZ & REPETTO [120], ORTIZ & STAINIER [121], CARSTENSENS, HACKL AND MIELKE [24]. The key idea can be described as follows: the general internal variable formulation of inelasticity for generalized standard media is governed by two scalar functions: the energy storage function and the dissipation function. The general set up of this generic type of material model can be related to the works BIOT [12], ZIEGLER & WEHRLI [157], GERMAIN [56], HALPEN & NGUYEN [59], see also the recent tratments by MAUGIN [100] and NGUYEN [117]. All the different variational formualtion which can be considered for the electro-mechanical coupled problem are describe in the recent work of MIEHE [109]. See also ROSATO & MIEHE [131].

1.2. Objectives and Overview

In recent years an increasing interest in functional materials such as ferroelectric polymers and ceramics has been shown. For those materials, viscous effects or electric polarizations cause hysteresis phenomena accompanied with possibly large remanent strains and rotations. Our final goal is to outline aspects of the formulation and numerical implementation of dissipative electro-mechanics at large strains. In particular we would like to develop continuous and discrete variational formulations for the treatment of the non-linear dissipative response of electro-mechanical solids and adapt these formulations to the modeling of the hysteretic material response of piezoceramics and ferroelectric polymers under electrical loading. The point of departure will be a general internal variable formulation that determines the hysteretic response of the material as a generalized standard medium in terms of an energy storage and a rate-dependent dissipation function. Consistent with this type of standard dissipative continua, we will develop an incremental variational formulation of the coupled electro-mechanical boundary-value-problem. We would like to specify the variational formulation for a setting based on a smooth rate-dependent dissipation function which governs the hysteretic response. Further, we underline the geometric

nature of dissipative electro-mechanics. An important aspect is the numerical implementation of the coupled problem. The discretization of the two-field problem will appear, as a consequence of the proposed incremental variational principle, in a symmetric and very compact format. Further, we would like to discuss constitutive assumptions which account for specific problems arising in the geometric nonlinear setting. With regard to the choice of the internal variables entering the constitutive functions, a critical point are the kinematic assumptions. Here, we will investigate the multiplicative decomposition of the local deformation gradient into reversible and remanent parts as well as the introduction of a remanent metric. Such a formulation allows us to reproduce the dielectric and butterfly hysteresis responses characteristic of the ferroelectric materials together with their rate-dependency and to account for macroscopically non-uniform distribution of the polarization in the specimen together with large attained deformations.

This work is organized as follows.

In **Chapter 2** we describe the micromechanical behavior of two classes of ferroelectric materials, i.e. piezoceramics and ferroelectric polymers, that are taken under consideration in this work as cases of study for the electro-mechanical dissipative response. The constitutive material response of these two classes of materials is based on two fundamental elements: first, the non-centrosymmetric molecular constitution, which yields to the appearance of elementary micro-dipoles characterized by a certain spontaneous polarization in the microstructure and additionally is responsible for the piezoelectric behavior of the unit cells; second the capability of aligning those elementary unit cells under a certain electro-mechanical loading and the ability of retaining this alignment after unloading. The first factor is responsible for the reversible part of the material response, while the second characteristic is the fundamental reason for the dissipative behavior of this class of materials.

Chapter 3 outlines the principal equations of non-linear continuum mechanics that describe the fundamental geometric mappings, basic stress measures, balance equations of a solid body undergoing finite mechanical deformations. In the Chapter 5 those equations will be modified in order to describe an electro-mechanically coupled problem.

The aim of **Chapter 4** is to construct the global and local equilibrium equations together with the constitutive equations of electrostatics by using an approach similar to the one used in Chapter 3 for the continuum mechanics. Those equations are written in the physical Eulerian configuration and later on the transformations to the current configuration are considered. The geometric nature of the electric objects is underlined.

The ultimate goal of **Chapter 5** is to derive the balance equations for the coupled electro-mechanical problem. The solution of those equations in combination with the constitutive equations gives us the independent electro-mechanical fields within the region under consideration. Since relativistic effects are considered the most general framework of balance laws for continua consists of a combination of Maxwell's equations of classical electro-statics and the classical balance equations of the thermomechanics. The latter are modified assuming that body force, body couple and energy supply can be decomposed into two parts: one due to the electric field and the other is supposed to be externally applied and known from the outset. The electric body force, body couple and energy supply are evaluated using the two-dipole model in the Chu formulation. Consequently the balance equations are modified through the introduction of a total stress and an amended energy functional accounting for the energy stored in the body and in the underlying free

space. No attempt to distinguish between mechanical and Maxwell stress is pursued in the proposed formulation.

The goal of **Chapter 6** is the discussion of a variational formulation for a generic dissipative electro-mechanical response. At first we concentrate on a purely local constitutive modeling for the constitutive dissipative material response and afterwards we focus on the global treatment of a multifield boundary-value-problem. Our considerations will be directed to the formalization of the coupled electro-mechanical boundary-value-problem through an energetic description. We focus first on local volume element of the solid which undergoes an electro-mechanical loading. The choice of the independent variables characterizing the local material response of an electro-mechanically coupled solid can be based on two different approaches: a physically-based approach which differentiates between actions and reactions and a geometry-based approach which considers dual objects in the geometric setting. The first type of approach yields in general to a minimization structure of the electro-mechanical boundary-value-problem, while the geometry-based approach delivers normally a saddle-point structure. In this work, we consider a formulation of the local constitutive material response based on a set of independent variables which have a geometric character. Thereafter, we deal with the formulation of the field equations in the form of variational principles and methods. The variational approach in various forms is often taken as the cornerstone for the development of discretization techniques such as the well established finite element methodology. Variational principles are particularly powerful and belong to the fundamental principles in mathematics and mechanics. It is important to note that the finite element method needs not necessarily to depend upon the existence of a variational principle. However, good approximate solutions are often related to weak forms of field equations, which are consequences of the stationarity condition of a functional.

In **Chapter 7** a phenomenological model for the ferroelectric material response at small strains is presented. The first objective of this chapter is the construction of energy and dissipation functionals which take into account the basic micro-effects characterizing ferroelectric materials. We construct simple functions which include in an elementary format all basic effects of electro-mechanical coupling suitable for the description of the piezoelectric non-dissipative material response. These functions contain a minimum number of material parameters, each of them related to an elementary experiment. These functions are later on modified in order to take the polarization dissipative mechanisms into account, which characterize ferroelectric materials. Based on the polarization mechanisms dissipation functionals are also constructed. A material model based on theses two functionals is developed and tested by means of a spectrum of benchmark problems.

In **Chapter 8** first we construct a simple model for a piezoelectric material response at large strains which contains the essential electro-mechanical coupling phenomena. This serves as basis for the construction of a model describing the dissipative response of ferroelectric materials at large strains. To this purpose we assume that the electric displacement can be additively decomposed into a reversible and irreversible contributions and we investigate the multiplicative decomposition of the local deformation gradient into reversible and remanent parts. Based on these kinematic assumptions we consider an energy storage functional derived from the piezoelectric one by replacing the independent variables with their reversible counterpart and by rendering the coupling dependent on the polarization process. An additional hardening term is added to such a functional. Based

on the polarization mechanisms dissipation functional are constructed. Finally the material model constructed on the energy storage and dissipation functional is tested by means of a spectrum of benchmark problems which eventually also show large deformations.

2. Micromechanical Motivation

Before starting with the modeling of electro-mechanically coupled materials and of the dissipative ferroelectric response, we would like to describe the micromechanical behavior of two classes of ferroelectric materials, i.e. piezoceramics and ferroelectric polymers, which will be taken under consideration in this work as cases of study for the electromechanical dissipative response. The constitutive material response of these two classes of materials is based on two fundamental elements: first the non-centrosymmetric molecular constitution, which yields to the appearance of elementary micro-dipoles characterized by a certain spontaneous polarization in the microstructure and additionally is responsible for the piezoelectric behavior of the unit cells; second, the capability of alignment of those elementary unit cells under a certain electro-mechanical loading and the ability of retaining this alignment after unloading. The first factor is responsible for the reversible part of the material response, while the second characteristic is the fundamental reason for the dissipative behavior of this class of materials. We will start by giving a description of the piezoelectric effect and we will focus later on the dissipative mechanisms which contradistinguish piezoceramics and ferroelectric polymers.

2.1. Piezoelectricity

Piezoelectricity is a linear coupling phenomenon possessing a direct and an inverse effect. Lets start the discussion with the *inverse piezoelectric effect* because it resembles the polarization mechanism. If a certain electric field $\mathbb{e}$ is applied to a mechanically unloaded piezoelectric specimen, one observes the strain ε

$$\varepsilon = c\,\mathbb{e}, \tag{2.1}$$

which is proportional to the electric field $\mathbb{e}$. The proportionality constant c is called *piezoelectric constant*. The electrically induced strain may be an elongation or a shortening, depending on the direction of the applied electric field and consequently on the sign of $\mathbb{e}$. To visualize this behavior, consider a unit cell of an unloaded polar material with a spontaneous polarization $\mathbb{p}_{spon}$, resulting from the different locations of the centers of positive and negative charges of a unit cell. Figure 2.1a displays a plane view of such a unit cell. Application of a constant voltage to the cell will result in a shifting of centers of the positive and negative ions with respect to each other. An electric field with the same direction as the spontaneous polarization will move the centers further apart from each other, while an electric field with the opposite direction will bring them closer together. The electro-mechanical coupling effect is caused by the fact that the shifting of the centers of the charges is accompanied by a corresponding elongation or shortening of the unit cell. In case the spontaneous polarization is oriented in the reverse direction with respect to a fixed frame of reference, the constant c has the same magnitude, but a different sign. As a consequence, the orientation of the electric field is an important ingredient of the effect. An exposure of the unit cell to mechanical loads will, of course, bring rise to a deformation in the structure of the cell and, accordingly, to a displacement in the relative positions of the centers of the charges. This displacement causes a transient current in the unit cell and, in turn, a change of polarization. This mechanically induced change of polarization is called *direct piezoelectric effect*. As a result of direct piezoelectric effect, application of even very small mechanical loads may lead to high electric voltages. This behavior suits to sensor applications. Besides, the inverse piezoelectric effect may
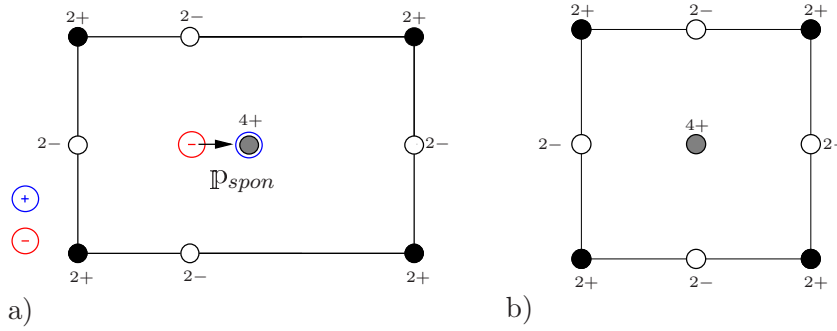
Figure 2.1: a) Plane view of a unit cell with different locations of the centers of positive and negative charges. The arrow indicates the corresponding spontaneous polarization $\mathbb{p}_{spon}$ which will be present even though the crystal lattice possesses no resultant electric charge. b) Plane view of a unit cell possessing a center of symmetry. In the unloaded state, both the centers of positive and negative charges will be in the center of the unit cell.

be employed in the actuator applications. The property of piezoelectricity is related to the polarity of the unit cell of a material. However, a spontaneous polarization is only possible in certain systems of crystal symmetry. Obviously, the unit cell must not possess a center of symmetry.

2.2. Piezoceramics

The common structure of the typical materials with piezoelectric properties, like $BaTiO_3$ and PZT, is polycrystalline as a result of ceramic processing techniques (for a more detailed description concerning the material science of ferroelectric piezoceramics see Jaffe et al. [70], Lines and Glass [93], and Moulson and Herbert [113]). The polycrystalline structure comprises grains of differently oriented crystal lattices. The unit cell consists of a structure of positively and negatively charged ions typical for a specific material. In this structure, the *centers* of the positive and negative charges of the unit cell have a certain location within the cell. If the centers of positive and negative charges are at different positions within the unit cell in the absence of any load giving rise to a permanent dipole, we say that the cell possesses *spontaneous polarization*. Although the direction of the lattice axes is fixed within a grain, it does not mean that the orientation of the spontaneous polarization is fixed as well. In fact, each grain may consist of substructures, *domains*, which are regions of unit cells with equal spontaneous polarization. A micrograph of a ferroelectric crystal is given in Figure 2.2, Arlt [3].

Let us consider $BaTiO_3$ or PZT. The crystal lattice of these materials has perovskite structure below material dependent *Curie temperature* θ_c. ($BaTiO_3 : \theta_c = 120 - 130\,°C$, $PZT : \theta_c = 250 - 350\,°C$). As in the Figure 2.3a, the unit cell is *cubic* in shape with a side length a_0 and $+4$ charged ion in the center. Since the centers of the positive and negative charges are at the same place, the material shows no instantaneous polarization and is in the *paraelectric phase*. Below the Curie temperature θ_c, the cubic configuration becomes unstable because of the shifting of the centers parallel to the one of the lattice axes leading to a *tetragonal* shape with the dimensions $a \times a \times c$. In this *ferroelectric* phase, as the centers no longer coexist, the unit cell has spontaneous polarization, and accordingly piezoelectric properties. Besides tetragonal, one may find additional ferroelectric phases too, Jaffe et al. [70]. For the sake of simplicity, tetragonal structure is considered here.
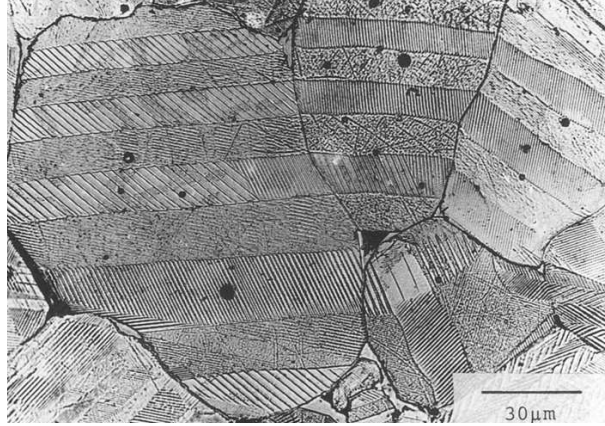
Figure 2.2: Micrograph of a ferroelectric ceramic crystal, ARLT [3]. The typical subdivision in grains and domains can be observed.

During the cooling period following the sintering process, held well above the Curie temperature, the ferroelectric materials experience a phase transition from the paraelectric phase to the ferroelectric one. There exist six possible directions in each unit cell for the rearrangement of the central ion, which are located along the axes of the original cube. This means, simultaneously, six different directions for the spontaneous polarization. That is the reason why there exists no unique spontaneous polarization direction for all unit cells of a grain upon cooling. In fact, the spontaneous polarization will be distributed with random orientations in a grain, and with uniform orientation only in the domains of a grain (see MOULSON AND HERBERT [113] for further details).

On macroscopic scale, after cooling below the Curie point, the randomly distributed spontaneous polarizations and the contributions of the corresponding microscopic piezo-electricities of the unit cells cancel each other. Thus, there is no residual macroscopic polarization and, accordingly, no macroscopic piezoelectricity in this *virgin* state of the material, also called *thermally depoled* state. Although the anisotropy of the individual unit cell is a fact, the random distribution of the spontaneous polarization in the thermally depoled state leads to a macroscopically isotropic state of a polycrystal.
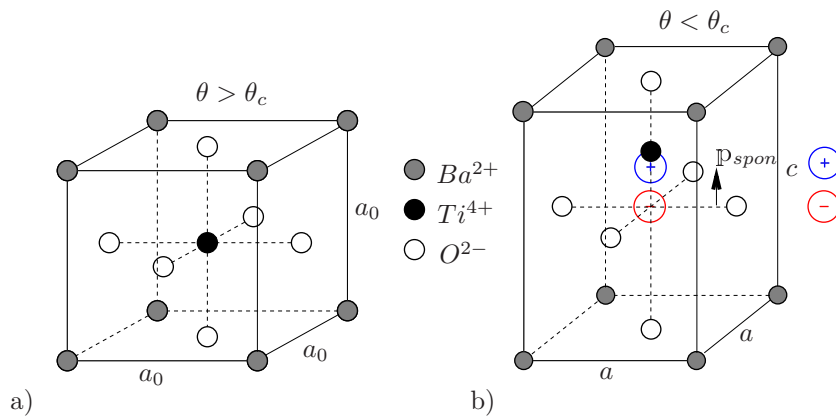
Figure 2.3: a) Unit cell of $BaTiO_3$ in the paraelectric phase. The symmetry of cubic shape does not allow for a spontaneous polarization. b) Unit cell of $BaTiO_3$ in the ferroelectric phase. The vector of spontaneous polarization $\mathbb{p}_{spon}$ is oriented in the direction of the displaced titanium ion.
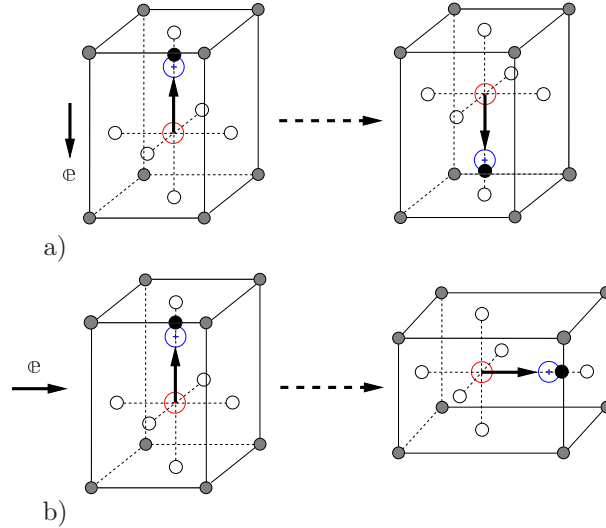
Figure 2.4: a) 180 ° and b) 90 ° switching of spontaneous polarization of a tetragonal unit cell under an electric field of magnitude above coercive electric field e_c.

The macroscopic electrical and mechanical response is the outcome of the domain structure. The domain state of a *ferroelectric material* can be modified under the loadings with sufficient magnitude by *domain switching*. For example, application of an electric field of magnitude above the *coercive field e_c* will switch the directions of spontaneous polarization by 90 ° or 180 ° to a direction more closely aligned with the applied electric field, as illustrated in Figure 2.4. In the 180 ° switching, the tetragonality of the unit cell remains unchanged while the 90 ° switching goes with the reorientation of the tetragonality.

After removal of the loading, the switched configuration retains. In the completely unloaded state, i.e. zero electric field, the material will have a non-zero residual macroscopic polarization, which is called *irreversible or remanent polarization*. The process to reach this ordered microscopic polarization state is named *poling*. The remanent polarization is the average of the spontaneous polarization of the unit cells over all of the corresponding crystals. In the ideal perfect crystals, the remanent polarization can achieve the value of spontaneous polarization as a maximum. However, in real ceramic structure the crystallographic axes are random from grain to grain within the polycrystal and thus there are mismatches of spontaneous polarization and strain from grain to grain, HUBER ET AL. [66]. Because of this kind of defects, i.e. dislocations and impurities, a maximum possible value reachable for the remanent polarization, *saturation polarization*, is defined, JAFFE ET AL. [70] and MOULSON AND HERBERT [113].

Arrangement of the formerly random orientation state of the unit cell by the poling process in the direction of the applied electric field causes a transversely isotropic material, whose anisotropy axis coincides with the remanent polarization vector, JAFFE ET AL. [70]. For the reason that the microscopic piezoelectric contribution of the individual unit cells do not cancel each other in this ordered state, a macroscopic piezoelectricity exists. Here, it should be emphasized that even in a fully poled state there is no ideal single domain grain in a real ferroelectric ceramic.

The reorientation of the unit cells in the direction of poling field also leads to a deformation of the polycrystal. Resulting macroscopic average of the spontaneous strains of the unit cells is called *irreversible* or *remanent strain*. As for the remanent polarization, there
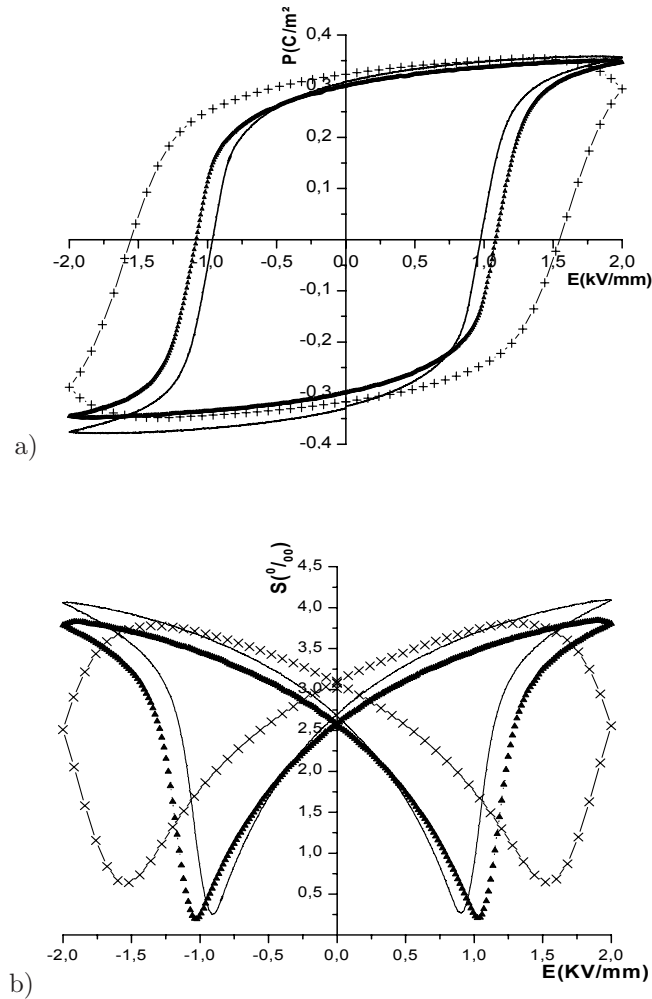
Figure 2.5: a) Electric hysteresis and b) butterfly curves in commercial soft PZT piezo-ceramic PIC151 for the loading rates of 0.01 (line with crosses), 0.1 (triangles) and 1 Hz (continuous line) according to ZHOU, KAMLAH AND MUNZ [156].

is also a maximum value for the remanent strain, called *saturation strain*, which cannot be greater than *spontaneous strain*. In the Figure 2.5 the typical macroscopic responses of a piezoceramic under a periodic electrical loading are shown. In Figure 2.5a we find the dielectric displacement vs. the electric field hysteresis, i.e. the dielectric hysteresis, while in Figure 2.5b the butterfly hysteresis is reported, i.e the strain vs. the electric field hysteresis. These hysteresis curves were already observed in the pioneering work of LYNCH [97] and are here extracted from the measurements in the work of ZHOU, KAMLAH AND MUNZ [156]. In these measurements the typical frequency dependence of the hysteresis curves is also put into evidence.

Mechanical stress with adequate magnitude, above *coercive stress* can trigger domain switching as well, LINES AND GLASS [93]. A mechanical stress can not give a unique switching direction of spontaneous polarization of a unit cell. Therefore, c-axes of the domains are oriented randomly in the plane perpendicular to the compression loading, accompanied by an irreversible deformation. Spontaneous polarization of a unit cell may take an orientation from alternatives shown in Figure 2.6. The resulting domain state is transversely isotropic and no macroscopic polarization is observed. Although the induced
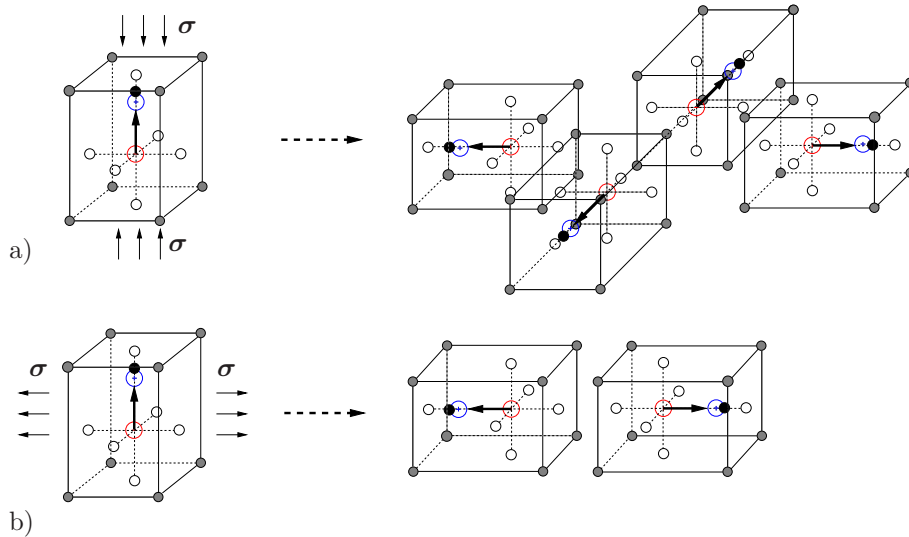
Figure 2.6: A mechanical stress $\boldsymbol{\sigma}$ of sufficient magnitude can switch a unit cell by $90\,°$. No specific orientation is given to spontaneous polarization vector. a) As consequence of a compression parallel to the spontaneous polarization we could have four possible $90\,°$ switching directions. b) Under a traction orthogonal to the spontaneous polarization two $90\,°$ switching directions are available.

deformations seem to be similar to those in metal plasticity, the saturation limit for the strains in domain switching mechanism makes the crucial difference between plastic strains caused by dislocation movement and strains due to domain switching. For a more detailed description of the microstructural and macrostructural material response of the ferroelectric ceramics see the review articles of Kamlah [73] and Landis [92] and references therein.

Ferroelectric ceramics are presently being used in a broad range of applications including sonar, MEMS devices, fuel injectors for high efficiency-low emission diesel engines, actuators for active control of helicopter rotor blades and underwater vehicle control surfaces, and ultrasonic rotary inchworm motors with high power and torque densities. Accurate modeling tools are required for the reliable design and optimized performance of these devices.

One of the most important characteristics of piezoceramics are the observed macroscopic hysteresis under purely electric loading. The macroscopic hysteresis phenomena will be discussed in the following in a qualitative manner disregarding the domain wall effects although their contribution to the performance of piezoceramics is significant, see Huber & Fleck [64], Weber, Kamlah & Munz [151], Kamlah, Liskowsky, McMeeking & Balke [75].

Let us consider a mechanically unclamped ferroelectric specimen which is loaded by a uniaxial cyclic electric field in a fixed direction, and for which polarization and strains in the same direction are recorded. The specimen is assumed to be initially in a thermally depoled state, in which it is isotropic due to the random distribution of the domain orientation by cooling below Curie temperature after sintering. In Figure 2.5a are the so called *dielectric hystereses*, the plots of polarization (or electric displacement) vs. applied electric field representing the dielectric behavior of the ferroelectric ceramic. To discuss these curves, consider the schematic sketch of Figure 2.7a. In the initial state ①, the
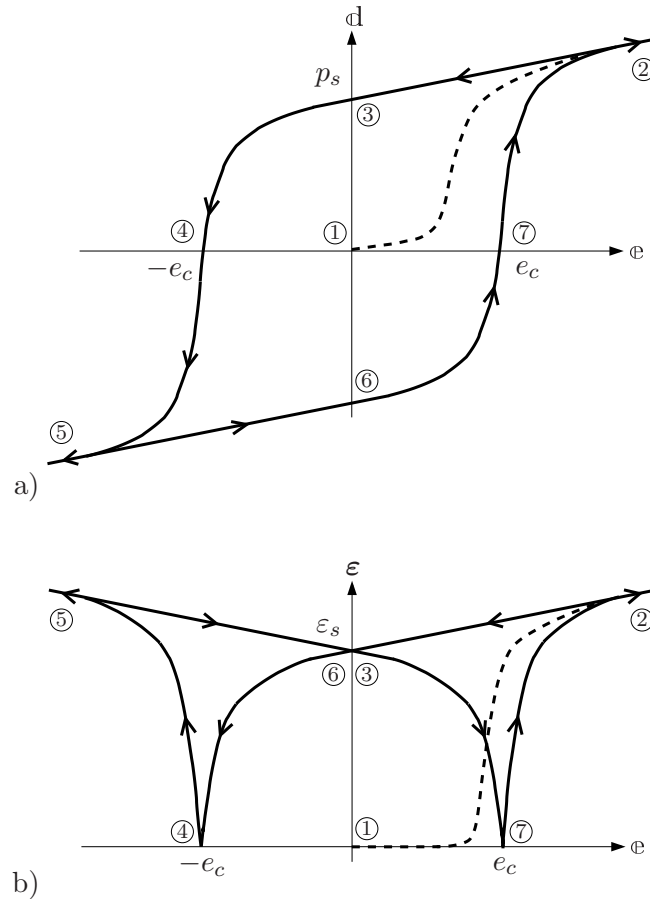
Figure 2.7: Schematic sketch of a) dielctric hysteresis b) butterfly hysteresis for a cyclic electric loading. The dashed lines belongs to the first polarization process of the unpoled material.

orientation of the polarization of the domains is randomly distributed and consequently there is no macroscopic polarization in this state. Application of electric fields with small magnitude causes only perturbation of the ions in the neighborhood of their equilibrium positions and no change in the domain structure is observed. The dielectric behavior of the material is reversible and approximately linear. As the electric field exceeds the *coercive field strength* e_c, the domain switching is initiated. This process is irreversible since certain ions within unit cells take new equilibrium positions. Microscopic polarization of all domains is oriented in the closest direction to the electric field. The increase of the polarization is much faster till the point ②, where reservoir of the switchable domains is exhausted. Further changes in the polarization state can only result from the shifting of the ions in the neighborhood of their new equilibrium positions. Such changes are essentially linear and reversible. Reversibility is clearly demonstrated during unloading part of the loading history. While reducing the electric field, the ions keep their new equilibrium positions and the switched domain state is preserved. Therefore, even in the absence of any electric field, at point ③, there exists a remanent i.e. residual polarization. In this example, it assumes the maximum possible value, *saturation polarization* due to complete alignment of the domains under the electric field of sufficient strength. This poled state is important for the technical application since it shows an approximately linear piezoelectric behavior under small electric fields. If the electric field in the opposite direction is increased beyond the coercive field strength, switching processes are again

initiated. The formerly fully oriented domain state is destructed such that the remanent polarization decreases till the point ④, where the material is in a more or less depoled state. Although at point ①, ④ and ⑦ in Figure 2.7a the resultant polarization is zero, the domain configurations for each point are different. Further loading will bring rise to a domain state oriented in the new direction of th electric field at point ⑤. After reversing the electric field again, the same mechanism applies for the points ⑥, ⑦ and ②. Summarizing, the material response is composed of three different ranges. In the initial state, a reversible behavior for small loads occurs, in a second state an initiation of irreversible process for the loading above a certain threshold value is recognized and at last a reversible character after the saturation of the irreversible process is observed.

The switching process also affects the deformation state of the material. In Figure 2.5b the *butterfly hystereses* are recorded for the normal strain in the direction of the electric field together with the dielectric hystereses in the Figure 2.5a. For a better understanding of this complex curves, consider the schematic representation of Figure 2.7b. The material is initially in a thermally depoled and macroscopically isotropic state at point ① as state of zero strain. For electric fields below the coercive field strength $e < e_c$, the polarization in the domains are distributed randomly and individual piezoelectric contributions of the domains will cancel each other. Therefore, there will be no electrically induced macroscopic strain. As one can see from Figure 2.7b, the curve is exactly horizontal until the electric field approaches the coercive field. As the coercive field is passed, switching occurs. Simultaneously, strain significantly increases by two contributions: at first the number of the domains with their long c-axes (cf. Figure 2.3) oriented along directions closest to the one of the electric field increases. Secondly, as we have seen before, a resultant macroscopic remanent polarization now occurs. This is accompanied by a macroscopic piezoelectric effect causing a reversible part of strain. After a fully switched domain state is reached with the completion of switching process, further changes in the strain state are only generated by macroscopic piezoelectricity, which is reflected by a reduced slope of the curve as point ② is approached. Switching strain and the strain due to piezoelectricity can be separated easily after unloading at zero electric field since macroscopic piezoelectric strain vanishes at point ③ and only strain due to the switching of domains remains. In the case of complete alignment of domains, this switching strain assumes the value of *saturation strain* as a maximum value. The poled state of the ceramic is the one employed in technical applications. In the neighborhood of point ③, there occur approximately linear changes in strain state under small electric fields due to macroscopic remanent polarization. The switching of domains in the microstructure during the poling process are of shape changing nature leading to volume preserving strain changes. Upon the reversal of electric field beyond the coercive field strength, back switching process will be initiated. The degree of order of domains is reduced and the distribution of the c-axes becomes more random. Here, an electric depolarization is recognized leading to a loss of piezoelectric properties. At the same time, the resultant switching strain is also reduced and at point ④ the strain goes through a sharp minimum. Notice that the electrically depoled state will be generally different from the thermally depoled initial state. However, based on the fact that the strain is close to zero at the point ④ in Figure 2.7, the domain structures will be similar up to some level for this material. From this minimum on, the alignment of the domains as well as switching strain and the piezoelectric strain start to increase again. At point ⑤, a fully oriented domain state in the new direction of the electric field is reached. The only difference to point ② is the direction of the
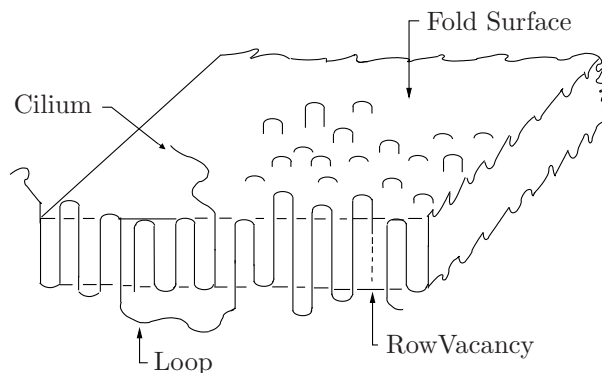
Figure 2.8: Schematic drawing of a chain folded polymer crystal (Figure redrawn from WANG, HERBERT AND GLASS [150].

alignment, which is opposite. The most significant feature of the butterfly hysteresis is its symmetry with respect to the strain axis at $\mathbb{e} = 0$, resulting from the properties of the switching strain and the piezoelectric strain. For the switching strains only the degree of alignment of c-axes counts and not the orientation of the spontaneous polarization vector. Particularly, two opposite polarization states will lead to the same remanent strain state. During poling by both a positive and a negative electric field, the induced piezoelectric strain will be positive, since it is caused by a corresponding positive or negative remanent polarization, respectively. The piezoelectric constants in the poled states ② and ⑤ have the same absolute magnitude, but opposite signs.

Figure 2.5 shows the time-dependent hysteretic behavior of piezoceramics, ZHOU, KAMLAH & MUNZ [156]. The dielectric hysteresis and the butterfly curve clearly demonstrate a strong frequency dependence. At slow rates very similar polarization and butterfly curves were observed at 0.01 Hz and 0.1 Hz, and the coercive field at 0.01 Hz is about 1 kV/mm. Note that the coercive field e_c increases with increasing measuring frequency. For higher loading frequencies, i.e. of 1Hz, polarization and strain were not saturated at the maximum electric field amplitude.

2.3. Ferroelectric Polymers

A ferroelectric polymer is a polymer possessing unit cells in the microstructure with a certain spontaneous polarization that can be reoriented between possible equilibrium directions by a realizable electric field which goes beyond a coercive value. A ferroelectric polymer can be in a single crystal form or, as in most of the cases encountered, a semicrystalline form in which the ferroelectric crystallites are embedded in an amorphous matrix. Crystal fields serve to keep the elementary dipoles aligned upon removal of the electric field. Examples of ferroelectric polymers include polyvinylfluoride (PVF) (FUKADA & NISHIYAMA [51], PHELAN, MAHLER, AND COOK [126]), polyvinylidene Fluoride (PVDF) (KAWAI [79], FUKADA & SAKURAI [52], MURAYAMA ET AL. [116]), copolymers of PVDF with trifluorethylene (TrFE) (HIGASHIHATA, SAKO AND YAGI [61]) or tetrafluorethylene (TFE) (BROADHURST ET AL. [16]), and odd-numbered nylons (KAWAI [79]). We will discuss PVDF and P(VDF-TrFE) in more detail.

As a poled piezoceramic, a poled ferroelectric polymer shows a piezoelectric-type behavior. The properties of polymers are very different from those of inorganics. They are much better sensors then ceramics. Piezoelectric polymeric sensors and actuators offer the ad-
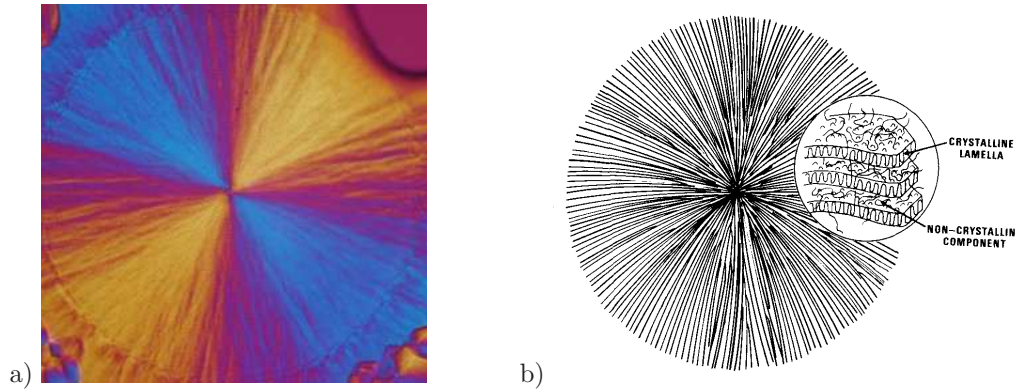
Figure 2.9: a) Photomicrograph of a rapidly coled melt of commercial unoriented PVDF between crossed polaroids; b) A schematic diagram of a spherulite and a detail of a section emphasizing the lamellar structure of the radiating branches.

vantage of processing flexibility because they are lightweight, tough, readily manufactured in large areas, and can be cut and formed into complex shapes. Polymers exhibit high strength and high impact resistance DAVIS [34]. Other notable features of polymers are low dielectric constant, low elastic stiffness, and low density, which result in high voltage sensitivity, and low acoustic and mechanical impedance. Polymers also typically possess high dielectric breakdown and high operating field strength, which means that they can withstand much higher driving field than piezoceramics. Polymers offer the ability to pattern electrodes on the film surface and pole only selected regions. Based on these features, piezoelectric polymers posses their own established area for technical applications and useful device configurations.

In order to understand the ferroelectric and piezoelectric properties of semicrystalline polymers, it is important to know something about their structure and morphology. Although many polymers with a regularly repeated structure can crystallize, the crystals are microscopic in size and usually comprise only 50 to 90% of the total volume. When crystalline polymers crystallize, the polymer molecules typically form lamellae of the order of 10 nm thick. The polymer molecules are oriented perpendicular to the surface of the lamellae and are folded in such a way that they have to penetrate the lamellae many times, KEPLER & ANDERSON [80]. A schematic representation of a lamella is reported in figure 2.8.

When crystallized from the melt, polymers usually exhibits spherulites. These spherical aggregates consist of radiating array of lamellae. Figure 2.9a is a photomicrograph of a spherulite in a melt-crystallized PVDF film. The volume fraction of crystalline material is typically 50% depending on the thermal history, see BROADHURST ET AL. [15] and references therein. Most of the uncrystallized molecules are in a metastable liquid phase. The glass transition temperature of this liquid phase is around $-50°$C. The structure of polymer spherulites is summarized in the schematic drawing in Figure 2.9b. Highly elongated chain folded lamellar crystals emanate radially from the center with the chain axis approximately tangential and a crystallographic axis frequently parallel to the radius. The diagram shows a lamellar twist which occurs in some cases. The non crystalline component between the lamellar crystals is presumed to consist of portions of molecules caught between participations in neighboring crystallites (tie molecules), portion of molecules which comprise "loose folds", dangling ends of molecules (cilia), tight
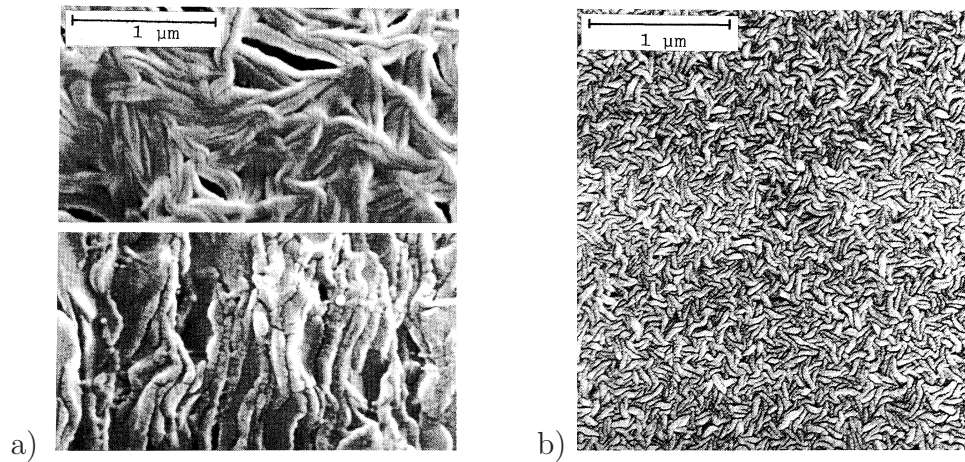
Figure 2.10: SEM images of P(VDF-TrFE) films; a) the upper is the surface and the lower the cross-section of a 60 μm-thick film, and b) the surface of a 0.1 μm-thick film. (From KIMURA & OHIGASHI [82])

folds, and non-crystallizable components such as branch points, bulky comonomer units, and low molecular weight polymer. As mentioned earlier the non-crystalline component can often occupy 50% or more of the total volume.

It is naturally presumed that the growth of large crystalline lamellae is suppressed by the thickness in very thin films, FURUKAWA [53]. This has been proved to be true by the images of scanning electron microscope (SEM) for 60μm and 0.1μm thick copolymer samples (cf. Figure 2.10). First of all, we may notice that surprisingly well grown crystalline lamellae are filling the space in both of the samples. The thinner sample consists of smaller lamellae. As the size of the lamellae decreases, a larger amounts of defects may be introduced and might have hindered full reversal of the polarization at low fields in thinner copolymer samples.

Thus, we can conclude that the morphology of such polymers consists of crystallites dispersed within amorphous regions, as shown in Figure 2.11a. The amorphous region has a glass transition temperature that dictates the mechanical properties of the polymer, and the melting temperature of the crystallites dictates the upper limit of the use temperature. Almost all polymers used in fibers or films are purposely oriented to improve physical properties such modulus, stiffness, and recovery. Orientation is achieved by stretching or rolling to several times the original length at temperatures below the crystallization temperature, cf. Figure 2.11b. During the process, the spherulites referred above are first deformed to an elliptical shape followed by disruption of the spherulite structure, particularly in a band corresponding to an equator normal to the direction of elongation. At large deformations (4 to 10 times), the morphology becomes fibrillar in appearance and the molecular chains become oriented preferentially parallel to the direction of the deformation. Depending on whether the stretch is uniaxial or biaxial, the electrical and mechanical properties are either highly anisotropic or isotropic in the plane of the polymer sheet. Electrical poling is accomplished by applying an electric field across the thickness, as depicted in Figure 2.11c. An electric field of the order of 50 MV/m is typically sufficient to effect crystalline orientation. The amorphous phase of semicrystalline polymers supports the crystal orientation, and polarization is stable up to the Curie temperature.

A brief discussion on the chain conformation and crystal structure is appropriate because
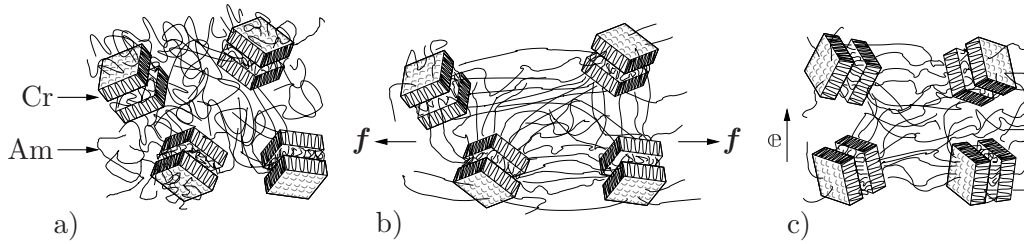
Figure 2.11: Schematic illustration of random stacks of amorphous and crystal lamellae in PVDF polymer: a) the morphology after the film is melt cast with schematization of the crystalline region (Cr) and the amorphous region (Am); b) after the reorientation of the film by mechanichally stretching several times its original length; and c) after depositing metal electrodes and poling through the film thickness.

of its importance in understanding piezoelectricity and ferroelectricity in crystalline polymers. Conformation of a molecule refers to the spatial arrangements of atoms which can be changed by rotations about chemical bonds. Figure 2.12 has been redrawn from Allock & Lampe [2] to show estimated variations in the potential energy as a function of the torsion angle between the two central carbon atoms of a four carbon segment in a polyethylene chain. The bond between the carbons being considered is perpendicular to the plane of the page. The solid lines represent tetrahedral bonds to the front carbon and the dotted lines represent tetrahedral bonds to the back carbon. The torsion angle is taken as 0° when the four carbons lie in the same plane. As the front carbon is twisted clockwise, the potential energy increase to a maximum as the atoms bonded to the front and back carbon reach an "eclipsed" position of maximum repulsion at 60°. Continued rotation results in a minimum when the atoms are furthest apart at 120°. The energy is not as low as at 0° when the carbons are further removed from overlap. Energy changes with continued rotations as shown in the Figure 2.12 with the position at 120° and 240° being equivalent. The lowest energy form is referred to as *trans* (T) and the two higher
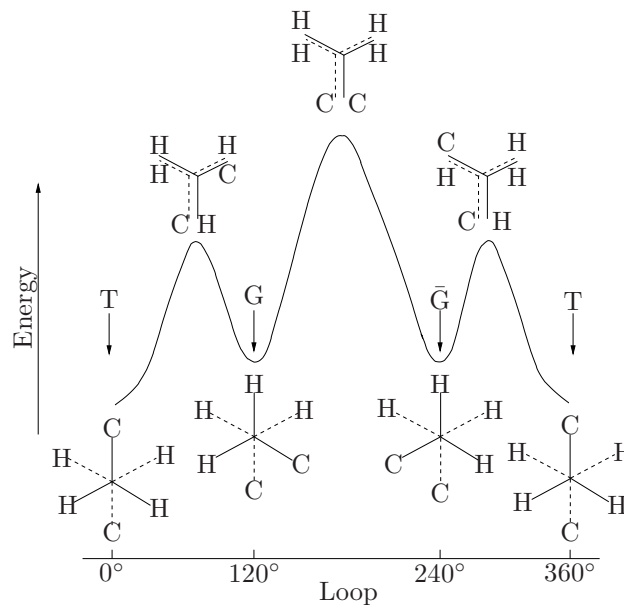
Figure 2.12: Potential energy of interaction between substituents on adjacent carbon atoms of polymer chain versus angle of rotation from planar zigzag conformation. *Trans-gauche*, and *gauche* prime positions are indicated by arrows, see Wang, Herbert and Glass [150].
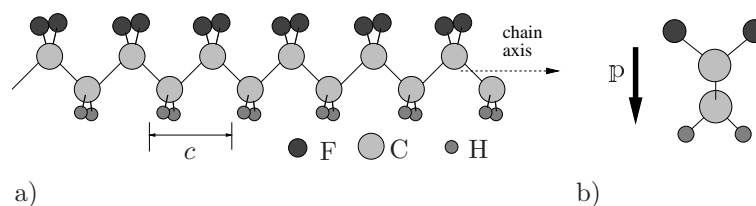
Figure 2.13: A schematic view of β-phase: a) polymer chain in the planar zigzag conformation with repeated crystal unit having lattice dimension $c = 2.56$ Å b) view parallel to the chain axis with spatial distribution of the charges inducing polarization.
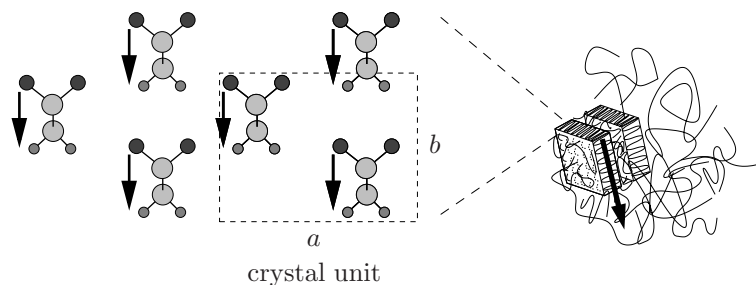
Figure 2.14: Crystal structure of β-phase containing two chains forming a crystal unit and having lattice dimensions $a = 8.58$ Å and $b = 4.90$ Å. Several chains alinged in the same direction form a crystallite in an amorph matrix (cf. Figure 2.11).

energy minima as *gauche* (G) and *gauche* prime ($\bar{G}$). Gauche energies are equivalent, but correspond to bond rotations of 120° in opposite directions.

As we already mentioned above, PVDF (molecular formula: CH_2F_2) and its copolymers exhibit the largest piezoelectric activity. PVDF is polymorphic and has at least four major crystalline phases LOVINGER [95]. Two of them, the form I (β-phase) and form II (α-phase), are the most relevant phases for practical ferroelectric and piezoelectric applications. In form I, which is also known as β-phase, two chains in all-*trans* planar zigzag conformation are packed into individual orthorhombic unit cells having lattice dimension $a = 8.58$ Å, $b = 4.90$ Å, and the chain direction or fiber axis $c = 2.56$ Å (Figure 2.13 and Figure 2.14). It is noted from Figure 2.13 that in the all-*transconformation*, the fluorine atoms are positioned on one side of the unit cell, resulting in a net dipole moment. As the structure of the unit cell of the form I crystal satisfies the symmetry requirement of a piezoelectric crystal, i.e. it is non-centrosymmetric, this is the form of PVDF that is responsible for its piezoelectric properties.

In form II, or α-phase, the chain conformations are represented as a sequence of alternating *trans* and *gauche* sequences, or TGT$\bar{G}$, Figure 2.15 and Figure 2.16. Each unit cell containing two chains is orthorhombic with lattice parameters $a = 4.96$ Å, $b = 9.64$ Å, and $c = 4.62$ Å. In the α-phase, adjacent chains are packed such that dipole moments of individual carbon-fluorine bonds are aligned perpendicular to chain direction, canceling one other out. The directions of the chains consist of a statistical average of up-up and up-down orientations.

When prepared using the melt crystallization or solution cast, in most cases PVDF will form α-phase which is not a polar phase. Mechanical stretching is often used in order to convert the α-phase to the ferroelectric β-phase. On the other hand, for P(VDF-TrFE) copolymers (TrFE, molecular formula: CF_2CFH) with VDF content less than approx-
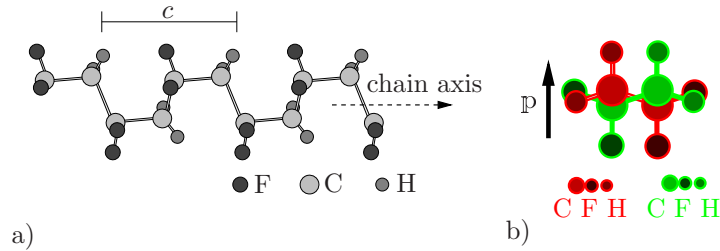
Figure 2.15: A schematic view of α-phase: a) single sequence with repeated crystal unit having lattice dimension $c = 4.62$ Å b) view parallel to the chain axis of a chain consisting of two sequences with spatial distribution of charges contributes to the polarization.
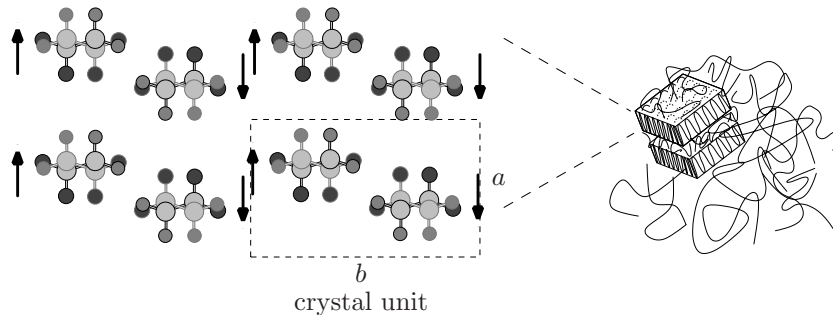
Figure 2.16: Crystal structure of α-phase. A crystal unit is composed of two chains, aligned such that dipole moments cancel out. Such a crystal unit has lattice dimensions $a = 4.96$ Å and $b = 9.64$ Å. Chains aligned in the same direction form a crystallite in an amorph matrix (cf. Figure 2.11).

imately 85 mol%, the β-phase will be formed directly. In the β-phase crystallites there are ferroelectric domains, which are polar, but oriented in all crystallographically allowed directions. Furthermore, in the semicrystalline polymer, these crystallites are randomly oriented within the sample. This accounts for the absence of any piezoelectric activity unless the sample is poled. Poling can be accomplished by electroding the polymer surfaces with metal, followed by application of a strong electric field to orient the crystallites.

The phase diagram of PVDF and P(VDF-TrFE) polymers (cf. Figure 2.17) shows a ferroelectric-paraelectric transition that signals a change from a ferroelectric (polar) phase to a paraelectric (nonpolar) phase. The ferroelectric-paraelectric (F-P) transition temperature increase with vinylidene fluoride mole fraction content. Below the F-P transition, the crystal is best represented as an ordered form I structure with ion sequences of all-*trans* bonds. As the temperature of the crystals rises and goes through the F-P transition, an increasing number of *gauche* bonds are introduced into the ordered all-*trans* structure. As a result, the polarization in the crystal regions tends toward disorder, leading to the formation of the *paraelectric* phase, cf. Lovinger [94]. One should note that PVDF as well as P(VDF-TrFE) copolymers with high VDF concentration do not appear to posses distinct F-P transitions. Rather melting takes place before F-P transition. However, it must be mentioned that even in the ferroelectric phase conformational defects can be introduced as the temperature of the polymers is raised.

As ferroelectric materials, PVDF and its copolymers with TrFE exhibit well-defined polarization hysteresis loops. For sinusoidal electric fields high enough to induce ferroelectric switching, the strain in the thickness direction draws a hysteresis loop of butterfly shape while the electric displacement draws a conventional square d-e hysteresis loop. As al-
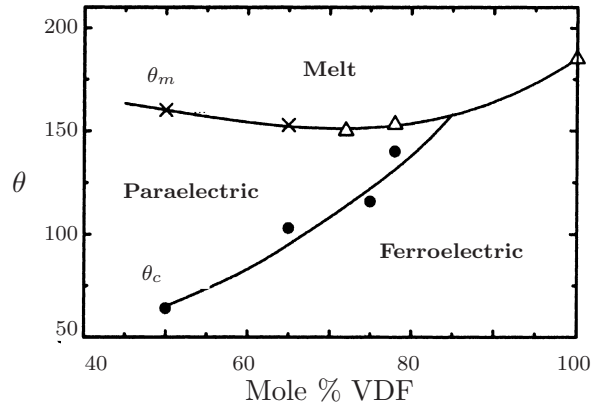
Figure 2.17: Phase diagram of PVDF and P(VDF-TrFE) copolymer. Where θ_m and θ_c are the melting temperature and the F-P phase transition temperatures, respectively (cf. CHENG ET AL. [26]).

ready suggested, the hysteretic behavior is due to switching mechanisms of the unit cells taking place through domain wall motions. Early x-ray studies demonstrated that the switching is primarily through successive 60° wall motions consistent with the pseudo hexagonal structure of the β-phase. It is retained that a kink of rotation propagates like a solitary wave along a PVDF molecule. We may, therefore, assume that each chain molecule instantaneously rotates like a rigid rod in a crystalline lamella (see FURUKAWA [53], BAR-COHEN [5]). According to the broad variety of material compositions and pre-treatments the shape of the hysteresis loops differs a lot. As an example, the butterfly hysteresis and the polarization hysteresis measured on a uniaxially drawn (PVDF) polymer are shown in Figure 2.18a. The polymer performs a conventional but rather rounded dielectric hysteresis loop compared to the hysteresis of undrawn (VDF-TrFE) copolymers illustrated in Figure 2.18b. The coercive field e_c, which marks the point where the hysteresis intersects the horizontal axis, is about 50 MV/m at room temperature for many ferroelectric polymers. The remanent polarization $\mathbb{p}^r$ corresponds to the point where the loop intersects the vertical axis. As one can see from the figures this material parameter can vary a lot. In spite of the difference in the shape of hysteresis loops, all polymers and copolymers of (VDF) become thickest when their polarization reverses and thinnest when the absolute value of the electric displacement is maximum. This behavior is inverse in comparison to ceramic ferroelectric material response, where the ceramic becomes thinnest when its polarization reverses, see Figure 2.7 (cf. FURUKAWA & SEO [54]). This behavior can be attributed to the geometry of the crystal unit cell, cf. Figure 2.13-2.16.

Most of the electro-mechanical applications that use PVDF and its copolymers exploit their piezoelectric properties. For ferroelectric PVDF and its copolymers, the sample as prepared usually have negligible piezoelectric responses due to the fact that the polarization at each domain orientates randomly, implying that the net sample polarization is zero. In order to establish the piezoelectric state, the polymers can be poled under a field several times higher than the coercive field to induce a stable remanent polarization.

In many polymeric materials, it is well known that there are large strain changes associated with transformation from one phase to another. For P(VDF-TrFE) copolymers, large lattice strains have been detected when the copolymer goes from the low-temperature (LT) ferroelectric phase to the high-temperature (HT) paraelectric phase. As revealed by
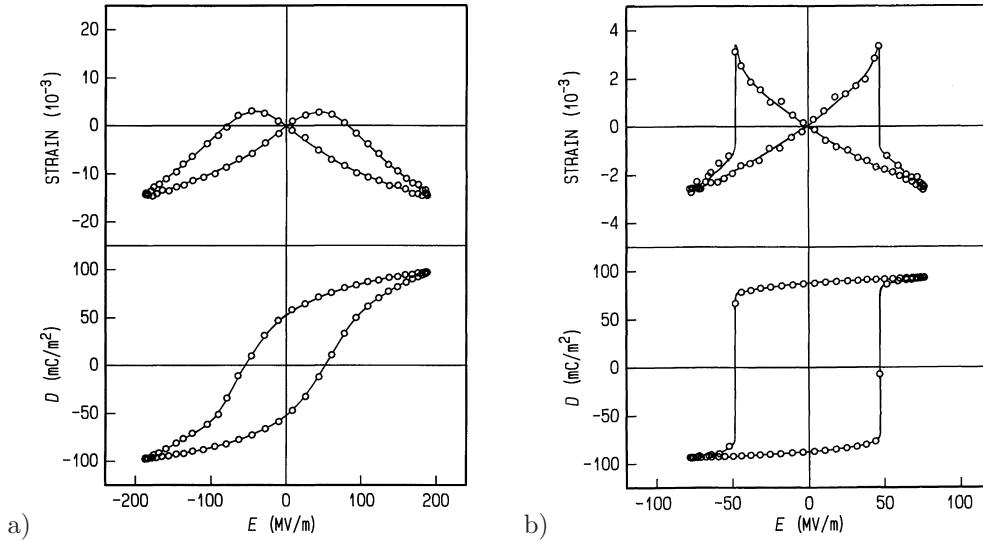
Figure 2.18: a) Butterfly hysteresis and dielectric hysteresis of uniaxially drawn (PVDF); b) butterfly hysteresis and dielectric hysteresis of undrawn (VDF-TrFE) copolymer with 65/35 mol% ratio, cf. FURUKAWA & SEO [54].

experimental data there is a lattice strain of -10% and 7% in the crystalline phase along and perpendicular to the polymer chain, respectively, as the copolymer goes through the (F-P) phase transition. Therefore, for a highly aligned copolymer with a high crystallinity ($> 50\%$ crystallinity), these strains can be translated to large macroscopic strains. In addition, for a ferroelectric polymer, the phase transformation can be controlled by an external field (both electric and mechanical), and hence, it is expected that a high field induced strain can be achieved in P(VDF-TrFE) copolymer by exploiting the lattice strain at F-P transformation. The temperature range in which the electric field can induce the phase transition from non-polar to polar phases depends strongly on the material. For most of the inorganic ferroelectrics, this temperature range is relatively narrow. For instance, the range is about 8°C for $BaTiO_3$. For P(VDF-TrFE) copolymers, it has been found that this temperature range is relatively large.

All these results indicate that one may be able to improve the electro-mechanical response of P(VDF-TrFE) copolymer significantly by operating the polymer near the F-P transition. However, there are several issues associated with the F-P transition in P(VDF-TrFE) copolymer that have to be addressed. As has been shown in the phase diagram (Figure 2.17), F-P transition in all P(VDF-TrFE) compositions occurs at temperatures higher than room temperature and the transition is relatively sharp (over a relatively narrow temperature range). In addition, large hystereses have been observed for the copolymers at the F-P transition, which is a basic feature for this type of transition. A large hysteresis is not desirable for practical applications. Therefore, to make use of the unique opportunities near the F-P transition in P(VDF-TrFE) copolymer systems, the copolymer should be modified as to broaden the phase transition region, move it to room temperature, and minimize the hysteresis.

In polymeric materials, high energy electron irradiation has been widely used to modify polymer properties. In P(VDF-TrFE) copolymers, LOVINGER [96] found that by using high energy electron irradiation, the ferroelectric phase at room temperature can be converted into a macroscopically paraelectric-like phase. Subsequent studies also found that
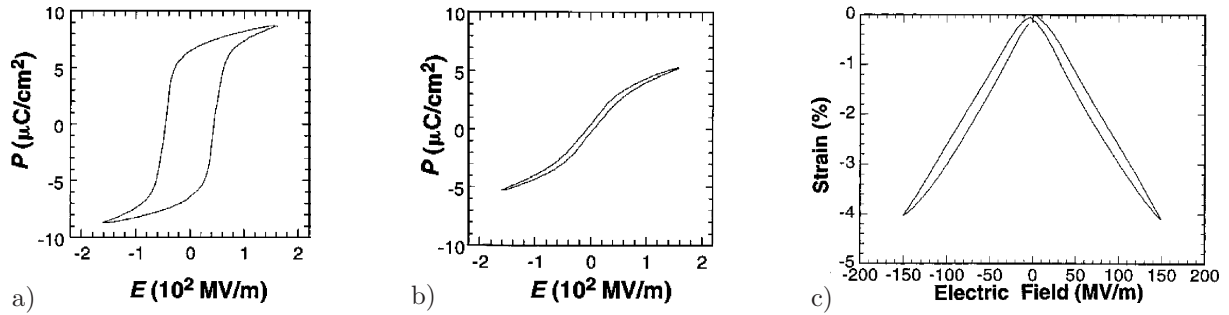
Figure 2.19: Polarization hysteresis for (VDF-TrFE) copolymer with 50/50 mol% ratio: a) before irradiation and b) after irradiation. c) Butterfly hysteresis after irradiation, cf. ZHANG, BHARTI & ZHAO [153].

a sharp dielectric constant peak from the F-P transition can be broadened markedly and moved to near room temperature, CHENG ET AL. [26] and references therein.

The irradiation effect is to introduce defect structures in the polymer to move the transformation process to near room temperature, reduce the hysteresis in the polarization response to the applied field, and broaden the transformation temperature region so that high electrostriction can be obtained over relatively broad temperature range. Extensive structural investigations indicate that electron irradiation disrupts the coherence of polarization domains (all-*trans* chains) and forms localized polar regions (nanometer-sized, all-*trans* chains interrupted by trans and gauche bonds). After irradiation, the material exhibits behavior analogous to that of relaxor ferroelectric systems in inorganic materials. The resulting material is no longer piezoelectric but rather exhibits a large electric field-induced strain (5% strain) due to electrostriction. The basis for such large electrostriction is the large change in the lattice strain as the polymer traverses the ferroelectric to paraelectric phase transition and the expansion and contraction of the polar regions.

Figure 2.19 (cf. ZHANG, BHARTI & ZHAO [153]) presents polarization loops measured at room temperature for unstreched (VDF-TrFE) copolymer film with 50/50 mol% ratio. For the unirradiated film, a typical polarization hysteresis loop was observed due to the high nucleation barrier when switching polarization from the coherent macroscopic polar domain. After irradiation, the polarization hysteresis is significantly reduced and the loop becomes quite slim due to the breaking up of macroscopic coherent polar domains to microscopic polar regions. In addition, the strain response is very high and exhibits only little butterfly hysteresis. The results indicate that the high energy irradiation is quite effective in eliminating the polarization hystereses in these polymers.

Of special interest is the discovery that in P(VDF-TrFE) copolymers, large anisotropy in the strain response exists along and perpendicular to the chain direction, as can be deduced from the change in the lattice parameters between the polar and non-polar phases. Therefore the tranverse strain can be tuned over a large range by varying the film processing conditions. For unstreched films, the transverse strain is relatively small ($\sim +1\%$). On the other hand, for stretched films, a large transverse strain along the stretching direction can be achieved ($\sim 4\text{-}5\%$).

Although high energy irradiation can be used to convert the normal ferroelectric P(VDF-TrFE) into a relaxor ferroelectric with high electrostriction, the irradiation also introduces many undesiderable defects to the copolymer, such as the formation of crosslinkings, rad-

icals and chain scissions. From the basic ferroelectric response point of view, the defects modifications of the ferroelectric properties can also be realized by introducing randomly in the polymer chain a third monomer, which is bulkier than VDF and TrFE. Furthermore, by a proper molecular design which enhances the degree of molecular level conformational changes in the polymer, the terpolymer can exhibit a higher electro-mechanical response than the high energy electron irradiated copolymer, as for terpolymer containing chlorofluoroethylene (CFE, -CH$_2$-CFCl-) as the monomer. This will be indicated with VDF$_x$-TrFE$_{1-x}$-CFE$_y$, where the mole ratio of VDF/TrFE is $x/(1-x)$ and y is the mol% of CFE in the terpolymer. Under a field of 130 MV/m, a thickness strain of -4.5% can be achieved, which is comparable to that observed in the irradiated copolymers.

By increasing the ratio of VDF/TrFE in the terpolymer, the field induced strain level can be raised due to the fact that the lattice strain between the polar conformation and non polar conformations increases with the VDF/TrFE ratio. A thickness strain of 7% can be reached. This demonstrates the potential of the terpolymers in achieving very high electro-mechanical responses through optimized composition.

3. Fundamentals of Continuum Mechanics

This chapter outlines the principal equations of non-linear continuum mechanics that describe the fundamental geometric mappings, basic stress measures, and balance equations of a solid body undergoing finite deformations. In the following chapters those equations will be modified in order to describe an electro-mechanically coupled problem. Most of the material treated here is based on the lecture notes of MIEHE [107, 108] and also well documented in the literature. For more comprehensive treatments the reader is referred to the monographs and books, for example, by ERINGEN [47], TRUESDELL & NOLL [143], CHADWICK [25], MARSDEN & HUGHES [98], OGDEN [119], HAUPT [60], MIEHE [105, 106] among others.

3.1. The Motion, Geometric Maps and Deformation Measures

A material body B is a physical object equipped with different kinds of properties and occupies regions of the Euclidian space $\mathbb{R}^3$. Formally the body B is defined as an open set of material points $P \in B$. The configuration of the body $B \subset \mathbb{R}^3$ at time t is described by a one-to-one relation

$$\boldsymbol{\chi}_t : \begin{cases} B & \to & \mathcal{B}_t \subset \mathbb{R}^3 \\ P & \mapsto & \boldsymbol{x}_t = \boldsymbol{\chi}_t(P) \end{cases} . \tag{3.1}$$

The configuration defined by $\boldsymbol{\chi}_t$, in equation (3.1), uniquely maps the material point P to the coordinate triple $\boldsymbol{x}_t \in \mathbb{R}^3$ with respect to the global Cartesian basis $\{\boldsymbol{E}_i\}_{i=1,2,3}$. While describing the motion of a solid body, it is common practice to name its placement at time t_0 as the reference configuration that generally possesses an undistorted stress-free state and is denoted as $\mathcal{B} = \boldsymbol{\chi}_{t_0}(B)$. On the other hand, the configuration of the body at current time t is denoted as $\mathcal{S} = \boldsymbol{\chi}_t(B)$. Commonly, the reference configuration is also denoted as material or Lagrangian configuration while the actual configuration of the body is also denoted as spacial or Eulerian. The reference and the spatial positions occupied by a material point P within the Euclidean space $\mathbb{R}^3$ are labeled by the reference coordinates $\boldsymbol{X} = \boldsymbol{\chi}_{t_0}(P) \in \mathcal{B}$ and the spatial coordinates $\boldsymbol{x} = \boldsymbol{\chi}_t(P) \in \mathcal{S}$, respectively. In order to describe the motion of the solid body in the Euclidean space, we introduce a non-linear deformation map $\boldsymbol{\varphi}_t(\boldsymbol{X})$ between $\boldsymbol{\chi}_{t_0}(P)$ and $\boldsymbol{\chi}_t(P)$

$$\boldsymbol{\varphi}_t : \begin{cases} \mathcal{B} & \to & \mathcal{S} \\ \boldsymbol{X} & \mapsto & \boldsymbol{x} = \boldsymbol{\varphi}_t(\boldsymbol{X}) := \boldsymbol{\chi}_t \circ \boldsymbol{\chi}_{t_0}^{-1}(\boldsymbol{X}) \end{cases} \tag{3.2}$$

that maps the material points $\boldsymbol{X} \in \mathcal{B}$ onto their deformed spatial positions $\boldsymbol{x} = \boldsymbol{\varphi}_t(\boldsymbol{X}) \in \mathcal{S}$ at time $t \in \mathbb{R}_+$, see Figure 3.1. Having the motion (3.2) defined, we are now in a position to introduce the material velocity

$$\boldsymbol{V}_t(\boldsymbol{X}) := \partial_t \boldsymbol{\varphi}(\boldsymbol{X}, t) = \frac{d}{dt} \boldsymbol{\varphi}_{\boldsymbol{X}}(t) , \tag{3.3}$$

and the material acceleration of the motion

$$\boldsymbol{A}_t(\boldsymbol{X}) := \partial_t \boldsymbol{V}(\boldsymbol{X}, t) = \frac{d}{dt} \boldsymbol{V}_{\boldsymbol{X}}(t) . \tag{3.4}$$

The spatial velocity is then expressed in terms of the material velocity

$$\boldsymbol{v}_t(\boldsymbol{x}, t) := \boldsymbol{V}_t(\boldsymbol{X}) \circ \boldsymbol{\varphi}_t^{-1}(\boldsymbol{x}) , \tag{3.5}$$
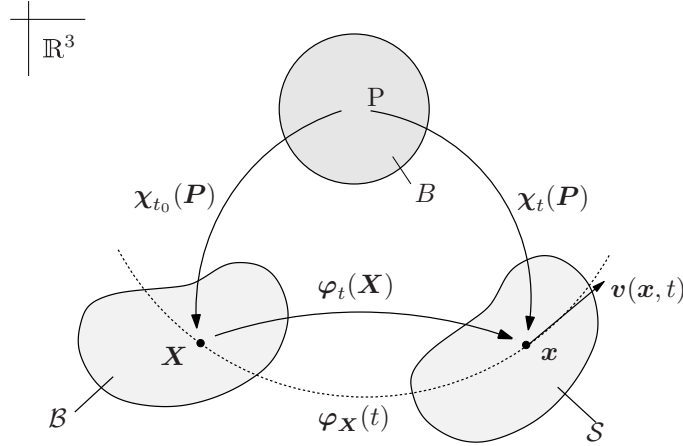
Figure 3.1: Mathematical description of the motion of a solid body in $\mathbb{R}^3$.

and the spatial acceleration is defined as the material time derivative of the spatial velocity

$$\boldsymbol{a}_t(\boldsymbol{x},t) := \boldsymbol{A}_t(\boldsymbol{X}) \circ \boldsymbol{\varphi}_t^{-1}(\boldsymbol{x}) = \partial_t \boldsymbol{v} + \nabla_{\boldsymbol{x}} \boldsymbol{v} \cdot \boldsymbol{v}\,, \tag{3.6}$$

where $\nabla_{\boldsymbol{x}}\boldsymbol{v} := \boldsymbol{l}$ stands for the spatial velocity gradient. The path $\boldsymbol{\varphi}_{\boldsymbol{X}}(t)$ is then called the integral curve of $\boldsymbol{v}$ as shown in Figure 3.1.

Apart from the global Cartesian coordinate system $\{\boldsymbol{E}_i\}_{i=1,2,3}$, Eulerian curvilinear coordinates θ^i are introduced oriented along the material lines which deform with the body in the Eulerian configuration. The spatial position vectors then have the representations $\boldsymbol{x} = x^i(\theta^1, \theta^2, \theta^3)\boldsymbol{E}_i$. This results in the definition of two dual co- and contra-variant bases $\{\boldsymbol{g}_i\}_{i=1,2,3}$ and $\{\boldsymbol{g}^i\}_{i=1,2,3}$ which are defined as follows

$$\boldsymbol{g}_i := \partial_{\theta^i}\boldsymbol{x} = \partial_{\theta^i}x^j(\theta^1,\theta^2,\theta^3)\boldsymbol{E}_j \quad \text{and} \quad \boldsymbol{g}^i := \partial_{\boldsymbol{x}}\theta^i = \partial_{x^j}\theta^i(\theta^1,\theta^2,\theta^3)\boldsymbol{E}^j \tag{3.7}$$

where the covariant basis $\{\boldsymbol{g}_i\}_{i=1,2,3}$ spans the so called tangent space $T_{\boldsymbol{x}}\mathcal{S}$ and the contravariant basis $\{\boldsymbol{g}^i\}_{i=1,2,3}$ spans the cotangent space $T_{\boldsymbol{x}}^*\mathcal{S}$ with the property $\boldsymbol{g}^i \cdot \boldsymbol{g}_j = \delta^i{}_j$ for the basis. In connection with the tangent and cotangent spaces the associated co- and contra-variant Eulerian metric tensors are defined as follows

$$\boldsymbol{g} := \boldsymbol{g}_i \cdot \boldsymbol{g}_j \boldsymbol{g}^i \otimes \boldsymbol{g}^j = g_{ij}\boldsymbol{g}^i \otimes \boldsymbol{g}^j \quad \text{and} \quad \boldsymbol{g}^{-1} := \boldsymbol{g}^i \cdot \boldsymbol{g}^j \boldsymbol{g}_i \otimes \boldsymbol{g}_j = g^{ij}\boldsymbol{g}_i \otimes \boldsymbol{g}_j \tag{3.8}$$

A similar development gives, after the introduction of the Lagrangian curvilinear coordinates Θ^I, the counterparts in the reference configuration, namely the co- and contravariant Lagrangian bases $\{\boldsymbol{G}_I\}_{I=1,2,3}$ and $\{\boldsymbol{G}^I\}_{I=1,2,3}$ and furthermore the respective Lagrangian metric tensors $\boldsymbol{G}$ and $\boldsymbol{G}^{-1}$. The covariant basis $\{\boldsymbol{G}_I\}_{I=1,2,3}$ spans the so called tangent space $T_{\boldsymbol{X}}\mathcal{B}$ and the contravariant basis $\{\boldsymbol{G}^I\}_{I=1,2,3}$ spans the cotangent space $T_{\boldsymbol{X}}^*\mathcal{B}$. The above explanations where presented for the general case of curvilinear coordinates, however, the relations simplify significantly for the choice of Cartesian bases for both the current and the reference configuration which results in

$$\{\boldsymbol{G}_I\} = \{\boldsymbol{g}_i\} = \{\boldsymbol{E}_i\} \tag{3.9}$$

For clarity a formal differentiation will be adopted in the following between the four Lagrangian and Eulerian tangent and cotangent spaces spanned by the bases $\{\boldsymbol{E}_A\}_{A=1,2,3}$,
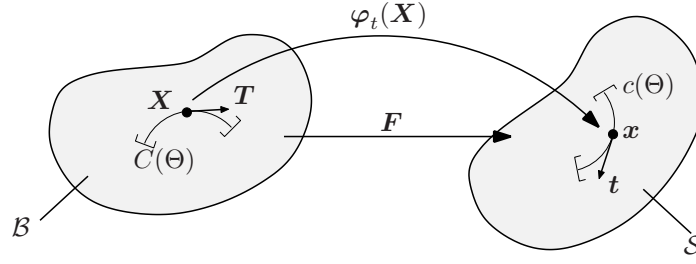
Figure 3.2: The deformation gradient $\boldsymbol{F}$ defined as a tangent map linearly transforming the material vector $\boldsymbol{T} \in T_{\boldsymbol{X}}\mathcal{B}$ tangent to the material curve $C(\Theta)$ at $\boldsymbol{X}$ onto the the spatial vector $\boldsymbol{t} \in T_{\boldsymbol{x}}\mathcal{S}$ tangent to the spatial curve $c(\Theta)$ at $\boldsymbol{x}$.

$\{\boldsymbol{E}^A\}_{A=1,2,3}$ and $\{\boldsymbol{e}_a\}_{a=1,2,3}$, $\{\boldsymbol{e}^a\}_{a=1,2,3}$ respectively. This gives the following specific form of the metric tensors

$$
\begin{aligned}
\boldsymbol{G} &= \delta_{AB}\boldsymbol{E}^A \otimes \boldsymbol{E}^B \\
\boldsymbol{G}^{-1} &= \delta^{AB}\boldsymbol{E}_A \otimes \boldsymbol{E}_B
\end{aligned}
\quad \text{and} \quad
\begin{aligned}
\boldsymbol{g} &= \delta_{ab}\boldsymbol{e}^a \otimes \boldsymbol{e}^b \\
\boldsymbol{g}^{-1} &= \delta^{ab}\boldsymbol{e}_a \otimes \boldsymbol{e}_b
\end{aligned}
\quad . \tag{3.10}
$$

Probably the most fundamental deformation measure used in kinematics of finite deformation is the deformation gradient. It can be considered as a linear map of the referential tangent vectors onto the spatial counterparts. To this end, let $C(\Theta)$ and $c(\Theta)$ be the material and spatial curves parameterized by a common variable $\Theta \in \mathbb{R}$ on $\mathcal{B}$ and $\mathcal{S}$, respectively. Furthermore, we consider that the spatial curve is related to the reference curve by the non-linear deformation map $c(\Theta) = \boldsymbol{\varphi}_t(C(\Theta))$ due to (3.2). Tangents of the curves belonging to the respective tangent spaces defined as the derivatives $\boldsymbol{T} := dC(\Theta)/d\Theta \in T_{\boldsymbol{X}}\mathcal{B}$ and $\boldsymbol{t} := dc(\Theta)/d\Theta \in T_{\boldsymbol{x}}\mathcal{S}$ are depicted in Figure 3.2. Through the chain rule, the spatial tangent $\boldsymbol{t}$ can be expressed in terms of the material tangent $\boldsymbol{T}$

$$
\boldsymbol{t} = \frac{d}{d\Theta}c(\Theta) = \nabla_{\boldsymbol{X}}\boldsymbol{\varphi}_t(\boldsymbol{X})\frac{d}{d\Theta}C(\Theta) = \boldsymbol{F}\boldsymbol{T} \qquad \text{with} \qquad t^a\boldsymbol{e}_a = F^a{}_A T^A \boldsymbol{e}_a . \tag{3.11}
$$

This already introduces the deformation gradient $\boldsymbol{F} = \nabla_{\boldsymbol{X}}\boldsymbol{\varphi}_t(\boldsymbol{X})$ with components $F^a{}_A \boldsymbol{g}_a \otimes \boldsymbol{G}^A = \partial\varphi^a/\partial X^A \boldsymbol{g}_a \otimes \boldsymbol{G}^A$ as the tangent map

$$
\boldsymbol{F} : \begin{cases} T_{\boldsymbol{X}}\mathcal{B} & \to \quad T_{\boldsymbol{x}}\mathcal{S} \\[4pt] \boldsymbol{T} & \mapsto \quad \boldsymbol{t} = \boldsymbol{F}\boldsymbol{T} \end{cases} \tag{3.12}
$$

between the tangent spaces $T_{\boldsymbol{X}}\mathcal{B}$ and $T_{\boldsymbol{x}}\mathcal{S}$ of the manifolds $\mathcal{B}$ and $\mathcal{S}$, respectively.

Once the deformation gradient has been defined, we can proceed with the other two fundamental maps. For this purpose, let dV and dv denote the infinitesimal volumes of parallelepipeds

$$
dV := d\boldsymbol{X}_1 \cdot (d\boldsymbol{X}_2 \times d\boldsymbol{X}_3) \qquad \text{and} \qquad dv := d\boldsymbol{x}_1 \cdot (d\boldsymbol{x}_2 \times d\boldsymbol{x}_3) \tag{3.13}
$$

defined as the scalar triple product of vectors $d\boldsymbol{X}_{i=1,2,3} \in T_{\boldsymbol{X}}\mathcal{B}$ and $d\boldsymbol{x}_{i=1,2,3} \in T_{\boldsymbol{x}}\mathcal{S}$, respectively. Each spatial tangent vector $d\boldsymbol{x}_i$ is defined as a tangential map of its material counterpart, i.e. $d\boldsymbol{x}_i = \boldsymbol{F}d\boldsymbol{X}_i$ for $i = 1, 2, 3$. This then leads to the definition of the volume map

$$
dv := \boldsymbol{F}d\boldsymbol{X}_1 \cdot (\boldsymbol{F}d\boldsymbol{X}_2 \times \boldsymbol{F}d\boldsymbol{X}_3) = \det[\boldsymbol{F}]dV =: JdV \tag{3.14}
$$

following the conventional coordinate-free definition of the determinant of a second order tensor. The value of the Jacobian J is restricted to positive real numbers $\mathbb{R}_+$, i.e. $J > 0$, in order to ensure the one-to-one relation between $\boldsymbol{x}$ and $\boldsymbol{X}$ and the impenetrability of a material. Then, we say that the volume map, $\det[\boldsymbol{F}]$, maps the reference volume elements onto their spatial counterparts

$$J = \det[\boldsymbol{F}] : \begin{cases} \mathbb{R}_+ & \to & \mathbb{R}_+ \\ dV & \mapsto & dv = \det[\boldsymbol{F}]dV \end{cases} . \tag{3.15}$$

The co-factor of the deformation gradient $\mathrm{cof}[\boldsymbol{F}]$ is defined as the derivative of the volume map $J := \det[\boldsymbol{F}]$ with respect to deformation gradient $\boldsymbol{F}$

$$\mathrm{cof}[\boldsymbol{F}] := \partial_{\boldsymbol{F}} \det[\boldsymbol{F}] = \det[\boldsymbol{F}]\boldsymbol{F}^{-T} . \tag{3.16}$$

In order to make the geometrical meaning of $\mathrm{cof}[\boldsymbol{F}]$ more transparent, let us define the reference and spatial area co-vectors $\boldsymbol{N}dA := d\boldsymbol{X}_2 \times d\boldsymbol{X}_3$ and $\boldsymbol{n}da := d\boldsymbol{x}_2 \times d\boldsymbol{x}_3$, respectively. With these definitions at hand, we can recast (3.15) into the following from

$$d\boldsymbol{x}_1 \cdot \boldsymbol{n}da = Jd\boldsymbol{X}_1 \cdot \boldsymbol{N}dA . \tag{3.17}$$

If we incorporate the identity $d\boldsymbol{x}_1 = \boldsymbol{F}d\boldsymbol{X}_1$ in (3.17) and solve this equality for $\boldsymbol{n}da$ for an arbitrary tangent vector $d\boldsymbol{X}_1$, we end up with the interpretation of co-factor as the area map

$$\boldsymbol{n}da = J\boldsymbol{F}^{-T}\boldsymbol{N}dA = \mathrm{cof}[\boldsymbol{F}]\boldsymbol{N}dA , \tag{3.18}$$

transforming the co-vectors (one-forms) of the material surfaces onto the normal vectors of spatial surfaces. Furthermore, we observe that the tensorial quantity carrying out the mapping operation in (3.18) is none other than $\boldsymbol{F}^{-T}$. Thus, we consider $\boldsymbol{F}^{-T}$ as the normal map transforming the reference co-vectors $\boldsymbol{N}$ onto the spatial co-vectors $\boldsymbol{n}$ belonging to the respective cotangent spaces $T_{\boldsymbol{X}}^*\mathcal{B}$ and $T_{\boldsymbol{x}}^*\mathcal{S}$. The normal map is then defined as

$$\boldsymbol{F}^{-T} : \begin{cases} T_{\boldsymbol{X}}^*\mathcal{B} & \to & T_{\boldsymbol{x}}^*\mathcal{S} \\ \boldsymbol{N} & \mapsto & \boldsymbol{n} = \boldsymbol{F}^{-T}\boldsymbol{N} \end{cases} . \tag{3.19}$$

Having the tangent and the cotangent spaces defined, we can now better interpret the covariant reference and the spatial metrics, $\boldsymbol{G}$ and $\boldsymbol{g}$ respectively,

$$\boldsymbol{G} : T_{\boldsymbol{X}}\mathcal{B} \to T_{\boldsymbol{X}}^*\mathcal{B} , \quad \boldsymbol{g} : T_{\boldsymbol{x}}\mathcal{S} \to T_{\boldsymbol{x}}^*\mathcal{S} \tag{3.20}$$

as the mappings from the tangent spaces $T_{\boldsymbol{X}}\mathcal{B}$ and $T_{\boldsymbol{x}}\mathcal{S}$ to the cotangent spaces $T_{\boldsymbol{X}}^*\mathcal{B}$ and $T_{\boldsymbol{x}}^*\mathcal{S}$, respectively. That is, $\boldsymbol{G}$ and $\boldsymbol{g}$ map tangents onto co-vectors by the index lowering operation

$$\begin{aligned} \boldsymbol{T}^* &= \boldsymbol{G}\boldsymbol{T} &, & T_A\boldsymbol{E}^A &= G_{AB}T^B\boldsymbol{E}^A \\ \boldsymbol{t}^* &= \boldsymbol{g}\boldsymbol{t} &, & t_a\boldsymbol{e}^a &= g_{ab}t^b\boldsymbol{e}^a . \end{aligned} \tag{3.21}$$

Analogously, we can further consider the inverse metrics $\boldsymbol{G}^{-1}$ and $\boldsymbol{g}^{-1}$

$$\begin{aligned} \boldsymbol{T} &= \boldsymbol{G}^{-1}\boldsymbol{T}^* &, & T^A\boldsymbol{E}_A &= G^{AB}T_B\boldsymbol{E}_A \\ \boldsymbol{t} &= \boldsymbol{g}^{-1}\boldsymbol{t}^* &, & t^a\boldsymbol{e}_a &= g^{ab}t_b\boldsymbol{e}_a , \end{aligned} \tag{3.22}$$
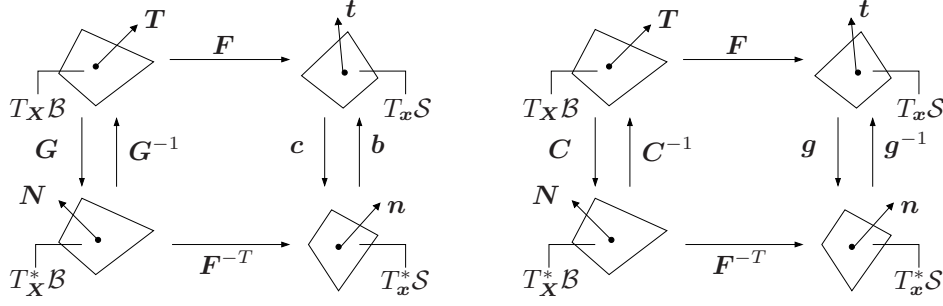
Figure 3.3: The push-forward and pull-back of the reference G and spatial g metrics and their contravariant inverse forms G^{-1} and spatial g^{-1} separately.

as the mappings from the cotangent spaces $T_X^*\mathcal{B}$ and $T_x^*\mathcal{S}$ to the tangent spaces $T_X\mathcal{B}$ and $T_x\mathcal{S}$ through the index raising. With the definitions (3.20)-(3.22) at hand, we are ready to construct the commutative diagrams, Figure 3.3, illustrating the pull-back and the push-forward operations on G and g and their contravariant inverse metrics G^{-1} and g^{-1}, separately. As shown in Figure 3.3a, the push-forward of the inverse of the reference metric $b := \varphi_*(G^{-1})$ and itself $c := \varphi_*(G)$ are defined by

$$
\begin{aligned}
b &:= \varphi_*(G^{-1}) &=& F G^{-1} F^T &,& \quad b^{ab} &=& F^a{}_A G^{AB} F^b{}_B \\
c = b^{-1} &:= \varphi_*(G) &=& F^{-T} G F^{-1} &,& \quad c_{ab} &=& (F^{-1})^A{}_a G_{AB} (F^{-1})^B{}_b
\end{aligned}
$$

(3.23)

and called the left Cauchy-Green tensor (Finger deformation tensor) and the inverse left Cauchy-Green tensor, respectively. Similarly, based on the commutative diagram depicted in Figure 3.3b, the pull-back of the spatial metric $C := \varphi^*(g)$ and its inverse $C^{-1} := \varphi^*(g^{-1})$ are defined by

$$
\begin{aligned}
C &:= \varphi^*(g) &=& F^T g F &,& \quad C_{AB} &=& F^a{}_A g_{ab} F^b{}_B \\
C^{-1} &:= \varphi^*(g^{-1}) &=& F^{-1} g^{-1} F^{-T} &,& \quad (C^{-1})^{AB} &=& (F^{-1})^A{}_a g^{ab} (F^{-1})^B{}_b
\end{aligned}
$$

(3.24)

and denoted as the right Cauchy-Green tensor (convected spatial metric) and the inverse right Cauchy-Green tensor, respectively.

As mentioned above, the both metric tensors and their inverse tensors are symmetric and positive definite and therefore so do their respective push-forwards (3.23) and pull-backs (3.24). The above introduced deformation tensors play a fundamental role in measuring the basic deformations. To illustrate this, let us consider tangent vectors $T \in T_X\mathcal{B}$ and $t \in T_x\mathcal{S}$, and define the stretch, $\bar{\lambda}$, as the ratio of the length of the deformed tangent vector t to the length of the reference tangent vector T, i.e. $\bar{\lambda} := |t|_g/|T|_G = \sqrt{t \cdot g t}/\sqrt{T \cdot G T} > 0$. Setting $|T|_G = 1$ as the reference value, the stretch can be expressed as

$$
\bar{\lambda} = \sqrt{t \cdot g t} = \sqrt{F T \cdot g F T} = \sqrt{T \cdot F^T g F T} = \sqrt{T \cdot C T} =: |T|_C \tag{3.25}
$$

in the so-called Lagrangian (material) description of the length deformation. This justifies the name convected spatial metric coined to the right Cauchy-Green tensor C. On the other hand, we can also set $|t|_g = 1$ in the so-called Eulerian (spatial) description of the deformation and express the inverse stretch

$$
\bar{\lambda}^{-1} = \sqrt{T \cdot G T} = \sqrt{F^{-1} t \cdot G F^{-1} t} = \sqrt{t \cdot F^{-T} G F^{-1} t} = \sqrt{t \cdot c t} =: |t|_c \tag{3.26}
$$
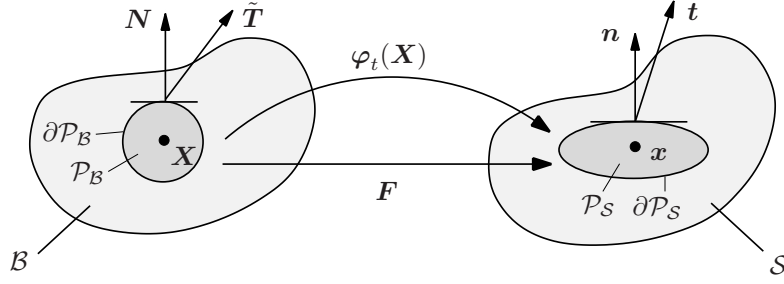
Figure 3.4: The material $\tilde{\boldsymbol{T}}(\boldsymbol{X}, t, \boldsymbol{N}) \in T_{\boldsymbol{X}}\mathcal{B}$ and spatial $\boldsymbol{t}(\boldsymbol{x}, t, \boldsymbol{n}) \in T_{\boldsymbol{x}}\mathcal{S}$ traction (stress) vectors representing the force action of the rest of the body at the vicinity, on the surfaces of the cut parts $\partial\mathcal{P}_{\mathcal{B}}$ and $\partial\mathcal{P}_{\mathcal{S}}$, respectively.

in terms of the inverse left Cauchy-Green tensor $\boldsymbol{c} = \boldsymbol{b}^{-1}$. We observe that $\boldsymbol{C}$ and $\boldsymbol{c}$ act as metric tensors in the respective Lagrangian and Eulerian description of the length deformation. Analogous to the length stretch $\bar{\lambda}$, we can also introduce the area stretch, $\bar{\nu}$, as the ratio of the length of the deformed normal $\boldsymbol{n} = \boldsymbol{F}^{-T}\boldsymbol{N} \in T_{\boldsymbol{x}}^*\mathcal{S}$ to the length of the reference normal $\boldsymbol{N} \in T_{\boldsymbol{X}}^*\mathcal{B}$ that is, $\bar{\nu} := |\boldsymbol{n}|_{\boldsymbol{g}^{-1}}/|\boldsymbol{N}|_{\boldsymbol{G}^{-1}} = \sqrt{\boldsymbol{n} \cdot \boldsymbol{g}^{-1}\boldsymbol{n}}/\sqrt{\boldsymbol{N} \cdot \boldsymbol{G}^{-1}\boldsymbol{N}} > 0$. Fixing the value $|\boldsymbol{N}|_{\boldsymbol{G}^{-1}} = 1$, we obtain the Lagrangian description of the area stretch

$$\bar{\nu} = \sqrt{\boldsymbol{n} \cdot \boldsymbol{g}^{-1}\boldsymbol{n}} = \sqrt{\boldsymbol{F}^{-T}\boldsymbol{N} \cdot \boldsymbol{g}^{-1}\boldsymbol{F}^{-T}\boldsymbol{N}} = \sqrt{\boldsymbol{N} \cdot \boldsymbol{F}^{-1}\boldsymbol{g}^{-1}\boldsymbol{F}^{-T}\boldsymbol{N}} =: |\boldsymbol{N}|_{\boldsymbol{C}^{-1}} \qquad (3.27)$$

as a norm of the material normal $\boldsymbol{N}$ with respect to the inverse right Cauchy-Green tensor $\boldsymbol{C}^{-1}$. In the spatial description, we set $|\boldsymbol{n}|_{\boldsymbol{g}^{-1}} = 1$ and express the inverse area stretch $\bar{\nu}^{-1}$ in terms of the Finger tensor

$$\bar{\nu}^{-1} = \sqrt{\boldsymbol{N} \cdot \boldsymbol{G}^{-1}\boldsymbol{N}} = \sqrt{\boldsymbol{F}^T\boldsymbol{n} \cdot \boldsymbol{G}^{-1}\boldsymbol{F}^T\boldsymbol{n}} = \sqrt{\boldsymbol{n} \cdot \boldsymbol{F}\boldsymbol{G}^{-1}\boldsymbol{F}^T\boldsymbol{n}} = \sqrt{\boldsymbol{n} \cdot \boldsymbol{b}\boldsymbol{n}} =: |\boldsymbol{n}|_{\boldsymbol{b}}. \qquad (3.28)$$

In order to have a local measure of the strains at a material point, the length of an infinitesimal line element is compared in both its reference as well as its current state

$$\delta := \tfrac{1}{2}\left\{ |d\boldsymbol{x}|_{\boldsymbol{g}}^2 - |d\boldsymbol{X}|_{\boldsymbol{G}}^2 \right\} = d\boldsymbol{X} \cdot \boldsymbol{E}d\boldsymbol{X} = d\boldsymbol{x} \cdot \boldsymbol{e}d\boldsymbol{x}. \qquad (3.29)$$

This comparison can be carried out either in the Lagrangian or in the Eulerian setting and yields to the definition of the Green-Lagrangian strain tensor $\boldsymbol{E} := \tfrac{1}{2}[\boldsymbol{C} - \boldsymbol{G}]$ and of the Almansi strain tensor $\boldsymbol{e} := \tfrac{1}{2}[\boldsymbol{g} - \boldsymbol{c}]$, respectively.

The foregoing examples concerning the elongation and area changes give a clear geometrical interpretation of the fundamental deformation tensors introduced by the pull-back and push-forward operations of the metrics. These deformation measures enter the various constitutive formulations of non-linear material theories.

3.2. Cauchy's Stress Theorem and the Stress Measures

Consider a part $\mathcal{P}_{\mathcal{B}} \subset \mathcal{B}$ cut off from the reference body $\mathcal{B}$ and its spatial counterpart $\mathcal{P}_{\mathcal{S}} \subset \mathcal{S}$ closed by the respective boundaries $\partial\mathcal{P}_{\mathcal{B}}$ and $\partial\mathcal{P}_{\mathcal{S}}$ as depicted in Figure 3.4. In the deformed configuration, we introduce the stress vector $\boldsymbol{t}$ that acts on the surface element da of $\partial\mathcal{P}_{\mathcal{S}}$ and represents the force action of the rest of the body at the vicinity $\mathcal{P}_{\mathcal{S}} \backslash \mathcal{S}$ on $\partial\mathcal{P}_{\mathcal{S}}$. The Cauchy stress theorem states that the spatial traction vector $\boldsymbol{t} \in T_{\boldsymbol{x}}\mathcal{S}$ linearly depends on the spatial normal $\boldsymbol{n} \in T_{\boldsymbol{x}}^*\mathcal{S}$ of the surface $\partial\mathcal{P}_{\mathcal{S}}$, i.e.

$$\boldsymbol{t}(\boldsymbol{x}, t, \boldsymbol{n}) := \boldsymbol{\sigma}(\boldsymbol{x}, t)\boldsymbol{n} \qquad (3.30)$$

through the Cauchy (true) stress tensor $\boldsymbol{\sigma}(\boldsymbol{x}, t)$. The Cauchy's stress theorem can be proven based on the force equilibrium on a tetrahedron. In the geometrical framework outlined so far, the Cauchy stress tensor can be understood as a contravariant mapping transforming normals $\boldsymbol{n} \in T_{\boldsymbol{x}}^* \mathcal{S}$ onto tangent vectors $\boldsymbol{t} \in T_{\boldsymbol{x}} \mathcal{S}$

$$\boldsymbol{\sigma} : \begin{cases} T_{\boldsymbol{x}}^* \mathcal{S} & \rightarrow & T_{\boldsymbol{x}} \mathcal{S} \\ \\ \boldsymbol{n} & \mapsto & \boldsymbol{t} = \boldsymbol{\sigma} \boldsymbol{n} \end{cases} . \tag{3.31}$$

Another spatial stress measure, the Kirchhoff stress tensor which is also known as the weighted Cauchy stress tensor, is defined as

$$\boldsymbol{\tau} := J \boldsymbol{\sigma} \tag{3.32}$$

and widely used in the spatial description of stress power terms in the reference volume. Owing to the scalar scaling by the Jacobian J, the Kirchhoff stresses retain the geometrical transformation characteristics of the Cauchy stress, i.e. $\boldsymbol{\tau} : T_{\boldsymbol{x}}^* \mathcal{S} \rightarrow T_{\boldsymbol{x}} \mathcal{S}$. Now let us consider another spatial traction vector $\boldsymbol{T} \in T_{\boldsymbol{x}} \mathcal{S}$ defined through the force equality $\boldsymbol{T} dA := \boldsymbol{t} da$ by scaling the spatial force term ($\boldsymbol{t} da$) through the reference area element dA. Based on this definition, we introduce the first Piola-Kirchhoff stress tensor by the reference Cauchy theorem $\boldsymbol{T} := \boldsymbol{P} \boldsymbol{N}$ leading to $\boldsymbol{P} \boldsymbol{N} dA = \boldsymbol{\sigma} \boldsymbol{n} da$. Using the area map (3.18), we obtain the relation $\boldsymbol{P} = \boldsymbol{\tau} \boldsymbol{F}^{-T} = J \boldsymbol{\sigma} \boldsymbol{F}^{-T}$ between the first Piola-Kirchhoff stress tensor and the spatial stress measures introduced in (3.31) and (3.32). Notice that $\boldsymbol{P}$ is a two-point tensor possessing the geometrical mapping properties

$$\boldsymbol{P} : \begin{cases} T_{\boldsymbol{X}}^* \mathcal{B} & \rightarrow & T_{\boldsymbol{x}} \mathcal{S} \\ \\ \boldsymbol{N} & \mapsto & \boldsymbol{T} = \boldsymbol{P} \boldsymbol{N} \end{cases} . \tag{3.33}$$

The transformation $(\circ) = J(\bullet) \boldsymbol{F}^{-T}$ devised in obtaining the first Piola-Kirchhoff stress tensor from the Cauchy stress tensor is called the Piola transformation. It is widely employed in transforming the objects acting on a spatial surface onto their material counterparts. The immediate outcome of the Piola transformation is the Piola-Identity

$$J \operatorname{div}[\bullet] = \operatorname{Div}[\circ] = \operatorname{Div}[J(\bullet) \boldsymbol{F}^{-T}] \tag{3.34}$$

that also implies the equality $\operatorname{Div}[J \boldsymbol{F}^{-T}] = \boldsymbol{0}$. The Lagrangian stress vector $\tilde{\boldsymbol{T}} \in T_{\boldsymbol{X}} \mathcal{B}$ may be defined through the pull-back of the spatial stress vector $\boldsymbol{T} \in T_{\boldsymbol{x}} \mathcal{S}$

$$\tilde{\boldsymbol{T}} = \varphi^*(\boldsymbol{t}) = \boldsymbol{F}^{-1} \boldsymbol{T} \in T_{\boldsymbol{X}} \mathcal{B} \quad , \quad \tilde{T}^A = (F^{-1})^A{}_a T^a , \tag{3.35}$$

as depicted in Figure 3.4. The third fundamental stress measure, the second Piola-Kirchhoff stress tensor $\boldsymbol{S}$, is then defined by $\tilde{\boldsymbol{T}} := \boldsymbol{S} \boldsymbol{N}$ yielding

$$\boldsymbol{S} : \begin{cases} T_{\boldsymbol{X}}^* \mathcal{B} & \rightarrow & T_{\boldsymbol{X}} \mathcal{B} \\ \\ \boldsymbol{N} & \mapsto & \tilde{\boldsymbol{T}} = \boldsymbol{S} \boldsymbol{N} \end{cases} . \tag{3.36}$$

Incorporating the definitions (3.31)-(3.33) in (3.36), we can express the second Piola-Kirchhoff stress tensor in terms of the other stress tensors

$$\begin{aligned} \boldsymbol{S} &:= \varphi^*(\boldsymbol{P}) = \boldsymbol{F}^{-1} \boldsymbol{P} &, \quad S^{AB} &= (F^{-1})^A{}_a P^{aB}, \\ \boldsymbol{S} &:= \varphi^*(\boldsymbol{\tau}) = \boldsymbol{F}^{-1} \boldsymbol{\tau} \boldsymbol{F}^{-T} &, \quad S^{AB} &= (F^{-1})^A{}_a \tau^{ab} (F^{-1})^B{}_b \end{aligned} \tag{3.37}$$
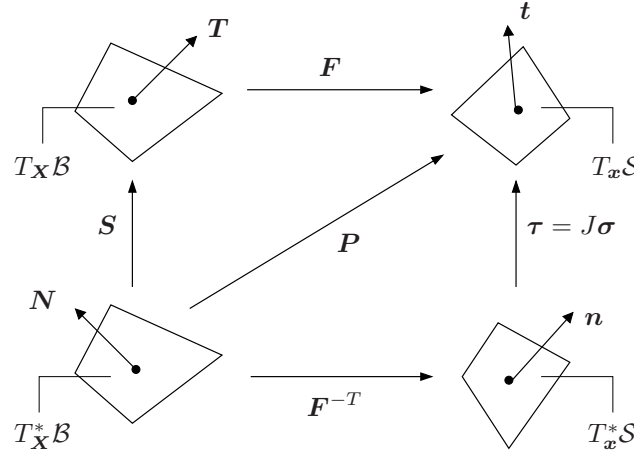
Figure 3.5: Commutative diagram illustrating the push-forward and pull-back operations among the stress measures.

as the pull-back of the contravariant two-point and spatial objects. Apparently the converse push-forward relations do also hold for the spatial stress tensors

$$\boldsymbol{\tau} = J\boldsymbol{\sigma} = \varphi_*(\boldsymbol{P}) = \boldsymbol{P}\boldsymbol{F}^T \qquad \text{and} \qquad \boldsymbol{\tau} = \varphi_*(\boldsymbol{S}) = \boldsymbol{F}\boldsymbol{S}\boldsymbol{F}^T \tag{3.38}$$

as shown in the commutative diagram, Figure 3.5.

3.3. Balance Principles of Continuum Thermomechanics

The balance laws of continuum mechanics serve as a basic set of equations required to solve an initial boundary-value-problem of thermomechanics for the primary variables. This section is devoted to derivation of the fundamental balance laws of continuum thermomechanics. In what follows, we consider a certain spatial volume $\mathcal{P}_\mathcal{S}$ closed by the boundary $\partial\mathcal{P}_\mathcal{S}$ as shown in Figure 3.4. For this part of the body, we write a balance equation where we will often have the volumetric source and the surface flux terms contributing a temporal change of the quantity for which the balance principle is constructed. In order to derive the local forms of the balance laws, we consider the following basic steps. First, we carry the surface flux terms into the body through the Gauß integral theorem. Once the balance equation is completely recast into a volume integral, the expression can be localized to its local form by stating that the integrand must also fulfill the equality for an infinitely small part $\mathcal{P}_\mathcal{S}$ provided that the continuity conditions are met. This spatial balance equation is then recast into its reference form.

Balance of Mass. The total mass of a closed system, the part of a body $\mathcal{P}_\mathcal{S}$ under consideration, remains constant; that is, the system is free of agencies that produce or destroy mass within the volume $\mathcal{P}_\mathcal{S}$ or is not subjected to flux terms that transfer mass over the surface $\partial\mathcal{P}_\mathcal{S}$. To this end, we define the spatial mass density $\rho(\boldsymbol{x}, t)$ and its material counterpart, the reference mass density $\rho_0(\boldsymbol{X})$, and require

$$\frac{d}{dt}M := \frac{d}{dt}\int_{\mathcal{P}_\mathcal{S}} \rho(\boldsymbol{x}, t)dv = \frac{d}{dt}\int_{\mathcal{P}_\mathcal{B}} J\rho(\boldsymbol{x}, t)dV = \frac{d}{dt}\int_{\mathcal{P}_\mathcal{B}} \rho_0(\boldsymbol{X})dV = 0\,. \tag{3.39}$$

Making use of the identity $\dot{J} := dJ/dt = \operatorname{cof}\boldsymbol{F} : \dot{\boldsymbol{F}} = J\operatorname{tr}(\boldsymbol{l}) = J\operatorname{div}[\boldsymbol{v}]$ in $(3.39)_3$ and equating the integrands of $(3.39)_2$ and $(3.39)_3$, we end up with the spatial and material

forms of the local mass balance equations

$$\dot{\rho} + \rho \operatorname{div}[\boldsymbol{v}] = 0 \qquad \text{and} \qquad J\rho(\boldsymbol{x}, t) = \rho_0(\boldsymbol{X}). \tag{3.40}$$

Balance of Linear Momentum. Being analogous to classical discrete mechanics, the time rate of linear momentum of the volume $\mathcal{P}_\mathcal{S}$ is equal to the sum of the forces acting on the body. Two types of forces are considered: the mass specific body forces $\boldsymbol{\gamma}(\boldsymbol{x}, t)$ due to the action of other bodies at a distance and the surface forces (stress vectors) $\boldsymbol{t}$ due to the action at a vicinity. These can also be regarded as momentum source and momentum flux terms, respectively. The balance of linear momentum then requires

$$\frac{d}{dt}\boldsymbol{L} := \frac{d}{dt}\int_{\mathcal{P}_\mathcal{S}} \rho\boldsymbol{v}(\boldsymbol{x}, t)dv = \int_{\mathcal{P}_\mathcal{S}} \rho\boldsymbol{\gamma}(\boldsymbol{x}, t)dv + \int_{\partial\mathcal{P}_\mathcal{S}} \boldsymbol{t}(\boldsymbol{x}, t, \boldsymbol{n})da. \tag{3.41}$$

Incorporating of the mass balance (3.40) in the time derivative, using the Cauchy stress theorem (3.30), and transforming through the Gauß integral theorem the surface integral into a volume integral, we obtain the local form of the spatial linear momentum balance

$$\rho\dot{\boldsymbol{v}} = \rho\boldsymbol{\gamma} + \operatorname{div}[\boldsymbol{\sigma}]. \tag{3.42}$$

Multiplication of the spatial form (3.42) with the Jacobian J, and incorporation of the mass balance $(3.40)_1$ and the Piola-Identity (3.34) yields the material form of the local linear momentum balance

$$\rho_0\dot{\boldsymbol{V}} = \rho_0\boldsymbol{\Gamma} + \operatorname{Div}[\boldsymbol{P}] \tag{3.43}$$

where $\boldsymbol{V}(\boldsymbol{X}, t)$ denotes the material velocity defined in (3.3) and $\boldsymbol{\Gamma} := \boldsymbol{\gamma}(\boldsymbol{x}, t) \circ \boldsymbol{\varphi}_t(\boldsymbol{X})$ stands for the material body force defined per unit mass.

It is believed to be illustrative that the integration of the product of spatial linear momentum balance (3.42) with the spatial velocity co-vector $\boldsymbol{v}^* = \boldsymbol{g}\boldsymbol{v}$ over the body $\mathcal{P}_\mathcal{S}$ yields

$$\frac{d}{dt}\int_{\mathcal{P}_\mathcal{S}} \frac{1}{2}\rho\boldsymbol{v} \cdot \boldsymbol{v}^* dv = \int_{\mathcal{P}_\mathcal{S}} \rho\boldsymbol{\gamma} \cdot \boldsymbol{v}^* dv + \int_{\mathcal{P}_\mathcal{S}} \operatorname{div}[\boldsymbol{\sigma}] \cdot \boldsymbol{v}^* dv. \tag{3.44}$$

Insertion of the equality $\int_{\mathcal{P}_\mathcal{S}} \operatorname{div}[\boldsymbol{\sigma}] \cdot \boldsymbol{v}^* dv = \int_{\partial\mathcal{P}_\mathcal{S}} (\boldsymbol{\sigma}\boldsymbol{n}) \cdot \boldsymbol{v}^* da - \int_{\mathcal{P}_\mathcal{S}} \boldsymbol{\sigma} : \boldsymbol{g}\boldsymbol{l}dv$ for the last term yields the so-called theorem of expended power

$$\frac{d}{dt}\int_{\mathcal{P}_\mathcal{S}} \frac{1}{2}\rho\boldsymbol{v} \cdot \boldsymbol{v}^* dv + \int_{\mathcal{P}_\mathcal{S}} \boldsymbol{\sigma} : \boldsymbol{g}\boldsymbol{l}dv = \int_{\mathcal{P}_\mathcal{S}} \rho\boldsymbol{\gamma} \cdot \boldsymbol{v}^* dv + \int_{\partial\mathcal{P}_\mathcal{S}} \boldsymbol{t} \cdot \boldsymbol{v}^* da \tag{3.45}$$

stating that the total power $\mathcal{P} = \int_{\mathcal{P}_\mathcal{S}} \rho\boldsymbol{\gamma} \cdot \boldsymbol{v}^* dv + \int_{\partial\mathcal{P}_\mathcal{S}} \boldsymbol{t} \cdot \boldsymbol{v}^* da$ due to the externally applied forces is equal to the summation of the temporal change of the kinetic energy $\dot{\mathcal{K}} = \frac{d}{dt}\int_{\mathcal{P}_\mathcal{S}} \frac{1}{2}\rho\boldsymbol{v} \cdot \boldsymbol{v}^* dv$ and the internal stress power $\dot{\mathcal{W}} = \int_{\mathcal{P}_\mathcal{S}} \boldsymbol{\sigma} : \boldsymbol{g}\boldsymbol{l}dv$.

Balance of Angular Momentum. The time derivative of the moment of linear momentum of $\mathcal{P}_\mathcal{S}$ is required to be equal to the sum of the moments of the forces acting on the body with respect to the same point. Without loss of generality, taking the moment with respect to the origin yields

$$\frac{d}{dt}\int_{\mathcal{P}_\mathcal{S}} \boldsymbol{x} \times \rho\boldsymbol{v}dv = \int_{\mathcal{P}_\mathcal{S}} \boldsymbol{x} \times \rho\boldsymbol{\gamma}dv + \int_{\partial\mathcal{P}_\mathcal{S}} \boldsymbol{x} \times \boldsymbol{t}da. \tag{3.46}$$

Exploiting the mass balance (3.40), the equality $\boldsymbol{v} \times \boldsymbol{v} = \boldsymbol{0}$ in $(3.46)_1$, using the Cauchy stress theorem (3.30) and converting through the Gauß integral theorem the surface integral $(3.46)_3$ into a volume integral, we obtain

$$\int_{\mathcal{P}_{\mathcal{S}}} \boldsymbol{x} \times (\rho \boldsymbol{a} - \rho \boldsymbol{\gamma} - \mathrm{div}[\boldsymbol{\sigma}]) dv = \int_{\mathcal{P}_{\mathcal{S}}} \boldsymbol{i} dv \tag{3.47}$$

where we demand $i_a := \epsilon_{abc} \sigma^{cb} = 0$. Since the permutation symbol ϵ_{abc} is skew symmetric with respect to two indices, e.g. $\epsilon_{abc} = -\epsilon_{acb}$, the equality (3.47) is fulfilled only for the symmetric Cauchy stresses. Thus, the balance of angular momentum results in

$$\boldsymbol{\sigma} = \boldsymbol{\sigma}^T \quad , \quad \sigma^{ab} = \sigma^{ba} . \tag{3.48}$$

Owing to the push-forward and pull-back relations derived in Section 3.2, the other two stress measures $\boldsymbol{\tau}$ and $\boldsymbol{S}$ are required to satisfy the following symmetry relations

$$\boldsymbol{\tau} = \boldsymbol{\tau}^T \quad , \quad \boldsymbol{P}\boldsymbol{F}^T = \boldsymbol{F}\boldsymbol{P}^T \quad , \quad \boldsymbol{S} = \boldsymbol{S}^T \tag{3.49}$$

as well. Observe that the first Piola-Kirchhoff stresses are generally non-symmetric.

Balance of Energy (The First Law of Thermodynamics). The first law of thermodynamics states that temporal change of total energy is equal to the sum of the mechanical and thermal power. The total energy is defined as a summation of the kinetic energy $\mathcal{K}$, see (3.45), and the internal energy $\mathcal{E} := \int_{\mathcal{P}_{\mathcal{S}}} \rho e(\boldsymbol{x}, t) dv$ where $e(\boldsymbol{x}, t)$ denotes the mass specific internal energy density. The external mechanical power $\mathcal{P}$ has already been introduced in (3.45). The thermal power $\mathcal{Q} := \int_{\mathcal{P}_{\mathcal{S}}} \rho r(\boldsymbol{x}, t) dv - \int_{\partial \mathcal{P}_{\mathcal{S}}} \boldsymbol{q} \cdot \boldsymbol{n} da$ is composed of the specific heat source $r(\boldsymbol{x}, t)$ and the surface heat flux vector $\boldsymbol{q}(\boldsymbol{x}, t)$, see Figure 3.6. The balance of energy has then the following global form

$$\frac{d}{dt}(\mathcal{K} + \mathcal{E}) = \mathcal{P} + \mathcal{Q} \tag{3.50}$$

where we immediately observe that $\dot{\mathcal{K}} - \mathcal{P} = -\dot{\mathcal{W}}$ due to the theorem of power expended introduced in (3.45). Incorporating this result in (3.50), we obtain $\dot{\mathcal{E}} = \dot{\mathcal{W}} + \mathcal{Q}$, localization of which through the integral theorem leads us to the spatial local form

$$\rho \dot{e} = \boldsymbol{\sigma} : (\boldsymbol{g}\boldsymbol{l}) + \rho r - \mathrm{div}[\boldsymbol{q}] \tag{3.51}$$

Analogous to the definition of the first Piola-Kirchhoff stress tensor, we introduce the reference heat flux vector $\boldsymbol{Q}$ that fulfills the equality $\boldsymbol{q} \cdot \boldsymbol{n} da = \boldsymbol{Q} \cdot \boldsymbol{N} dA$ through the area map $\boldsymbol{Q} := J\boldsymbol{q}\boldsymbol{F}^{-T} = J\boldsymbol{F}^{-1}\boldsymbol{q}$ as introduced in (3.18) and depicted in Figure 3.6. This immediately implies that $\boldsymbol{Q}$ is none other than the Piola transform of the spatial heat flux vector $\boldsymbol{q}$ and therefore the equality $J\,\mathrm{div}[\boldsymbol{q}] = \mathrm{Div}[\boldsymbol{Q}]$ is satisfied identically. Having defined the reference heat flux vector $\boldsymbol{Q}$, the spatial energy balance equation (3.52) can be recast into the reference local form by following the obvious steps

$$\rho_0 \dot{e} = \boldsymbol{\tau} : (\boldsymbol{g}\boldsymbol{l}) + \rho_0 R - \mathrm{Div}[\boldsymbol{Q}] \tag{3.52}$$

with $R(\boldsymbol{X}, t) := r(\boldsymbol{x}, t) \circ \boldsymbol{\varphi}_t(\boldsymbol{X})$.

For the forthcoming developments, it is important to note that the volume specific stress power term $\rho_0 \mathscr{P} := J\boldsymbol{\sigma} : (\boldsymbol{gl}) = \boldsymbol{\tau} : (\boldsymbol{gl})$ appears as a scalar product the stress measures and their work conjugate variable the spatial velocity gradient $\boldsymbol{gl}$. Since $\boldsymbol{\tau}$ or $\boldsymbol{\sigma}$ is symmetric, the stress power term $\rho_0 \mathscr{P}$ can be rewritten as $\rho_0 \mathscr{P} = \boldsymbol{\tau} : \boldsymbol{d}$ with $\boldsymbol{d} := \text{sym}(\boldsymbol{gl}) = \frac{1}{2}(\boldsymbol{gl} + \boldsymbol{lg})$ denoting the rate of deformation tensor, which is equivalent to the half of the Lie derivative of the spatial metric $\boldsymbol{g}$. The Lie derivative of a spatial object is geometrically defined as the push-forward of the material time derivative of its pull-back, that is,

$$\boldsymbol{\mathcal{L}_v}(\bullet) := \boldsymbol{\varphi}_* (\frac{d}{dt}\boldsymbol{\varphi}^*(\bullet)) \tag{3.53}$$

With this definition at hand, the rate of deformation gradient $\boldsymbol{d}$ can be obtained as

$$\boldsymbol{\mathcal{L}_v}(\boldsymbol{g}) = \boldsymbol{\varphi}_* \left(\frac{d}{dt}\boldsymbol{\varphi}^*(\boldsymbol{g})\right) = \boldsymbol{\varphi}_* \left(\frac{d}{dt}\boldsymbol{C}\right) = \boldsymbol{F}^{-T}\dot{\boldsymbol{C}}\boldsymbol{F}^{-1} = (\boldsymbol{gl} + \boldsymbol{lg}) = 2\boldsymbol{d}\,, \tag{3.54}$$

where $\boldsymbol{l} := \nabla_{\boldsymbol{x}}\boldsymbol{v} = \dot{\boldsymbol{F}}\boldsymbol{F}^{-1}$ denotes the spatial velocity gradient. Therefore, the analogous representations of the stress power $\rho_0 \mathscr{P}$ can also be derived in terms of $\boldsymbol{P}$

$$\rho_0 \mathscr{P} := \boldsymbol{\tau} : (\boldsymbol{gl}) = \boldsymbol{P}\boldsymbol{F}^T : \boldsymbol{g}\dot{\boldsymbol{F}}\boldsymbol{F}^{-1} = \boldsymbol{g}\boldsymbol{P} : \dot{\boldsymbol{F}} \tag{3.55}$$

and also for $\boldsymbol{S}$

$$\rho_0 \mathscr{P} := \boldsymbol{\tau} : \boldsymbol{d} = \boldsymbol{\tau} : \tfrac{1}{2}\boldsymbol{\mathcal{L}_v}(\boldsymbol{g}) = \boldsymbol{F}\boldsymbol{S}\boldsymbol{F}^T : \tfrac{1}{2}\boldsymbol{F}^{-T}\dot{\boldsymbol{C}}\boldsymbol{F}^{-1} = \boldsymbol{S} : \tfrac{1}{2}\dot{\boldsymbol{C}}\,. \tag{3.56}$$

The alternative representations of the stress power per unit of reference volume $\rho_0 \mathscr{P} := \boldsymbol{\tau} : \boldsymbol{d} = \boldsymbol{g}\boldsymbol{P} : \dot{\boldsymbol{F}} = \boldsymbol{S} : \frac{1}{2}\dot{\boldsymbol{C}}$ manifest the distinct work conjugate couples

$$(\boldsymbol{\tau}, \boldsymbol{d})\quad,\quad (\boldsymbol{g}\boldsymbol{P}, \dot{\boldsymbol{F}})\quad\text{and}\quad \left(\boldsymbol{S}, \tfrac{1}{2}\dot{\boldsymbol{C}}\right). \tag{3.57}$$

Balance of Entropy (The Second Law of Thermodynamics). The second law of thermodynamics, which is in fact an inequality unlike the other balance principles, serves as a major mathematical restriction on the constitutive equations governing, for instance, heat conduction or evolution of internal variables describing an internal dissipative mechanism. For the part of the body $\mathcal{P}_\mathcal{S}$ under consideration, we define the total entropy by integrating the specific entropy η over the volume, i.e. $\int_{\mathcal{P}_\mathcal{S}} \rho\eta dv$. The temporal change of the entropy has two contributions, namely the reversible and the irreversible parts, see e.g. DE GROOT & MAZUR [57]. The reversible change of the entropy is due to external heat sources. The irreversible part of the entropy change, however, stems from internal dissipative mechanisms. The second law of thermodynamics states that the irreversible part of the entropy rate is always positive. For this purpose, we introduce the specific rate of entropy production $\gamma(\boldsymbol{x}, t)$ whose integration over the volume leads us to the total rate of entropy production $\int_{\mathcal{P}_\mathcal{S}} \rho\gamma(\boldsymbol{x}, t)dv \geq 0$. The balance of entropy can then be expressed as

$$\int_{\mathcal{P}_\mathcal{S}} \rho\gamma dv := \frac{d}{dt}\int_{\mathcal{P}_\mathcal{S}} \rho\eta dv - \left(\int_{\mathcal{P}_\mathcal{S}} \frac{\rho r}{\theta}dv - \int_{\partial\mathcal{P}_\mathcal{S}} \frac{\boldsymbol{q}\cdot\boldsymbol{n}}{\theta}da\right) \geq 0 \tag{3.58}$$

where θ stands for the absolute temperature restricted to the positive values $\theta > 0$. Following the conventional steps, we end up with the local spatial entropy balance

$$\rho\gamma = \rho\dot{\eta} - \rho\frac{r}{\theta} + \text{div}\left[\frac{\boldsymbol{q}}{\theta}\right] = \rho\dot{\eta} - \rho\frac{r}{\theta} + \frac{1}{\theta}\text{div}[\boldsymbol{q}] - \frac{1}{\theta^2}\boldsymbol{q}\cdot\nabla_{\boldsymbol{x}}\theta \geq 0\,. \tag{3.59}$$
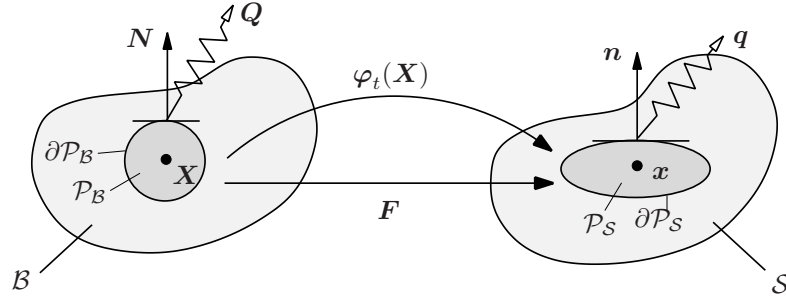
Figure 3.6: The material $Q(X,t) \in T_X\mathcal{B}$ and spatial $q(x,t) \in T_x\mathcal{S}$ heat flux vectors representing the production of heat through the rest of the body over the surfaces of the cut parts $\partial\mathcal{P}_\mathcal{B}$ and $\partial\mathcal{P}_\mathcal{S}$, respectively.

The inequality $(3.59)_3$ can also be written in the form commonly referred to as the Clausius-Duhem inequality

$$\rho\dot{\eta} \geq \rho\frac{r}{\theta} - \frac{1}{\theta}\operatorname{div}[\boldsymbol{q}] + \frac{1}{\theta^2}\boldsymbol{q} \cdot \nabla_{\boldsymbol{x}}\theta \,. \tag{3.60}$$

The material version of (3.59) then reads as

$$\rho_0\dot{\eta} \geq \rho_0\frac{R}{\theta} - \frac{1}{\theta}\operatorname{Div}[\boldsymbol{Q}] + \frac{1}{\theta^2}\boldsymbol{Q} \cdot \nabla_{\boldsymbol{X}}\theta \,. \tag{3.61}$$

3.4. The Entropy Production Inequality

The spatial dissipation is defined as the product of the rate of entropy production in (3.59) with the absolute temperature θ, i.e. $\rho\mathscr{D} := \rho\gamma\theta \geq 0$. Owing to the nature of the terms in (3.59), it is common practice to additively split the dissipation into the local (intrinsic) $\mathscr{D}_{loc}$ and the conductive (thermal) $\mathscr{D}_{con}$ parts, $\mathscr{D} = \mathscr{D}_{loc} + \mathscr{D}_{loc}$. We then require a more strict condition than (3.59) by demanding the positiveness of the both terms $\mathscr{D}_{loc}$ and $\mathscr{D}_{con}$ separately. To this end, we introduce the Clausius-Planck inequality

$$\rho\mathscr{D}_{loc} := \rho\dot{\eta}\theta - (\rho r - \operatorname{div}[\boldsymbol{q}]) \geq 0 \,, \tag{3.62}$$

and the Fourier inequality

$$\rho\mathscr{D}_{con} := -\frac{1}{\theta}\boldsymbol{q} \cdot \nabla_{\boldsymbol{x}}\theta \geq 0 \,, \tag{3.63}$$

that can also be expressed in the following Lagrangian form

$$\rho_0\mathscr{D}_{con} = J\rho\mathscr{D}_{con} = -\frac{1}{\theta}J\boldsymbol{q} \cdot \nabla_{\boldsymbol{x}}\theta = -\frac{1}{\theta}\boldsymbol{Q} \cdot \nabla_{\boldsymbol{X}}\theta \geq 0 \,. \tag{3.64}$$

Incorporation of the spatial energy balance equation (3.52) in the first version of the Clausius-Planck inequality (3.62) leads to the equation formulated in terms of the internal energy density

$$\rho\mathscr{D}_{loc} := \rho\dot{\eta}\theta - \rho\dot{e} + \boldsymbol{\sigma} : (\boldsymbol{gl}) \geq 0. \tag{3.65}$$

This form can be rewritten per unit reference volume by multiplying (3.66) with the Jacobian J, i.e.

$$\rho_0\mathscr{D}_{loc} = J\rho\mathscr{D}_{loc} = \rho_0\dot{\eta}\theta - \rho_0\dot{e} + \boldsymbol{gP} : \dot{\boldsymbol{F}} \geq 0 \,. \tag{3.66}$$

There are four basic thermomechanical potentials widely encountered in the thermome-chanics literature. The choice of an appropriate potential is generally made according to circumstances of experiments or properties of the material at hand. In the context of continuum thermomechanics, these potentials generally depend on a set of variables which is formed through a mutual combination between the sets $\{\boldsymbol{gP}, \boldsymbol{F}\}$ and $\{\eta, \theta\}$. The first set can, of course, be replaced with any of the work conjugate pairs given in (3.57). For inelastic materials, these sets are supplemented by additional internal variables, say $\{\mathfrak{Q}\}$, employed for the description of inelastic dissipative processes. The concept of internal variables has widely been used in the constitutive formulation of dissipative materials through the initial value problems governing their temporal evolution. The set $\{\mathfrak{Q}\}$ may have scalar, tensorial or n-vector character. The internal variables may be observable but generally cannot be externally controlled, see MAUGIN [101] for an excellent review. The thermodynamical forces, say $\{\mathfrak{M}\}$, conjugate to the set $\{\mathfrak{Q}\}$ on the bases of dissipa-tion, generally are not externally defined. Thus, it should also be noted that the internal variables do not explicitly appear up to the energy balance equation (3.52).

By looking at the time derivatives of the fields in the Clausius-Planck inequality (3.66) one can readily conclude that the internal energy e can be considered as a thermodynamical potential depending primarily upon the deformation $\boldsymbol{F}$ and the entropy η, i.e. $e = \hat{e}(\boldsymbol{F}, \eta, \ldots)$. We then define the Helmholtz free energy through the partial Legendre transformation $\psi := \sup_\eta\{e - \theta\eta\}$ implying the functional dependency $\psi = \hat{\psi}(\boldsymbol{F}, \theta, \ldots)$. Similarly, we can also introduce the Gibbs free energy $g = \hat{g}(\boldsymbol{gP}, \theta, \ldots) := \sup_{\boldsymbol{F}}\{\psi - \boldsymbol{gP} : \boldsymbol{F}\}$ and the enthalpy $h = \hat{h}(\boldsymbol{gP}, \eta, \ldots) := \sup_{\boldsymbol{F}}\{e - \boldsymbol{gP} : \boldsymbol{F}\}$. Commonly, in the modeling of the material behavior we utilize the Helmholtz free energy. Hence, the version of the Clausius-Planck inequality in terms of the Helmholtz free energy, or simply free energy, is of interest. Inserting its definition $\psi := \sup_\eta\{e - \theta\eta\}$ into (3.66), we end up with

$$\rho_0 \mathscr{D}_{loc} := \boldsymbol{gP} : \dot{\boldsymbol{F}} - \rho_0\dot{\psi} - \rho_0\eta\dot{\theta} \geq 0\,. \tag{3.67}$$

To fix the ideas, let us focus on a problem of thermoelasticity for a homogeneous material where the free energy does not depend on the internal variables. Being consistent with the principle of equipresence, we assume that the constitutive equations, the free energy ψ and the heat flux vector $\boldsymbol{Q}$, depend upon the same set of field variables

$$\psi = \hat{\psi}(\boldsymbol{g}, \boldsymbol{F}, \theta, \boldsymbol{\mathcal{G}}) \qquad \text{and} \qquad \boldsymbol{Q} = \hat{Q}(\boldsymbol{g}, \boldsymbol{F}, \theta, \boldsymbol{\mathcal{G}}) \tag{3.68}$$

where $\boldsymbol{\mathcal{G}} := \nabla_{\boldsymbol{X}}\theta$ denotes the material gradient of the temperature field and the spatial metric $\boldsymbol{g}$ is needed to compute the deformation measures in the reference configuration. Based on this assumption, we can include the time derivative of the free energy $\dot{\psi} = \partial_{\boldsymbol{F}}\psi : \dot{\boldsymbol{F}} + \partial_\theta\psi\dot{\theta} + \partial_{\boldsymbol{\mathcal{G}}}\psi \cdot \dot{\boldsymbol{\mathcal{G}}}$ in the Clausius-Planck inequality given in (3.67). Gathering the coefficients of the time rates of the common terms, we obtain

$$\rho_0 \mathscr{D}_{loc} := [\boldsymbol{gP} - \rho_0\partial_{\boldsymbol{F}}\psi] : \dot{\boldsymbol{F}} - \rho_0[\eta + \partial_\theta\psi]\dot{\theta} - \rho_0\partial_{\boldsymbol{\mathcal{G}}}\psi \cdot \dot{\boldsymbol{\mathcal{G}}} \geq 0 \tag{3.69}$$

Following the celebrated reasoning of COLEMAN & NOLL [33] and COLEMAN & GURTIN [32] within the framework of thermodynamics with internal variables, we contend that the thermodynamic restriction should be fulfilled for an arbitrary rate of the deformation gradient, temperature and temperature gradient. Therefore, (3.69) implies a particular form of constitutive equations such that

$$\boldsymbol{gP} := \rho_0\partial_{\boldsymbol{F}}\psi \quad , \qquad \eta := -\partial_\theta\psi \qquad \text{and} \qquad \partial_{\boldsymbol{\mathcal{G}}}\psi = \boldsymbol{0}\,. \tag{3.70}$$

The first two equations of (3.70) state that the free energy acts as a potential for the stresses and the entropy while $(3.70)_3$ implies that the free energy does not depend on the temperature gradient $\boldsymbol{G}$, i.e. $\psi = \hat{\psi}(\boldsymbol{g}, \boldsymbol{F}, \theta)$. From the results (3.70), it is also clear that the local dissipation $\mathscr{D}_{loc}$ vanishes identically for thermoelastic problems. In a general problem of thermoinelasticity, however, the free energy is also a function of the internal variables $\{\mathfrak{Q}\}$. With the results obtained in (3.70), the Clausius-Planck inequality can be recast into its reduced form

$$\rho_0 \mathscr{D}_{loc} := \mathfrak{M} : \dot{\mathfrak{Q}} \geq 0 \qquad \text{with} \qquad \mathfrak{M} := -\rho_0 \partial_{\mathfrak{Q}} \psi \,. \tag{3.71}$$

The principle of material frame invariance requires the invariance of the energy stored under rigid body rotations superimposed on the current spatial configuration. Therefore, we locally demand $\psi(\boldsymbol{g}, \boldsymbol{F}, \theta) = \psi(\tilde{\boldsymbol{g}}, \tilde{\boldsymbol{F}}, \theta)$ where $\tilde{\boldsymbol{F}} := \boldsymbol{Q}_*(\boldsymbol{F}) := \boldsymbol{Q}\boldsymbol{F}$ and $\tilde{\boldsymbol{g}} := \boldsymbol{Q}_*(\boldsymbol{g}) := \boldsymbol{Q}^{-T}\boldsymbol{g}\boldsymbol{Q}^{-1}$ for all $\boldsymbol{Q} \in \mathcal{SO}(3)$. Observe that the right Cauchy-Green tensor $\boldsymbol{C} = \boldsymbol{F}^T\boldsymbol{g}\boldsymbol{F} = \tilde{\boldsymbol{F}}^T\tilde{\boldsymbol{g}}\tilde{\boldsymbol{F}}$ automatically satisfies this condition. Therefore, the storage function $\hat{\psi}$ in terms of $\boldsymbol{C} = \boldsymbol{F}^T\boldsymbol{g}\boldsymbol{F}$ is a priori objective and the form $\hat{\psi}(\boldsymbol{C}, \theta) = \hat{\psi}(\boldsymbol{F}^T\boldsymbol{g}\boldsymbol{F}, \theta)$ represents its reduced form. Based on this restriction, we can rewrite the term $[\boldsymbol{g}\boldsymbol{P} - \rho_0 \partial_{\boldsymbol{F}}\psi] : \dot{\boldsymbol{F}}$ in (3.69) as $[\boldsymbol{S} - 2\rho_0 \partial_{\boldsymbol{C}}\psi] : \frac{1}{2}\dot{\boldsymbol{C}}$ due to the stress power equalities (3.60), (3.61). This yields the functional definition of the second Piola-Kirchhoff stress tensor

$$\boldsymbol{S} = 2\rho_0 \partial_{\boldsymbol{C}} \psi. \tag{3.72}$$

Starting from this equality, we can further continue to obtain

$$[\boldsymbol{S} - 2\rho_0 \partial_{\boldsymbol{C}}\psi] : \tfrac{1}{2}\dot{\boldsymbol{C}} = \boldsymbol{\tau} : \tfrac{1}{2}\,\pounds_{\boldsymbol{v}}\boldsymbol{g} - 2\rho_0 \partial_{\boldsymbol{C}}\psi : \boldsymbol{F}^T\,\pounds_{\boldsymbol{v}}\boldsymbol{g}\boldsymbol{F} = [\boldsymbol{\tau} - 2\rho_0 \boldsymbol{F}\partial_{\boldsymbol{C}}\psi\boldsymbol{F}^T] : \tfrac{1}{2}\,\pounds_{\boldsymbol{v}}\boldsymbol{g}. \tag{3.73}$$

where it can be shown through the chain rule that $2\rho_0 \boldsymbol{F}\partial_{\boldsymbol{C}}\psi\boldsymbol{F}^T = 2\partial_{\boldsymbol{g}}\psi$ see MARSDEN & HUGHES [98], p.197. This equality leads us to the Doyle-Ericksen formula

$$\boldsymbol{\tau} = 2\partial_{\boldsymbol{g}}\psi(\boldsymbol{g}, \boldsymbol{F}, \theta) \tag{3.74}$$

originally derived by DOYLE & ERICKSEN [44].

4. Electrostatics

The aim of this chapter is to construct the global and local equilibrium equations together with the constitutive equations of electrostatics by using an approach similar to the one used for the continuum mechanics. Those equations will be written in the physical Eulerian configuration $\mathcal{S}$ and later on transformed to the current configuration $\mathcal{B}$ will be considered. The material treated here is assembled by referring to different books and lecture notes, see LANDAU & LIFSCHITZ [88], SCHELKUNOFF [132], PENFIELD & HAUS [125], FLEURY & MATHIEU [50], POHL [127], TONTI [142], STRATTON [140] among the others.

4.1. The Electric field

Historically two kinds of *electric charge*, positive and negative, each conceived as some sort of invisible fluid, were postulated to explain primitive experiments with wax and ebonite rubbed with fur and with bodies brought in contact with them. Simple experiments suffice to demonstrate that charges of the same sign repeal each other, those of opposite signs attract, and that equal charges of opposite signs can neutralize each other as far as external action is concerned. The Coulomb's law of force between charged particles and bodies is analogous to Newton's law of gravitation

$$f^e = k^e \frac{q_1 q_2}{r^2} \tag{4.1}$$

where q_1 and q_2 are the electric charges on the particles, r is their distance and the force acts along the line joining the particles. The entity of the constant k^e will be specified in the following subchapters.

The evidence that the charges attract or repel themselves suggests the institution of a physical variable which measures the intensity of such an action. Thus we define a new field, the *electric field*, and we say that an electric charge is surrounded by such a field and is the source of the same. In order to define the electric field generated by an arbitrary system of charges we observe that a test charge q^e placed in such a field experiences a force $\boldsymbol{f}^e$ which depends on the position $\boldsymbol{x}$, on the charge q^e, and converges to zero for $q^e \to 0$ (see Figure 4.1). The force $\boldsymbol{f}^e$ could be expressed in polynomial form as

$$\boldsymbol{f}^e(\boldsymbol{x}, q^e) = \mathbb{e}(\boldsymbol{x})q^e + \mathbb{g}(\boldsymbol{x})\left(q^e\right)^2 + \mathbb{s}(\boldsymbol{x})\left(q^e\right)^3 + HOT(q^e) \tag{4.2}$$

being $\mathbb{e}$, $\mathbb{g}$, $\mathbb{s}$ vectorial coefficients and $HOT(q^e)$ higher order terms in q^e. In particular, if q^e is small the following approximation holds

$$\boldsymbol{f}^e(\boldsymbol{x}, q^e) = \mathbb{e}(\boldsymbol{x})q^e \qquad \text{with} \qquad \mathbb{e}(\boldsymbol{x}) := \lim_{q^e \to 0} \frac{\boldsymbol{f}^e(\boldsymbol{x}, q^e)}{q^e} \ . \tag{4.3}$$

The vector $\mathbb{e}$ defined in equation $(4.3)_2$ is called the *electric field vector*. The unit of the electric field intensity is *one newton per coulomb* $\left[\frac{\text{N}}{\text{C}}\right]$ or, as we will see in the following, the *volt per meter* $\left[\frac{\text{V}}{\text{m}}\right]$.

From equation (4.1) and $(4.3)_2$ we conclude that the intensity of the electric field generated from a charged particle q^e is given by

$$|\mathbb{e}|(\boldsymbol{x}, q^e) = k^e \frac{q^e}{r^2} \tag{4.4}$$
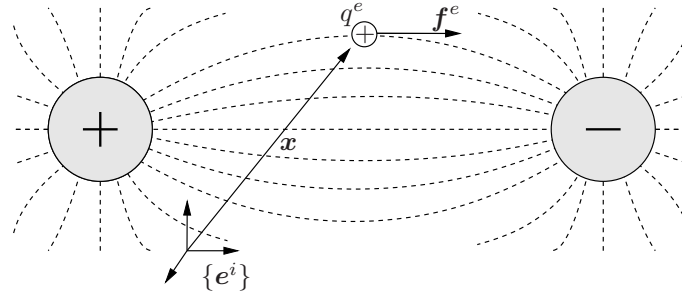
Figure 4.1: Measuring of the electric field with a test charge q^e. The dashed lines represent the electric field lines.

being r the distance from q^e. We observe that the introduction of a test charge in an electric field alters the position of the charges originally generating the field (Pohl [127]). Thus the ratio $\boldsymbol{f}^e/q^e$ gives a measure of the field altered from the presence of the test charge. This ratio is a measure of the pre-existing field in one of the three following situation (see Schelkunoff [132]):

- The sources of the field are held fixed.

- The point $\boldsymbol{x}$ in which the test charge is placed is so far away from the sources that the test charge does not affect their position.

- The test charge is so small that it does not affect the position of the sources.

Since the distortion gets smaller for a smaller value of the test charge one does the limit of the ratio $\boldsymbol{f}^e/q^e$ as in $(4.3)_2$. On the other hand, the smallest possible charge is the charge of the electron and thus such a limit operation is in contrast with physics. For this reason we have to be satisfied with a model of the electric field which ignores the discrete nature of the electric charge.

From a spatial point of view we have two different types of charges: the contained charge q^{ec} and the flowing charge q^{ef}. The contained charge is associated with a certain volume $\mathcal{S}$, i.e. $q^{ec} = \hat{q}^{ec}(\mathcal{S})$. The flowing charge, whose rate is called electric current, has the property of inducing a magnetic field. In the electrostatic case $q^{ef} = 0$, i.e. the charges are not flowing.

4.2. The First Law of Electrostatics

The first law of electrostatic, known also under the name of *Gauß-Law*, involves two physical variables which we are going to define in the next subchapters. These variables are the electric flux or electric surface charge h^e and the electric induction vector or electric displacement vector ⅆ.

4.2.1. Charge Distribution in Conductors

Conducting bodies are normally electrically neutral. They contain equal numbers of protons and electrons so distributed that their forces on an external charge cancel such that no external field as well as no internal field are produced. If a quantity of electrons is removed from a body, the body becomes positively charged. It is negatively charged when there is an excess of electrons. If electrons are introduced into a conductor, the
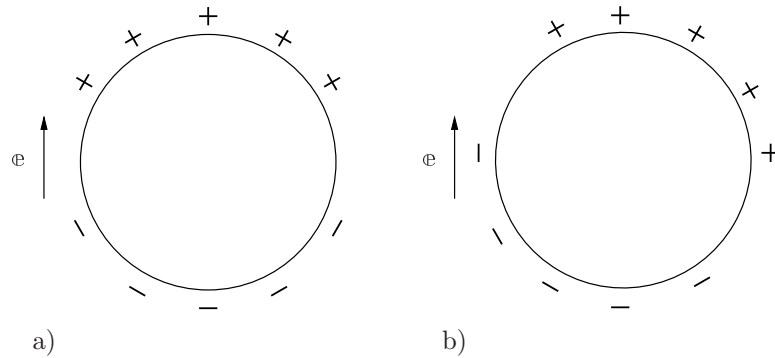
Figure 4.2: The displacement of charge under the influence of an electric field: a) on a neutral metallic sphere in an isotropic medium, b) on a neutral metallic sphere in an anisotropic medium.

forces of repulsion will disperse them. They will keep moving as long as there is an electric intensity inside the conductor and a tangential component of ℮ on the surface. The normal component of ℮ will try to pull them out unless the opposite pushing force is extremely strong. A static state is reached when the field inside the conductor and its tangential component on the surface vanish. Thus, in a static state the electric field is normal to the surface of any conductor.

The above argument was based on an excess of electrons. The same argument applies when there is an electron deficiency. The protons will pull the electrons until the positive field inside the conductor disappears so that the deficiency of electrons will exist only on the surface, and there the final distribution will be such that the tangential component of ℮ is zero.

If a neutral conductor is introduced in an electric field, the free electrons are displaced, Figure 4.2a, in such a way that the electric intensity due to their displacement within the conducting body is equal and opposite to the external field. Thus, the tangential component of the electric field due to the displaced charge is equal and opposite to the impressed tangential component. This phenomenon is known as *electrostatic induction*.

If the medium outside a metal sphere is crystalline, the electrons are usually displaced in some directions other than that of ℮ (Figure 4.2b), except when ℮ is along a "principal" axis of the medium.

4.2.2. Farady's Law of Electrostatic Induction

Faraday discovered that if a charge q^e is enclosed by a neutral metal sphere, an equal charge of the same sign appears on the external surface of the sphere. He found that the external field is symmetric weather the sphere is placed concentric within the enclosed charge or not (cf. Figure 4.3). Also, if the charge on the external surface is removed from the sphere by momentarily grounding it, a charge equal and opposite to the enclosed charge will be left on the inner part of the sphere. This is true regardless of the nonconducting medium surrounding the charge q^e. The induced charge is also independent of the shape of the metallic closed conducting shell and of its dimension.

Faraday's observations are explained in view of the present-day knowledge about free electrons in conductors. The enclosed charge will either repel or attract the electrons, depending on its sign. Hence the same charge will always be on the external surface and
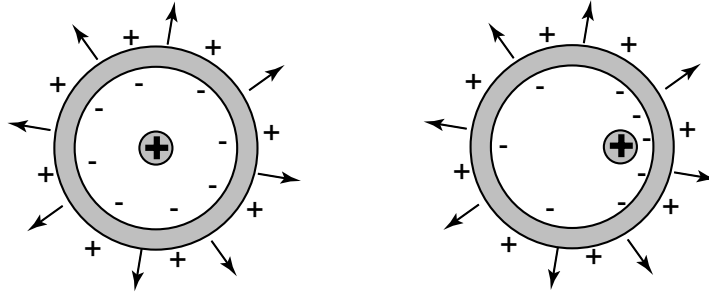
Figure 4.3: The charge induced on the external surface of the metallic spherical shell is equal to the enclosed charge.

the opposite charge on the internal surface. When the displacement of charge has taken place, there will be no field in the metallic shell. Hence the charge on the external surface is free to distribute itself according to its own forces.

The law of the electric induction represents the experimental point of departure of the so called *Gauß-Law*: "*the electric charge which appears on the external surface of a conducting closed shell is equal to the total enclosed charge*".

4.2.3. Electric Displacement or Induction

If we approach with a charge q^e a metallic shell of arbitrary shape, closed or opened, because of the electric induction two charges of opposite sign will raise on his two surfaces. We consider an infinitesimal oriented conducting shell $d\boldsymbol{s} = ds\,\boldsymbol{n}$ of area ds and normal $\boldsymbol{n}$. We assume as positive side $d\boldsymbol{s}^+$ of $d\boldsymbol{s}$ the one from which the normal $\boldsymbol{n}$ is outgoing. We define the charge raising on $d\boldsymbol{s}^+$ as the *electric flux* or *electric surface charge* h^e. Obviously the charge induced on the negative side $d\boldsymbol{s}^-$ of $d\boldsymbol{s}$ is equal to $-h^e$, i.e.

$$h^e(d\boldsymbol{s}^+) = -h^e(d\boldsymbol{s}^-) \qquad \text{or} \qquad h^e(d\boldsymbol{s}) = -h^e(-d\boldsymbol{s})\,. \tag{4.5}$$

In $(4.5)_2$ we identified $d\boldsymbol{s}$ with its positive side. Experimental evidences show that (cf. Figure 4.4):

1. The displaced or induced charge h^e depends on the relative orientation of the plate with respect to the electric field orientation $\mathtt{e}$.

2. h^e is proportional to the area ds of the test plate.
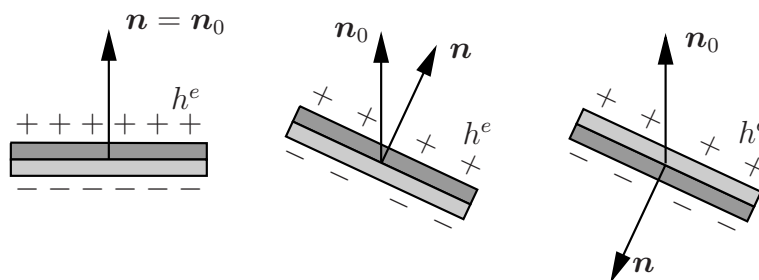
Figure 4.4: The measure of the electric flux on an oriented surface element in an electric field $\mathtt{e}$ depending on the surface normal $\boldsymbol{n}$.
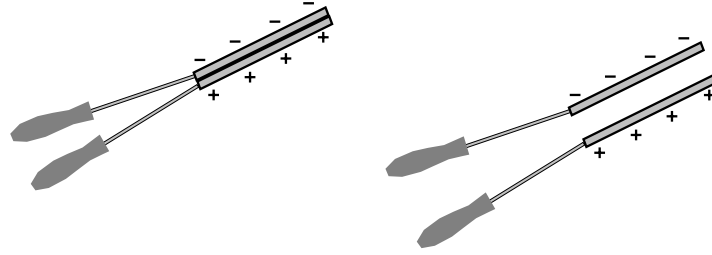
Figure 4.5: The electric flux ϕ^e can be measured by using a probe made up of two identical metallic shells with two isolating handles. In an electric field a concentration of opposite charges will raise on the external faces of the two shells.

3. When the orientation $\boldsymbol{n}$ of the plate is parallel to a certain direction $\boldsymbol{n}_0$, the displaced charge h^e is a maximum.

4. The charge displaced in any other orientation equals the maximum displaced charge multiplied by the cosine of the angle between $\boldsymbol{n}$ and $\boldsymbol{n}_0$.

5. The displaced charge depends not only on the electric field e but also on the medium surrounding the plate.

For small discs the charge h^e (in Coulomb) is proportional to the area. The quantity

$$\sigma^e := \lim_{ds \to 0} \frac{h^e}{ds} \tag{4.6}$$

is defined as electric surface density charge. The flux h^e can be measured with a probe made up of two identical metallic discs provided with two isolating handles as in Figure 4.5. If the two parts are in contact and are immerged in an electric field, because of the electric induction a concentration of opposite charges will raise on the external faces of the two shells. If we now detouch the two metallic surfaces the induced charges will remain on the two shells and could be measured. If we fix one of the two shells as positive, we define the electric charge on it as *electric flux h^e*. The fact that *the induced charge is independent of the material of the conducting disc* is of primary importance: this allows us to *link the electric flux directly to the geometrical surface.*

The surface density σ^e is a variable depending on the position $\boldsymbol{x}$ and on the orientation $\boldsymbol{n}$. We would like to define a vector $\mathrm{d}(\boldsymbol{x})$ depending only on the position $\boldsymbol{x}$, such that we could write

$$\sigma^e(\boldsymbol{x}, \boldsymbol{n}) = \mathrm{d}(\boldsymbol{x}) \cdot \boldsymbol{n} \tag{4.7}$$

We consider first of all the direction $\boldsymbol{n}_0$ in correspondence of which the surface density σ^e reaches its maximal value σ_0^e. Experimental evidences show that for a generic orientation $\boldsymbol{n}$ the following relationship holds

$$\sigma^e(\boldsymbol{x}, \boldsymbol{n}) = \sigma_0^e(\boldsymbol{x}) cos(\alpha) = \sigma_0^e(\boldsymbol{x})(\boldsymbol{n}_0 \cdot \boldsymbol{n}), \tag{4.8}$$

with α angle between $\boldsymbol{n}$ and $\boldsymbol{n}_0$. It becomes natural at this point to define the vector

$$\mathrm{d} := \sigma_0^e(\boldsymbol{x})\boldsymbol{n}_0 \tag{4.9}$$

which is called *electric induction vector* or *displacement density* or *electric displacement vector* and is necessary for a complete quantitative description of the electric field. This vector depends only on the position $\boldsymbol{x}$. We can now write equation (4.8) in the desired form (4.7). It is then obvious that the electric flux on the positive surface $\partial\mathcal{S}$ could be written in the form

$$h^e[\partial\mathcal{S}] = \int_{\partial\mathcal{S}} \mathrm{d}(\boldsymbol{x}) \cdot d\boldsymbol{s}\,. \tag{4.10}$$

with $d\boldsymbol{s} = ds\boldsymbol{n}$ and $\boldsymbol{n}$ normal to $\partial\mathcal{S}$. Equation (4.10) has to be interpreted as the definition of the electric induction vector d since the flux h^e is the quantity which can be measured. Finally we could express Farady's electrostatic induction law as follow:

First Law of Electrostatics: The electric flux h^e relative to the boundary $\partial\mathcal{S}$ of the closed region $\mathcal{S}$ is equal to the electric charge q^e enclosed in the volume $\mathcal{S}$, i.e.

$$h^e[\partial\mathcal{S}] = q^e[\mathcal{S}]\,. \tag{4.11}$$

4.2.4. The Gauß Theorem

Using equation (4.10) we could rewrite Farady's law of electrostatic induction (4.11) in the form

$$\int_{\partial\mathcal{S}} \mathrm{d}(\boldsymbol{x}) \cdot d\boldsymbol{s} = q^e[\mathcal{S}]\,. \tag{4.12}$$

If the charge $q^e[\mathcal{S}]$ is distributed in $\mathcal{S}$ with a volume density $\bar{\rho}^e(\boldsymbol{x})$ we can write $q^e[\mathcal{S}] = \int_{\mathcal{S}} \bar{\rho}^e(\boldsymbol{x})dv$ and thus equation (4.12) reads

$$\int_{\partial\mathcal{S}} \mathrm{d}(\boldsymbol{x}) \cdot d\boldsymbol{s} = \int_{\mathcal{S}} \bar{\rho}^e(\boldsymbol{x})dv\,, \tag{4.13}$$

representing the global or integral form of the Gauß-Law. Using successively the divergence theorem and the localization theorem, we could derive the local or differential form of the first law of electrostatics

$$\mathrm{div}[\mathrm{d}(\boldsymbol{x})] = \bar{\rho}^e(\boldsymbol{x}) \qquad \text{in } \mathcal{S}\,. \tag{4.14}$$

Equation (4.14) becomes on the boundary $\partial\mathcal{S}$ of $\mathcal{S}$

$$\mathrm{d}(\boldsymbol{x}) \cdot \boldsymbol{n} = \sigma^e(\boldsymbol{x}) \qquad \text{on } \partial\mathcal{S}\,. \tag{4.15}$$

4.3. The Second Law of Electrostatics

The second law of electrostatics involves together with the electric field e defined in the previous sections, the electric tension U^e and the electric potential ϕ^e which are going to be defined in the next subchapters.

4.3.1. Constitutive Equations

In order to study the electric field we have introduced two vectors: the electric displacement vector d which describes the charge distribution on a surface and the electric field

vector $\mathbb{e}$ which describes the forces acting on charges. It is obvious to expect a relationship between these two vectors. We could write a constitutive equation of the general form

$$\mathbb{d} = \hat{\mathbb{d}}(\mathbb{e}, \mathbf{q}) \tag{4.16}$$

which will depend on the medium on which the electric field acts. $\mathbf{q}$ is a set of parameters describing eventual dissipative phenomena. Equation (4.16) could be approximated in the non-dissipative case in terms of a linearization in the form

$$\mathbb{d} = \boldsymbol{\epsilon}\mathbb{e} \tag{4.17}$$

with second order tensor $\boldsymbol{\epsilon}$ referred as *dielectric permittivity tensor*. In vacuum the tensor $\boldsymbol{\epsilon}$ reduces to a constant

$$\mathbb{d} = \epsilon_0\mathbb{e} \tag{4.18}$$

with ϵ_0 as the dielectric permittivity constant in vacuum. Equation (4.18) is experimentally verified, see HALLIDAY, RESNICK AND KRANE [58]. We can observe indeed that in vacuum the vectors $\mathbb{e}$ and $\mathbb{d}$ have the same direction.

4.3.2. The Polarization Vector

Different from vacuum, in a generic material $\mathbb{e}$ and $\mathbb{d}$ could have different directions and their relationship could either be linear or non-linear. Although the two vectors $\mathbb{e}$ and $\mathbb{d}$ are sufficient to characterize completely an electrostatic field in any medium, it is convenient to introduce a third vector $\mathbb{p}$, the *polarization vector*, defined as the difference between $\mathbb{e}$ and $\mathbb{d}$ or, more precisely, as the difference between the electric displacement vector in matter and the electric displacement vector in vacuum, i.e.

$$\mathbb{p}(\mathbb{e}, \mathbf{q}) := \mathbb{d}(\mathbb{e}, \mathbf{q}) - \epsilon_0\mathbb{e}\,, \tag{4.19}$$

see STRATTON [140]. Materials in which $\mathbb{p}$ can assume a value different from zero are called dielectric materials. The polarization vector $\mathbb{p}$ vanishes in the free space and therefore is associated with the constitution of the dielectric. Insertion of (4.19) in the form $\mathbb{d} = \mathbb{p} + \epsilon_0\mathbb{e}$ into the local form of the Gauß-Law (4.14) reads

$$\text{div}[\mathbb{e}(\boldsymbol{x})] = \frac{1}{\epsilon_0}\left\{\bar{\rho}^e(\boldsymbol{x}) - \text{div}[\mathbb{p}(\boldsymbol{x})]\right\} \tag{4.20}$$

from which we can conclude that the effect of a dielectric on the field may be accounted for by an equivalent charge distribution whose volume density is

$$\rho^p(\boldsymbol{x}) = -\text{div}[\mathbb{p}(\boldsymbol{x})] \tag{4.21}$$

called the volume density of the polarization charge. The concept will be more clear in Section 4.6 where we will give a micro-mechanical motivation of (4.21). In some dielectrics the relationship between $\mathbb{p}$ and $\mathbb{e}$ is of linear type and we write

$$\mathbb{p}(\mathbb{e}) = \epsilon_0\boldsymbol{\chi}^e\mathbb{e} \tag{4.22}$$

with $\boldsymbol{\chi}^e$ as the dielectric susceptibility tensor. Insertion of (4.22) into (4.19) gives the following constitutive relationship for the non-dissipative dielectric materials

$$\mathbb{d}(\mathbb{e}) = \epsilon_0\boldsymbol{1}\mathbb{e} + \epsilon_0\boldsymbol{\chi}^e\mathbb{e} = \epsilon_0(\boldsymbol{1} + \boldsymbol{\chi}^e)\mathbb{e} = \epsilon_0\boldsymbol{\epsilon}_r\mathbb{e} = \boldsymbol{\epsilon}\mathbb{e} \tag{4.23}$$
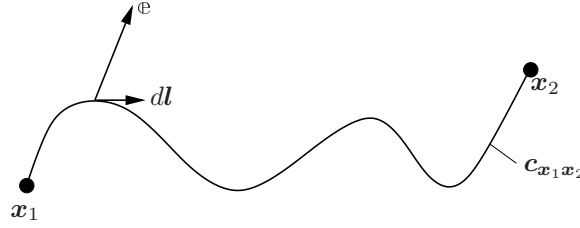
Figure 4.6: An illustration of equation (4.26) which defines the electromotive force (the "voltage") between the two points $\boldsymbol{x}_1$ and $\boldsymbol{x}_2$ along a given curve $\boldsymbol{c}_{\boldsymbol{x}_1\boldsymbol{x}_2}$.

with $\boldsymbol{\epsilon}_r = \boldsymbol{1} + \boldsymbol{\chi}^e$ and $\boldsymbol{\epsilon} = \epsilon_0\boldsymbol{\epsilon}_r$, being $\boldsymbol{\epsilon}_r$ the *relative dielectric permittivity tensor*. For dissipative dielectrics, we could additively split the polarization $\mathbb{p}$ in a reversible part $\mathbb{p}^e(\mathbb{e})$ depending on the electric field $\mathbb{e}$ and an irreversible part $\mathbb{p}^r$

$$\mathbb{p}(\mathbb{e}, \mathbb{p}^r) = \mathbb{p}^e(\mathbb{e}) + \mathbb{p}^r \tag{4.24}$$

which inserted into (4.19) yields

$$\mathbb{d}(\mathbb{e}, \mathbb{p}^r) = \mathbb{p}^e(\mathbb{e}) + \epsilon_0\mathbb{e} + \mathbb{p}^r = \mathbb{d}^e(\mathbb{e}) + \mathbb{p}^r \tag{4.25}$$

with $\mathbb{d}^e(\mathbb{e}) = \mathbb{p}^e(\mathbb{e}) + \epsilon_0\mathbb{e}$ reversible part of the electric displacement.

4.3.3. The Electromotive Force

The *electromotive force* or the *voltage* along a given path $\boldsymbol{c}_{\boldsymbol{x}_1\boldsymbol{x}_2}$ between the point $\boldsymbol{x}_1$ and $\boldsymbol{x}_2$ (cf. Figure 4.6) is the line integral of the tangential component of the electric field

$$U^e[\boldsymbol{c}_{\boldsymbol{x}_1\boldsymbol{x}_2}] = \int_{\boldsymbol{c}} \mathbb{e} \cdot d\boldsymbol{l} \,. \tag{4.26}$$

It is clear that $U^e[\boldsymbol{c}_{\boldsymbol{x}_1\boldsymbol{x}_2}] = -U^e[\boldsymbol{c}_{\boldsymbol{x}_2\boldsymbol{x}_1}]$. Suppose that a charged particle q^e is carried along $\boldsymbol{c}_{\boldsymbol{x}_1\boldsymbol{x}_2}$. Multiplying equation (4.26) by q^e, we have

$$q^e U^e[\boldsymbol{c}_{\boldsymbol{x}_1\boldsymbol{x}_2}] = \int_{\boldsymbol{c}_{\boldsymbol{x}_1\boldsymbol{x}_2}} q^e \mathbb{e} \cdot d\boldsymbol{l} \,. \tag{4.27}$$

Here $q^e\mathbb{e}$ is the force $\boldsymbol{f}^e$ acting on q^e and the line integral is the work $w[\boldsymbol{c}_{\boldsymbol{x}_1\boldsymbol{x}_2}, q^e]$ done by this force, i.e.

$$w[\boldsymbol{c}_{\boldsymbol{x}_1\boldsymbol{x}_2}, q^e] = \int_{\boldsymbol{c}_{\boldsymbol{x}_1\boldsymbol{x}_2}} \boldsymbol{f}^e \cdot d\boldsymbol{l} = \int_{\boldsymbol{c}_{\boldsymbol{x}_1\boldsymbol{x}_2}} q^e \mathbb{e} \cdot d\boldsymbol{l} = q^e U^e[\boldsymbol{c}_{\boldsymbol{x}_1\boldsymbol{x}_2}] \,. \tag{4.28}$$

Hence, if $\mathbb{e}$ does not vary with time, the voltage $U^e[\boldsymbol{c}_{\boldsymbol{x}_1\boldsymbol{x}_2}]$ is the work done by the field per unit charge carried along the path $\boldsymbol{c}_{\boldsymbol{x}_1\boldsymbol{x}_2}$. If $\mathbb{e}$ varies with time but the transit time of the particle is so short that $\mathbb{e}$ has not changed appreciably in this time, $U^e[\boldsymbol{c}_{\boldsymbol{x}_1\boldsymbol{x}_2}]$ is still substantially the work done by the field per unit charge carried along $\boldsymbol{c}_{\boldsymbol{x}_1\boldsymbol{x}_2}$. Otherwise $U^e[\boldsymbol{c}_{\boldsymbol{x}_1\boldsymbol{x}_2}]$ is just the line integral of $\mathbb{e}$ which plays an important role in electromagnetic theory.
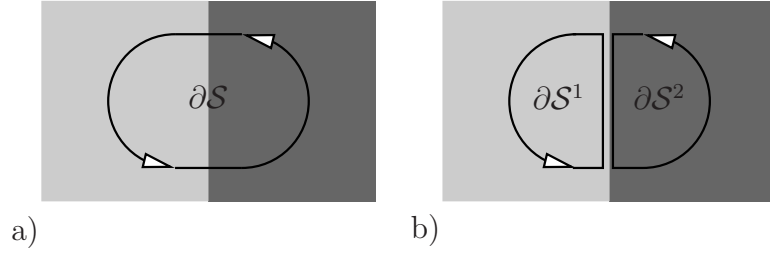
Figure 4.7: The electric tension along a closed line crossing different materials is equal to zero.

In the remaining part of this subsection we will prove that in the case of electrostatic fields it is permissible to speak of *voltage between two points* because the voltage is independent of the path joining the two points. Furthermore, this is often approximately true even for time-varying fields.

Since $q^e U^e[\boldsymbol{c}_{\boldsymbol{x}_1 \boldsymbol{x}_2}]$ is in the nature of work or energy, its unit is the *joule* ([J]). Therefore, the unit of electromotive force is one *joule per coulomb* ([J/C]), which is called the *volt* ([V]). From equation (4.26) is clear that the unit of the electric field may be called volt/meter ([V/m]) as well as newton/coulomb ([N/C]).

It is easy to prove that in a Coulombian field generated by one charge, the electric tension along a generic closed line $\boldsymbol{c}$ is equal to zero since the force between two charges is conservative:

$$U^e[\boldsymbol{c}] = 0 \qquad \text{with} \qquad \boldsymbol{c} \text{ closed}. \qquad (4.29)$$

Let us consider an homogeneous and isotropic medium and in it the electric field produced from several charges. Assuming the superposition property to be valid we conclude that the electric field in each point is the sum of the electric fields $\mathbb{e}_k$ generated by the single charges, i.e.

$$U^e[\boldsymbol{c}] = \int_{\boldsymbol{c}} \mathbb{e} \cdot d\boldsymbol{l} = \int_{\boldsymbol{c}} \sum_{k=1}^n \mathbb{e}_k \cdot d\boldsymbol{l} = \sum_{k=1}^n \int_{\boldsymbol{c}} \mathbb{e}_k \cdot d\boldsymbol{l} = \sum_{k=1}^n U_k^e[\boldsymbol{c}] = 0. \qquad (4.30)$$

Since each of the fields $\mathbb{e}_k$ is a Coulombian field and thus the property (4.29) holds we conclude that also for the resulting field the property (4.29) holds. In the case of an anisotropic medium the property (4.29) is still valid. The anisotropy in fact affects only the relationship between $\mathbb{d}$ and $\mathbb{e}$, but the electric tension is defined using the vector $\mathbb{e}$ only and thus the anisotropy has no consequence on (4.29).

Let us consider now two homogeneous media as in Figure 4.7a. Let the closed line $\boldsymbol{c}$ be the border of a surface ∂S which crosses the two media. This closed path can be decomposed in two paths each of which lays in just one medium. Let us label with ∂S^1 and ∂S^2 the two surfaces into which ∂S is decomposed, as in Figure 4.7b. For each of these two surfaces the property (4.29) holds, i.e.

$$U^e[\boldsymbol{c}^1] = 0 \qquad \text{and} \qquad U^e[\boldsymbol{c}^2] = 0. \qquad (4.31)$$

being $\boldsymbol{c}^1$ and $\boldsymbol{c}^2$ the closed curves surrounding ∂S^1 and ∂S^2. Since the common piece of the two closed lines $\boldsymbol{c}^1$ and $\boldsymbol{c}^2$ is covered twice in different directions we conclude that

$$U^e[\boldsymbol{c}] = U^e[\boldsymbol{c}^1] + U^e[\boldsymbol{c}^2] = 0. \qquad (4.32)$$

and thus also along a closed line crossing two different materials the electric tension is equal to zero. This property is also valid if the closed line crosses several different materials. In particular, a material whose homogeneity varies continuously can be approximated by a series of infinitesimal portions having different physical properties. As consequence the property (4.29) is also valid for materials generically not homogeneous and thus we come to the

Second Law of Electrostatics: The electric tension along any reducible closed line $\boldsymbol{c}$ is equal to zero, i.e.

$$U^e[\boldsymbol{c}] = \int_{\boldsymbol{c}} \mathbb{e} \cdot d\boldsymbol{l} = 0 \, . \tag{4.33}$$

Because of (4.28) we could state the second law of electrostatics also by saying that *the work done to move the unit charge along a generic closed path is equal to zero*.

From (4.33) we can also conclude that *the electrostatic field is conservative*, i.e. the work done to move a unit charge from a point $\boldsymbol{x}_0$ to a point $\boldsymbol{x}$ is independent of the path. In fact, if we decompose the closed path $\boldsymbol{c}$ passing through the points $\boldsymbol{x}_0$ and $\boldsymbol{x}$ as $\boldsymbol{c} = \boldsymbol{c}^1_{\boldsymbol{x}_0\boldsymbol{x}} \cup \boldsymbol{c}^2_{\boldsymbol{x}\boldsymbol{x}_0}$ (cf. Figure 4.8) we could write using (4.33)

$$\int_{\boldsymbol{c}^1_{\boldsymbol{x}_0\boldsymbol{x}}} \mathbb{e} \cdot d\boldsymbol{l} = - \int_{\boldsymbol{c}^2_{\boldsymbol{x}\boldsymbol{x}_0}} \mathbb{e} \cdot d\boldsymbol{l} = \int_{\boldsymbol{c}^2_{\boldsymbol{x}_0\boldsymbol{x}}} \mathbb{e} \cdot d\boldsymbol{l} \, . \tag{4.34}$$

The integral in (4.33) is nothing but the circulation of the electric field $\mathbb{e}$ around the closed path $\boldsymbol{c}$ surrounding the surface $\partial\boldsymbol{S}$ of area S. Using Stokes' theorem we could write

$$\int_{\boldsymbol{c}} \mathbb{e} \cdot d\boldsymbol{l} = \int_{\partial\boldsymbol{S}} \operatorname{curl}[\mathbb{e}] \cdot \boldsymbol{n} \, ds = 0 \tag{4.35}$$

with $\boldsymbol{n}$ unit normal to $\partial\boldsymbol{S}$. The equation (4.35) represents the global form of the second law of electrostatics. An immediate consequence of (4.35) in conjunction with (4.33) is the fact that the electric field is irrotational. We have in fact

$$\operatorname{curl}[\mathbb{e}] \cdot \boldsymbol{n} = \lim_{S \to 0} \frac{1}{S} \int_{\boldsymbol{c}} \mathbb{e} \cdot d\boldsymbol{l} = 0 \tag{4.36}$$

from which we deduce the local form of the second law of electrostatics as

$$\operatorname{curl}[\mathbb{e}] = \boldsymbol{0} \, . \tag{4.37}$$

4.3.4. The Electric Potential

The second law of electrostatics (4.33) implies that the electromotive force from any point $\boldsymbol{x}$ to another point $\boldsymbol{x}_0$ (cf. Figure 4.8) is independent from the path along which it is taken. Hence, we can choose a fixed point $\boldsymbol{x}_0$ and define for any other point $\boldsymbol{x}$ a *unique* quantity $\phi^e(\boldsymbol{x})$ equal to the electromotive force from $\boldsymbol{x}$ to the reference point

$$\phi^e(\boldsymbol{x}) = \int_{\boldsymbol{x}}^{\boldsymbol{x}_0} \mathbb{e} \cdot d\boldsymbol{l} = - \int_{\boldsymbol{x}_0}^{\boldsymbol{x}} \mathbb{e} \cdot d\boldsymbol{l} \, . \tag{4.38}$$
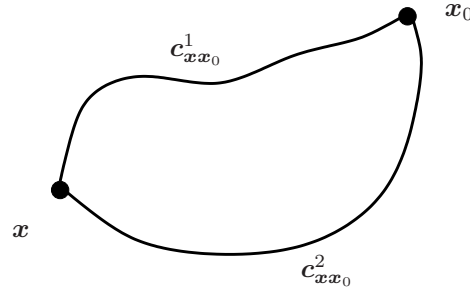
Figure 4.8: The electromotive force is independent of the path on which is taken.

The function $\phi^e(\boldsymbol{x})$, defined unless an arbitrary constant, is called *electric potential* of the point $\boldsymbol{x}$. The reference point is often chosen at infinity.

The lines and surfaces of equal potential are called *equipotential lines* and *equipotential surfaces*. They have the property that the electric field is always orthogonal to them. In the case of a static charge distribution, the potential on the surface of any conductor must be constant because if it were not constant, there would be a tangential component of $\mathbb{e}$ and a flow of charge would take place. In electrostatics conducting surfaces are equipotential surfaces. Any equipotential surface may be replaced by a conducting surface without disturbing the field.

Reciprocally, we can obtain the electric field in any point $\boldsymbol{x}$ from the potential distribution $\phi^e(\boldsymbol{x})$ as its gradient

$$\mathbb{e}(\boldsymbol{x}) = -\nabla_{\boldsymbol{x}}\phi^e(\boldsymbol{x})\,. \tag{4.39}$$

It is important to remember that the concept of potential is based on equation (4.33) and does not apply in all its generality to time variable fields. However, if strong magnetic fields are confined to certain regions, the equation (4.33) is approximately true outside these regions. Also in certain regions we may have an electric field varying strongly with the time and relatively weak magnetic fields. In such regions equation (4.33) is approximately true and we can introduce the concept of a *local potential*.

4.4. The Boundary-Value-Problem of Electrostatics

The equation governing the boundary-value-problem for the electrostatic case in a given region $\mathcal{S} \in \mathbb{R}^3$ of boundary $\partial\mathcal{S}$ occupied by a dielectric material and surrounded by free space could be summarized as in Table 4.1 where the boundary $\partial\mathcal{S}$ has been decomposed in a portion $\partial\mathcal{S}_{\mathbb{d}}$, where the free surface charges are placed, and a portion $\partial\mathcal{S}_{\phi}^e$, where the electric potential can be assigned, as follows

$$\partial\mathcal{S} = \partial\mathcal{S}_{\phi^e} \cup \partial\mathcal{S}_{\mathbb{d}} \quad \text{with} \quad \partial\mathcal{S}_{\phi^e} \cap \partial\mathcal{S}_{\mathbb{d}} = \emptyset\,. \tag{4.40}$$

4.4.1. Remark on the Boundary Conditions

We should notice that the electric field $\mathbb{e}$ and the electric displacement $\mathbb{d}$ are not only confined to the region $\mathcal{S}$, but they "live" also in the free space surrounding it. The electric property of the dielectricum is in general different from the property of the medium (free space in the considered case) surrounding it. Thus the surface $\partial\mathcal{S}$ has to be seen as a surface of discontinuity. The local equation (4.14) and (4.37) should be satisfied in each point $\boldsymbol{x}$ of $\mathcal{S}$ and in each point $\boldsymbol{x}$ of the surrounding free space $\mathbb{R}^3\backslash\mathcal{S}$ and the fields $\mathbb{e}(\boldsymbol{x})$

Table 4.1: Boundary-Value-Problem of Electrostatics

1.	Kinematic equations	$\mathbb{e}(\boldsymbol{x})$	$= -\ \nabla_{\boldsymbol{x}}\phi^e(\boldsymbol{x})$	$(\mathrm{curl}[\mathbb{e}(\boldsymbol{x})] = \boldsymbol{0})$
2.	Equilibrium equation	$\mathrm{div}[\mathbb{d}(\boldsymbol{x})] =$	$\bar{\rho}^e(\boldsymbol{x})$	
3.	Constitutive law	$\mathbb{d}(\boldsymbol{x})$	$=\quad \hat{\mathbb{d}}(\mathbb{e})$	
4.	Boundary conditions	$\mathbb{d}(\boldsymbol{x})\cdot\boldsymbol{n}$	$= -\ \bar{\sigma}^e(\boldsymbol{x},\boldsymbol{n})$	on $\partial\mathcal{S}_{\mathbb{d}}$
		$\phi^e(\boldsymbol{x})$	$=\quad \bar{\phi}^e(\boldsymbol{x})$	on $\partial\mathcal{S}_{\phi}^e$

and $\mathbb{d}(\boldsymbol{x})$ should continuously change. However, across $\partial\mathcal{S}$ we may expect a discontinuity of the fields $\mathbb{e}(\boldsymbol{x})$ and $\mathbb{d}(\boldsymbol{x})$ which could be specified by writing the global form of the electrostatic laws across the boundary $\partial\mathcal{S}$.

Let $\boldsymbol{n}$ be the outgoing normal of $\mathcal{S}$ on $\partial\mathcal{S}$ and let us contradistinguish with the subscript "$\mathcal{S}$" the properties and fields of the dielectricum occupying the region $\mathcal{S}$ and with the subscript "free" the properties and fields of the surrounding free space $\mathbb{R}^3\backslash\mathcal{S}$.

We draw through the boundary $\partial\mathcal{S}$ a right cylinder as indicated in Figure 4.9a occupying the region $\mathcal{P}\in\mathbb{R}^3$ with boundary $\partial\mathcal{P}$. The walls of the cylinder are normal to $\partial\mathcal{S}$ and its bases of area Δa lie in the two different media and are separated by a height Δl. Fixing our attention on the field of the vector $\mathbb{d}(\boldsymbol{x})$ we have

$$\int_{\partial\mathcal{P}} \mathbb{d}(\boldsymbol{x})\cdot d\boldsymbol{s} = \int_{\mathcal{P}} \bar{\rho}^e(\boldsymbol{x})dv \tag{4.41}$$

when integrated over the walls and basis $\partial\mathcal{P}$ of the cylinder $\mathcal{P}$. If the base is made sufficiently small, it may be assumed that $\mathbb{d}$ has a constant value over it. Further if Δl is small enough, the volume charge density $\bar{\rho}^e$ may be considered constant within the region $\mathcal{P}$. Neglecting differentials of higher order we may approximate (4.41) by

$$\left[\mathbb{d}_{\mathrm{free}}\cdot(\boldsymbol{n}) + \mathbb{d}_{\mathcal{S}}\cdot(-\boldsymbol{n})\right]\Delta a + LL = \bar{\rho}^e\Delta a\Delta l \tag{4.42}$$

were LL represents the contribution of the walls to the surface integral which is directly proportional to Δl. In the limit $\Delta l \to 0$, the bases of the cylinder lie just on either side of $\partial\mathcal{S}$ and the walls' contribution becomes vanishingly small. $q^e = \bar{\rho}^e\Delta a\Delta l$ is the charge contained in $\mathcal{P}$ distributed with a volume density $\bar{\rho}^e$. As $\Delta l \to 0$, the total charge q^e remains constant, for it cannot be destroyed, and the volume density $\bar{\rho}^e$ becomes infinity. It is convenient to replace $\bar{\rho}^e\Delta l$ by a surface density $\bar{\sigma}^e$, defined as the charge per unit area. Then as $\Delta l \to 0$ and $\Delta a \to 0$ we have

$$(\mathbb{d}_{\mathrm{free}} - \mathbb{d}_{\mathcal{S}})\cdot\boldsymbol{n} = \bar{\sigma}^e\,. \tag{4.43}$$

The presence of a density charge on $\partial\mathcal{S}$ results in an abrupt change in the normal component of the electric displacement $\mathbb{d}$, the amount of the discontinuity being equal to the
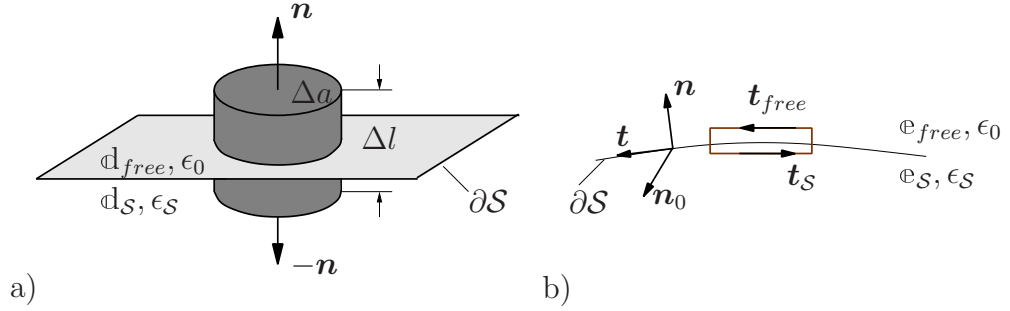
Figure 4.9: a) Bondary conditions on the electric displacement $\mathbb{d}$. b) Bondary conditions on the electric field $\mathbb{e}$

surface charge density σ^e. If the medium surrounding the dielectricum $\mathcal{S}$ is, as in the case under consideration, the free space, it follows that

$$|\mathbb{d}_{\mathcal{S}}| \gg |\mathbb{d}_{\text{free}}|\,, \tag{4.44}$$

i.e. $\mathbb{d}_{\text{free}}$ is negligible with respect to $\mathbb{d}_{\mathcal{S}}$ since the permittivity of the free space is much smaller then the permittivity of the dielectricum (normally 100-1000 smaller), so that (4.43) can be written as

$$\mathbb{d}_{\mathcal{S}} \cdot \boldsymbol{n} = -\bar{\sigma}^e\,. \tag{4.45}$$

Let us consider now a rectangular path $\boldsymbol{c}_0$ across the surface $\partial\mathcal{S}$. The sides of the rectangle of length Δs lie in either the dielectric material in the region $\mathcal{S}$ or in the free space while the other two edges of length Δl cross $\partial\mathcal{S}$. About the rectangle $\boldsymbol{c}_0$ we have

$$\int_{\boldsymbol{c}_0} \mathbb{e} \cdot d\boldsymbol{l} = 0\,. \tag{4.46}$$

Let $\boldsymbol{t}_{\text{free}}$ and $\boldsymbol{t}_{\mathcal{S}}$ be the vectors in the circulation direction along the lower and the upper sides of the rectangle as shown in the Figure 4.9b. Neglecting differentials of higher order, one may approximate (4.46) by

$$[\mathbb{e} \cdot \boldsymbol{t}_{\text{free}} + \mathbb{e} \cdot \boldsymbol{t}_{\mathcal{S}}]\,\Delta s + ll = 0\,, \tag{4.47}$$

being ll the contribution of Δl to the line integral. If $\boldsymbol{n}_0$ is the normal to the rectangular surface, we may write

$$\boldsymbol{t}_{\text{free}} = -\boldsymbol{t}_{\mathcal{S}} = \boldsymbol{n}_0 \times \boldsymbol{n}\,. \tag{4.48}$$

In the limit $\Delta l \to 0$ and $\Delta s \to 0$ we have

$$\boldsymbol{n}_0 \cdot [\boldsymbol{n} \times (\mathbb{e}_{\text{free}} - \mathbb{e}_{\mathcal{S}})] = 0\,. \tag{4.49}$$

Since $\boldsymbol{n}_0$ is arbitrary, we finally obtain

$$\boldsymbol{n} \times (\mathbb{e}_{\text{free}} - \mathbb{e}_{\mathcal{S}}) = \boldsymbol{0}\,. \tag{4.50}$$

The transition of the tangential components of the vector $\mathbb{e}$ through a surface of discontinuity is continuous. If $\mathbb{e} = -\nabla_{\boldsymbol{x}}\phi^e$ and $\boldsymbol{t}$ is the unit vector tangent to the surface $\partial\mathcal{S}$,
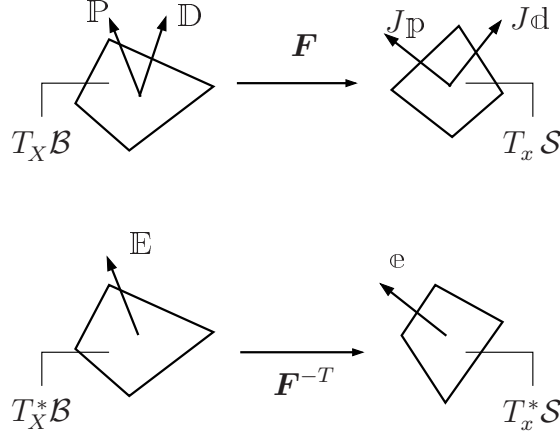
Figure 4.10: Geometrical representation of the electric objects.

$\partial_{\boldsymbol{t}}\phi^e$ represent the rate of change of the electric potential ϕ^e in the tangential direction. Then the boundary condition (4.50) can be expressed in terms of the electric potential by

$$(\partial_{\boldsymbol{t}}\phi^e)_{\text{free}} - (\partial_{\boldsymbol{t}}\phi^e)_{\mathcal{S}} = \boldsymbol{0} \,. \tag{4.51}$$

From the conservative nature of the field it follows also that the electric potential itself must be continuous across $\partial\mathcal{S}$, for the work required to carry a small charge from infinity to either two adjacent points located on opposite sides of $\partial\mathcal{S}$ must be the same

$$\phi^e_{\text{free}} = \phi^e_{\mathcal{S}} \,. \tag{4.52}$$

4.5. Geometrical Transformations of Electric Objects

In the Section 4.3.4 we have defined the electric potential $\phi^e(\boldsymbol{x})$ in terms of the electric field in the current configuration. By using the transformation of line elements (3.11) we can transform the integration on the actual configuration in (4.38) in an integration on the reference configuration and define a Lagrangian electric field $\mathbb{E}$ as follows

$$\phi^e(\boldsymbol{X}) = -\int_{\boldsymbol{X}_0}^{\boldsymbol{X}} \mathbb{e} \cdot \boldsymbol{F} d\boldsymbol{L} = -\int_{\boldsymbol{X}_0}^{\boldsymbol{X}} \boldsymbol{F}^T \mathbb{e} \cdot d\boldsymbol{L} = -\int_{\boldsymbol{X}_0}^{\boldsymbol{X}} \mathbb{E} \cdot d\boldsymbol{L} \tag{4.53}$$

yielding the transformation

$$\mathbb{e} = \boldsymbol{F}^{-T}\mathbb{E} \,. \tag{4.54}$$

As $\boldsymbol{F}^{-T}$ being the normal map, we identify $\mathbb{e}$ as a geometric object of the Eulerian cotangent space $T^*_{\boldsymbol{x}}\mathcal{S}$ and $\mathbb{E}$ as an object of the Lagrangian cotangent space $T^*_{\boldsymbol{X}}\mathcal{B}$ (cf. Figure 4.10).

The formal definition of the electric displacement was given in Section 4.2.3, equation (4.10). By using the area transformation given in (3.18), we can define an electric displacement $\mathbb{D}$ in the reference configuration as follows

$$h^e[\partial\mathcal{S}] = \int_{\partial\mathcal{S}} \mathbb{d}(\boldsymbol{x}) \cdot d\boldsymbol{s} = \int_{\partial\mathcal{B}} \mathbb{d} \cdot J\boldsymbol{F}^{-T} d\boldsymbol{S} = \int_{\partial\mathcal{B}} J\boldsymbol{F}^{-1}\mathbb{d} \cdot d\boldsymbol{S} = \int_{\partial\mathcal{B}} \mathbb{D} \cdot d\boldsymbol{S} = h^e[\partial\mathcal{B}] \,. \tag{4.55}$$
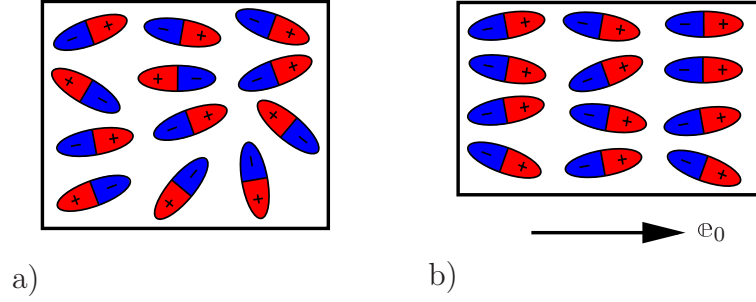
Figure 4.11: Orientation of polar molecules when a) $\mathbb{e}_0 = \boldsymbol{0}$ and b) $\mathbb{e}_0 \neq \boldsymbol{0}$.

Thus, the transformation of the material to the spatial electric displacement vector reads

$$\mathbb{d} = J^{-1}\boldsymbol{F}\mathbb{D}\,, \tag{4.56}$$

which is a typical Piola-transformation and allows us to identify $J\mathbb{d}$ as a geometric object of the Eulerian tangent space $T_{\boldsymbol{x}}\mathcal{S}$ and $\mathbb{D}$ as an object of the Lagrangian tangent space $T_{\boldsymbol{X}}\mathcal{B}$ (cf. Figure 4.10). The polarization vector transforms analogously to the electric displacement vector

$$\mathbb{p} = J^{-1}\boldsymbol{F}\mathbb{P} \tag{4.57}$$

with $\mathbb{P}$ polarization in the Lagrangian configuration. To take into account the different geometric nature of the electric field $\mathbb{e}$, the electric displacement $\mathbb{d}$, and the polarization $\mathbb{p}$, we need to modify (4.19) as follows

$$\mathbb{p} := \mathbb{d} - \epsilon_0 \boldsymbol{g}^{-1}\mathbb{e}\,. \tag{4.58}$$

Insertion of (4.54), (4.56) and (4.57) into (4.58) gives the relationship between the Lagrangian quantities $\mathbb{E}$, $\mathbb{D}$ and $\mathbb{P}$

$$\mathbb{P} = \mathbb{D} - \epsilon_0 J \boldsymbol{C}^{-1}\mathbb{E}\,. \tag{4.59}$$

with $\boldsymbol{C}^{-1} = \boldsymbol{F}^{-1}\boldsymbol{g}^{-1}\boldsymbol{F}^{-T}$. $J\mathbb{p}$ is a geometric object of the Eulerian tangent space $T_{\boldsymbol{x}}\mathcal{S}$ and $\mathbb{P}$ an object of the Lagrangian tangent space $T_{\boldsymbol{X}}\mathcal{B}$ (cf. Figure 4.10).

4.6. Dielectrics

The dielectrics are insulating material and can be of two types. The first type are polar dielectrics, which are dielectrics that have permanent electric dipole moments $\mathbb{p}_d$. An example of this type of dielectric is water. With dipole moment $\mathbb{p}_d$ we intend the vector pointing from the barycenter of the negative charges q^- in a molecule to the barycenter of the positive charges q^+, i.e. $\mathbb{p}_d = q^+\boldsymbol{d}$ with $\boldsymbol{d}$ unit vector pointing from q^- to q^+ and assuming $q^- = -q^+$.

As depicted in Figure 4.11, the orientation of polar molecules is random in the absence of an external field. When an external electric field $\mathbb{e}_0$ is present, a torque is set up and causes the molecules to align with $\mathbb{e}_0$. However, the alignment is not complete due to random thermal motion. The aligned molecules then generate an electric field that is opposite to the applied field but smaller in magnitude.

The second type of dielectrics are the non-polar dielectrics, which are dielectrics that do not possess permanent electric dipole moments. Electric dipole moments can be induced
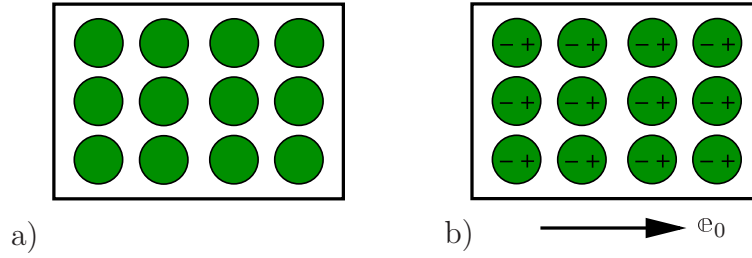
Figure 4.12: Orientation of non-polar molecules when a) $e_0 = \boldsymbol{0}$ and b) $e_0 \neq \boldsymbol{0}$.

by placing the materials in an externally applied electric field. Figure 4.12 illustrates the orientation of non-polar molecules with and without an external field e_0. The induced surface charges on the faces produce an electric field e_P in the direction opposite to e_0, leading to $e = e_0 + e_P$, with $|e| < |e_0|$. Below we show how the induced electric field is calculated.

4.6.1. Polarization

We have shown that dielectric materials consist of many permanent or induced electric dipoles. One of the concepts crucial to the understanding of dielectric materials is the average electric field produced by many little electric dipoles which are all aligned. Suppose we have a piece of material in the form of a cylinder with area A and height h, as shown in Figure 4.13, and that it consists of N electric dipoles, each with electric dipole moment p_d spread uniformly throughout the volume of the cylinder. We furthermore assume for the moment that all the electric dipole moments p_d are aligned with the axis of the cylinder. Since each electric dipole has its own electric field associated with it, in the absence of any external electric field, if we average over all the individual fields produced by the dipole, we will have an average electric field just due to the presence of the aligned dipoles.

To determine such a field, let us consider an infinitesimal volume dv and define the polarization vector p to be the net electric dipole moment vector per unit volume:

$$p = \frac{1}{dv} \sum_{i=1}^{N} p_d^i \tag{4.60}$$

with N number of dipoles p_d^i contained in the volume dv. In the case of our cylinder, where all the dipoles are perfectly aligned, the magnitude of p is equal to

$$|p| = \frac{N|p_d|}{Ah} \tag{4.61}$$

and the direction of p is parallel to the aligned dipoles. The key to figuring out the average electric field these dipoles produce is realizing that the situation shown in Figure 4.13a is equivalent to that shown in Figure 4.13b, where all the little $\pm$ charges associated with the electric dipoles in the interior of the cylinder are replaced with two equivalent charges, $\pm q^p$, on the top and bottom of the cylinder, respectively. The equivalence can be seen by noting that in the interior of the cylinder, positive charge at the top of any one of the electric dipoles is canceled on average by the negative charge of the dipole just above it. The only place where cancellation does not take place is for electric dipoles at the top of the cylinder, since there are no adjacent dipoles further up. Thus, the interior of the cylinder appears uncharged in an average sense (averaging over many dipoles),
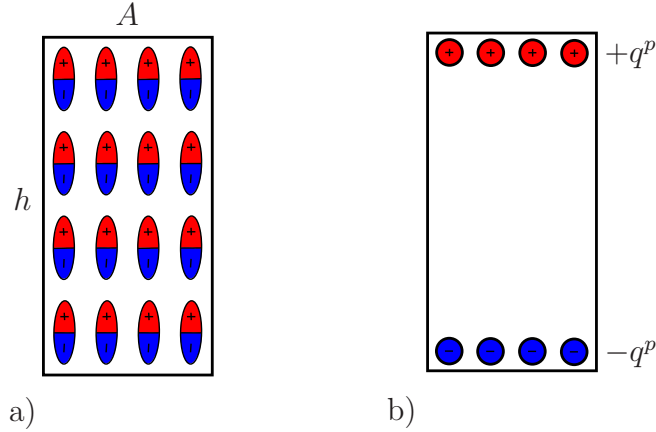
Figure 4.13: a) A cylinder with uniform dipole distribution. b) Equivalent charge distribution.

whereas the top surface of the cylinder appears to carry a net positive charge. Similarly, the bottom surface of the cylinder will appear to carry a net negative charge.

To find an expression for the equivalent charge q^p in terms of quantities we require that the electric dipole moment $q^p h$ that q^p produces is equal to the total electric dipole moment of all the little electric dipoles. This gives $q^p h = N|\mathbb{p}_d|$, or

$$q^p = \frac{N|\mathbb{p}_d|}{h} \,. \tag{4.62}$$

To compute the electric field produced by q^p, we note that the equivalent charge distribution resembles that of a parallel-plate capacitors, with an equivalent surface charge density σ_P that is equal to the magnitude of the polarization:

$$\sigma^p = \frac{q^p}{A} = \frac{N|\mathbb{p}_d|}{Ah} = |\mathbb{p}| \,. \tag{4.63}$$

The case of non-uniformly distributed $\mathbb{p}$ may be introduced as follows. A volume of $\mathcal{P}_\mathcal{S}$ with boundary $\partial\mathcal{P}_\mathcal{S}$ in a dielectric medium is considered. If equation (4.63) is generalized, the polarization density on $\partial\mathcal{P}_\mathcal{S}$ may be written as

$$\sigma^p = \mathbb{p} \cdot \boldsymbol{n} \tag{4.64}$$

in terms of $\boldsymbol{n}$ as the outward normal to $\partial\mathcal{P}_\mathcal{S}$. In contrast to the previous case, now, there is a volume charge density because of the non-uniform displacement of the charges in $\mathcal{P}_\mathcal{S}$. If the charge in $\mathcal{P}_\mathcal{S}$ is represented by q^p, as a result of the electro-neutrality, it may be written as

$$q^p = -\int_{\partial\mathcal{P}_\mathcal{S}} \mathbb{p} \cdot \boldsymbol{n} da \,. \tag{4.65}$$

If q^p is related to a volume charge density ρ^p in $\mathcal{P}_\mathcal{S}$, one may write

$$q^p = \int_{\mathcal{P}_\mathcal{S}} \rho^p dv = -\int_{\partial\mathcal{P}_\mathcal{S}} \mathbb{p} \cdot \boldsymbol{n} da \,. \tag{4.66}$$

Employing *Gauß Theorem* one gets

$$\text{div}[\mathbb{p}(\boldsymbol{x})] = -\rho^p(\boldsymbol{x}) . \tag{4.67}$$

Equation (4.67) gives the general relationship between the polarization vector and the polarization charge. Thus, our equivalent charge system will produce an average electric field of magnitude $|\mathbb{e}_P| = |\mathbb{p}|/\epsilon_0$. Since the direction of this electric field is opposite to the direction of $\mathbb{p}$, in vector notation, we have

$$\mathbb{e}_P = -\frac{\mathbb{p}}{\epsilon_0} . \tag{4.68}$$

Thus, the average electric field of all these dipoles is opposite to the direction of the dipoles themselves. It is important to realize that this is just the average field due to all the dipoles. If we go close to any individual dipole, we will see a very different field. We have assumed here that all our electric dipoles are aligned. In general, if these dipoles are randomly oriented, then the polarization $\mathbb{p}$ given in equation (4.60) will be zero, and there will be no average field due to their presence. If the dipoles have some tendency toward a preferred orientation, then $\mathbb{p} \neq \boldsymbol{0}$, leading to a non-vanishing average field $\mathbb{e}_P$.

Let us now examine the effects of introducing dielectric material into a system. We shall first assume that the atoms or molecules comprising the dielectric material have a permanent electric dipole moment. If left to themselves, these permanent electric dipoles in a dielectric material never line up spontaneously, so that in the absence of any applied external electric field $\mathbb{p} = \boldsymbol{0}$ due to the random alignment of dipoles and the average electric field $\mathbb{e}_P$ is zero as well. However, when we place the dielectric material in an external field $\mathbb{e}_0$, the dipoles will tend to align in a direction close to $\mathbb{e}_0$. The effect is a net polarization $\mathbb{p}$ parallel to $\mathbb{e}_0$, and therefore an average electric field of the dipoles $\mathbb{e}_P$ anti-parallel to $\mathbb{e}_0$, i.e. that will tend to reduce the total electric field strength below $\mathbb{e}_0$. The total electric field $\mathbb{e}$ is the sum of these two fields

$$\mathbb{e} = \mathbb{e}_0 + \mathbb{e}_P . \tag{4.69}$$

In the case of a dielectric material where there are no permanent electric dipoles, a similar effect is observed due to the presence of an external field $\mathbb{e}_0$ which induces electric dipole moments in the atoms or molecules. These induced electric dipoles are parallel to $\mathbb{e}_0$, again leading to a polarization $\mathbb{p}$ parallel to $\mathbb{e}_0$, and a reduction of the total electric field strength.

5. Balance Equations for the Electro-Mechanics

The ultimate goal of this chapter is to derive the balance equations for the coupled electro-mechanical problem. The solution of those equations in combination with the constitutive equations gives us the independent electro-mechanical fields within the region under consideration. For more comprehensive treatments the reader is referred to LANDAU & LIFSCHITZ [88], PENFIELD & HAUS [125], HUTTER, VAN DE VEN AND URESCU [67], PAO [122], MAUGIN [99], ERINGEN AND MAUGIN [48], KOVETZ [87], DORFMAN AND OGDEN [40], BUSTAMANTE AND OGDEN [21]. Right at the beginning of our considerations we introduce a first simplification: *any relativistic effects are neglected.* Thus the most general framework of balance laws for continua consists of a combination of Maxwell's equations of classical electro-statics and the classical balance equations of the thermomechanics.

5.1. The Balance Laws of Mechanics

We start with the modified balance laws of mechanics. The integral expressions of the laws of conservation of mass, balance of momentum, moment of momentum and energy in the spatial and material description were derived in Section 3. Considering a generic part $\mathcal{P}_\mathcal{S}$ of the domain $\mathcal{S} \subset \mathbb{R}^3$ they read in the actual configuration:

conservation of mass

$$\frac{d}{dt} \int\limits_{\mathcal{P}_s} \rho \, dv = 0 \tag{5.1}$$

conservation of linear momentum

$$\frac{d}{dt} \int\limits_{\mathcal{P}_s} \rho \boldsymbol{v} \, dv = \int\limits_{\mathcal{P}_s} \rho \boldsymbol{\gamma} \, dv + \int\limits_{\partial\mathcal{P}_s} \boldsymbol{\sigma} \boldsymbol{n} \, da \tag{5.2}$$

conservation of angular momentum

$$\frac{d}{dt} \int\limits_{\mathcal{P}_s} \boldsymbol{x} \times \rho \boldsymbol{v} \, dv = \int\limits_{\mathcal{P}_s} (\boldsymbol{x} \times \rho \boldsymbol{\gamma} + \rho \boldsymbol{m}) \, dv + \int\limits_{\partial\mathcal{P}_s} \boldsymbol{x} \times \boldsymbol{\sigma} \boldsymbol{n} \, da \tag{5.3}$$

conservation of energy

$$\frac{d}{dt} \int\limits_{\mathcal{P}_s} (\frac{1}{2} \rho \boldsymbol{v} \cdot \boldsymbol{v}^* + \rho e) \, dv = \int\limits_{\mathcal{P}_s} (\rho \boldsymbol{\gamma} \cdot \boldsymbol{v}^* + \rho r) \, dv + \int\limits_{\partial\mathcal{P}_s} (\boldsymbol{\sigma} \boldsymbol{n} \cdot \boldsymbol{v}^* - \boldsymbol{q} \cdot \boldsymbol{n}) \, da \,. \tag{5.4}$$

Here, ρ is the mass density per unit volume, $\boldsymbol{\sigma}$ is the Cauchy stress tensor, $\boldsymbol{\gamma}$ is the total body force due to electric fields and external actions, $\boldsymbol{m}$ is the body couple, e is the internal energy per unit mass, $\boldsymbol{q}$ is the heat flux, r the total energy supply due to electromagnetic fields and to heat, and $\boldsymbol{n}$ the outward unit normal to $\partial\mathcal{P}_s$. It is assumed that body force, body couple and energy supply can be decomposed into two parts: one is due to the electric field and indicated with the superscript "e", the other is supposed to be externally applied and known from the outset and contradistinguished with a bar. Hence

$$\rho \boldsymbol{\gamma} = \rho \boldsymbol{\gamma}^e + \rho \bar{\boldsymbol{\gamma}} \qquad , \qquad \rho \boldsymbol{m} = \rho \boldsymbol{m}^e \qquad , \qquad \rho r = \rho r^e + \rho \bar{r} \,. \tag{5.5}$$

Here $\rho\boldsymbol{\gamma}^e$, $\rho\boldsymbol{m}^e$, and ρr^e are thought to be expressed in terms of electric field quantities while $\rho\bar{\boldsymbol{\gamma}}$ and $\rho\bar{r}$ are known. We have assumed that there are no externally applied body couples. If the considered fields are sufficiently smooth, the global balance equations (5.1) - (5.4) assume the local forms:

conservation of mass

$$\dot{\rho} + \rho \operatorname{div}[\boldsymbol{v}] = 0 \quad \text{in} \quad \mathcal{S} \tag{5.6}$$

conservation of linear momentum

$$\rho\dot{\boldsymbol{v}} = \operatorname{div}[\boldsymbol{\sigma}] + \rho\bar{\boldsymbol{\gamma}} + \rho\boldsymbol{\gamma}^e \quad \text{in} \quad \mathcal{S} \tag{5.7}$$

conservation of angular momentum

$$\operatorname{skew}[\boldsymbol{\sigma}] = \rho\hat{\boldsymbol{m}}^e \quad \text{in} \quad \mathcal{S} \tag{5.8}$$

conservation of energy

$$\rho\dot{e} = \boldsymbol{\sigma} : \boldsymbol{gl} - \operatorname{div}[\boldsymbol{q}] + \rho\bar{r} + \rho r^e \quad \text{in} \quad \mathcal{S}. \tag{5.9}$$

where use of (5.5) has been made. The second order tensor $\hat{\boldsymbol{m}}^e$ is the dual of the electric body couple $\boldsymbol{m}^e$ or $\boldsymbol{m}^e$ is the axial vector of $\hat{\boldsymbol{m}}^e$, i.e. for a generic vector $\boldsymbol{a}$, $\hat{\boldsymbol{m}}^e\boldsymbol{a} = \boldsymbol{m}^e \times \boldsymbol{a}$. As follows from (5.6), the present density is related to the density in the reference configuration ρ_0 by $J\rho = \rho_0$, with $J := \det[\boldsymbol{F}]$.

5.2. Reduced Maxwell's Equations

Before we get into equations, let us make a second assumption which means no loss of generality with respect to the problem that we are going to treat here: *the partial derivative of the magnetic induction and the magnetic induction itself can be neglected*, i.e.

$$\frac{\partial\mathbb{b}}{\partial t} \approx \boldsymbol{0} \quad \text{and} \quad \mathbb{b} = \boldsymbol{0} \quad \text{in} \quad \mathcal{S}. \tag{5.10}$$

Here, the first relation is the usual "electro-quasi-static" assumption. Additionally, static magnetic induction is disregarded for convenience by the second relation, as it allows to eliminate a magnetic dependence of the quantities $\rho\boldsymbol{\gamma}^e$, $\rho\boldsymbol{m}^e$ and ρr^e in the balance equations. In our case the assumption (5.10) is justified since the treated materials are really bad conductors. Thus, for weak electric currents the magnetic fields are taken to be negligible.

On the other hand, the idealization as perfect insulator is not necessarily adequate for actuator applications with a quasi-static rate of change of loading. In this case, there may be enough time for the migration of free charges due to external or depolarization electric fields to modify the electro-mechanical state of the body under consideration. Further the conduction current is assumed to vanish

$$\mathbb{j} = \boldsymbol{0} \quad \text{in} \quad \mathcal{S}. \tag{5.11}$$

As the main simplification, this assumption makes the conservation of the charge trivial. The balance equations for the electrostatic case, under the hypothesis of neglecting the magnetic field, are described by two equations which were described in Section 4

Gauß-Law

$$\int_{\mathcal{P}_s} \bar{\rho}^e \, dv = \int_{\partial \mathcal{P}_s} \mathrm{d} \cdot \boldsymbol{n} da \tag{5.12}$$

Faraday-Law

$$\int_{\boldsymbol{c}} \mathrm{e} \cdot d\boldsymbol{l} = 0 \tag{5.13}$$

with $\bar{\rho}^e$ volume free-charge density, d electric displacement vector, e electric field vector and $\boldsymbol{c}$ closed curve in $\mathcal{S}$. Again, assuming sufficient smoothness of the fields, the balance laws (5.12) and (5.13) may be brought into the following local forms

Gauß-Law

$$\mathrm{div}[\mathrm{d}] = \bar{\rho}^e \quad \text{in} \quad \mathcal{S} \tag{5.14}$$

Faraday-Law

$$\mathrm{curl}\,[\mathrm{e}] = \boldsymbol{0} \quad \text{in} \quad \mathcal{S}\,. \tag{5.15}$$

5.3. Material Description

The balance laws listed in the previous two subsections are written in the spatial or Eulerian formulation. Corresponding to these equations, there is a material or Lagrangian description. The following well known identities, introduced in Section 3, hold for transformations on infinitesimal volume, area, and line elements:

$$dv = JdV \quad , \quad d\boldsymbol{a} = J\boldsymbol{F}^{-T}d\boldsymbol{A} \quad , \quad d\boldsymbol{l} = \boldsymbol{F}d\boldsymbol{L}\,. \tag{5.16}$$

With (5.16) at hand, we can transform the balance laws (5.1)-(5.4) into the following forms:

conservation of mass

$$\frac{d}{dt}\int_{\mathcal{P}_B} \rho_0 dV = 0 \tag{5.17}$$

conservation of linear momentum

$$\frac{d}{dt}\int_{\mathcal{P}_B} \rho_0 \boldsymbol{V} dV = \int_{\partial \mathcal{P}_B} \boldsymbol{P}\boldsymbol{N} dA + \int_{\mathcal{P}_B} \rho_0 \boldsymbol{\Gamma} dV \tag{5.18}$$

conservation of angular momentum

$$\frac{d}{dt}\int_{\mathcal{P}_B} \rho_0 \boldsymbol{x} \times \boldsymbol{V} dV = \int_{\partial \mathcal{P}_B} \boldsymbol{x} \times \boldsymbol{P}\boldsymbol{N} dA + \int_{\mathcal{P}_B} \rho_0 (\boldsymbol{M} + \boldsymbol{x} \times \boldsymbol{\Gamma}) dV \tag{5.19}$$

conservation of energy

$$\frac{d}{dt}\int_{\mathcal{P}_B} (\frac{1}{2}\rho_0 \boldsymbol{V} \cdot \boldsymbol{V}^* + \rho_0 e) dV = \int_{\mathcal{P}_B} (\boldsymbol{V}^* \cdot \rho_0 \boldsymbol{\Gamma} + \rho_0 R) dV + \int_{\partial \mathcal{P}_B} (\boldsymbol{P}\boldsymbol{N} \cdot \boldsymbol{V}^* - \boldsymbol{Q} \cdot \boldsymbol{N}) dA\,. \tag{5.20}$$

Here, the integrations are performed over the reference volume $\mathcal{P}_\mathcal{B} \subset \mathcal{B}$ having surface $\partial \mathcal{P}_\mathcal{B}$ and outward normal $\boldsymbol{N}$. Further, $\boldsymbol{P}$ is the first Piola-Kirchhoff stress tensor, $\boldsymbol{Q}$ is the material energy flux vector, $\boldsymbol{\Gamma}$ is the material body force, $\boldsymbol{M}$ the material body couple, R the heat source in the reference configuration which are related to $\boldsymbol{\sigma}$, $\boldsymbol{q}$, $\boldsymbol{\gamma}$, $\boldsymbol{m}$, and r according to

$$
\begin{aligned}
\boldsymbol{P} &= J\boldsymbol{\sigma}\boldsymbol{F}^{-T} & , & & \boldsymbol{Q} &= J\boldsymbol{F}^{-1}\boldsymbol{q}\,, \\
\boldsymbol{\Gamma}(\boldsymbol{X},t) &= \boldsymbol{\gamma}(\boldsymbol{x},t) \circ \boldsymbol{\varphi}_t(\boldsymbol{X}) & , & & \boldsymbol{M}(\boldsymbol{X},t) &= \boldsymbol{m}(\boldsymbol{x},t) \circ \boldsymbol{\varphi}_t(\boldsymbol{X})\,, \quad (5.21) \\
R(\boldsymbol{X},t) &= r(\boldsymbol{x},t) \circ \boldsymbol{\varphi}_t(\boldsymbol{X})
\end{aligned}
$$

and ρ_0 is the density of mass in the reference configuration. Assuming for the external source terms decompositions similar to those listed in (5.5) and supposing sufficient smoothness of the fields involved, we find the following local forms of (5.18)-(5.20):

conservation of linear momentum

$$
\rho_0 \dot{\boldsymbol{V}} = \mathrm{Div}\,[\boldsymbol{P}] + \rho_0 \bar{\boldsymbol{\Gamma}} + \rho_0 \boldsymbol{\Gamma}^e \quad \text{in} \quad \mathcal{B} \tag{5.22}
$$

conservation of angular momentum

$$
\mathrm{skew}[\boldsymbol{P}\boldsymbol{F}^T] = \rho_0 \hat{\boldsymbol{M}}^e \quad \text{in} \quad \mathcal{B} \tag{5.23}
$$

conservation of energy

$$
\rho_0 \dot{e} = \boldsymbol{g}\boldsymbol{P} : \dot{\boldsymbol{F}} - \mathrm{Div}\,[\boldsymbol{Q}] + \rho_0 \bar{R} + \rho_0 R^e \quad \text{in} \quad \mathcal{B}\,. \tag{5.24}
$$

$\hat{\boldsymbol{M}}^e$ is the dual tensor of the electric body couple $\boldsymbol{M}^e$ in the reference configuration. Using (5.16) we can also transform the Gauß-Law (5.12) and Faraday-Law (5.13) obtaining

Gauß-Law

$$
\int_{\partial \mathcal{P}_B} \mathbb{D} \cdot \boldsymbol{N} dA = \int_{\mathcal{P}_B} \rho_0^e dV \tag{5.25}
$$

Faraday-Law

$$
\int_c \mathbb{E} \cdot d\boldsymbol{L} = 0\,. \tag{5.26}
$$

Here $\mathbb{D}$, $\mathbb{E}$ and ρ_0^e are the material counterparts of $\mathbb{d}$, $\mathbb{e}$ and $\bar{\rho}^e$ and are related as follows:

$$
J\mathbb{d} = \boldsymbol{F}\mathbb{D} \quad , \quad \mathbb{e} = \boldsymbol{F}^{-T}\mathbb{E} \quad , \quad J\bar{\rho}^e = \rho_0^e\,. \tag{5.27}
$$

Again, assuming sufficient smoothness of the fields, the balance laws (5.25) and (5.26) may be brought into the following local forms

Gauß-Law

$$
\mathrm{Div}[\mathbb{D}] = \rho_0^e \quad \text{in} \quad \mathcal{B} \tag{5.28}
$$

Faraday-Law

$$
\mathrm{Curl}\,[\mathbb{E}] = \boldsymbol{0} \quad \text{in} \quad \mathcal{B}\,. \tag{5.29}
$$
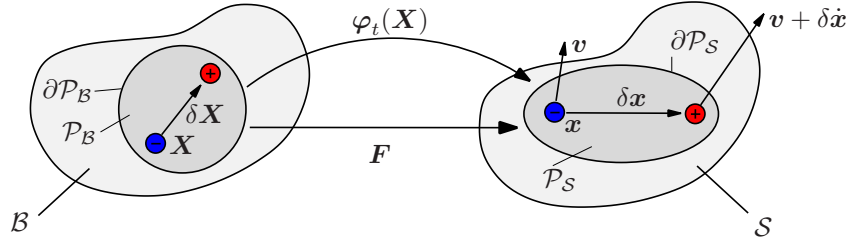
Figure 5.1: Moving body at the reference (material) configuration and the current (spatial) configuration and the dipoles within a volume element $\mathcal{P}_\mathcal{S}$.

5.4. Force, Couple, and Energy Supply

The body force $\boldsymbol{\gamma}^e$, couple $\boldsymbol{m}^e$, and energy supply r^e must be determined in terms of the electric field variables that satisfy a particular formulation of the Maxwell equations. In order to concentrate on the physical meaning of $\boldsymbol{\gamma}^e$, $\boldsymbol{m}^e$, and r^e, the different geometric nature of of the electric field $\mathbb{e}$, the electric displacement $\mathbb{d}$, and the polarization $\mathbb{p}$ is here neglected. There exist *several formulations* expressing those quantities. In this work, we follow the approach of postulating a model for the effect of polarization in moving matter. In particular we adopt the two-dipole model in the Chu formulation to evaluate the electric forces. We follow all the assumptions leading to the global laws for electromagnetism in moving matter step up from Chu based on the two-dipole model, see PAO & HUTTER [123, 124]. In addition, we assume that the forces acting on the charges of the electric dipoles are

$$\boldsymbol{f}_{q^e} = q^e \mathbb{e} + q^e \boldsymbol{v} \times (\mu_0 \mathbb{h}) \tag{5.30}$$

where q^e is the electric charge, $\mathbb{e}$ and $\mathbb{h}$ are the electric and magnetic fields inside a moving body, and $\boldsymbol{v}$ is the velocity of the material particle. The assumption of the force $\boldsymbol{f}_{q^e}$ has its origin in the Lorenz theory of electrons. The Lorentz force $\boldsymbol{f}_l$ is generally stated as

$$\boldsymbol{f}_l = q^e \mathbb{e} + \mathbb{j} \times (\mathbb{b}) , \tag{5.31}$$

valid for an electron with charge q^e moving with velocity $\boldsymbol{v}$ in free space ($\mathbb{j} = q^e \boldsymbol{v}$). Macroscopically, the first term in (5.31) is the definition of an electrostatic field $\mathbb{e}$ and the second term is the interaction force between the charge q^e moving with velocity $\boldsymbol{v}$ and the magnetic induction $\mathbb{b}$ in free space. Only in free space $\mathbb{b}$ and $\mu_0 \mathbb{h}$ coincide. Thus the adoption of the Lorentz's formula for macroscopic charges inside a continuum as in (5.30) is a postulate. Based on this two assumptions the body force $\boldsymbol{\gamma}^e$, body couple $\boldsymbol{m}^e$, and energy supply r^e can be calculated by an averaging and a limiting process.

5.4.1. Body Force

Let us consider the electric dipoles and let the negative charge q^e_- be at $\boldsymbol{x}$, the actual position of a material particle, while the positive charge q^e_+ is at $\boldsymbol{x} + \delta\boldsymbol{x}$ (cf. Figure 5.1). The respective velocities of the moving charges are

$$\boldsymbol{v}^e_- = \boldsymbol{v} \quad , \quad \boldsymbol{v}^e_+ = \boldsymbol{v} + \delta\dot{\boldsymbol{x}} . \tag{5.32}$$

Using (5.30) by means of a Taylor series expansion the force on the charge can be expressed

as

$$
\begin{aligned}
\boldsymbol{f}_{q_-^e} &= - && q^e \mathbb{e}(\boldsymbol{x}) - q^e \boldsymbol{v} \times \mu_0 \mathbb{h}(\boldsymbol{x}) \\
\boldsymbol{f}_{q_+^e} &= && q^e \mathbb{e}(\boldsymbol{x} + \delta\boldsymbol{x}) + q^e[\boldsymbol{v} + \delta\dot{\boldsymbol{x}}] \times \mu_0 \mathbb{h}(\boldsymbol{x} + \delta\boldsymbol{x}) \\
&= && q^e \mathbb{e}(\boldsymbol{x}) + q^e \delta\boldsymbol{x} \cdot \nabla_{\boldsymbol{x}} \mathbb{e}(\boldsymbol{x}) + q^e \boldsymbol{v} \times \mu_0 \mathbb{h}(\boldsymbol{x}) \\
&+ && q^e \boldsymbol{v} \times \mu_0 \nabla_{\boldsymbol{x}} \mathbb{h}(\boldsymbol{x}) \cdot \delta\boldsymbol{x} + q^e \delta\dot{\boldsymbol{x}} \times \mu_0 \mathbb{h}(\boldsymbol{x}) + \dots .
\end{aligned}
\tag{5.33}
$$

We consider a unit material volume element which contains N^e electric dipoles. No broken dipoles are taken under consideration. Since the force on each dipole is $\boldsymbol{f}_{q_+^e} + \boldsymbol{f}_{q_-^e}$ the total force on the volume element due to the polarization only is

$$
\rho\boldsymbol{\gamma}^p = \lim_{|\delta\boldsymbol{x}|\to 0} N^e(\boldsymbol{f}_{q_+^e} + \boldsymbol{f}_{q_-^e}) = [\nabla_{\boldsymbol{x}}\mathbb{e}]\,\mathbb{p} + \mu_0 \boldsymbol{v} \times [\nabla_{\boldsymbol{x}}\mathbb{h}]\,\mathbb{p} + \mu_0 \rho \frac{d}{dt}\left(\frac{\mathbb{p}}{\rho}\right) \times \mathbb{h}
\tag{5.34}
$$

with $\mathbb{p}$ polarization vector defined as

$$
\mathbb{p} = \lim_{|\delta\boldsymbol{x}|\to 0} N^e q^e \delta\boldsymbol{x} .
\tag{5.35}
$$

In addition to the force due to polarization, there is a force due to the free charge $\bar{\rho}^e$. Thus, the total force on an element of unit volume is

$$
\rho\boldsymbol{\gamma}^e = \bar{\rho}^e \mathbb{e} + \rho\boldsymbol{\gamma}^p .
\tag{5.36}
$$

For the quasi-static case ($\boldsymbol{v} \approx \boldsymbol{0}$) under consideration equation (5.36) reduces to

$$
\rho\boldsymbol{\gamma}^e = \bar{\rho}^e \mathbb{e} + [\nabla_{\boldsymbol{x}}\mathbb{e}]\,\mathbb{p} .
\tag{5.37}
$$

5.4.2. Body Couple

In an analogous manner the body couple $\boldsymbol{m}^e$ is determined. Since the position of the negative charge of an electric dipole is assumed to coincide with that of the material particle, the couple acting upon the particle may be determined by evaluating the torque exerted on the positive charges. From (5.33) follows that the torque on a unit volume with N^e electric dipoles for the quasi-static case is

$$
\rho\boldsymbol{m}^e = \lim_{|\delta\boldsymbol{x}|\to 0} N^e(\delta\boldsymbol{x} \times \boldsymbol{f}_{q_+^e}) = \mathbb{p} \times \mathbb{e} \qquad \text{or} \qquad \rho\hat{\boldsymbol{m}}^e = \text{skew}[\mathbb{p} \otimes \mathbb{e}] .
\tag{5.38}
$$

5.4.3. Energy Supply

The energy supply r^e is determined by evaluating the rate of work done on an electric dipole by the forces $\boldsymbol{f}_{q_-^e}$ and $\boldsymbol{f}_{q_+^e}$ in (5.33) for the N^e electric dipoles in the unit volume

$$
\rho r^e = \lim_{|\delta\boldsymbol{x}|\to 0} N^e \left(\boldsymbol{f}_{q_+^e} \cdot \boldsymbol{v}_+^e + \boldsymbol{f}_{q_-^e} \cdot \boldsymbol{v}_-^e\right) = \rho\mathbb{e} \cdot \frac{d}{dt}\left(\frac{\mathbb{p}}{\rho}\right) + [\nabla_{\boldsymbol{x}}\mathbb{e}]\,\mathbb{p} \cdot \boldsymbol{v} .
\tag{5.39}
$$

For the quasi-static case equation (5.39) reads

$$
\rho r^e = \rho\mathbb{e} \cdot \frac{d}{dt}\left(\frac{\mathbb{p}}{\rho}\right) .
\tag{5.40}
$$

5.5. Balance of Momentum Equations in Terms of Maxwell's Stress Tensor

It is often convenient to define the Maxwell stress tensor $\boldsymbol{\sigma}^M$ such that

$$\mathrm{div}[\boldsymbol{\sigma}^M] = \rho \boldsymbol{\gamma}^e \qquad \text{and} \qquad \mathrm{skew}[\boldsymbol{\sigma}^M] = \rho \hat{\boldsymbol{m}}^e \ . \tag{5.41}$$

With the introduction of $\boldsymbol{\sigma}^M$, the conservation of linear momentum, equation (5.7), can be rewritten as

$$\mathrm{div}[\boldsymbol{\sigma}^{tot}] + \rho \bar{\boldsymbol{\gamma}} = \rho \dot{\boldsymbol{v}} \qquad \text{with} \qquad \boldsymbol{\sigma}^{tot} = \boldsymbol{\sigma} + \boldsymbol{\sigma}^M \ . \tag{5.42}$$

The total stress $\boldsymbol{\sigma}^{tot}$ has the advantage of being symmetric, i.e. the balance of angular momentum, equation (5.8), takes the form

$$\mathrm{skew}[\boldsymbol{\sigma}^{tot}] = \boldsymbol{0} \ . \tag{5.43}$$

For the two-dipole model in the Chu formulation considered here the following form of the Maxwell stress tensor is formulated

$$\boldsymbol{\sigma}^M = \epsilon_0 \, \mathbb{e} \otimes \mathbb{e} + \mathbb{e} \otimes \mathbb{p} - \frac{1}{2}\epsilon_0 |\mathbb{e}|^2 \boldsymbol{1} = \mathbb{e} \otimes \mathbb{d} - \frac{1}{2}\epsilon_0 |\mathbb{e}|^2 \boldsymbol{1} \ . \tag{5.44}$$

It can be shown that by using the Gauß-Law $\mathrm{div}[\mathbb{d}] = \bar{\rho}^e$ and the definition of the polarization vector $\mathbb{d} = \epsilon_0 \mathbb{e} + \mathbb{p}$ one indeed obtains

$$\begin{aligned} \mathrm{div}[\boldsymbol{\sigma}^M] &= \mathrm{div}[\mathbb{d}] \, \mathbb{e} + (\nabla_{\boldsymbol{x}} \, \mathbb{e}) \, \mathbb{d} - (\nabla_{\boldsymbol{x}} \, \mathbb{e})^T \epsilon_0 \, \mathbb{e} \\ &= \bar{\rho}^e \mathbb{e} + (\nabla_{\boldsymbol{x}} \, \mathbb{e})^T (\mathbb{d} - \epsilon_0 \, \mathbb{e}) \\ &= \bar{\rho}^e \mathbb{e} + (\nabla_{\boldsymbol{x}} \, \mathbb{e})^T \mathbb{p} \ . \end{aligned} \tag{5.45}$$

In (5.45), the Faraday-Law $\mathrm{curl}[\mathbb{e}] = \boldsymbol{0}$ was used in the sense

$$\mathrm{curl}[\mathbb{e}] \times \boldsymbol{a} = (\nabla \mathbb{e} - \nabla \mathbb{e}^T)\boldsymbol{a} = \boldsymbol{0} \ . \tag{5.46}$$

It can be also confirmed that the above definition of the Maxwell stress tensor leads to a symmetric total stress, or by using the relation derived from (5.8) in combination with (5.38)$_2$

$$\boldsymbol{\sigma} - \boldsymbol{\sigma}^T = \mathbb{p} \otimes \mathbb{e} - \mathbb{e} \otimes \mathbb{p} \tag{5.47}$$

or

$$\boldsymbol{\sigma} + \mathbb{e} \otimes \mathbb{p} \qquad \text{symmetric} \ . \tag{5.48}$$

We have indeed

$$\boldsymbol{\sigma}^{tot} = \boldsymbol{\sigma} + \mathbb{e} \otimes \mathbb{p} + \epsilon_0 \, \mathbb{e} \otimes \mathbb{e} - \frac{1}{2} \, \epsilon_0 |\mathbb{e}|^2 \boldsymbol{1} \tag{5.49}$$

with $\epsilon_0 \, \mathbb{e} \otimes \mathbb{e} - \frac{1}{2} \epsilon_0 |\mathbb{e}|^2 \boldsymbol{1}$ symmetric. $\boldsymbol{\sigma}^{tot}$ has to be considered as total Cauchy stress tensor and obviously the modified balance equations (5.42) and (5.43) are written in the deformed configuration. In an analogous way, we can define a total first Piola stress

$$\boldsymbol{P}^{tot} = \boldsymbol{P} + \boldsymbol{P}^M \quad \text{with} \quad \boldsymbol{P}^M = \boldsymbol{F}^{-T}\mathbb{E} \otimes \mathbb{D} - \frac{1}{2}J\epsilon_0(\boldsymbol{C}^{-1} : \mathbb{E} \otimes \mathbb{E})\boldsymbol{F}^{-T} := J \, \boldsymbol{\sigma}^M \boldsymbol{F}^{-T} \tag{5.50}$$

and we can modify the balance of linear momentum and the balance of angular momentum in the reference configuration:

balance of linear momentum

$$\text{Div}\,[\boldsymbol{P}^{tot}] + \rho_0 \bar{\boldsymbol{\Gamma}} = \rho_0 \dot{\boldsymbol{V}} \quad \text{in} \quad \mathcal{B} \tag{5.51}$$

balance of angular momentum

$$\text{skew}[\boldsymbol{P}^{tot}\boldsymbol{F}^T] = \boldsymbol{0} \quad \text{in} \quad \mathcal{B}\,. \tag{5.52}$$

Notice that as consequence of neglecting the different geometric nature of the electric field ℯ, the electric displacement ⅆ, and the polarization ℗ as in Section 5.4, we automatically extended this assumption in giving the definition of the Maxwell stress tensors $\boldsymbol{\sigma}^M$ and $\boldsymbol{P}^M$. Since we intend to underline the geometrical aspects of the electro-mechanical formulation, the proper definition of the Maxwell stress tensors reads

$$\begin{aligned}
\boldsymbol{\sigma}^M &= (\boldsymbol{g}^{-1}ℯ) \otimes ⅆ - \tfrac{1}{2}\epsilon_0 |ℯ|^2_{\boldsymbol{g}^{-1}} \boldsymbol{g}^{-1} \qquad \text{and} \\
\boldsymbol{P}^M &= \boldsymbol{g}^{-1}\boldsymbol{F}^{-T}\mathbb{E} \otimes \mathbb{D} - \tfrac{1}{2}J\epsilon_0(\boldsymbol{C}^{-1}:\mathbb{E}\otimes\mathbb{E})\boldsymbol{g}^{-1}\boldsymbol{F}^{-T}
\end{aligned} \tag{5.53}$$

with $|ℯ|^2_{\boldsymbol{g}^{-1}} = (ℯ \otimes ℯ):\boldsymbol{g}^{-1}$ and $\boldsymbol{C}^{-1} = \boldsymbol{F}^{-1}\boldsymbol{g}^{-1}\boldsymbol{F}^{-T}$.

5.6. Jump Conditions

Across a surface of discontinuity within the boundary or across the boundary $\partial\mathcal{S}$, the fields ℯ and ⅆ have to satisfy certain continuity conditions. They are derived from the global Maxwell equations (5.28) and (5.29) considering limit of vanishing volume $\mathcal{P}_\mathcal{S}$ or surface enclosed by $\boldsymbol{c}$ across those discontinuity surfaces as in Section 4. Here, we do not consider internal surfaces of discontinuity and therefore the continuity conditions refer only to $\partial\mathcal{S}$. Then the continuity conditions satisfied by the electric field ℯ and electric displacement ⅆ are

$$[\![ℯ]\!] \times \boldsymbol{n} = \boldsymbol{0} \quad \text{and} \quad [\![ⅆ]\!] \cdot \boldsymbol{n} = \bar{\sigma}^e \quad \text{on} \quad \partial\mathcal{S} \tag{5.54}$$

with $\bar{\sigma}^e$ surface charge density. $[\![\Phi]\!] = \Phi^+ - \Phi^-$ denotes the jump of the quantity Φ across $\partial\mathcal{S}$. The positive side of the surface $\partial\mathcal{S}$ is defined by the direction of its outward normal $\boldsymbol{n}$. The jump conditions (5.54) could be simplified by following the assumptions of Section 4.

The boundary conditions associated to the equilibrium of linear momentum (5.42) is

$$\big[\!\big[\boldsymbol{\sigma}^{tot}\big]\!\big]\boldsymbol{n} = \boldsymbol{0} \quad \text{on} \quad \partial\mathcal{S}\,. \tag{5.55}$$

If $\bar{\boldsymbol{t}}$ is the applied traction per unit area on $\partial\mathcal{S}$, then the stress $\boldsymbol{\sigma}^{tot}$ calculated inside the material must satisfy

$$\boldsymbol{\sigma}^{tot}\boldsymbol{n} = \bar{\boldsymbol{t}} \quad \text{on} \quad \partial\mathcal{S}\,. \tag{5.56}$$

In general, $\bar{\boldsymbol{t}}$ may be prescribed on only part of $\partial\mathcal{S}$ indicated with $\partial\mathcal{S}_{\boldsymbol{t}}$. On the remanent part $\partial\mathcal{S}_{\boldsymbol{\varphi}}$ of $\partial\mathcal{S}$ the deformation path is prescribed.

The conditions (5.54)-(5.56) were written in the actual configuration. The counterpart of the jump condition (5.54) in the reference configuration are

$$[\![\mathbb{E}]\!] \times \boldsymbol{N} = \boldsymbol{0} \quad \text{and} \quad [\![\mathbb{D}]\!] \cdot \boldsymbol{N} = \bar{\Sigma}^e \quad \text{on} \quad \partial\mathcal{B} \tag{5.57}$$

where $\boldsymbol{N}$ is the outward normal on $\partial\mathcal{B}$ and $\bar{\Sigma}^e = \bar{\sigma}^e \circ \boldsymbol{\varphi}_t(\boldsymbol{X})$ is the prescribed surface charge density in the reference configuration. The traction boundary conditions associated with (5.51) and analogous to (5.55) are

$$\llbracket \boldsymbol{P}^{tot} \rrbracket \, \boldsymbol{N} = \boldsymbol{0} \quad \text{on} \quad \partial\mathcal{B}_{\boldsymbol{T}} \tag{5.58}$$

and equation (5.56) can be recast as

$$\boldsymbol{P}^{tot} \boldsymbol{N} = \bar{\boldsymbol{T}} \quad \text{on} \quad \partial\mathcal{B}_{\boldsymbol{T}} \tag{5.59}$$

where we used the Nanson's formula $\boldsymbol{n} da = J\boldsymbol{F}^{-T}\boldsymbol{N} dA$ relating area elements to define $\bar{\boldsymbol{T}}$ by $\bar{\boldsymbol{T}} dA = \bar{\boldsymbol{t}} da$ as the traction per unit of reference area.

5.7. The Entropy Production Inequality

It is a fact of experience that real physical processes are irreversible. This means that processes cannot, in general, be traversed back in time. This fact is called the second law of thermodynamics and its mathematical realization is the entropy production inequality. It is based on the assumption that there exists an additive quantity η, the entropy, which satisfy the balance

$$\int_{\mathcal{P}_S} \rho\gamma dv = \frac{d}{dt}\int_{\mathcal{P}_S} \rho\eta dv - \left(\int_{\mathcal{P}_S} \rho\frac{\bar{r}}{\theta} dv - \int_{\partial\mathcal{P}_S} \frac{\boldsymbol{q}\cdot\boldsymbol{n}}{\theta} da\right). \tag{5.60}$$

Here $\mathcal{P}_S \subset \mathcal{S}$ is part of the body $\mathcal{S}$ in the reference configuration, γ is the rate of entropy production, $\bar{r}/\theta$ the entropy supply, $(\boldsymbol{q}\cdot\boldsymbol{n})/\theta$ the entropy flux coinciding with the heat flux $\boldsymbol{q}\cdot\boldsymbol{n}$ over the absolute temperature θ. The second law of thermodynamics states that the irreversible part of the entropy rate γ is always positive. Thus for sufficiently smooth fields (5.60) implies the Clausius-Duhem-Inequality

$$\rho\gamma = \rho\dot{\eta} - \rho\frac{\bar{r}}{\theta} + \frac{1}{\theta}\operatorname{div}[\boldsymbol{q}] - \frac{1}{\theta^2}\boldsymbol{q}\cdot\nabla_{\boldsymbol{x}}\theta \geq 0. \tag{5.61}$$

The spatial dissipation is defined as the product of the rate of entropy production in (5.61) with the absolute temperature θ, i.e. $\rho\mathscr{D} = \rho\gamma\theta \geq 0$. Owing to the nature of terms in (5.61), it is common practice to additively split the dissipation into the local $\mathscr{D}_{loc}$ and $\mathscr{D}_{con}$ parts, $\mathscr{D} = \mathscr{D}_{loc} + \mathscr{D}_{con}$. We then require a stricter condition than (5.61) by demanding the positiveness of both terms $\mathscr{D}_{loc}$ and $\mathscr{D}_{con}$ separately. To this end, we introduce the Clausius-Planck-Inequality (CPI in the following),

$$\rho\mathscr{D}_{loc} := \rho\dot{\eta}\theta - (\rho\bar{r} - \operatorname{div}[\boldsymbol{q}]) \geq 0, \tag{5.62}$$

and the Fourier inequality (FI in the following)

$$\rho\mathscr{D}_{con} = -\frac{1}{\theta}\boldsymbol{q}\cdot\nabla_{\boldsymbol{x}}\theta \geq 0. \tag{5.63}$$

Incorporating the spatial energy balance equation (5.9) in the CPI (5.62) we get a formulation of this inequality in terms of the internal energy

$$\rho\mathscr{D}_{loc} := \boldsymbol{\sigma} : (\boldsymbol{g}\boldsymbol{l}) + \rho\dot{\eta}\theta + \rho r^e - \rho\dot{e} \geq 0. \tag{5.64}$$

The FI (5.63) and CPI (5.64) could be also written in the reference configuration

$$\begin{aligned}
\rho_0 \mathscr{D}_{con} &= -\frac{1}{\theta} \boldsymbol{Q} \cdot \nabla_{\boldsymbol{X}} \theta \geq 0, \\
\rho_0 \mathscr{D}_{loc} &= \boldsymbol{g} \boldsymbol{P} : \dot{\boldsymbol{F}} + \rho_0 \dot{\eta} \theta + \rho_0 R^e - \rho_0 \dot{e} \geq 0 \,.
\end{aligned} \tag{5.65}$$

By choosing the two-dipole model for the description of the electric body force, body couple and energy supply, it follows that

$$\begin{aligned}
\rho_0 R^e &= \rho_0 \mathbb{e} \cdot \left[\frac{d}{dt} \left(\frac{\mathbb{p}}{\rho} \right) \right] = \rho_0 \boldsymbol{F}^{-T} \mathbb{E} \cdot \left(\overline{\frac{\boldsymbol{F} \mathbb{P}}{J\rho}} \right) \\
&= \rho_0 \boldsymbol{F}^{-T} \mathbb{E} \cdot \frac{1}{\rho_0} (\overline{\boldsymbol{F} \mathbb{P}}) = \mathbb{E} \cdot \dot{\mathbb{P}} + \boldsymbol{F}^{-T} (\mathbb{E} \otimes \mathbb{P}) : \dot{\boldsymbol{F}}
\end{aligned} \tag{5.66}$$

which inserted into $(5.65)_2$ gives

$$\rho_0 \mathscr{D}_{loc} = [\boldsymbol{g} \boldsymbol{P} + \boldsymbol{F}^{-T} (\mathbb{E} \otimes \mathbb{P})] : \dot{\boldsymbol{F}} + \mathbb{E} \cdot \dot{\mathbb{P}} + \rho_0 \dot{\eta} \theta - \rho_0 \dot{e} \geq 0 \,. \tag{5.67}$$

By considering the rates appearing in the CPI (5.67), we can conclude that the internal energy is a thermodynamical potential depending primarily upon the deformation gradient $\boldsymbol{F}$, the entropy η, and the polarization $\mathbb{P}$, i.e. $e = \hat{e}(\boldsymbol{F}, \mathbb{P}, \eta, ...)$. Since the entropy η is not a measurable quantity, the internal energy is replaced usually by the Helmholtz free energy ψ and related to the former through a Legendre transformation

$$\psi = \sup_{\eta} \{ e - \theta \eta \} \,, \tag{5.68}$$

implying the functional dependence $\psi = \hat{\psi}(\boldsymbol{F}, \mathbb{P}, \theta, ...)$. Similarly other thermodynamical potentials could be considered. The version of the CPI in terms of Helmholtz free energy is obtained by inserting the partial Legendre transformation (5.68) into (5.67)

$$\rho_0 \mathscr{D}_{loc} = [\boldsymbol{g} \boldsymbol{P} + \boldsymbol{F}^{-T} (\mathbb{E} \otimes \mathbb{P})] : \dot{\boldsymbol{F}} + \mathbb{E} \cdot \dot{\mathbb{P}} - \rho_0 \eta \dot{\theta} - \rho_0 \dot{\psi} \geq 0 \,. \tag{5.69}$$

From now on we will confine our consideration to isothermal processes ($\dot{\theta} = 0$). For those processes the constitutive material response will be thermodynamically consistent if only the CPI (5.69) with $\theta = 0$ is verified, i.e.

$$\rho_0 \mathscr{D}_{loc} = [\boldsymbol{g} \boldsymbol{P} + \boldsymbol{F}^{-T} (\mathbb{E} \otimes \mathbb{P})] : \dot{\boldsymbol{F}} + \mathbb{E} \cdot \dot{\mathbb{P}} - \rho_0 \dot{\psi} \geq 0 \,. \tag{5.70}$$

We would like to use the last form of the CPI (5.70) to derive a thermodynamically consistent formulation of the constitutive equations based on the argumentation of COLEMAN & NOLL [33] and COLEMAN & GURTIN [32]. Being consistent with the principle of equipresence, we assume that the constitutive equations depend upon the same set of variables

$$\psi = \hat{\psi}(\boldsymbol{g}, \boldsymbol{F}, \mathbb{P}, \boldsymbol{\mathfrak{Q}}) \tag{5.71}$$

with $\boldsymbol{\mathfrak{Q}}$ set of Lagrangian internal variables, employed for the description of inelastic dissipative processes. The spatial metric $\boldsymbol{g}$ is needed to compute the deformation measures in the reference configurations. Based on this assumption, we can include the time derivative of the free energy function ψ, i.e. $\dot{\psi} = \partial_{\boldsymbol{F}} \psi : \dot{\boldsymbol{F}} + \partial_{\mathbb{P}} \psi \cdot \dot{\mathbb{P}} + \partial_{\boldsymbol{\mathfrak{Q}}} \psi \cdot \dot{\boldsymbol{\mathfrak{Q}}}$, in the CPI (5.70)

$$\rho_0 \mathscr{D}_{loc} = [\boldsymbol{g} \boldsymbol{P} + \boldsymbol{F}^{-T} (\mathbb{E} \otimes \mathbb{P}) - \rho_0 \partial_{\boldsymbol{F}} \psi] : \dot{\boldsymbol{F}} + [\mathbb{E} - \rho_0 \partial_{\mathbb{P}} \psi] \cdot \dot{\mathbb{P}} - \rho_0 \partial_{\boldsymbol{\mathfrak{Q}}} \psi \cdot \dot{\boldsymbol{\mathfrak{Q}}} \geq 0 \,. \tag{5.72}$$

Contending that the thermodynamic restriction should be fulfilled for an arbitrary rate of the deformation gradient $\boldsymbol{F}$ and of the polarization $\mathbb{P}$ we obtain the particular form of the constitutive equations

$$
\begin{aligned}
\boldsymbol{gP} &= \rho_0 \partial_{\boldsymbol{F}} \hat{\psi}(\boldsymbol{g}, \boldsymbol{F}, \mathbb{P}, \mathfrak{Q}) - \boldsymbol{F}^{-T}(\mathbb{E} \otimes \mathbb{P}) , \\
\mathbb{E} &= \rho_0 \partial_{\mathbb{P}} \hat{\psi}(\boldsymbol{g}, \boldsymbol{F}, \mathbb{P}, \mathfrak{Q})
\end{aligned}
\tag{5.73}
$$

which inserted into (5.72) gives the reduced form of local dissipation together with the definition of Lagrangian thermodynamical forces $\{\mathfrak{M}\}$, conjugated to the set $\{\mathfrak{Q}\}$ on the basis of the local dissipation, i.e.

$$
\rho_0 \mathscr{D}_{loc}^{red} := \mathfrak{M} \cdot \dot{\mathfrak{Q}} \geq 0 \quad \text{with} \quad \mathfrak{M} = -\rho_0 \partial_{\mathfrak{Q}} \hat{\psi}(\boldsymbol{g}, \boldsymbol{F}, \mathbb{P}, \mathfrak{Q}) .
\tag{5.74}
$$

We observe that the CPI (5.70) could be expressed in terms of the electro-mechanical power per unit volume $\rho_0 \mathscr{P}$ as

$$
\rho_0 \mathscr{D}_{loc} := \rho_0 \mathscr{P} - \rho_0 \dot{\psi} \geq 0 \quad \text{with} \quad \rho_0 \mathscr{P} = \left[\boldsymbol{gP} + \boldsymbol{F}^{-T}(\mathbb{E} \otimes \mathbb{P}) \right] : \dot{\boldsymbol{F}} + \mathbb{E} \cdot \dot{\mathbb{P}} .
\tag{5.75}
$$

(5.75) states that the difference between the electro-mechanical power $\rho_0 \mathscr{P}$ and the rate of the energy stored into the material is the rate of dissipated energy. The energy stored into the material could be expressed in terms of the mixed energy-enthalpy function ψ', related to the free energy function ψ through a partial Legendre transformation

$$
\psi' = \inf_{\mathbb{P}} \{ \psi - \mathbb{E} \cdot \mathbb{P} \}
\tag{5.76}
$$

which inserted into (5.75) gives

$$
\begin{aligned}
\rho_0 \mathscr{D}_{loc} &:= \rho_0 \mathscr{P}' - \rho_0 \dot{\psi}' \geq 0 \\
\rho_0 \mathscr{P}' &:= \rho_0 \mathscr{P} - \frac{d}{dt}(\mathbb{E} \cdot \mathbb{P}) = [\boldsymbol{gP} + \boldsymbol{F}^{-T}(\mathbb{E} \otimes \mathbb{P})] : \dot{\boldsymbol{F}} - \mathbb{P} \cdot \dot{\mathbb{E}} .
\end{aligned}
\tag{5.77}
$$

Exploiting $(5.77)_1$ with the Coleman-Noll-Gurtin arguments we get the set of thermodynamically consistent constitutive equations

$$
\begin{aligned}
\boldsymbol{gP} &= \rho_0 \partial_{\boldsymbol{F}} \hat{\psi}'(\boldsymbol{g}, \boldsymbol{F}, \mathbb{E}, \mathfrak{Q}) - \boldsymbol{F}^{-T}(\mathbb{E} \otimes \mathbb{P}) , \\
\mathbb{P} &= -\rho_0 \partial_{\mathbb{E}} \hat{\psi}'(\boldsymbol{g}, \boldsymbol{F}, \mathbb{E}, \mathfrak{Q}) , \\
\mathfrak{M} &= -\rho_0 \partial_{\mathfrak{Q}} \hat{\psi}'(\boldsymbol{g}, \boldsymbol{F}, \mathbb{E}, \mathfrak{Q}) .
\end{aligned}
\tag{5.78}
$$

We would now like to consider an amended energy balance $(5.77)_1$ which takes also the electrostatic energy stored in the free space underlying the domain under consideration. To this purpose, we consider the modified thermodynamical potential

$$
\rho_0 \psi'_{amnd} = \rho_0 \psi' + \rho_0 u^e
\tag{5.79}
$$

with $\rho_0 u^e$ electrostatic energy in the reference configuration in the form of a mixed energy-enthalpy functional, derived from the true expression in the actual configuration ρu^e

$$
\begin{aligned}
\rho u^e &= -\frac{1}{2} \epsilon_0 \boldsymbol{g}^{-1} : (\mathbb{e} \otimes \mathbb{e}), \\
\rho_0 u^e &= J \rho u^e = -\frac{1}{2} J \epsilon_0 \boldsymbol{C}^{-1} : (\mathbb{E} \otimes \mathbb{E}) .
\end{aligned}
\tag{5.80}
$$

The rate of the electrostatic energy $\rho_0 u^e$

$$\rho \dot{u}^e = \left[-\frac{1}{2}\epsilon_0 J(\boldsymbol{C}^{-1} : \mathbb{E} \otimes \mathbb{E})\boldsymbol{F}^{-T} + \epsilon_0 J\boldsymbol{F}^{-T}(\mathbb{E} \otimes \boldsymbol{C}^{-1}\mathbb{E}) \right] : \dot{\boldsymbol{F}} - (\epsilon_0 J\boldsymbol{C}^{-1}\mathbb{E}) \cdot \dot{\mathbb{E}}, \quad (5.81)$$

should be entirely compensated by a counterpart in the extend electro-mechanical power $\rho_0 \mathscr{P}'_{amnd}$ derived from $\rho_0 \mathscr{P}'$ as

$$\rho_0 \mathscr{P}'_{amnd} = \rho_0 \mathscr{P}' + \rho \dot{u}^e = \boldsymbol{g}\boldsymbol{P}^{tot} : \dot{\boldsymbol{F}} - \mathbb{D} \cdot \dot{\mathbb{E}}. \quad (5.82)$$

Recalling the definition of the polarization vector and of the Maxwell stress tensor in the reference configuration

$$\begin{aligned} \mathbb{D} &= \mathbb{P} + \epsilon_0 J\boldsymbol{C}^{-1}\mathbb{E}, \\ \boldsymbol{g}\boldsymbol{P}^M &= \boldsymbol{F}^{-T}(\mathbb{E} \otimes \mathbb{D}) - \frac{1}{2}\epsilon_0 J(\boldsymbol{C}^{-1} : \mathbb{E} \otimes \mathbb{E})\boldsymbol{F}^{-T}, \end{aligned} \quad (5.83)$$

we can indeed write the amended electro-mechanical power in terms of the total first Piola stress tensor $\boldsymbol{P}^{tot} = \boldsymbol{P} + \boldsymbol{P}^M$ and of the electric displacement $\mathbb{D}$. The CPI in terms of the amended quantities then will read

$$\rho_0 \mathscr{D}_{loc} = \rho_0 \mathscr{P}'_{amnd} - \rho_0 \dot{\psi}'_{amnd} = \boldsymbol{g}\boldsymbol{P}^{tot} : \dot{\boldsymbol{F}} - \mathbb{D} \cdot \dot{\mathbb{E}} - \rho_0 \dot{\psi}'_{amnd} \geq 0. \quad (5.84)$$

From (5.84) we can conclude that the amended mixed energy-enthalpy ψ'_{amnd} depends upon the deformation gradient $\boldsymbol{F}$, the electric field $\mathbb{E}$ and the set of internal variables $\{\boldsymbol{\mathfrak{Q}}\}$ and its derivatives with respect to those arguments give the thermodynamically consistent constitutive equations for the total first Piola stress tensor $\boldsymbol{P}^{tot}$, the electric displacement $\mathbb{D}$, and the internal forces, $\{\boldsymbol{\mathfrak{M}}\}$ respectively

$$\begin{aligned} \boldsymbol{g}\boldsymbol{P}^{tot} &= \rho_0 \partial_{\boldsymbol{F}} \psi'_{amnd}(\boldsymbol{g}, \boldsymbol{F}, \mathbb{E}, \boldsymbol{\mathfrak{Q}}), \\ \mathbb{D} &= -\rho_0 \partial_{\mathbb{E}} \psi'_{amnd}(\boldsymbol{g}, \boldsymbol{F}, \mathbb{E}, \boldsymbol{\mathfrak{Q}}), \\ \boldsymbol{\mathfrak{M}} &= -\rho_0 \partial_{\boldsymbol{\mathfrak{Q}}} \psi'_{amnd}(\boldsymbol{g}, \boldsymbol{F}, \mathbb{E}, \boldsymbol{\mathfrak{Q}}). \end{aligned} \quad (5.85)$$

By considering a partial Legendre transformation of ψ'_{amnd} with respect to the electric slot, we obtain an amended free energy

$$\psi_{amnd} = \sup_{\mathbb{E}}\{\psi'_{amnd} + \mathbb{D} \cdot \mathbb{E}\} \quad \text{with} \quad \psi_{amnd} = \hat{\psi}(\boldsymbol{g}, \boldsymbol{F}, \mathbb{D}, \boldsymbol{\mathfrak{Q}}). \quad (5.86)$$

In terms of the amended free energy ψ_{amnd} the CPI would be written as

$$\rho_0 \mathscr{D}_{loc} = \rho_0 \mathscr{P}_{amnd} - \rho_0 \dot{\psi}_{amnd} \geq 0 \quad \text{with} \quad \rho_0 \mathscr{P}_{amnd} = \boldsymbol{g}\boldsymbol{P}^{tot} : \dot{\boldsymbol{F}} + \mathbb{E} \cdot \dot{\mathbb{D}}. \quad (5.87)$$

Exploitation of (5.87) with the usage of Coleman-Noll-Gurtin's arguments yields the following set of thermodynamically consistent constitutive equations

$$\begin{aligned} \boldsymbol{g}\boldsymbol{P}^{tot} &= \rho_0 \partial_{\boldsymbol{F}} \psi_{amnd}(\boldsymbol{g}, \boldsymbol{F}, \mathbb{D}, \boldsymbol{\mathfrak{Q}}), \\ \mathbb{E} &= \rho_0 \partial_{\mathbb{D}} \psi_{amnd}(\boldsymbol{g}, \boldsymbol{F}, \mathbb{D}, \boldsymbol{\mathfrak{Q}}), \\ \boldsymbol{\mathfrak{M}} &= -\rho_0 \partial_{\boldsymbol{\mathfrak{Q}}} \psi_{amnd}(\boldsymbol{g}, \boldsymbol{F}, \mathbb{D}, \boldsymbol{\mathfrak{Q}}). \end{aligned} \quad (5.88)$$

The forms (5.84) and (5.87) represent the starting point for our successive formulation which will take into account only the total stresses and the electric displacement. Once

the field equations are solved, the Maxwell stress tensor and the polarization vector can be determined as post processing by using the proper definition. For the sake of clarity we will not use anymore in the following the subscript "amnd" and the superscript "tot".

The electro-mechanical stress power per unit of reference volume $\rho_0 \mathscr{P}$ and $\rho_0 \mathscr{P}'$ could be written alternatively in terms of the second Piola-Kirchhoff stress $\boldsymbol{S}$ and the rate of the Cauchy-Green strain tensor $\boldsymbol{C}$. We have in fact

$$
\begin{aligned}
\rho_0 \mathscr{P} &= \boldsymbol{g}\boldsymbol{P} : \dot{\boldsymbol{F}} + \mathbb{E} \cdot \dot{\mathbb{D}} = \boldsymbol{S} : \frac{1}{2}\dot{\boldsymbol{C}} + \mathbb{E} \cdot \dot{\mathbb{D}} \\
\rho_0 \mathscr{P}' &= \boldsymbol{g}\boldsymbol{P} : \dot{\boldsymbol{F}} - \mathbb{D} \cdot \dot{\mathbb{E}} = \boldsymbol{S} : \frac{1}{2}\dot{\boldsymbol{C}} - \mathbb{D} \cdot \dot{\mathbb{E}} \,.
\end{aligned}
\tag{5.89}
$$

Thus, we could define the set of constitutive equations in terms of a free energy $\psi = \tilde{\psi}(\boldsymbol{C}, \mathbb{D}, \boldsymbol{\mathfrak{Q}})$ as

$$
\boldsymbol{S} := 2\rho_0 \partial_{\boldsymbol{C}} \tilde{\psi}(\boldsymbol{C}, \mathbb{D}, \boldsymbol{\mathfrak{Q}}), \quad \mathbb{E} := \rho_0 \partial_{\mathbb{D}} \tilde{\psi}(\boldsymbol{C}, \mathbb{D}, \boldsymbol{\mathfrak{Q}}), \quad \mathfrak{M} := -\rho_0 \partial_{\boldsymbol{\mathfrak{Q}}} \tilde{\psi}(\boldsymbol{C}, \mathbb{D}, \boldsymbol{\mathfrak{Q}}), \tag{5.90}
$$

or in terms of the mixed energy-enthalpy $\psi' = \tilde{\psi}'(\boldsymbol{C}, \mathbb{E}, \boldsymbol{\mathfrak{Q}})$

$$
\boldsymbol{S} := 2\rho_0 \partial_{\boldsymbol{C}} \tilde{\psi}'(\boldsymbol{C}, \mathbb{E}, \boldsymbol{\mathfrak{Q}}), \quad \mathbb{D} := -\rho_0 \partial_{\mathbb{E}} \tilde{\psi}'(\boldsymbol{C}, \mathbb{E}, \boldsymbol{\mathfrak{Q}}), \quad \mathfrak{M} := -\rho_0 \partial_{\boldsymbol{\mathfrak{Q}}} \tilde{\psi}'(\boldsymbol{C}, \mathbb{E}, \boldsymbol{\mathfrak{Q}}) \,.
\tag{5.91}
$$

An alternative representation of the stress power $\rho_0 \mathscr{P}$ and $\rho_0 \mathscr{P}'$ would be in terms of the Kirchhoff stresses $\boldsymbol{\tau}$, the rate of the geometric mapping $\boldsymbol{g}$, the electric field e in the current configuration, and the rate of the current electric displacement d or vice versa in terms of d and the rate of e. We have indeed

$$
\begin{aligned}
\rho_0 \mathscr{P} &= \boldsymbol{S} : \tfrac{1}{2}\dot{\boldsymbol{C}} + \mathbb{E} \cdot \dot{\mathbb{D}} = \boldsymbol{F}\boldsymbol{S}\boldsymbol{F}^T : \tfrac{1}{2} \boldsymbol{F}^{-T}\dot{\boldsymbol{C}}\boldsymbol{F}^{-1} + \boldsymbol{F}^{-T}\mathbb{E} \cdot \boldsymbol{F}\dot{\mathbb{D}} \\
&= \boldsymbol{\tau} : \tfrac{1}{2} \boldsymbol{\mathcal{L}}_{\boldsymbol{v}}(\boldsymbol{g}) + \mathrm{e} \cdot \boldsymbol{\mathcal{L}}_{\boldsymbol{v}}(\tilde{\mathrm{d}}) \\
\rho_0 \mathscr{P}' &= \boldsymbol{S} : \tfrac{1}{2}\dot{\boldsymbol{C}} - \mathbb{D} \cdot \dot{\mathbb{E}} = \boldsymbol{F}\boldsymbol{S}\boldsymbol{F}^T : \tfrac{1}{2} \boldsymbol{F}^{-T}\dot{\boldsymbol{C}}\boldsymbol{F}^{-1} - \boldsymbol{F}\mathbb{D} \cdot \boldsymbol{F}^{-T}\dot{\mathbb{E}} \\
&= \boldsymbol{\tau} : \tfrac{1}{2} \boldsymbol{\mathcal{L}}_{\boldsymbol{v}}(\boldsymbol{g}) - \tilde{\mathrm{d}} \cdot \boldsymbol{\mathcal{L}}_{\boldsymbol{v}}(\mathrm{e})
\end{aligned}
\tag{5.92}
$$

with $\tilde{\mathrm{d}} = J\mathrm{d}$ being a Kirchhoff-type electric displacement. The Lie derivative of a spatial object is geometrically defined as the push-forward of the material time derivative of its pull-back, that is

$$
\boldsymbol{\mathcal{L}}_{\boldsymbol{v}}(\bullet) := \boldsymbol{\varphi}_* \left(\frac{d}{dt} \boldsymbol{\varphi}^*(\bullet) \right) \,.
\tag{5.93}
$$

With this definition at hand, the rate of deformation tensor $\boldsymbol{d}$, the rate of the electric displacement $\boldsymbol{\mathcal{L}}_{\boldsymbol{v}}(\tilde{\mathrm{d}})$, and the rate of the electric field $\boldsymbol{\mathcal{L}}_{\boldsymbol{v}}(\mathrm{e})$ can be computed as follows

$$
\begin{aligned}
\boldsymbol{\mathcal{L}}_{\boldsymbol{v}}(\boldsymbol{g}) &= \boldsymbol{\varphi}_* \left(\frac{d}{dt} \boldsymbol{\varphi}^*(\boldsymbol{g}) \right) = \boldsymbol{\varphi}_* \left(\frac{d}{dt}\boldsymbol{C} \right) = (\boldsymbol{g}\boldsymbol{l} + \boldsymbol{l}^T \boldsymbol{g}) = 2\boldsymbol{d} \\
\boldsymbol{\mathcal{L}}_{\boldsymbol{v}}(\tilde{\mathrm{d}}) &= \boldsymbol{\varphi}_* \left(\frac{d}{dt} \boldsymbol{\varphi}^*(\tilde{\mathrm{d}}) \right) = \boldsymbol{\varphi}_* \left(\frac{d}{dt}\mathbb{D} \right) = \boldsymbol{F}\dot{\mathbb{D}} \\
\boldsymbol{\mathcal{L}}_{\boldsymbol{v}}(\mathrm{e}) &= \boldsymbol{\varphi}_* \left(\frac{d}{dt} \boldsymbol{\varphi}^*(\mathrm{e}) \right) = \boldsymbol{\varphi}_* \left(\frac{d}{dt}\mathbb{E} \right) = \boldsymbol{F}^{-T}\dot{\mathbb{E}} \,.
\end{aligned}
\tag{5.94}
$$

According to the expressions (5.92), we could define the set of constitutive equations in terms of the free energy $\psi = \bar{\psi}(\boldsymbol{g}; \boldsymbol{F}, \tilde{\mathrm{d}}, \mathbf{q})$ or in terms of the mixed energy-enthalpy $\psi' = \bar{\psi}'(\boldsymbol{g}; \boldsymbol{F}, \mathrm{e}, \mathbf{q})$

$$\boldsymbol{\tau} := 2\rho_0 \partial_{\boldsymbol{g}} \bar{\psi}(\boldsymbol{g}; \boldsymbol{F}, \tilde{\mathrm{d}}, \mathbf{q}), \quad \mathrm{e} := \rho_0 \partial_{\mathrm{d}} \bar{\psi}(\boldsymbol{g}; \boldsymbol{F}, \tilde{\mathrm{d}}, \mathbf{q}), \quad \mathfrak{m} := -\rho_0 \partial_{\mathbf{q}} \bar{\psi}(\boldsymbol{g}; \boldsymbol{F}, \tilde{\mathrm{d}}, \mathbf{q}), \quad (5.95)$$

or

$$\boldsymbol{\tau} := 2\rho_0 \partial_{\boldsymbol{g}} \bar{\psi}'(\boldsymbol{g}; \boldsymbol{F}, \mathrm{e}, \mathbf{q}), \quad \tilde{\mathrm{d}} := -\rho_0 \partial_{\mathrm{e}} \bar{\psi}'(\boldsymbol{g}; \boldsymbol{F}, \mathrm{e}, \mathbf{q}), \quad \mathfrak{m} := -\rho_0 \partial_{\mathbf{q}} \bar{\psi}'(\boldsymbol{g}; \boldsymbol{F}, \mathrm{e}, \mathbf{q}). \quad (5.96)$$

with $\{\mathbf{q}\}$ set of Eulerian internal variables and $\{\mathfrak{m}\}$ dual Eulerian set of internal forces. The alternative expressions of the electro-mechanical power manifest the distinct work conjugate couples

$$\left(\{\boldsymbol{gP}, \mathbb{E}\}; \{\dot{\boldsymbol{F}}, \dot{\mathbb{D}}\} \right), \quad \left(\{\boldsymbol{S}, \mathbb{E}\}; \{\tfrac{1}{2}\dot{\boldsymbol{C}}, \dot{\mathbb{D}}\} \right), \quad \left(\{\boldsymbol{\tau}, \mathrm{e}\}; \{\tfrac{1}{2}\boldsymbol{\mathcal{L}}_{\boldsymbol{v}}(\boldsymbol{g}), \boldsymbol{\mathcal{L}}_{\boldsymbol{v}}(\tilde{\mathrm{d}})\} \right), \quad (5.97)$$

or

$$\left(\{\boldsymbol{gP}, \mathbb{D}\}; \{\dot{\boldsymbol{F}}, \dot{\mathbb{E}}\} \right), \quad \left(\{\boldsymbol{S}, \mathbb{D}\}; \{\tfrac{1}{2}\dot{\boldsymbol{C}}, \dot{\mathbb{E}}\} \right), \quad \left(\{\boldsymbol{\tau}, \tilde{\mathrm{d}}\}; \{\tfrac{1}{2}\boldsymbol{\mathcal{L}}_{\boldsymbol{v}}(\boldsymbol{g}), \boldsymbol{\mathcal{L}}_{\boldsymbol{v}}(\mathrm{e})\} \right), \quad (5.98)$$

with respect to the representation in terms of $\mathscr{P}$ or $\mathscr{P}'$, respectively. As we will understand in the following, (5.97) are the "physical" work conjugate couples, while (5.98) are the "geometrical" work conjugate couples.

5.8. Small Deformations

While dealing with materials like piezoceramics we are usually confronted with electrically and mechanically induced strains which do not exceed the order of magnitude of one percent. Thus if we consider the polar decomposition of the deformation gradient $\boldsymbol{F} = \boldsymbol{RU}$, the right stretch tensor $\boldsymbol{U}$ will be approximatively equal to the unit tensor, $\boldsymbol{U} \approx \boldsymbol{1}$, and this implies that the deformation gradient nearly coincides with the rotation tensor $\boldsymbol{F} \approx \boldsymbol{R}$. This assumption would result already in a simplification of the above derived balance and constitutive equations. However, we can employ the classical small deformation assumption leading to a geometrically linear theory

$$\boldsymbol{F} = \boldsymbol{RU} \approx \boldsymbol{1} \quad , \quad \boldsymbol{R} \approx \boldsymbol{1} \quad , \quad \boldsymbol{U} \approx \boldsymbol{1}. \quad (5.99)$$

It must be noted that the exclusion of the finite rotations may be not appropriate for the case of bending devices, where finite rotations may occur even though stretches are small.

The small deformation assumptions (5.99) imply an approximate coincidence of the reference and actual configurations, $\boldsymbol{x} \approx \boldsymbol{X}$ and consequently a constant mass density, $\dot{\rho} \approx 0$ and $\mathrm{div}[\boldsymbol{v}] \ll 1$. Thus, material and spatial space and time derivatives are no longer distinguished. Further, there is no need to geometrically distinguish between strain measures and stress tensors. The strain measures are replaced by the small strain tensor

$$\boldsymbol{\varepsilon} := \tfrac{1}{2}\left(\nabla \boldsymbol{u} + \nabla^T \boldsymbol{u} \right) \quad (5.100)$$

with $\boldsymbol{u} = \boldsymbol{\varphi}_t(\boldsymbol{X}) - \boldsymbol{X}$ displacement vector and consequently the nonlinear terms are dropped to yield a linear geometrical setting. The stresses are represented through the true Cauchy stress tensor $\boldsymbol{\sigma}$. Additionally we describe the electric balance and constitutive

equations in terms of the physically existent electric field in the actual configuration $\mathbb{e}$ and the Eulerian electric displacement $\mathbb{d}$.

The relevant equations in the local form for the geometrically linear setting are summarized as follows:

Gauß -Law

$$\mathrm{div}[\mathbb{d}] = \bar{\rho}^e \tag{5.101}$$

Farady-Law

$$\mathrm{curl}[\mathbb{e}] = \boldsymbol{0} \tag{5.102}$$

balance of linear momentum

$$\mathrm{div}[\boldsymbol{\sigma}] + \rho\bar{\boldsymbol{\gamma}} = \rho\dot{\boldsymbol{v}} \tag{5.103}$$

balance of angular momentum

$$\boldsymbol{\sigma} = \boldsymbol{\sigma}^T \tag{5.104}$$

balance of energy

$$\rho\dot{e} = \boldsymbol{\sigma} : \dot{\boldsymbol{\varepsilon}} + \mathbb{e} \cdot \dot{\mathbb{d}} - \mathrm{div}[\boldsymbol{q}] + \rho\bar{r} \tag{5.105}$$

Clausius-Plank-Inequality (CPI)

$$\rho\mathscr{D}_{loc} = \boldsymbol{\sigma} : \dot{\boldsymbol{\varepsilon}} + \mathbb{e} \cdot \dot{\mathbb{d}} + \rho\theta\dot{\eta} - \rho\dot{e} \geq 0 \tag{5.106}$$

Fourier-Inequality (FI)

$$\rho\mathscr{D}_{con} = -\frac{1}{\theta}\boldsymbol{q} \cdot \nabla\theta \geq 0 \,. \tag{5.107}$$

Observe that the considered stress is the total stress $\boldsymbol{\sigma}^{tot}$ which is the sum of the purely mechanical stress $\boldsymbol{\sigma}$ and of the Maxwell stress $\boldsymbol{\sigma}^M$

$$\boldsymbol{\sigma}^{tot} = \boldsymbol{\sigma} + \boldsymbol{\sigma}^M \qquad \text{with} \qquad \boldsymbol{\sigma}^M = \mathbb{e} \otimes \mathbb{d} - \frac{1}{2}\epsilon_0|\mathbb{e}|^2\boldsymbol{1} \,. \tag{5.108}$$

Further, the considered internal energy is the amended one, sum of the energy stored in the body and the electrostatic energy stored in the free space. By restricting our considerations to the isothermal case, we can formulate the CPI in terms of the free energy $\psi = \hat{\psi}(\boldsymbol{\varepsilon}, \mathbb{d}, \mathbf{q})$

$$\rho\mathscr{D}_{loc} = \rho\mathscr{P} - \rho\dot{\psi} \geq 0 \qquad \text{with} \qquad \rho\mathscr{P} = \boldsymbol{\sigma} : \dot{\boldsymbol{\varepsilon}} + \mathbb{e} \cdot \dot{\mathbb{d}} \tag{5.109}$$

with $\rho\mathscr{P}$ rate of the electro-mechanical work. Exploitation of (5.109) using the Coleman-Noll-Gurtin's arguments yields to the set of thermodynamically consistent constitutive equations

$$\boldsymbol{\sigma} := \rho\partial_{\boldsymbol{\varepsilon}}\hat{\psi}(\boldsymbol{\varepsilon}, \mathbb{d}, \mathbf{q}), \quad \mathbb{e} := \rho\partial_{\mathbb{d}}\hat{\psi}(\boldsymbol{\varepsilon}, \mathbb{d}, \mathbf{q}), \quad \mathfrak{m} := -\rho\partial_{\mathbf{q}}\hat{\psi}(\boldsymbol{\varepsilon}, \mathbb{d}, \mathbf{q}) \,. \tag{5.110}$$

By considering a partial Legendre transformation of the free energy function ψ with respect to the electric slot we obtain the mixed energy-enthalpy function $\psi' = \sup_{\mathbb{d}}\{\psi - \mathbb{d} \cdot \mathbb{e}\}$ in terms of which the CPI reads

$$\rho\mathscr{D}_{loc} = \rho\mathscr{P}' - \rho\dot{\psi}' \geq 0 \qquad \text{with} \qquad \rho\mathscr{P}' = \boldsymbol{\sigma} : \dot{\boldsymbol{\varepsilon}} - \mathbb{d} \cdot \dot{\mathbb{e}} \tag{5.111}$$

which exploited with the Coleman-Noll-Gurtin procedure yields to a modified set of thermodynamically consistent constitutive equations

$$\boldsymbol{\sigma} := \rho\partial_{\boldsymbol{\varepsilon}}\hat{\psi}'(\boldsymbol{\varepsilon}, \mathbb{e}, \mathbf{q}), \quad \mathbb{d} := -\rho\partial_{\mathbb{e}}\hat{\psi}'(\boldsymbol{\varepsilon}, \mathbb{e}, \mathbf{q}), \quad \mathfrak{m} := -\rho\partial_{\mathbf{q}}\hat{\psi}'(\boldsymbol{\varepsilon}, \mathbb{e}, \mathbf{q}) \,, \tag{5.112}$$

which will be taken under consideration in the following.

6. Variational Formulation in Electro-Mechanics

The goal of this chapter is the discussion of a variational formulation for a generic dissipative electro-mechanical response. At first we will concentrate on a purely *local* constitutive modeling and afterwards focus on the *global* treatment of a multifield boundary-value-problem. Our considerations will be directed to the formalization of the coupled electro-mechanical boundary-value-problem through an energetical description. The arguments derived here are mainly based on the concepts found in MIEHE [109]. See also NOWAKI [118], MIEHE [108], MIEHE, SCHOTTE AND LAMBRECHT [110], MCMEEKING & LANDIS [103], MCMEEKING, LANDIS AND JIMENEZ [104], MIELKE & TIMOFTE [111, 112].

6.1. Local Constitutive Variational Principle

We focus first on a local volume element of the solid which undergoes an electro-mechanical loading. The *choice of the independent variables* characterizing the local material response of an electro-mechanically coupled solid can be based on two different approaches: a *physically-based* approach which differentiate between actions and reactions and a *geometry-based* approach which considers dual objects in the geometric setting. The first type of approach yields in general to a minimization structure of the electro-mechanical boundary-value-problem, while the geometry-based approach delivers normally a saddle-point structure, see MIEHE [109].

We consider in this work a formulation of the local constitutive material response based on a set of independent variables which have a geometric character. In particular we consider a description in terms of *generalized vectors* and *generalized covectors*. Generalized vectors are the variables for which a Cauchy-type theorem is applicable, and thus those contravariant objects having basis in the tangent spaces and which can be contracted without any metric with normals, which are elements of the cotangent spaces. We know indeed that the stresses applied linearly to a normal give the traction vector acting on the surface having that normal, see (3.30). Further, we know also that the scalar product between the negative electric displacement and the normal of a surface element gives the charge induced on that surface, see (4.7). Thus, the stresses and the negative electric displacement represent the generalized vectors. The dual quantities produced by the tractions and charges are deformations and electric field which can be then considered as the generalized covectors.

It is important to underline that those dual geometric objects do not coincide with the dual physical objects. The latter are *actions* or *generalized forces* caused by *reactions* or *generalized deformations*. We know that a force applied on a point-mass causes a displacement of the same. In a similar way stresses on a local volume element of a solid produces deformations while an electric field gives raise to a movement of charges or electric displacement. Based on this argumentation we define the stresses and electric field as *actions* and the deformation and electric displacement as *reactions*.

In particular, we may consider three types of generalized vectors and three correspondent types of generalized covectors which refers to a two-point formulation, Lagrangian formulation and Eulerian formulation, respectively. For the sake of clarity we will consider only the first and third type of sets. We will indicate the generalized vector for a two-point formulation with $\mathfrak{S}'$ and the one in the Eulerian configuration with $\mathfrak{s}'$, i.e.

$$\mathfrak{S}' := [\boldsymbol{g}\boldsymbol{P}, -\mathbb{D}]^T \qquad \text{and} \qquad \mathfrak{s}' := [\boldsymbol{\tau}, -\tilde{\mathbb{d}}]^T . \tag{6.1}$$

The correspondent generalized covectors will be contradistinguished with $\tilde{\mathfrak{F}}'$ and $\mathfrak{f}'$ meaning the sets

$$\tilde{\mathfrak{F}}' := [\boldsymbol{F}, \mathbb{E}]^T \qquad \text{and} \qquad \mathfrak{f}' := [\tfrac{1}{2}\boldsymbol{g}, \mathrm{e}]^T. \tag{6.2}$$

The third possible description in terms of the Lagrangian vector $[\boldsymbol{S}, -\mathbb{D}]^T$ and covector $[\tfrac{1}{2}\boldsymbol{C}, \mathbb{E}]^T$ can be easily determined starting from the formulation in terms of $\mathfrak{S}'$ and $\tilde{\mathfrak{F}}'$. With the definition of generalized vectors and covectors at hand, the electro-mechanical power per unit of the reference volume $\rho_0 \mathscr{P}'$ expressed in the equations $(5.89)_2$ and $(5.92)_2$ can be written in a more compact fashion as

$$\rho_0 \mathscr{P}' = \mathfrak{S}' \star \dot{\tilde{\mathfrak{F}}}' \qquad , \qquad \rho_0 \mathscr{P}' = \mathfrak{s}' \star \boldsymbol{\mathcal{L}_v}(\mathfrak{f}'). \tag{6.3}$$

Here the star indicates a generalized inner product that produces a scalar according to $(5.89)_2$ and $(5.92)_2$. Thus, the electro-mechanical power is the inner product between the generalized vectors and the rate of the generalized covectors. Notice that

$$\rho_0 \mathscr{P}' = \rho_0 \mathscr{P} - \frac{d}{dt}(\mathbb{E} \cdot \mathbb{D}) \qquad \text{and} \qquad \rho_0 \mathscr{P}' = \rho \mathscr{P} - \boldsymbol{\mathcal{L}_v}(\mathrm{e} \cdot \tilde{\mathrm{d}}). \tag{6.4}$$

The prime for the generalized vectors and covectors is used in order to be consistent with the different formulations of the electro-mechanical power given in Section 5.7.

6.1.1. Formulation of Non-Dissipative Response

Consider the time interval $[0, t] \in \mathbb{R}^+$ in which a certain electro-mechanical loading process takes place. Let

$$W_0^t := \int_0^t \rho_0 \mathscr{P}' d\tau \tag{6.5}$$

be the work per unit of reference volume done to the material element within this process. Let us first focus on a non-dissipative electro-mechanical response which implies a path-independency of the work done to the material element defined in (6.5) and which could be expressed with a potential character of the electro-mechanical power $\mathscr{P}'$, i.e.

$$W_0^t := \rho_0 \hat{\psi}'(t) - \rho_0 \hat{\psi}'(0) \qquad \text{or} \qquad W_0^t := \rho_0 \tilde{\psi}'(t) - \rho_0 \tilde{\psi}'(0) \tag{6.6}$$

with $\rho_0 \hat{\psi}'(t)$ and $\rho_0 \tilde{\psi}'(t)$ mixed energy-enthalpy for the two-point and Eulerian representation, respectively, which is stored in the material element at time t. We assume that the mixed energy-enthalpy for a non-dissipative material response depend exclusively on generalized covectors

$$\rho_0 \hat{\psi}'(t) = \rho_0 \psi'(\tilde{\mathfrak{F}}'(t)) \qquad \text{and} \qquad \rho_0 \tilde{\psi}'(t) = \rho_0 \psi'(\mathfrak{f}'(t)). \tag{6.7}$$

The above expressions simply state that the work done to the material element in the time interval $[0, t]$ is fully stored in the material and the free space in background. The property (6.7) implies

$$\rho_0 \mathscr{P}' = \frac{d}{dt}\rho_0 \psi'(\tilde{\mathfrak{F}}'(t)) \qquad \text{and} \qquad \rho_0 \mathscr{P}' = \frac{d}{dt}\rho_0 \psi'(\mathfrak{f}'(t)). \tag{6.8}$$

Combination of (6.3) and (6.8) gives the identities

$$\mathfrak{S}' \star \dot{\tilde{\mathfrak{F}}}' = \rho_0 \partial_{\tilde{\mathfrak{F}}'} \psi' \star \dot{\tilde{\mathfrak{F}}}' \qquad \text{and} \qquad \mathfrak{s}' \star \boldsymbol{\mathcal{L}_v}(\mathfrak{f}') = \rho_0 \partial_{\mathfrak{f}'} \psi' \star \boldsymbol{\mathcal{L}_v}(\mathfrak{f}'), \tag{6.9}$$

that must be satisfied for all possible rates of the generalized covectors, yielding the potential constitutive equations

$$\boldsymbol{\mathfrak{S}}' = \rho_0 \partial_{\boldsymbol{\mathfrak{F}}'} \psi'(\boldsymbol{\mathfrak{F}}'(t)) \qquad \text{and} \qquad \boldsymbol{\mathfrak{s}}' = \rho_0 \partial_{\mathbf{f}'} \psi'(\mathbf{f}'(t)) \,, \tag{6.10}$$

which define the generalized vectors in terms of the generalized covectors. Equations (6.10) are the compact versions of equations $(5.85)_1$ and $(5.85)_2$, and $(5.96)_1$ and $(5.96)_2$, respectively.

The mixed energy-enthalpy function ψ' is related to the free energy function ψ through a partial Legendre transformation with respect to the electric slot, i.e.

$$\rho_0 \psi'(\boldsymbol{F}, \mathbb{E}) := \inf_{\mathbb{D}} \{ \rho_0 \psi(\boldsymbol{F}, \mathbb{D}) - \mathbb{E} \cdot \mathbb{D} \} \quad \text{and} \quad \rho_0 \psi'(\boldsymbol{g}, \mathrm{e}) := \inf_{\tilde{\mathrm{d}}} \left\{ \rho_0 \psi(\boldsymbol{g}, \tilde{\mathrm{d}}) - \mathrm{e} \cdot \tilde{\mathrm{d}} \right\} . \tag{6.11}$$

The free energy is in general a convex function and consequently the mixed energy-enthalpy results to be a convex-concave function, see ROCKAFELLAR [129]. Thus a formulation in terms of actions and reactions can yield to a minimization structure of the electro-mechanical boundary-value-problem while on the other hand a formulation in terms of vectors and covectors is generally combined to a saddle-point character of the electro-mechanical boundary-value-problem. Similar considerations are also valid for the dissipative response.

6.1.2. Formulation of Dissipative Response

We now extend the previous treatment in order to account for a dissipative electro-mechanical material response which appears for example in ferroelectric materials. The difference with respect to the case of non-dissipative materials is the fact that the work done to the material element defined in (6.5) is now not fully stored, but it is in part dissipated. Thus equation (6.6) must be reformulated as follows

$$W_0^t = \rho_0 \hat{\psi}'(t) - \rho_0 \hat{\psi}'(0) + D_0^t \qquad \text{and} \qquad W_0^t = \rho_0 \tilde{\psi}'(t) - \rho_0 \tilde{\psi}'(0) + D_0^t \,, \tag{6.12}$$

where

$$D_0^t = \int\limits_0^t \rho_0 \mathscr{D}_{loc} d\tau \geq 0 \tag{6.13}$$

is the part of the electro-mechanical work which dissipates into heat while $\rho_0 \hat{\psi}'(t) - \rho_0 \hat{\psi}'(0)$ or $\rho_0 \tilde{\psi}'(t) - \rho_0 \tilde{\psi}'(0)$ constitutes the stored one. Recall that $\rho_0 \mathscr{D}_{loc}$ is the dissipation per unit of reference volume. The statement (6.13) expresses the second law of thermodynamics which was already introduced in Section 5 and states a positive dissipation for arbitrary processes. Considering (6.12) we may extend (6.8) to

$$\rho_0 \mathscr{P}' = \frac{d}{dt} \rho_0 \psi'(\boldsymbol{\mathfrak{F}}'(t)) + \rho_0 \mathscr{D}_{loc} \qquad \text{and} \qquad \rho_0 \mathscr{P}' = \frac{d}{dt} \rho_0 \psi'(\mathbf{f}'(t)) + \rho_0 \mathscr{D}_{loc} \,, \tag{6.14}$$

from which it becomes clear that the energy storage function ψ' cannot be only a function of the generalized covectors $\boldsymbol{\mathfrak{F}}'$ or $\mathbf{f}'$, but has to depend additionally on a set of internal variables $\boldsymbol{\mathfrak{Q}} \in \mathbb{R}^m$ for the two-point formulation or $\mathbf{q} \in \mathbb{R}^m$ for the Eulerian formulation. Thus we may write

$$\rho_0 \psi'(t) = \rho_0 \hat{\psi}'(\boldsymbol{\mathfrak{F}}'(t), \boldsymbol{\mathfrak{Q}}(t)) \qquad \text{and} \qquad \rho_0 \psi'(t) = \rho_0 \tilde{\psi}'(\mathbf{f}'(t), \mathbf{q}(t)) \,. \tag{6.15}$$

Following the Coleman-Noll-Gurtin's arguments recalled in Section 5, we identify the generalized vectors and the internal forces $\mathfrak{M}$ and $\mathfrak{m}$ dual to $\mathfrak{Q}$ and $\mathfrak{q}$ by

$$
\begin{aligned}
\mathfrak{S}' &= \rho_0 \partial_{\mathfrak{F}'} \psi'(\mathfrak{F}', \mathfrak{Q}) & \mathfrak{s}' &= \rho_0 \partial_{\mathfrak{f}'} \psi'(\mathfrak{f}', \mathfrak{q}) \\
& & \text{and} & & & \\
\mathfrak{M} &= - \rho_0 \partial_{\mathfrak{Q}'} \psi'(\mathfrak{F}', \mathfrak{Q}) & \mathfrak{m} &= - \rho_0 \partial_{\mathfrak{q}'} \psi'(\mathfrak{f}', \mathfrak{q})
\end{aligned}
\tag{6.16}
$$

Usage of (6.16) gives the reduced dissipation

$$
\rho_0 \mathscr{D}_{loc} = \mathfrak{M} \star \dot{\mathfrak{Q}} \geq 0 \qquad \text{and} \qquad \rho_0 \mathscr{D}_{loc} = \mathfrak{m} \star \pounds_v(\mathfrak{q}) \geq 0
\tag{6.17}
$$

as an inner product of the internal forces, driving the evolution of the internal variables, and the time rate of the internal variables.

6.1.3. Evolution Equations

The constitutive setting for dissipative materials is completed by the evolution equations for the internal variables. Those equations can be formulated by postulating the existence of a dissipation potential $\phi : \mathbb{R}^m \to \mathbb{R}$. This function is assumed to depend on the flux $\dot{\mathfrak{Q}}$ or $\pounds_v(\mathfrak{q})$ of the internal variables and determine the evolution of $\mathfrak{Q}$ or $\mathfrak{q}$ in terms of the constitutive differential equations

$$
\begin{aligned}
\rho_0 \partial_{\mathfrak{Q}} \psi'(\mathfrak{F}', \mathfrak{Q}) + \rho_0 \partial_{\dot{\mathfrak{Q}}} \phi(\dot{\mathfrak{Q}}) &= \mathbf{0} & \mathfrak{Q}(0) &= \mathfrak{Q}_0 \\
& & \text{with} & & , \\
\rho_0 \partial_{\mathfrak{q}} \psi'(\mathfrak{f}', \mathfrak{q}) + \rho_0 \partial_{\pounds_v(\mathfrak{q})} \phi(\pounds_v(\mathfrak{q})) &= \mathbf{0} & \mathfrak{q}(0) &= \mathfrak{q}_0
\end{aligned}
\tag{6.18}
$$

often referred to as Biot's equation of standard dissipative systems. The constitutive equations (6.16) and (6.18) determine the generalized vector response of a smooth normal electro-mechanically coupled material in a generalized-covector driven process where the generalized covector is prescribed. The insertion of the evolution equation (6.18) into the reduced dissipation inequality (6.17) gives the form

$$
\rho_0 \partial_{\dot{\mathfrak{Q}}} \phi(\dot{\mathfrak{Q}}) \star \dot{\mathfrak{Q}} \geq 0 \qquad \text{and} \qquad \rho_0 \partial_{\pounds_v(\mathfrak{q})} \phi(\pounds_v(\mathfrak{q})) \star \pounds_v(\mathfrak{q}) \geq 0 \,,
\tag{6.19}
$$

which serves as fundamental physically-based constraint on the dissipation function ϕ. The thermodynamic constraint (6.19) is a priori satisfied by assuming the dissipation function to be normalized and positive

$$
\phi(\mathbf{0}) = 0 \qquad \text{and} \qquad \phi(\mathbf{A}) \geq 0 \,,
\tag{6.20}
$$

and additionally convex

$$
\alpha \phi(\mathbf{A}_1) + (1 - \alpha) \phi(\mathbf{A}_2) > \phi(\alpha \mathbf{A}_1 + (1 - \alpha) \mathbf{A}_2) \,,
\tag{6.21}
$$

for $\alpha \in [0, 1]$. Depending on particular applications, the dissipation function may be assumed to be homogeneous of degree p

$$
\phi(\alpha \mathbf{A}) = \alpha^p \phi(\mathbf{A}) \qquad \text{for} \qquad \alpha > 0 \,.
\tag{6.22}
$$

An important case is $p = 1$ which characterizes a rate-independent response. Then, differentiation of (6.22) with respect to α gives $\partial_{\mathbf{A}} \phi(\mathbf{A}) \star \mathbf{A} = \phi(\mathbf{A})$, which identifies for the rate-independent case the dissipation $\mathscr{D}_{loc}$ with the dissipation function ϕ, i.e. $\mathscr{D}_{loc} =$

$\phi(\dot{\mathfrak{Q}}) \geq 0$ or $\mathscr{D}_{loc} = \phi(\boldsymbol{\mathcal{L}}_v(q)) \geq 0$. Such a function has a cone-like graph and is not differentiable at the point $\boldsymbol{A} = \boldsymbol{0}$. A generalization of the above formulation needs a generalization of the differential operator $\partial_{\dot{\mathfrak{Q}}}$ or $\partial_{\boldsymbol{\mathcal{L}}_v(\mathbf{q})}$ for smooth functions to the notion of sub-differential operator representing a set. For smooth dissipation functions $\partial_{\dot{\mathfrak{Q}}}$ or $\partial_{\boldsymbol{\mathcal{L}}_v(\mathbf{q})}$ is the standard derivative. Using the definition of sub-differential operator, in what follows we formally understand the Biot-type equation (6.18) to be generalized to

$$\boldsymbol{0} \in \rho_0 \partial_{\mathbf{q}} \psi'(\boldsymbol{\mathfrak{F}}', \mathfrak{Q}) + \rho_0 \partial_{\dot{\mathfrak{Q}}} \phi(\dot{\mathfrak{Q}}) \qquad \boldsymbol{\mathfrak{M}} \in \partial_{\dot{\mathfrak{Q}}} \rho_0 \phi(\dot{\mathfrak{Q}})$$

$$\text{or} \qquad\qquad\qquad\qquad . \qquad (6.23)$$

$$\boldsymbol{0} \in \rho_0 \partial_{\mathbf{q}} \psi'(\mathbf{f}', \mathbf{q}) + \rho_0 \boldsymbol{\mathcal{L}}_v(\mathbf{q}) \phi(\boldsymbol{\mathcal{L}}_v(\mathbf{q})) \qquad \mathbf{m} \in \partial_{\boldsymbol{\mathcal{L}}_v(\mathbf{q})} \rho_0 \phi(\boldsymbol{\mathcal{L}}_v(\mathbf{q}))$$

Based on the definition $(6.16)_3$ and $(6.16)_4$, we may introduce a dual dissipation function $\phi^* : \mathbb{R}^m \to \mathbb{R}$ depending on the internal forces $\boldsymbol{\mathfrak{M}}$ or $\mathbf{m}$ by the Legendre-Fenchel transformation

$$\rho_0 \phi^*(\boldsymbol{\mathfrak{M}}) := \sup_{\dot{\mathfrak{Q}}} \left\{ \boldsymbol{\mathfrak{M}} \star \dot{\mathfrak{Q}} - \rho_0 \phi(\dot{\mathfrak{Q}}) \right\} ,$$

$$\rho_0 \phi^*(\mathbf{m}) := \sup_{\boldsymbol{\mathcal{L}}_v(\mathbf{q})} \left\{ \mathbf{m} \star \boldsymbol{\mathcal{L}}_v(\mathbf{q}) - \rho_0 \phi(\boldsymbol{\mathcal{L}}_v(\mathbf{q})) \right\} . \qquad (6.24)$$

The dual dissipation function defines directly the evolution of the internal variables by

$$\dot{\mathfrak{Q}} \in \rho_0 \partial_{\boldsymbol{\mathfrak{M}}} \phi^*(\boldsymbol{\mathfrak{M}}) \qquad \text{or} \qquad \boldsymbol{\mathcal{L}}_v(\mathbf{q}) \in \rho_0 \partial_{\mathbf{m}} \phi^*(\mathbf{m}) , \qquad (6.25)$$

dual to $(6.23)_3$ and $(6.23)_4$, degenerating for a smooth response to $\dot{\mathfrak{Q}} = \rho_0 \partial_{\boldsymbol{\mathfrak{M}}} \phi^*(\boldsymbol{\mathfrak{M}})$ and $\boldsymbol{\mathcal{L}}_v(\mathbf{q}) = \rho \partial_{\mathbf{m}} \phi^*(\mathbf{m})$.

6.1.4. Rate-Independent Dissipation Functions

Rate-independent dissipation functions are often derived by invoking the so-called principle of maximum dissipation by extension of the arguments used to model the case of rate independent plasticity. Here, the dissipation function is defined by the constraint maximum problems

$$\rho_0 \phi(\dot{\mathfrak{Q}}) = \sup_{\boldsymbol{\mathfrak{M}} \in \mathcal{A}} \{ \boldsymbol{\mathfrak{M}} \star \dot{\mathfrak{Q}} \} \qquad \text{and} \qquad \rho_0 \phi(\dot{\mathbf{q}}) = \sup_{\mathbf{m} \in a} \{ \mathbf{m} \star \boldsymbol{\mathcal{L}}_v(\mathbf{q}) \} , \qquad (6.26)$$

where $\mathcal{A}$ and a model reversible domains in the space of the driving forces $\boldsymbol{\mathfrak{M}}$ and $\mathbf{m}$,

$$\mathcal{A} := \{ \boldsymbol{\mathfrak{M}} \in \mathbb{R}^m | f(\boldsymbol{\mathfrak{M}}) \leq C \} \qquad \text{and} \qquad a := \{ \mathbf{m} \in \mathbb{R}^m | f(\mathbf{m}) \leq c \} , \qquad (6.27)$$

in terms of a set-level function $f : \mathbb{R}^m \to \mathbb{R}$, which is positive $f(\boldsymbol{\mathfrak{M}})$, $f(\mathbf{m}) \geq 0$, normalized $f(\boldsymbol{0}) = 0$, convex and homogeneous of order one $f(\alpha \boldsymbol{A}) = \alpha f(\boldsymbol{A})$ for $\alpha > 0$. The threshold values $C > 0$ and $c > 0$ bound the driving forces $\boldsymbol{\mathfrak{M}}$ and $\mathbf{m}$. The constrained maximum problems (6.26) can be solved by a Lagrange method

$$\rho_0 \phi(\dot{\mathbf{q}}) = \sup_{\boldsymbol{\mathfrak{M}}, \lambda \geq 0} \left\{ \boldsymbol{\mathfrak{M}} \star \dot{\mathfrak{Q}} - \lambda(f(\boldsymbol{\mathfrak{M}}) - C) \right\} ,$$

$$\rho_0 \phi(\boldsymbol{\mathcal{L}}_v(\mathbf{q})) = \sup_{\mathbf{m}, \lambda \geq 0} \left\{ \mathbf{m} \star \boldsymbol{\mathcal{L}}_v(\mathbf{q}) - \lambda(f(\mathbf{m}) - c) \right\} . \qquad (6.28)$$

By exploitation of the necessary conditions for the maximum problem (6.28) we obtain the evolution equation for the internal variables

$$\dot{\mathfrak{Q}} = \lambda \partial_{\boldsymbol{\mathfrak{M}}} f(\boldsymbol{\mathfrak{M}}) \qquad \text{and} \qquad \boldsymbol{\mathcal{L}}_v(\mathbf{q}) = \lambda \partial_{\mathbf{m}} f(\mathbf{m}) , \qquad (6.29)$$

along with the loading-unloading conditions

$$\lambda \geq 0 \quad , \quad f(\mathfrak{M}) \leq C \quad , \quad \lambda(f(\mathfrak{M}) - C) = 0 \,, \tag{6.30}$$

for $(6.29)_1$ and

$$\lambda \geq 0 \quad , \quad f(\mathfrak{m}) \leq c \quad , \quad \lambda(f(\mathfrak{m}) - c) = 0 \,, \tag{6.31}$$

for $(6.29)_2$. The latter determine the non-smooth dissipative response by the set-level function f. Note that the insertion of (6.29) into (6.28) gives the simple expression for the dissipation function $\rho_0 \mathscr{D}_{loc} = \rho_0 \phi(\dot{\mathfrak{Q}}) = \lambda C \geq 0$ and $\rho_0 \mathscr{D}_{loc} = \rho_0 \phi(\boldsymbol{\mathcal{L}_v}(\mathfrak{q})) = \lambda c \geq 0$. The combination of (6.29) and (6.30) or (6.31) is a specific form of (6.25) for a rate-independent response governed by a switching function f.

6.1.5. Rate-Dependent Dissipation Functions

A rate-dependent class of dissipation functions with reversible range $\mathcal{A}$ or a governed by the set-level function f is obtained by an approximate penalty-type solution of the maximum problem (6.26)

$$\rho_0 \phi(\dot{\mathfrak{Q}}) = \sup_{\mathfrak{M}} \left\{ \mathfrak{M} \star \dot{\mathfrak{Q}} - \frac{C}{\eta(m+1)} \langle f(\mathfrak{M})/C - 1 \rangle^{m+1} \right\} \,,$$

$$\rho_0 \phi(\boldsymbol{\mathcal{L}_v}(\mathfrak{q})) = \sup_{\mathfrak{m}} \left\{ \mathfrak{m} \star \boldsymbol{\mathcal{L}_v}(\mathfrak{q}) - \frac{c}{\eta(m+1)} \langle f(\mathfrak{m})/c - 1 \rangle^{m+1} \right\} \,, \tag{6.32}$$

where the constants $\eta > 0$ and $m > 0$ are interpreted as material parameters associated with the viscosity of the electro-mechanical process. $\langle x \rangle = \frac{1}{2}(x + |x|)$ is the ramp function, expressed by the McAuley brackets. The necessary conditions of (6.32) provides the non-linear evolution equations

$$\dot{\mathfrak{Q}} = \frac{1}{\eta} \langle f(\mathfrak{M})/C - 1 \rangle^m \partial_{\mathfrak{M}} f(\mathfrak{M}) \,,$$

$$\boldsymbol{\mathcal{L}_v}(\mathfrak{q}) = \frac{1}{\eta} \langle f(\mathfrak{m})/c - 1 \rangle^m \partial_{\mathfrak{m}} f(\mathfrak{m}) \,. \tag{6.33}$$

This evolution equations may be directly obtained from (6.25) based on the dual dissipation function

$$\rho_0 \phi^*(\mathfrak{M}) = \frac{C}{\eta(m+1)} \langle f(\mathfrak{M})/C - 1 \rangle^{m+1} \,,$$

$$\rho_0 \phi^*(\mathfrak{m}) = \frac{c}{\eta(m+1)} \langle f(\mathfrak{m})/c - 1 \rangle^{m+1} \,, \tag{6.34}$$

which follows from (6.32), if the penalty-type variational principle is eventually interpreted as Legendre-Fenchel transformation. For $\eta \to 0$ we obtain in the limit the rate-independent form (6.29) combined with (6.30) or (6.31).

6.1.6. Incremental Variational Principle for Dissipative Response

Incremental Potential for Generalized Vectors. We consider now an incremental electro-mechanical loading process in the time interval $[t_n, t_{n+1}]$. We assume that the state of the material at the time t_n is known and in particular the internal state, characterized by the value $\mathfrak{Q}_n$ or $\mathfrak{q}_n$ of the internal variables at the time t_n is assumed to be known.

Our aim is to determine the new generalized vector state at t_{n+1} when advancing the generalized covector from $\mathfrak{F}'_n$ or $\mathfrak{f}'_n$ at time t_n to $\mathfrak{F}'_{n+1}$ or $\mathfrak{f}'_{n+1}$ at time t_{n+1}. To this purpose we define an *incremental potential* W depending only on the current generalized covector $\mathfrak{F}'_{n+1}$ or $\mathfrak{f}'_{n+1}$ that determines the current generalized vector by the *quasi-hyperelastic function evaluation*

$$\mathfrak{S}'_{n+1} = \partial_{\mathfrak{F}'_{n+1}} W(\mathfrak{F}'_{n+1}) \qquad \text{and} \qquad \mathfrak{s}'_{n+1} = \partial_{\mathfrak{f}'_{n+1}} W(\mathfrak{f}'_{n+1})\,. \tag{6.35}$$

We will omit from now on the subscript "$n{+}1$" indicating the variables at the current time step t_{n+1} with an exception for t_{n+1} itself. Further derivations of the potential W, and thus of the generalized vectors $\mathfrak{S}'$ and $\mathfrak{s}'$ give the coupled electro-mechanical consistent tangent moduli

$$\mathfrak{C}' := \partial_{\mathfrak{F}'} \mathfrak{S}' = \partial^2_{\mathfrak{F}'\mathfrak{F}'} W(\mathfrak{F}') \quad \text{and} \quad \mathfrak{c}' := \partial_{\mathfrak{f}'} \mathfrak{s}' = \partial^2_{\mathfrak{f}'\mathfrak{f}'} w(\mathfrak{f}')\,. \tag{6.36}$$

The incremental potential $W(\mathfrak{F}')$ or $W(\mathfrak{f}')$ represents the incremental electro-mechanical work done on the infinitesimal material volume element in the time window $[t_n, t_{n+1}]$ which accounts not only for the energy stored in the material, but also for the dissipated energy. Equations (6.35) and (6.36) suggests that the incremental potential W can be considered as an extension of the mixed energy-enthalpy function ψ' used to characterized a non-dissipative material response.

Clearly, this functional must cover characteristics of the storage function ψ' and the dissipation function ϕ introduced above. To this end we propose a definition of the incremental functional W through the following variational problems

$$W(\mathfrak{F}') = \inf_{\dot{\mathfrak{Q}}} \left\{ \int_{t_n}^{t_{n+1}} \left[\frac{d}{dt} \rho_0 \psi'(\mathfrak{F}', \mathfrak{Q}) + \rho_0 \phi(\dot{\mathfrak{Q}}) \right] d\tau \right\} \quad \text{with} \quad \mathfrak{Q}(t_n) = \mathfrak{Q}_n\,,$$

$$W(\mathfrak{f}') = \inf_{\mathcal{L}_v(\mathfrak{q})} \left\{ \int_{t_n}^{t_{n+1}} \left[\frac{d}{dt} \rho_0 \psi'(\mathfrak{f}', \mathfrak{q}) + \rho_0 \phi(\mathcal{L}_v(\mathfrak{q})) \right] d\tau \right\} \quad \text{with} \quad \mathfrak{q}(t_n) = \mathfrak{q}_n\,. \tag{6.37}$$

For prescribed generalized covectors, these problems define the incremental potential function W as a minimum of the generalized work $\int_{t_n}^{t_{n+1}} \left[\rho_0 \dot{\psi}' + \rho_0 \phi \right] d\tau$ done on the material in the time increment under consideration. Starting with the given initial condition $\mathfrak{Q}(t_n) = \mathfrak{Q}_n$ or $\mathfrak{q}(t_n) = \mathfrak{q}_n$, the minimum problem defines an optimum path of the internal variables $\mathfrak{Q}(t)$ or $\mathfrak{q}(t)$ for $t \in [t_n, t_{n+1}]$ including the right boundary value $\mathfrak{Q} = \mathfrak{Q}(t_{n+1})$ or $\mathfrak{q} = \mathfrak{q}(t_{n+1})$.

Equations (6.35) and (6.37) provide an approximate variational counterpart of the continuous setting (6.16) and (6.18) of the constitutive equations in the discrete time step $[t_n, t_{n+1}]$ under consideration. In order to show the consistency, we at first recast (6.37) into the form

$$W(\mathfrak{F}') = \inf_{\dot{\mathfrak{Q}}} \left\{ [\rho_0 \psi'(\mathfrak{F}', \mathfrak{Q})]_{t_n}^{t_{n+1}} + \int_{t_n}^{t_{n+1}} \rho_0 \phi(\dot{\mathfrak{Q}}) d\tau \right\}\,,$$

$$W(\mathfrak{f}') = \inf_{\mathcal{L}_v(\mathfrak{q})} \left\{ [\rho_0 \psi'(\mathfrak{f}', \mathfrak{q})]_{t_n}^{t_{n+1}} + \int_{t_n}^{t_{n+1}} \rho_0 \phi(\mathcal{L}_v(\mathfrak{q})) d\tau \right\}\,. \tag{6.38}$$

The necessary condition for the minimum problem is that the variation with respect to the internal variables of the term in curly brackets vanishes, i.e.

$$[\rho_0 \partial_{\mathfrak{Q}} \psi' \star \delta\mathfrak{Q}]_{t_n}^{t_{n+1}} + \int_{t_n}^{t_{n+1}} \left[\partial_{\dot{\mathfrak{Q}}} \rho_0 \phi \star \delta\dot{\mathfrak{Q}}\right] d\tau = 0,$$

$$[\rho_0 \partial_{\mathbf{q}} \psi' \star \delta\mathbf{q}]_{t_n}^{t_{n+1}} + \int_{t_n}^{t_{n+1}} \left[\rho_0 \partial_{\boldsymbol{\mathcal{L}}_v(\mathbf{q})} \phi \star \delta\boldsymbol{\mathcal{L}}_v(\mathbf{q})\right] d\tau = 0. \tag{6.39}$$

For smooth functions, integration by parts of the integrals appearing in (6.39) yields the expressions

$$\left[(\rho_0 \partial_{\mathfrak{Q}} \psi' + \rho_0 \partial_{\dot{\mathfrak{Q}}} \phi) \star \delta\mathfrak{Q}\right]_{t_n}^{t_{n+1}} + \int_{t_n}^{t_{n+1}} \left[-\frac{d}{dt}(\rho_0 \partial_{\dot{\mathfrak{Q}}} \phi)\right] \star \delta\mathfrak{Q} \, d\tau = 0,$$

$$\left[(\rho_0 \partial_{\mathbf{q}} \psi' + \rho_0 \partial_{\boldsymbol{\mathcal{L}}_v(\mathbf{q})} \phi) \star \delta\mathbf{q}\right]_{t_n}^{t_{n+1}} + \int_{t_n}^{t_{n+1}} \left[-\frac{d}{dt}(\rho_0 \partial_{\boldsymbol{\mathcal{L}}_v(\mathbf{q})} \phi)\right] \star \delta\mathbf{q} \, d\tau = 0, \tag{6.40}$$

which have to be verified for arbitrary increments $\delta\mathfrak{Q}$ and $\delta\mathbf{q}$. Thus the variational problem (6.37) yields the Biot's equation (6.23)

$$\rho_0 \partial_{\mathfrak{Q}} \psi' + \rho_0 \partial_{\dot{\mathfrak{Q}}} \phi = \boldsymbol{0} \quad \text{and} \quad \rho_0 \partial_{\mathbf{q}} \psi' + \rho_0 \partial_{\boldsymbol{\mathcal{L}}_v(\mathbf{q})} \phi = \boldsymbol{0} \quad \text{for} \quad t = t_{n+1} \tag{6.41}$$

at the discrete right boundary of the interval $[t_n, t_{n+1}]$. The minimizing path of the internal variables inside the interval is determined by the Euler equations

$$-\frac{d}{dt}(\rho_0 \partial_{\dot{\mathfrak{Q}}} \phi) = \boldsymbol{0} \qquad \text{and} \qquad -\frac{d}{dt}(\rho_0 \partial_{\boldsymbol{\mathcal{L}}_v(\mathbf{q})} \phi) = \boldsymbol{0} \qquad \text{for} \qquad t \in [t_n, t_{n+1}]. \tag{6.42}$$

For the limit $t_{n+1} \to t_n$, the form of the minimization path becomes irrelevant, because the time increment degenerates to a discrete time t. Because (6.41) still holds in this case, it is shown that the variational formulation (6.37) represents a consistent point–wise approximation of Biot's normal–dissipative evolution equation (6.23). Furthermore, taking the derivative of the incremental potential function with respect to the generalized covectors $\mathfrak{F}'$ or $\mathfrak{f}'$, we have

$$\partial_{\mathfrak{F}'} W(\mathfrak{F}') = \rho_0 \partial_{\mathfrak{F}'} \psi'(\mathfrak{F}', \mathfrak{Q}) \qquad , \qquad \partial_{\mathfrak{f}'} W(\mathfrak{f}') = \rho_0 \partial_{\mathfrak{f}'} \psi'(\mathfrak{f}', \mathbf{q}). \tag{6.43}$$

where $\mathfrak{Q}$ or $\mathbf{q}$ is assumed to be given by the minimization problem (6.37). Comparison with (5.85) and (5.96) then shows the consistency of the potential equations (6.35) with the continuous setting.

For finite time increments Δt, the minimization problem (6.37) is understood to have the algorithmic form

$$W^h(\mathfrak{F}') = \inf_{\mathfrak{Q}} \tilde{W}(\mathfrak{F}', \mathfrak{Q}) \qquad \text{and} \qquad W^h(\mathfrak{f}') = \inf_{\mathbf{q}} \hat{W}(\mathfrak{f}', \mathbf{q}) \tag{6.44}$$

in terms of the algorithmic expression for the (generalized) incremental electro-mechanical work

$$\tilde{W}(\mathfrak{F}', \mathfrak{Q}) = \rho_0 \psi'(\mathfrak{F}', \mathfrak{Q}) - \rho_0 \psi'(\mathfrak{F}'_n, \mathfrak{Q}_n) + \Delta t \, \rho_0 \phi\left(\tfrac{\mathfrak{Q} - \mathfrak{Q}_n}{\Delta t}\right),$$

$$\hat{W}(\mathfrak{f}', \mathbf{q}) = \rho_0 \psi'(\mathfrak{f}', \mathbf{q}) - \rho_0 \psi'(\mathfrak{f}'_n, \mathbf{q}_n) + \Delta t \, \rho_0 \phi\left(\tfrac{\mathbf{q} - \mathbf{q}_n}{\Delta t}\right). \tag{6.45}$$

Note that the algorithmic expression in (6.45) is based on an approximation of the integrals $\int_{t_n}^{t_{n+1}} \rho_0 \phi(\dot{\mathfrak{Q}}) d\tau \approx \Delta t \rho_0 \phi\left(\frac{\mathfrak{Q}-\mathfrak{Q}_n}{\Delta t}\right)$ and $\int_{t_n}^{t_{n+1}} \rho_0 \phi(\dot{\mathbf{q}}) d\tau \approx \Delta t \rho_0 \phi\left(\frac{\mathbf{q}-\mathbf{q}_n}{\Delta t}\right)$ in (6.37) through the algorithmic simplification of the rates $\dot{\mathfrak{Q}}$ of $\mathfrak{Q}$ and $\mathcal{L}_v(\mathbf{q})$ of $\mathbf{q}$ with the constant values $\dot{\mathfrak{Q}} = [\mathfrak{Q} - \mathfrak{Q}_n]/\Delta t$ and $\mathcal{L}_v(\mathbf{q}) = [\mathbf{q} - \mathbf{q}_n]/\Delta t$ in the interval $[t_n, t_{n+1}]$. Note further that the last approximation should be performed in an objective manner, see SIMO & HUGHES [137]. The exploitation of the necessary condition for the algorithmic minimization problem (6.44) provides the algorithmic forms

$$\mathbf{0} \in \rho_0 \partial_{\mathfrak{Q}} \psi'(\mathfrak{F}', \mathfrak{Q}) + \Delta t \rho_0 \partial_{\mathfrak{Q}} \phi(\tfrac{\mathfrak{Q}-\mathfrak{Q}_n}{\Delta t}) \,,$$

$$\mathbf{0} \in \rho_0 \partial_{\mathbf{q}} \psi'(\mathbf{f}', \mathbf{q}) + \Delta t \rho_0 \partial_{\mathbf{q}} \phi(\tfrac{\mathbf{q}-\mathbf{q}_n}{\Delta t}) \,,$$

$$\text{(6.46)}$$

of the Biot's equation (6.23). In other words, the algorithmic minimization problem (6.44) determines the update of the internal variables.

A Two-Point Formulation for Rate-Independent Response. For rate independent dissipative processes characterized by a reversible range $\mathcal{A}$ defined in $(6.27)_1$ in terms of the switching function f, we may modify the variational problem $(6.37)_1$ by inserting the specific dissipation function $(6.28)_1$

$$W(\mathfrak{F}') = \inf_{\dot{\mathfrak{Q}}} \sup_{\mathfrak{M}, \lambda \geq 0} \left\{ \int\limits_{t_n}^{t_{n+1}} \left[\frac{d}{dt} \rho_0 \psi' + \mathfrak{M} \star \dot{\mathfrak{Q}} - \lambda(f(\mathfrak{M}) - C) \right] d\tau \right\} . \qquad \text{(6.47)}$$

For finite time increments, this principle has the algorithmic form

$$W^h(\mathfrak{F}') = \inf_{\mathfrak{Q}} \sup_{\mathfrak{M}, \gamma \geq 0} \tilde{W}(\mathfrak{F}', \mathfrak{Q}, \mathfrak{M}, \gamma) \,, \qquad \text{(6.48)}$$

in terms of the approximated expression for the incremental electro-mechanical work

$$\tilde{W} = \rho_0 \psi'(\mathfrak{F}', \mathfrak{Q}) - \rho_0 \psi'(\mathfrak{F}'_n, \mathfrak{Q}_n) + \mathfrak{M} \star [\mathfrak{Q} - \mathfrak{Q}_n] - \gamma(f(\mathfrak{M}) - C) \,. \qquad \text{(6.49)}$$

Here, $\gamma := \lambda \Delta t$ is the Lagrange parameter associated with the increment $[t_n, t_{n+1}]$. For the loading case $\gamma > 0$, the necessary conditions of the constitutive variational problem (6.48) give the non-linear system of equations

$$\tilde{\mathbf{r}} := \begin{bmatrix} \partial_{\mathfrak{Q}} \tilde{W} \\ \partial_{\mathfrak{M}} \tilde{W} \\ \partial_{\gamma} \tilde{W} \end{bmatrix} = \begin{bmatrix} \rho_0 \partial_{\mathfrak{Q}} \psi' + \mathfrak{M} \\ \mathfrak{Q} - \mathfrak{Q}_n - \gamma \partial_{\mathfrak{M}} f \\ -f + C \end{bmatrix} = \mathbf{0} \qquad \text{(6.50)}$$

along with the discrete version of the loading-unloading conditions (6.30)

$$\gamma \geq 0 \quad , \quad f(\mathfrak{M}) \leq C \quad , \quad \gamma(f(\mathfrak{M}) - C) = 0 \,. \qquad \text{(6.51)}$$

The first equation of the system (6.50) represents the algorithmic definition of the conjugate internal force $\mathfrak{M}$. The second equation of (6.50) is the discrete counterpart of the evolution equation $(6.18)_1$. The above non-linear system (6.50) can be solved at given generalized covector $\mathfrak{F}'$ by a local Newton-type algorithm for the current variables $\tilde{\mathbf{v}} := \{\mathfrak{Q}, \mathfrak{M}, \gamma\}$

$$\tilde{\mathbf{v}} \Leftarrow \tilde{\mathbf{v}} - \tilde{\mathbf{a}}^{-1} \tilde{\mathbf{r}} \qquad \text{(6.52)}$$

until convergence is achieved in the sense $|\tilde{\boldsymbol{r}}| < tol$. The tangent matrix of the Newton iteration has the form

$$
\tilde{\boldsymbol{a}} := \begin{bmatrix} \partial^2_{\mathfrak{Q}\mathfrak{Q}}\tilde{W} & \partial^2_{\mathfrak{Q}\mathfrak{M}}\tilde{W} & \partial^2_{\mathfrak{Q}\gamma}\tilde{W} \\[2mm] \partial^2_{\mathfrak{M}\mathfrak{Q}}\tilde{W} & \partial^2_{\mathfrak{M}\mathfrak{M}}\tilde{W} & \partial^2_{\mathfrak{M}\gamma}\tilde{W} \\[2mm] \partial^2_{\gamma\mathfrak{Q}}\tilde{W} & \partial^2_{\gamma\mathfrak{M}}\tilde{W} & \partial^2_{\gamma\gamma}\tilde{W} \end{bmatrix} = \begin{bmatrix} \rho_0\partial^2_{\mathfrak{Q}\mathfrak{Q}}\psi' & \boldsymbol{1} & \boldsymbol{0} \\[2mm] \boldsymbol{1} & -\gamma\partial^2_{\mathfrak{M}\mathfrak{M}}f & -\partial_{\mathfrak{M}}f \\[2mm] \boldsymbol{0} & -\partial_{\mathfrak{M}}f & \boldsymbol{0} \end{bmatrix} . \tag{6.53}
$$

Using the implicit function theorem, we may derive a closed-form solution of the coupled electro-mechanical tangent moduli operators defined in $(6.36)_1$

$$
\mathfrak{C}' := \partial^2_{\mathfrak{F}'\mathfrak{F}'}W = \rho_0\partial^2_{\mathfrak{F}'\mathfrak{F}'}\psi' - s \begin{bmatrix} \rho_0\partial^2_{\mathfrak{F}'\mathfrak{Q}}\psi' \\[1mm] \boldsymbol{0} \\[1mm] \boldsymbol{0} \end{bmatrix} \cdot (\tilde{\boldsymbol{a}})^{-1} \cdot \begin{bmatrix} \rho_0\partial^2_{\mathfrak{Q}\mathfrak{F}'}\psi' \\[1mm] \boldsymbol{0} \\[1mm] \boldsymbol{0} \end{bmatrix} \tag{6.54}
$$

in terms of a dissipative loading flag

$$
s := \begin{cases} 1 & \text{for} \quad \gamma > 0 , \\ 0 & \text{otherwise} . \end{cases} \tag{6.55}
$$

Note that the second part of (6.54) characterizes the softening of the fully coupled electro-mechanical tangent moduli due to the evolution of the internal variables. Note also that due to the variational structure the moduli are symmetric.

An Eulerian Formulation for a Rate-Independent Response. For rate independent dissipative processes characterized by a reversible range a defined in $(6.27)_2$ in terms of the switching function f, we may modify the variational problem $(6.37)_2$ by inserting the specific dissipation function $(6.28)_2$

$$
W(\mathbf{f}') = \inf_{\boldsymbol{\mathcal{L}_v}(\mathbf{q})} \sup_{\mathfrak{m},\lambda\geq 0} \left\{ \int_{t_n}^{t_{n+1}} \left[\frac{d}{dt}\rho_0\psi' + \mathfrak{m} \star \boldsymbol{\mathcal{L}_v}(\mathbf{q}) - \lambda(f(\mathfrak{m}) - c) \right] d\tau \right\} . \tag{6.56}
$$

For finite time increments, this principle has the algorithmic form

$$
W^h(\mathbf{f}') = \inf_{\mathbf{q}} \sup_{\mathfrak{m},\gamma\geq 0} \hat{W}(\mathbf{f}', \mathbf{q}, \mathfrak{m}, \gamma) \tag{6.57}
$$

in terms of the approximated expression for the incremental electro-mechanical work

$$
\hat{W} = \rho_0\psi'(\mathbf{f}', \mathbf{q}) - \rho_0\psi'(\mathbf{f}'_n, \mathbf{q}_n) + \mathfrak{m} \star [\mathbf{q} - \boldsymbol{\varphi}_*(\mathfrak{Q}_n)] - \gamma(f(\mathfrak{m}) - c) . \tag{6.58}
$$

Here, $\gamma := \lambda\Delta t$ is the Lagrange parameter associated with the increment $[t_n, t_{n+1}]$. Observe that in order to get an objective approximation of the Lie derivative, we need to first pull-back, then make the approximation of the time derivative and finally to push forward the obtained quantity as follows

$$
\boldsymbol{\mathcal{L}_v}(\mathbf{q}) \approx \boldsymbol{\varphi}_* \left(\frac{[\boldsymbol{\varphi}^*(\mathbf{q})]_{t=t_{n+1}} - [\boldsymbol{\varphi}^*(\mathbf{q})]_{t=t_n}}{\Delta t} \right) = \frac{\boldsymbol{\varphi}_*(\mathfrak{Q} - \mathfrak{Q}_n)}{\Delta t} = \frac{\mathbf{q} - \boldsymbol{\varphi}_*(\mathfrak{Q}_n)}{\Delta t} . \tag{6.59}
$$

with $\boldsymbol{\varphi}^*(\bullet)$ and $\boldsymbol{\varphi}_*(\bullet)$ pull-back and push-forward operators, respectively. For the loading case $\gamma > 0$, the necessary conditions of the constitutive variational problem (6.57) give the non-linear system of equations

$$\hat{\boldsymbol{r}} := \begin{bmatrix} \partial_{\mathbf{q}}\hat{W} \\ \partial_{\mathbf{m}}\hat{W} \\ \partial_{\gamma}\hat{W} \end{bmatrix} = \begin{bmatrix} \rho_0 \partial_{\mathbf{q}}\psi' + \mathbf{m} \\ \mathbf{q} - \boldsymbol{\varphi}_*(\mathfrak{Q}_n) - \gamma\partial_{\mathbf{m}}f \\ -f + c \end{bmatrix} = \boldsymbol{0} \tag{6.60}$$

along with the discrete version of the loading-unloading conditions (6.31)

$$\gamma \geq 0 \quad , \quad f(\mathbf{m}) \leq c \quad , \quad \gamma(f(\mathbf{m}) - c) = 0 \,. \tag{6.61}$$

The first equation of the system (6.60) represents the algorithmic definition of the conjugate internal force $\mathbf{m}$. The second equation of (6.60) is the discrete counterpart of the evolution equation $(6.18)_2$. The above non-linear system (6.60) can be solved at given generalized covector $\mathfrak{f}'$ by a local Newton-type algorithm for the current variables $\hat{\boldsymbol{v}} := \{\mathbf{q}, \mathbf{m}, \gamma\}$

$$\hat{\boldsymbol{v}} \Leftarrow \hat{\boldsymbol{v}} - \hat{\boldsymbol{a}}^{-1}\hat{\boldsymbol{r}} \tag{6.62}$$

until convergence is achieved in the sense $|\hat{\boldsymbol{r}}| < tol$. The tangent matrix of the Newton iteration has the form

$$\hat{\boldsymbol{a}} := \begin{bmatrix} \partial_{\mathbf{qq}}^2\hat{W} & \partial_{\mathbf{qm}}^2\hat{W} & \partial_{\mathbf{q}\gamma}^2\hat{W} \\ \partial_{\mathbf{mq}}^2\hat{W} & \partial_{\mathbf{mm}}^2\hat{W} & \partial_{\mathbf{m}\gamma}^2\hat{W} \\ \partial_{\gamma\mathbf{q}}^2\hat{W} & \partial_{\gamma\mathbf{m}}^2\hat{W} & \partial_{\gamma\gamma}^2\hat{W} \end{bmatrix} = \begin{bmatrix} \rho_0\partial_{\mathbf{qq}}^2\psi' & \boldsymbol{1} & \boldsymbol{0} \\ \boldsymbol{1} & -\gamma\partial_{\mathbf{mm}}^2 f & -\partial_{\mathbf{m}}f \\ \boldsymbol{0} & -\partial_{\mathbf{m}}f & \boldsymbol{0} \end{bmatrix} . \tag{6.63}$$

Using the implicit function theorem, we may derive a closed-form solution of the coupled electro-mechanical tangent moduli operators defined in $(6.36)_2$

$$\mathfrak{c}' := \partial_{\mathfrak{f}'\mathfrak{f}'}^2 W = \rho_0\partial_{\mathfrak{f}'\mathfrak{f}'}^2\psi' - s\begin{bmatrix} \rho_0\partial_{\mathfrak{f}'\mathbf{q}}^2\psi' \\ \boldsymbol{0} \\ \boldsymbol{0} \end{bmatrix} \cdot (\hat{\boldsymbol{a}})^{-1} \cdot \begin{bmatrix} \rho_0\partial_{\mathbf{q}\mathfrak{f}'}^2\psi' \\ \boldsymbol{0} \\ \boldsymbol{0} \end{bmatrix} \tag{6.64}$$

in terms of a dissipative loading flag

$$s := \begin{cases} 1 & \text{for} \quad \gamma > 0 \,, \\ 0 & \text{otherwise} \,. \end{cases} \tag{6.65}$$

Note that the second part of (6.64) characterizes the softening of the fully coupled electro-mechanical tangent moduli due to the evolution of the internal variables. Note also that due to the variational structure the moduli are symmetric.

A Two-Point Formulation for Rate-Dependent Response. For rate dependent dissipative processes characterized by a reversible range $\mathcal{A}$ defined in $(6.27)_1$ in terms of the switching function f, we may modify the variational problem $(6.37)_1$ by inserting the specific dissipation function $(6.32)_1$

$$W(\mathfrak{F}') = \inf_{\dot{\mathfrak{Q}}} \sup_{\mathfrak{M}} \left\{ \int_{t_n}^{t_{n+1}} \left[\frac{d}{dt}\rho_0\psi' + \mathfrak{M} \star \dot{\mathfrak{Q}} - \frac{C}{\eta(m+1)}\langle f(\mathfrak{M})/C - 1\rangle^{m+1} \right] d\tau \right\} . \tag{6.66}$$

For finite time increments, this principle has the algorithmic form

$$W^h(\boldsymbol{\mathfrak{F}}') = \inf_{\boldsymbol{\mathfrak{Q}}} \sup_{\boldsymbol{\mathfrak{M}}} \bar{W}(\boldsymbol{\mathfrak{F}}', \boldsymbol{\mathfrak{Q}}, \boldsymbol{\mathfrak{M}}) \tag{6.67}$$

in terms of the approximated expression for the incremental electro-mechanical work

$$\bar{W} = \rho_0 \psi'(\boldsymbol{\mathfrak{F}}', \boldsymbol{\mathfrak{Q}}) - \rho_0 \psi'(\boldsymbol{\mathfrak{F}}_n', \boldsymbol{\mathfrak{Q}}_n) + \boldsymbol{\mathfrak{M}} \star [\boldsymbol{\mathfrak{Q}} - \boldsymbol{\mathfrak{Q}}_n] - \frac{C\Delta t}{\eta(m+1)} \langle f(\boldsymbol{\mathfrak{M}})/C - 1 \rangle^{m+1} . \tag{6.68}$$

The necessary conditions of the constitutive variational problem (6.67) give the non-linear system of equations

$$\bar{\boldsymbol{r}} := \begin{bmatrix} \partial_{\boldsymbol{\mathfrak{Q}}} \bar{W} \\ \partial_{\boldsymbol{\mathfrak{M}}} \bar{W} \end{bmatrix} = \begin{bmatrix} \rho_0 \partial_{\boldsymbol{\mathfrak{Q}}} \psi' + \boldsymbol{\mathfrak{M}} \\ \boldsymbol{\mathfrak{Q}} - \boldsymbol{\mathfrak{Q}}_n - \frac{\Delta t}{\eta} \langle f/C - 1 \rangle^m \partial_{\boldsymbol{\mathfrak{M}}} f \end{bmatrix} = \boldsymbol{0} . \tag{6.69}$$

The first equation of the system (6.69) represents the algorithmic definition of the conjugate internal force $\boldsymbol{\mathfrak{M}}$. The second equation of (6.69) is the discrete counterpart of the evolution equation $(6.33)_1$. The above non-linear system (6.69) can be solved at given generalized covector $\boldsymbol{\mathfrak{F}}'$ by a local Newton-type algorithm for the current variables $\bar{\boldsymbol{v}} := \{\boldsymbol{\mathfrak{Q}}, \boldsymbol{\mathfrak{M}}\}$

$$\bar{\boldsymbol{v}} \Leftarrow \bar{\boldsymbol{v}} - \bar{\boldsymbol{a}}^{-1} \bar{\boldsymbol{r}} \tag{6.70}$$

until convergence is achieved in the sense $|\bar{\boldsymbol{r}}| < tol$. The tangent matrix of the Newton iteration has the form

$$\bar{\boldsymbol{a}} := \begin{bmatrix} \partial^2_{\boldsymbol{\mathfrak{Q}}\boldsymbol{\mathfrak{Q}}} \bar{W} & \partial^2_{\boldsymbol{\mathfrak{Q}}\boldsymbol{\mathfrak{M}}} \bar{W} \\ \partial^2_{\boldsymbol{\mathfrak{M}}\boldsymbol{\mathfrak{Q}}} \bar{W} & \partial^2_{\boldsymbol{\mathfrak{M}}\boldsymbol{\mathfrak{M}}} \bar{W} \end{bmatrix} = \begin{bmatrix} \rho_0 \partial^2_{\boldsymbol{\mathfrak{Q}}\boldsymbol{\mathfrak{Q}}} \psi' & \boldsymbol{1} \\ \boldsymbol{1} & \begin{matrix} -\frac{m\Delta t}{\eta C} \langle f/C - 1 \rangle^{m-1} \partial_{\boldsymbol{\mathfrak{M}}} f \otimes \partial_{\boldsymbol{\mathfrak{M}}} f \\ -\frac{\Delta t}{\eta} \langle f/C - 1 \rangle^m \partial^2_{\boldsymbol{\mathfrak{M}}\boldsymbol{\mathfrak{M}}} f \end{matrix} \end{bmatrix} . \tag{6.71}$$

Using the implicit function theorem, we may derive a closed-form solution of the coupled electro-mechanical tangent moduli operators defined in $(6.36)_1$

$$\boldsymbol{\mathfrak{C}}' := \partial^2_{\boldsymbol{\mathfrak{F}}'\boldsymbol{\mathfrak{F}}'} W = \rho_0 \partial^2_{\boldsymbol{\mathfrak{F}}'\boldsymbol{\mathfrak{F}}'} \psi' - \begin{bmatrix} \rho_0 \partial^2_{\boldsymbol{\mathfrak{F}}'\boldsymbol{\mathfrak{Q}}} \psi' \\ \boldsymbol{0} \end{bmatrix} \cdot (\bar{\boldsymbol{a}})^{-1} \cdot \begin{bmatrix} \rho_0 \partial^2_{\boldsymbol{\mathfrak{Q}}\boldsymbol{\mathfrak{F}}'} \psi' \\ \boldsymbol{0} \end{bmatrix} . \tag{6.72}$$

Note that the second part of (6.72) characterizes the softening of the fully coupled electro-mechanical tangent moduli due to the evolution of the internal variables. Note also that due to the variational structure the moduli are symmetric.

An Eulerian Formulation for Rate-Dependent Response. For rate dependent dissipative processes characterized by a reversible range a defined in $(6.27)_2$ in terms of the switching function f, we may modify the variational problem $(6.37)_2$ by inserting the specific dissipation function $(6.32)_2$

$$W(\mathbf{f}') = \inf_{\boldsymbol{\mathcal{L}}_v(\mathbf{q})} \sup_{\mathbf{m}} \left\{ \int_{t_n}^{t_{n+1}} \left[\frac{d}{dt} \rho \psi' + \mathbf{m} \star \boldsymbol{\mathcal{L}}_v(\mathbf{q}) - \frac{c}{\eta(m+1)} \langle f(\mathbf{m})/c - 1 \rangle^{m+1} \right] d\tau \right\} . \tag{6.73}$$

For finite time increments, this principle has the algorithmic form

$$W^h(\mathbf{f}') = \inf_{\mathbf{q}} \sup_{\mathbf{m}} \check{W}(\mathbf{f}', \mathbf{q}, \mathbf{m}) \tag{6.74}$$

in terms of the approximated expression for the incremental electro-mechanical work

$$\check{W} = \rho\psi'(\mathfrak{f}', \mathfrak{q}) - \rho\psi'(\mathfrak{f}'_n, \mathfrak{q}_n) + \mathfrak{m} \star [\mathfrak{q} - \boldsymbol{\varphi}_*(\mathfrak{Q}_n)] - \frac{c\Delta t}{\eta(m+1)}\langle f(\mathfrak{m})/c - 1\rangle^{m+1}, \quad (6.75)$$

where we made use of the approximation (6.59). The necessary conditions of the constitutive variational problem (6.74) give the non-linear system of equations

$$\check{\boldsymbol{r}} := \begin{bmatrix} \partial_{\mathfrak{q}}\check{W} \\ \partial_{\mathfrak{m}}\check{W} \end{bmatrix} = \begin{bmatrix} \rho\partial_{\mathfrak{q}}\psi' + \mathfrak{m} \\ \mathfrak{q} - \boldsymbol{\varphi}_*(\mathfrak{Q}_n) - \frac{\Delta t}{\eta}\langle f/c - 1\rangle^m \partial_{\mathfrak{m}}f \end{bmatrix} = \boldsymbol{0}. \quad (6.76)$$

The first equation of the system (6.76) represents the algorithmic definition of the conjugate internal force $\mathfrak{m}$. The second equation of (6.76) is the discrete counterpart of the evolution equation $(6.33)_2$. The above non-linear system (6.76) can be solved at given generalized covector $\mathfrak{f}'$ by a local Newton-type algorithm for the current variables $\check{\boldsymbol{v}} := \{\mathfrak{q}, \mathfrak{m}\}$

$$\check{\boldsymbol{v}} \Leftarrow \check{\boldsymbol{v}} - \check{\boldsymbol{a}}^{-1}\check{\boldsymbol{r}} \quad (6.77)$$

until convergence is achieved in the sense $|\check{\boldsymbol{r}}| < tol$. The tangent matrix of the Newton iteration has the form

$$\check{\boldsymbol{a}} := \begin{bmatrix} \partial^2_{\mathfrak{q}\mathfrak{q}}\check{W} & \partial^2_{\mathfrak{q}\mathfrak{m}}\check{W} \\ \partial^2_{\mathfrak{m}\mathfrak{q}}\check{W} & \partial^2_{\mathfrak{m}\mathfrak{m}}\check{W} \end{bmatrix} = \begin{bmatrix} \rho\partial^2_{\mathfrak{q}\mathfrak{q}}\psi' & \boldsymbol{1} \\ \boldsymbol{1} & -\frac{m\Delta t}{\eta c}\langle f/c - 1\rangle^{m-1}\partial_{\mathfrak{m}}f \otimes \partial_{\mathfrak{m}}f \\ & -\frac{\Delta t}{\eta}\langle f/c - 1\rangle^m \partial^2_{\mathfrak{m}\mathfrak{m}}f \end{bmatrix}. \quad (6.78)$$

Using the implicit function theorem, we may derive a closed-form solution of the coupled electro-mechanical tangent moduli operators defined in $(6.36)_2$

$$\mathfrak{c}' := \partial^2_{\mathfrak{f}'\mathfrak{f}'}w = \rho\partial^2_{\mathfrak{f}'\mathfrak{f}'}\psi' - \begin{bmatrix} \rho\partial^2_{\mathfrak{f}'\mathfrak{q}}\psi' \\ \boldsymbol{0} \end{bmatrix} \cdot (\check{\boldsymbol{a}})^{-1} \cdot \begin{bmatrix} \rho\partial^2_{\mathfrak{q}\mathfrak{f}'}\psi' \\ \boldsymbol{0} \end{bmatrix}. \quad (6.79)$$

Note that the second part of (6.79) characterizes the softening of the fully coupled electro-mechanical tangent moduli due to the evolution of the internal variables. Note also that due to the variational structure the moduli are symmetric.

6.2. Global Variational Principles

This chapter deals with the formulation of the field equations in the form of variational principles and methods. The variational approach in various forms is often taken as the *cornerstone* for the development of discretization techniques such as the well established finite element methodology. Variational principles are particularly powerful and belong to the fundamental principles in mathematics and mechanics. It is important to note that the finite element method needs not necessarily to depend upon the existence of a variational principle. However, good approximate solutions are often related to weak forms of field equations which are consequences of the stationarity condition of a functional.

6.2.1. Compact Form of the Electro-Mechanical Boundary-Value-Problem

A Two-Point Formulation. We start by giving a short summary of the equations describing the quasi-static electro-mechanical boundary-value-problem using a compact

notation compatible with the one introduced in the previous chapter. Here, we consider a two-point formulation. The coupled boundary-value-problem is a two field problem. It is described by choosing as primary variables the deformation map $\boldsymbol{\varphi}(\boldsymbol{X}, t)$

$$\boldsymbol{\varphi} : \begin{cases} \mathcal{B} \times [0, t] & \to & \mathcal{S} \subset \mathbb{R}^3 \\ (\boldsymbol{X}, t) & \mapsto & \boldsymbol{x} = \boldsymbol{\varphi}(\boldsymbol{X}, t) \end{cases} \tag{6.80}$$

and the electric potential $\phi^e(\boldsymbol{X}, t)$

$$\phi^e : \begin{cases} \mathcal{B} \times [0, t] & \to & \mathbb{R} \\ (\boldsymbol{X}, t) & \mapsto & \phi^e(\boldsymbol{X}, t) \end{cases}. \tag{6.81}$$

In order to express the governing equations by using a compact notation, we introduce the generalized deformation map $\mathfrak{U}'$ defined as

$$\mathfrak{U}' := [\boldsymbol{\varphi}(\boldsymbol{X}, t), -\phi^e(\boldsymbol{X}, t)]^T. \tag{6.82}$$

As we already saw in Section 3, the Fréchet derivative of the deformation map is the deformation gradient

$$\boldsymbol{F} := \nabla_{\boldsymbol{X}} \boldsymbol{\varphi}(\boldsymbol{X}, t). \tag{6.83}$$

Further in Section 4 we established that in the quasi static case the electric field has to be a curl-free field (see equation (4.37)). This property is automatically satisfied if the electric field $\mathbb{E}$ is chosen to be the gradient of the electric potential

$$\mathbb{E} := -\nabla_{\boldsymbol{X}} \phi^e(\boldsymbol{X}, t). \tag{6.84}$$

The kinematic equations (6.83) and (6.84) can be expressed in terms of the generalized deformation map $\mathfrak{U}'$ and a generalized material gradient operator $\mathscr{G}$ as

$$\mathfrak{F}' := \mathscr{G}[\mathfrak{U}'], \tag{6.85}$$

with $\mathfrak{F}'$ generalized covector for the two-point formulation introduced in $(6.2)_1$. The key equations for the solution of the boundary-value-problem are the equilibrium equations. These are the balance of linear momentum

$$\mathrm{Div}[\boldsymbol{P}] + \rho_0 \bar{\boldsymbol{\Gamma}} = \boldsymbol{0} \tag{6.86}$$

and the Gauß-Law

$$\mathrm{Div}[\mathbb{D}] - \bar{\rho}_0^e = 0, \tag{6.87}$$

respectively. By using the definition of the two-point generalized vector given in $(6.1)_1$ and the definition of a generalized divergence operator $\mathscr{D}_v$, we can recast (6.86) and (6.87) in the compact format

$$\mathscr{D}_v[\mathfrak{S}'] + \bar{\mathfrak{B}}' = \boldsymbol{0}, \tag{6.88}$$

with $\bar{\mathfrak{B}}'$ array of generalized body forces

$$\bar{\mathfrak{B}}' = [\rho_0 \bar{\boldsymbol{\Gamma}}, \bar{\rho}_0^e]^T. \tag{6.89}$$

Recall that the generalized vector $\mathfrak{S}'$ can be determined in terms of an incremental function W as

$$\mathfrak{S}' = \partial_{\mathfrak{F}'} W(\mathfrak{F}'; \boldsymbol{X}), \tag{6.90}$$

with W defined in the Section 6.1.6. The last equation is valid for both the dissipative and non-dissipative material response. In the last case we have indeed the identification of W with the mixed energy-enthalpy function $\rho_0\psi'$, i.e. $W(\mathfrak{F}'; \boldsymbol{X}) = \rho_0\psi'(\mathfrak{F}'; \boldsymbol{X})$. Insertion of (6.85) and (6.90) into (6.88) finally yields the coupled system of quasi-static electromechanics

$$\mathscr{D}_v[\partial_{\mathfrak{F}'}W(\boldsymbol{\mathscr{G}}[\mathfrak{U}']; \boldsymbol{X})] + \bar{\mathfrak{B}}' = \boldsymbol{0} \tag{6.91}$$

providing twelve coupled scalar differential equations for the determination of the generalized deformation map $\mathfrak{U}'$ in the reference domain $\mathcal{B}$ under consideration. Those equations are in general non-linear. In order to be able to solve the system (6.91) we have to impose the boundary conditions. For the two-point formulation they read for the mechanical problem

$$\boldsymbol{\varphi} = \bar{\boldsymbol{\varphi}}(\boldsymbol{X}, t) \quad \text{on} \quad \partial\mathcal{B}_{\boldsymbol{\varphi}} \qquad \text{and} \qquad \boldsymbol{P}\boldsymbol{N} = \bar{\boldsymbol{T}}(\boldsymbol{X}, t) \quad \text{on} \quad \partial\mathcal{B}_{\boldsymbol{T}}, \tag{6.92}$$

and for the electrical problem

$$\phi^e = \bar{\phi}^e(\boldsymbol{X}, t) \quad \text{on} \quad \partial\mathcal{B}_{\phi} \qquad \text{and} \qquad \mathbb{D} \cdot \boldsymbol{N} = -\bar{\Sigma}^e(\boldsymbol{X}, t) \quad \text{on} \quad \partial\mathcal{B}_{\Sigma}. \tag{6.93}$$

Consistent with the above compact notation, we may write the boundary conditions as

$$\mathfrak{U}' = \bar{\mathfrak{U}}'(\boldsymbol{X}, t) \quad \text{on} \quad \partial\mathcal{B}_{\mathfrak{U}'} \qquad \text{and} \qquad \mathfrak{S}' \cdot \mathfrak{N} = \bar{\mathfrak{T}}'(\boldsymbol{X}, t) \quad \text{on} \quad \partial\mathcal{B}_{\mathfrak{T}'}. \tag{6.94}$$

In equation (6.94) $\bar{\mathfrak{U}}' := [\bar{\boldsymbol{\varphi}}(\boldsymbol{X}, t), -\bar{\phi}^e(\boldsymbol{X}, t)]^T$ assembles the prescribed primary variables on the Dirichlet boundary $\partial\mathcal{B}_{\mathfrak{U}'} := \{\partial\mathcal{B}_{\boldsymbol{\varphi}}, \partial\mathcal{B}_{\phi}\}$. Furthermore $\bar{\mathfrak{T}}' := [\bar{\boldsymbol{T}}(\boldsymbol{X}, t), \bar{\Sigma}^e(\boldsymbol{X}, t)]^T$ assembles the prescribed variables on the Neumann boundaries $\partial\mathcal{B}_{\mathfrak{T}'} := \{\partial\mathcal{B}_{\boldsymbol{T}}, \partial\mathcal{B}_{\Sigma}\}$. The generalized normal vector $\mathfrak{N} := [\boldsymbol{N}, \boldsymbol{N}]^T$ provides the outward surface normals for each partial field of the coupled problem.

6.2.2. Variational Principle. A Two-Point Formulation

Continuous Formulation. Let us assume the existence of an incremental energy functional $I'(\mathfrak{U}')$ for both generalized vectors and loads. This assumption is common in many fields of solid mechanics. A formulation based on energy functionals is very useful, for example, for the development of robust numerical algorithms that are based on optimization techniques.

From now on we assume that the loads do not depend on the motion of the body. It means that the directions of the loads remain parallel and their values unchanged throughout the deformation process. We say such loads are "dead".

We consider a body in static equilibrium under the action of specific "dead" loadings and boundary conditions specified in (6.94). Then the total generalized incremental energy functional $I'(\mathfrak{U}')$ of the system is the difference between the internal energy $I'_{\text{int}}(\mathfrak{U}')$ stored in the body and the underlying free space in the time interval $[t_n, t_{n+1}]$ and the incremental work done by the external loads $I'_{\text{ext}}(\mathfrak{U}')$, i.e.

$$I'(\mathfrak{U}') = I'_{\text{int}}(\mathfrak{U}') - I'_{\text{ext}}(\mathfrak{U}'), \tag{6.95}$$

with

$$\begin{aligned} I'_{\text{int}}(\mathfrak{U}') &= \int_{\mathcal{B}} W(\boldsymbol{\mathscr{G}}[\mathfrak{U}']; \boldsymbol{X})dV \\[2mm] I'_{\text{ext}}(\mathfrak{U}') &= \int_{\mathcal{B}} \bar{\mathfrak{B}}' \star (\hat{\mathfrak{U}}' - \hat{\mathfrak{U}}'_n)dV + \int_{\partial\mathcal{B}_{\mathfrak{T}}} \bar{\mathfrak{T}}' \star (\hat{\mathfrak{U}}' - \hat{\mathfrak{U}}'_n)dA \end{aligned} \tag{6.96}$$

in terms of the generalized deformation map vector defined in (6.82) and of the generalized quantities introduced in Section 6.1. In (6.96) the quantity $\hat{\mathfrak{U}}'$ is defined as $\hat{\mathfrak{U}}' = \mathfrak{U}' - [\boldsymbol{X},\, 0]^T$. The energy functional $I'(\mathfrak{U}')$ has to be stationary with respect to generalized deformation map $\mathfrak{U}'$ satisfying the Dirichlet boundary conditions given in $(6.94)_1$. Thus, our main objective is to find the state of equilibrium for which the potential $I'(\mathfrak{U}')$ is stationary, i.e.

$$\mathfrak{U}' = \text{Arg}\left\{ \underset{\mathfrak{U}' \in \mathcal{W}}{\text{stat}}\, I'(\mathfrak{U}') \right\} = \text{Arg}\left\{ \inf_{\boldsymbol{\varphi}} \sup_{-\phi^e} I'(\boldsymbol{\varphi}, -\phi^e) \right\} \tag{6.97}$$

for admissible generalized deformation map

$$\mathfrak{U}' \in \mathcal{W} := \left\{ \mathfrak{U}' \mid \mathfrak{U}' = \bar{\mathfrak{U}}'(\boldsymbol{X}, t) \quad \text{on} \quad \partial\mathcal{B}_{\mathfrak{U}'} \right\}. \tag{6.98}$$

Note that $I'(\mathfrak{U}')$ has to be minimized with respect to the mechanical primary variable $\boldsymbol{\varphi}$ and maximized with respect to the electrical primary variable $-\phi^e$. This confers to the problem a *saddle-point character*. The stationarity position of the functional $I'(\mathfrak{U}')$ is obtained by requiring the directional derivative with respect to the generalized deformation map $\mathfrak{U}'$ to vanish in all directions $\delta\mathfrak{U}'$, i.e.

$$\delta I'(\mathfrak{U}', \delta\mathfrak{U}') = \left[\frac{d}{d\epsilon} I'(\mathfrak{U}' + \epsilon\delta\mathfrak{U}') \right]_{\epsilon=0} = 0\,, \tag{6.99}$$

which could be regarded as an extension of the principle of minimum potential energy of elastostatics to a stationarity principle for the fully coupled electro-mechanical problem. In particular for the non-dissipative case, the principle is in line with the variational framework of ALLIK & HUGHES [1] and BENJEDDOU [11] for piezoelectricity. Equation (6.99) requires that the first variation of the functional $I'(\mathfrak{U}')$ denoted with $\delta I'$ vanishes. This variation is clearly a function of both $\mathfrak{U}'$ and $\delta\mathfrak{U}'$. The arbitrary vector field $\delta\mathfrak{U}'$ has to be consistent with the conditions imposed on the continuum body and the underlying free space. Thus, $\delta\mathfrak{U}' = \boldsymbol{0}$ over $\partial\mathcal{B}_{\mathfrak{U}'}$, where the generalized deformation map is prescribed. Taking this constraint into account, we can write (6.99) explicitly by using the definition (6.95) and (6.96)

$$\delta I'(\mathfrak{U}', \delta\mathfrak{U}') = \int_{\mathcal{B}} \left\{ \partial_{\tilde{\mathfrak{F}}'} W \star \boldsymbol{\mathscr{G}}[\delta\mathfrak{U}'] - \bar{\boldsymbol{\mathfrak{B}}}' \star \delta\mathfrak{U}' \right\} dV - \int_{\partial\mathcal{B}_{\mathfrak{T}'}} \boldsymbol{\mathfrak{T}}' \star \delta\mathfrak{U}' dA = 0\,. \tag{6.100}$$

By using the Gauß theorem in terms of the generalized deformation map field, we get

$$\delta I' = -\int_{\mathcal{B}} \left\{ \mathscr{D}_v[\partial_{\tilde{\mathfrak{F}}'} W] + \bar{\boldsymbol{\mathfrak{B}}}' \right\} \star \delta\mathfrak{U}' dV + \int_{\partial\mathcal{B}_{\mathfrak{T}'}} \left\{ \partial_{\tilde{\mathfrak{F}}'} W \cdot \boldsymbol{\mathfrak{N}} - \boldsymbol{\mathfrak{T}}' \right\} \star \delta\mathfrak{U}' dA = 0\,. \tag{6.101}$$

Since $\delta\mathfrak{U}'$ has to be arbitrary, we obtain from the necessary condition for the stationarity of the energy functional $I'(\mathfrak{U}')$, the Euler-Lagrange equations associated with the variational principle (6.97)

$$\mathscr{D}_v[\partial_{\tilde{\mathfrak{F}}'} W] + \bar{\boldsymbol{\mathfrak{B}}}' = \boldsymbol{0} \quad \text{in} \quad \mathcal{B}\,,$$

$$\tag{6.102}$$

$$\partial_{\tilde{\mathfrak{F}}'} W \boldsymbol{\mathfrak{N}} = \boldsymbol{\mathfrak{T}}' \quad \text{on} \quad \partial\mathcal{B}_{\mathfrak{T}'}\,.$$

By including the constitutive equations (6.90), we recognize that equation $(6.102)_1$ represents the generalized balance equation (6.88) and equation $(6.102)_2$ are the generalized Neumann boundary conditions$(6.94)_2$.

Finite Element Discretization. The variational problem (6.97) is approximately solved by a finite element method. To this end, the generalized deformation map and its gradient are discretized within N finite element domains $\mathcal{B}^e \subset \mathcal{B}^h$ in which the discretized solid $\mathcal{B}^h$ is decomposed, such that

$$\mathfrak{U}'^h(\boldsymbol{X}) = \mathfrak{X}' + \mathfrak{N}'^e(\boldsymbol{X})\mathfrak{D}'^e \quad \text{and} \quad \mathscr{G}[\mathfrak{U}'^h] = \mathfrak{J}' + \mathfrak{B}'^e(\boldsymbol{X})\mathfrak{D}'^e \quad \text{in} \quad \mathcal{B}^e . \quad (6.103)$$

Here $\mathfrak{D}'^e$ is the element generalized displacement vector

$$\mathfrak{D}'^e := [\boldsymbol{d}^e, -\boldsymbol{\phi}^e]^T \quad (6.104)$$

which contains the element nodal displacements $\boldsymbol{d}^e$ and the negative electric nodal potential $-\boldsymbol{\phi}^e$ at the current time t_{n+1}. Further $\mathfrak{N}'^e(\boldsymbol{X})$ is the matrix of element interpolation functions and $\mathfrak{B}'^e(\boldsymbol{X})$ the associated gradient matrix. The arrays $\mathfrak{X}'$ and $\mathfrak{J}'$ are defined as follows

$$\mathfrak{X}' = \begin{bmatrix} \boldsymbol{X} \\ \boldsymbol{0} \end{bmatrix} \quad \text{and} \quad \mathfrak{J}' = \begin{bmatrix} \boldsymbol{1} & \boldsymbol{0} \\ \boldsymbol{0} & \boldsymbol{0} \end{bmatrix} . \quad (6.105)$$

After assembling the element quantities in global arrays

$$\mathfrak{D}' = \overset{N}{\underset{e=1}{\mathbf{A}}} \mathfrak{D}'^e \quad , \quad \mathfrak{N}'(\boldsymbol{X}) = \overset{N}{\underset{e=1}{\mathbf{A}}} \mathfrak{N}'^e(\boldsymbol{X}) \quad , \quad \mathfrak{B}'(\boldsymbol{X}) = \overset{N}{\underset{e=1}{\mathbf{A}}} \mathfrak{B}'^e(\boldsymbol{X}) , \quad (6.106)$$

we may express the approximated generalized deformation map $\mathfrak{U}'^h$ and its generalized gradient $\mathscr{G}[\mathfrak{U}'^h]$ in the discretized domain $\mathcal{B}^h$ as follows

$$\mathfrak{U}'^h(\boldsymbol{X}) = \mathfrak{X}' + \mathfrak{N}'(\boldsymbol{X})\mathfrak{D}' \quad \text{and} \quad \mathscr{G}[\mathfrak{U}'^h] = \mathfrak{J}' + \mathfrak{B}'(\boldsymbol{X})\mathfrak{D}' \quad \text{in} \quad \mathcal{B}^h . \quad (6.107)$$

With the approximation (6.107) at hand, the energy functional (6.95) appears approximated in the form

$$I'^h(\mathfrak{D}') = \int_{\mathcal{B}^h} \left\{ W(\mathfrak{J}' + \mathfrak{B}'\mathfrak{D}'; \boldsymbol{X}) - \bar{\mathfrak{B}}' \star \mathfrak{N}'\Delta\mathfrak{D}' \right\} dV - \int_{\partial\mathcal{B}^h_{\mathfrak{T}'}} \bar{\mathfrak{T}}' \star \mathfrak{N}'\Delta\mathfrak{D}' dA \quad (6.108)$$

with $\Delta\mathfrak{D}' := (\mathfrak{D}' - \mathfrak{D}'_n)$. The discrete energy functional (6.108) has to be stationary with respect to the global generalized nodal displacement $\mathfrak{D}'$ and thus we search for the global generalized nodal displacement $\mathfrak{D}'$ which satisfy the variational principle

$$\mathfrak{D}' = \mathrm{Arg} \left\{ \underset{\mathfrak{D}'\in\mathcal{W}^h}{\mathrm{stat}} I'^h(\mathfrak{D}') \right\} = \mathrm{Arg} \left\{ \underset{\boldsymbol{D}}{\inf}\,\underset{-\boldsymbol{\phi}}{\sup} I'^h(\boldsymbol{D}, -\boldsymbol{\phi}) \right\} , \quad (6.109)$$

which results to be the discrete counterpart of (6.97). Here, $\boldsymbol{D} = \overset{N}{\underset{e=1}{\mathbf{A}}} \boldsymbol{d}^e$, $\boldsymbol{\phi} = \overset{N}{\underset{e=1}{\mathbf{A}}} \boldsymbol{\phi}^e$, and $\mathcal{W}^h$ is the set of admissible nodal variables which satisfy the discrete Dirichlet boundary conditions

$$\mathcal{W}^h := \left\{ \mathfrak{D}' \mid \mathfrak{D}' = \bar{\mathfrak{D}}' \quad \text{on} \quad \partial\mathcal{B}^h_{\mathfrak{U}'} \right\} . \quad (6.110)$$

The necessary conditions for the solution of the discrete stationary problem (6.109) are given by setting to zero the variation of $I'^h(\mathfrak{D}')$

$$I'^h_{,\mathfrak{D}'}(\mathfrak{D}') = \boldsymbol{0} . \quad (6.111)$$

The equations (6.111) provide a system of non-linear equations from which the discrete generalized displacements, i.e. the mechanical nodal displacements and the electric nodal potentials, are determined. The solution vector may be obtained through an iterative method as the Newton-Raphson method, yielding the update equations

$$\mathfrak{D}' = \mathfrak{D}' - \left[I'^h_{,\mathfrak{D}'\mathfrak{D}'}(\mathfrak{D}')\right]^{-1}\left[I'^h_{,\mathfrak{D}'}(\mathfrak{D}')\right] \tag{6.112}$$

performed by some solver of linear equations. Due to the variational structure of the coupled electro-mechanical problem, the coupled tangent $\boldsymbol{\mathfrak{K}}' = I'^h_{\mathfrak{D}'\mathfrak{D}'}$ is symmetric. The update (6.112) is performed till convergence is reached in the sense

$$\left\|I'^h_{,\mathfrak{D}'}(\mathfrak{D}')\right\| < \mathrm{tol}\,, \tag{6.113}$$

i.e. till the norm of the residuum $\boldsymbol{\mathfrak{R}}' = I'^h_{,\mathfrak{D}'}$ is smaller than a certain predefined tolerance. The first and second derivatives of the discrete variational functional (6.108) give all the finite element arrays needed for the solution of the coupled electro-mechanical boundary-value-problem by means of the finite element method. These arrays are the finite element residual

$$\boldsymbol{\mathfrak{R}}' := I'^h_{,\mathfrak{D}'} = \int\limits_{\mathcal{B}^h} \left\{\boldsymbol{\mathfrak{B}}'^T\boldsymbol{\mathfrak{S}}'^h - \boldsymbol{\mathfrak{N}}'^T\bar{\boldsymbol{\mathfrak{B}}}'\right\}dV - \int\limits_{\partial\mathcal{B}'_{\bar{\mathfrak{T}}'}} \boldsymbol{\mathfrak{N}}'^T\bar{\boldsymbol{\mathfrak{T}}}'dA \tag{6.114}$$

and the finite element tangent matrix

$$\boldsymbol{\mathfrak{K}}' := I'^h_{,\mathfrak{D}'\mathfrak{D}'} = \int\limits_{\mathcal{B}^h} \boldsymbol{\mathfrak{B}}'^T\boldsymbol{\mathfrak{C}}'^h\boldsymbol{\mathfrak{B}}'dV\,. \tag{6.115}$$

These arrays are expressed in terms of the first and second derivatives of the incremental functional W which give the generalized approximated vector $\boldsymbol{\mathfrak{S}}'^h$ and moduli $\boldsymbol{\mathfrak{C}}'^h$

$$\boldsymbol{\mathfrak{S}}'^h := \partial_{\boldsymbol{\mathfrak{F}}'^h}W(\boldsymbol{\mathfrak{I}}' + \boldsymbol{\mathfrak{B}}'\mathfrak{D}';\boldsymbol{X}) \qquad \text{and} \qquad \boldsymbol{\mathfrak{C}}'^h := \partial^2_{\boldsymbol{\mathfrak{F}}'^h\boldsymbol{\mathfrak{F}}'^h}W(\boldsymbol{\mathfrak{I}}' + \boldsymbol{\mathfrak{B}}'\mathfrak{D}';\boldsymbol{X}) \tag{6.116}$$

of the coupled problem. Clearly, due to the variational structure of the coupled constitutive problem, the moduli $\boldsymbol{\mathfrak{C}}'^h$ are symmetric. However, they are not positive definite due to the saddle-point structure. As a consequence, also the finite element tangent matrix $\boldsymbol{\mathfrak{K}}'$ is not positive definite and this excludes the application of certain fast and efficient solvers for the solution of the linear iterative update (6.112).

6.3. Small Strain Approximation

In this section, we adapt the above described variational formulation for large strain to the case of small deformations and we will focus again on a formulation based on *generalized vectors* and *generalized covectors*. We recall that the generalized vectors are the stresses and the electric displacement while the generalized covectors are the strains and the electric field. In this case we deal only with one type of generalized vectors and covectors which will be indicated with $\boldsymbol{\mathfrak{s}}'$ and $\boldsymbol{\mathfrak{f}}'$, respectively, and are defined as follows

$$\boldsymbol{\mathfrak{s}}' := [\boldsymbol{\sigma}, -\mathrm{d}]^T \qquad , \qquad \boldsymbol{\mathfrak{f}}' := [\boldsymbol{\varepsilon}, \mathbb{e}]^T\,. \tag{6.117}$$

In terms of the generalized vectors and covectors, the electro-mechanical power $\rho\mathscr{P}'$ expressed in the equation (5.109) can be written in a more compact fashion as

$$\rho\mathscr{P}' = \boldsymbol{\mathfrak{s}}' \star \dot{\boldsymbol{\mathfrak{f}}}'\,. \tag{6.118}$$

Here the star indicates a generalized inner product that produces a scalar according to (5.109). Thus, the electro-mechanical power is the inner product between the generalized vector and the rate of the generalized covector.

6.3.1. Dissipative Response

We directly consider a dissipative electro-mechanical material response which appears for example in ferroelectric materials. The case of non-dissipative materials can be recovered by dropping the dissipation contribution. Thus, we may write the work done to the material element as sum of stored and dissipated contributions

$$w_0^t := \int\limits_0^t \rho \mathscr{P}' d\tau = \rho \hat{\psi}'(t) - \rho \hat{\psi}'(0) + d_0^t \,, \tag{6.119}$$

where

$$d_0^t := \int\limits_0^t \rho \mathscr{D}_{loc} d\tau \geq 0 \,, \tag{6.120}$$

is the part of the electro-mechanical work which dissipates into heat while $\rho \hat{\psi}'(t) - \rho \hat{\psi}'(0)$ constitutes the stored one. The statement (6.120) expresses the second law of thermodynamics which was already introduced in Section 5 and states a positive dissipation for arbitrary processes. Considering (6.119) we may write

$$\rho \mathscr{P}' = \frac{d}{dt} \rho \hat{\psi}'(\mathbf{f}'(t)) + \rho_0 \mathscr{D}_{loc} \,, \tag{6.121}$$

from which it becomes clear that the energy storage function ψ' cannot be only a function of the generalized covector $\mathbf{f}'$, but has to depend additionally on a set of internal variables $\mathbf{q} \in \mathbb{R}^m$, i.e.

$$\rho \psi'(t) = \rho \hat{\psi}'(\mathbf{f}'(t), \mathbf{q}(t)) \,. \tag{6.122}$$

Following the Coleman-Noll-Gurtin's arguments recalled in Section 5, we identify the generalized vector and the internal forces $\mathfrak{m}$ dual to $\mathbf{q}$ by

$$\mathbf{s}' = \rho \partial_{\mathbf{f}'} \psi'(\mathbf{f}', \mathbf{q}) \qquad , \qquad \mathfrak{m} = -\rho \partial_{\mathbf{q}'} \psi'(\mathbf{f}', \mathbf{q}) \,. \tag{6.123}$$

Usage of (6.123) gives the reduced dissipation

$$\rho \mathscr{D}_{loc} = \mathfrak{m} \star \dot{\mathbf{q}} \geq 0 \tag{6.124}$$

as an inner product of the internal forces, driving the evolution of the internal variables, and the time rate of the internal variables.

6.3.2. Evolution Equations

The constitutive setting for dissipative materials is completed by the evolution equations for the internal variables. Those equations can be formulated by postulating the existence of a dissipation potential $\phi : \mathbb{R}^m \to \mathbb{R}$. This function is assumed to depend on the flux $\dot{\mathbf{q}}$ of the internal variables and determine the evolution of $\mathbf{q}$ in terms of the constitutive differential equations

$$\boldsymbol{0} \in \rho \partial_{\mathbf{q}} \psi'(\mathbf{f}', \mathbf{q}) + \rho \partial_{\dot{\mathbf{q}}} \phi(\dot{\mathbf{q}}) \qquad \text{or} \qquad \mathfrak{m} \in \rho \partial_{\dot{\mathbf{q}}} \phi(\dot{\mathbf{q}}) \qquad \text{with} \qquad \mathbf{q}(0) = \mathbf{q}_0 \tag{6.125}$$

often referred to as Biot's equation of standard dissipative systems. The constitutive equations (6.123) and (6.125) determine the generalized vector response of a smooth normal electro-mechanically coupled material in a generalized-covector driven process where the generalized covector is prescribed. The insertion of the evolution equation (6.125) into the reduced dissipation inequality (6.124) gives the form

$$\rho \partial_{\dot{\mathbf{q}}} \phi(\dot{\mathbf{q}}) \star \dot{\mathbf{q}} \geq 0 \,, \tag{6.126}$$

which serves as fundamental physically-based constraint on the dissipation function ϕ.

Based on the definition (6.123), we may introduce a dual dissipation function $\phi^* : \mathbb{R}^m \to \mathbb{R}$ depending on the internal forces $\mathfrak{m}$ by the Legendre-Fenchel transformation

$$\rho \phi^*(\mathfrak{m}) := \sup_{\dot{\mathbf{q}}} \{ \mathfrak{m} \star \dot{\mathbf{q}} - \rho \phi(\dot{\mathbf{q}}) \} \,. \tag{6.127}$$

The dual dissipation function defines directly the evolution of the internal variables by

$$\dot{\mathbf{q}} \in \rho \partial_{\mathfrak{m}} \phi^*(\mathfrak{m}) \,, \tag{6.128}$$

dual to $(6.125)_2$, degenerating for a smooth response to $\dot{\mathbf{q}} = \rho \partial_{\mathfrak{m}} \phi^*(\mathfrak{m})$.

6.3.3. Rate-Independent Dissipation Functions

Rate-independent dissipation functions are often derived by invoking the so-called principle of maximum dissipation by extension of the arguments used to model the case of rate independent plasticity. Here, the dissipation function is defined by the constraint maximum problem

$$\rho \phi(\dot{\mathbf{q}}) = \sup_{\mathfrak{m} \in a} \{ \mathfrak{m} \star \dot{\mathbf{q}} \} \,, \tag{6.129}$$

where a models a reversible domain in the space of the driving forces $\mathfrak{m}$,

$$a := \{ \mathfrak{m} \in \mathbb{R}^m | f(\mathfrak{m}) \leq c \} \tag{6.130}$$

in terms of a set-level function $f : \mathbb{R}^m \to \mathbb{R}$, which is positive $f(\mathfrak{m}) \geq 0$, normalized $f(\mathbf{0}) = 0$, convex and homogeneous of order one $f(\alpha \mathbf{A}) = \alpha f(\mathbf{A})$ for $\alpha > 0$. The threshold value $c > 0$ bounds the driving force $\mathfrak{m}$. The constrained maximum problems (6.129) can be solved by a Lagrange method

$$\rho \phi(\dot{\mathbf{q}}) = \sup_{\mathfrak{m}, \lambda \geq 0} \{ \mathfrak{m} \star \dot{\mathbf{q}} - \lambda(f(\mathfrak{m}) - c) \} \,. \tag{6.131}$$

By exploitation of the necessary conditions for the maximum problem (6.131) we obtain the evolution equation for the internal variables

$$\dot{\mathbf{q}} = \lambda \partial_{\mathfrak{m}} f(\mathfrak{m}) \tag{6.132}$$

along with the loading-unloading conditions

$$\lambda \geq 0 \quad , \quad f(\mathfrak{m}) \leq c \quad , \quad \lambda(f(\mathfrak{m}) - c) = 0 \,. \tag{6.133}$$

The latter determine the non-smooth dissipative response by the set-level function f. Note that the insertion of (6.132) into (6.131) gives the simple expression for the dissipation function $\rho \mathscr{D}_{loc} = \rho \phi(\dot{\mathbf{q}}) = \lambda c \geq 0$. The combination of (6.132) and (6.133) is a specific form of (6.128) for a rate-independent response governed by a switching function f.

6.3.4. Rate-Dependent Dissipation Functions

A rate-dependent class of dissipation functions with reversible range a governed by the set-level function f is obtained by an approximate penalty-type solution of the maximum problem (6.129)

$$\rho\phi(\dot{\mathfrak{q}}) = \sup_{\mathfrak{m}} \left\{ \mathfrak{m} \star \dot{\mathfrak{q}} - \frac{c}{\eta(m+1)} \langle f(\mathfrak{m})/c - 1 \rangle^{m+1} \right\}, \tag{6.134}$$

where the constants $\eta > 0$ and $m > 0$ are interpreted as material parameters associated with the viscosity of the electro-mechanical process. The necessary conditions of (6.134) provides the non-linear evolution equations

$$\dot{\mathfrak{q}} = \frac{1}{\eta} \langle f(\mathfrak{m})/c - 1 \rangle^{m} \partial_{\mathfrak{m}} f(\mathfrak{m}). \tag{6.135}$$

This evolution equations may be directly obtained from (6.129) based on the dual dissipation function

$$\rho\phi^*(\mathfrak{m}) = \frac{c}{\eta(m+1)} \langle f(\mathfrak{m})/c - 1 \rangle^{m+1}, \tag{6.136}$$

which follows from (6.134), if the penalty-type variational principle is interpreted as Legendre-Fenchel transformation. For $\eta \to 0$ we obtain in the limit the rate-independent form (6.132) combined with (6.133).

6.3.5. Variational Principle for Dissipative Response

Incremental Potential for Generalized Vectors. We consider now an incremental electro-mechanical loading process in the time interval $[t_n, t_{n+1}]$. We assume that the state of the material at the time t_n is known and in particular the internal state, characterized by the value $\mathfrak{q}_n$ of the internal variables at the time t_n is assumed to be known. Our aim is to determine the new generalized vector state at t_{n+1} when advancing the generalized covector from $\mathfrak{f}'_n$ at time t_n to $\mathfrak{f}'_{n+1}$ at time t_{n+1}. To this purpose we define an *incremental potential w* depending only on the current generalized covector $\mathfrak{f}'_{n+1}$ that determines the current generalized vector by the *quasi-hyperelastic function evaluation*

$$\mathfrak{s}'_{n+1} = \partial_{\mathfrak{f}'_{n+1}} w(\mathfrak{f}'_{n+1}). \tag{6.137}$$

We will omit from now on the subscript "$n + 1$" indicating the variables at the current time step t_{n+1} with an exception for t_{n+1} itself. A further derivation of the potential w, and thus of the generalized vector $\mathfrak{s}'$ gives the coupled electro-mechanical consistent tangent moduli

$$\mathfrak{c}' := \partial_{\mathfrak{f}'} \mathfrak{s}' = \partial^2_{\mathfrak{f}'\mathfrak{f}'} w(\mathfrak{f}'). \tag{6.138}$$

The incremental potential $w(\mathfrak{f}')$ represents the incremental electro-mechanical work done on the infinitesimal material volume element in the time window $[t_n, t_{n+1}]$ which accounts not only for the energy stored in the material, but also for the dissipated energy. Equations (6.137) and (6.138) suggests that the incremental potential w can be considered as an extension of the mixed energy-enthalpy function ψ' used to characterized a non-dissipative material response. Clearly, this functional must cover characteristics of the storage function ψ' and the dissipation function ϕ introduced above. To this end we

propose a definition of the incremental functional w through the following variational problem

$$w(\mathbf{f}') = \inf_{\dot{\mathbf{q}}} \left\{ \int_{t_n}^{t_{n+1}} \left[\frac{d}{dt} \rho \psi'(\mathbf{f}', \mathbf{q}) + \rho \phi(\dot{\mathbf{q}}) \right] d\tau \right\} \quad \text{with} \quad \mathbf{q}(t_n) = \mathbf{q}_n. \tag{6.139}$$

For the prescribed generalized covector, this problem defines the incremental potential function w as a minimum of the generalized work $\int_{t_n}^{t_{n+1}} \left[\rho \dot{\psi}' + \rho \phi \right] d\tau$ done on the material in the time increment under consideration. Starting with the given initial condition $\mathbf{q}(t_n) = \mathbf{q}_n$, the minimum problem defines an optimum path of the internal variables $\mathbf{q}(t)$ for $t \in [t_n, t_{n+1}]$ including the right boundary value $\mathbf{q} = \mathbf{q}(t_{n+1})$.

Equations (6.137) and (6.139) provide an approximate variational counterpart of the continuous setting (6.123) and (6.125) of the constitutive equations in the discrete time step $[t_n, t_{n+1}]$ under consideration. For finite time increments Δt, the minimization problem (6.139) is understood to have the algorithmic form

$$w^h(\mathbf{f}') = \inf_{\mathbf{q}} \tilde{w}(\mathbf{f}', \mathbf{q}) \tag{6.140}$$

in terms of the algorithmic expression for the (generalized) incremental electro-mechanical work

$$\tilde{w}(\mathbf{f}', \mathbf{q}) = \rho \psi'(\mathbf{f}', \mathbf{q}) - \rho \psi'(\mathbf{f}'_n, \mathbf{q}_n) + \Delta t \, \rho \phi \left(\frac{\mathbf{q} - \mathbf{q}_n}{\Delta t} \right). \tag{6.141}$$

Note that the algorithmic expression in (6.141) is based on an approximation of the integrals $\int_{t_n}^{t_{n+1}} \rho \phi(\dot{\mathbf{q}}) d\tau \approx \Delta t \rho \phi \left(\frac{\mathbf{q} - \mathbf{q}_n}{\Delta t} \right)$ in (6.139) through the algorithmic simplification of the rates $\dot{\mathbf{q}}$ of $\mathbf{q}$ with the constant value $\dot{\mathbf{q}} \approx [\mathbf{q} - \mathbf{q}_n]/\Delta t$ in the interval $[t_n, t_{n+1}]$. The exploitation of the necessary condition for the algorithmic minimization problem (6.140) provides the algorithmic form

$$\mathbf{0} \in \rho \partial_{\mathbf{q}} \psi'(\mathbf{f}', \mathbf{q}) + \Delta t \rho \partial_{\mathbf{q}} \phi \left(\frac{\mathbf{q} - \mathbf{q}_n}{\Delta t} \right) \tag{6.142}$$

of Biot's equation (6.125). In other words, the algorithmic minimization problem (6.140) determines the update of the internal variables.

A Variational Principle for Rate-Independent Response. For rate independent dissipative processes characterized by a reversible range a defined in (6.130) in terms of the switching function f, we may modify the variational problem (6.139) by inserting the specific dissipation function (6.131)

$$w(\mathbf{f}') = \inf_{\dot{\mathbf{q}}} \sup_{\mathbf{m}, \lambda \geq 0} \left\{ \int_{t_n}^{t_{n+1}} \left[\frac{d}{dt} \rho \psi' + \mathbf{m} \star \dot{\mathbf{q}} - \lambda(f(\mathbf{m}) - c) \right] d\tau \right\}. \tag{6.143}$$

For finite time increments, this principle has the algorithmic form

$$w^h(\mathbf{f}') = \inf_{\mathbf{q}} \sup_{\mathbf{m}, \gamma \geq 0} \tilde{w}(\mathbf{f}', \mathbf{q}, \mathbf{m}, \gamma) \tag{6.144}$$

in terms of the approximated expression for the incremental electro-mechanical work

$$\tilde{w} = \rho\psi'(\mathbf{f}',\mathbf{q}) - \rho\psi'(\mathbf{f}'_n,\mathbf{q}_n) + \mathbf{m} \star [\mathbf{q} - \mathbf{q}_n] - \gamma(f(\mathbf{m}) - c). \tag{6.145}$$

Here, $\gamma := \lambda\Delta t$ is the Lagrange parameter associated with the increment $[t_n, t_{n+1}]$. For the loading case $\gamma > 0$, the necessary conditions of the constitutive variational problem (6.144) give the non-linear system of equations

$$\tilde{r} := \begin{bmatrix} \partial_{\mathbf{q}}\tilde{w} \\ \partial_{\mathbf{m}}\tilde{w} \\ \partial_{\gamma}\tilde{w} \end{bmatrix} = \begin{bmatrix} \rho\partial_{\mathbf{q}}\psi' + \mathbf{m} \\ \mathbf{q} - \mathbf{q}_n - \gamma\partial_{\mathbf{m}}f \\ -f + c \end{bmatrix} = \mathbf{0} \tag{6.146}$$

along with the discrete version of the loading-unloading conditions (6.133)

$$\gamma \geq 0 \quad , \quad f(\mathbf{m}) \leq c \quad , \quad \gamma(f(\mathbf{m}) - c) = 0. \tag{6.147}$$

The first equation of the system (6.146) represents the algorithmic definition of the conjugate internal force $\mathbf{m}$. The second equation of (6.146) is the discrete counterpart of the evolution equation $(6.125)_1$. The above non-linear system (6.146) can be solved at given generalized covector $\mathbf{f}'$ by a local Newton-type algorithm for the current variables $\tilde{v} := \{\mathbf{q}, \mathbf{m}, \gamma\}$

$$\tilde{v} \Leftarrow \tilde{v} - \tilde{a}^{-1}\tilde{r} \tag{6.148}$$

until convergence is achieved in the sense $|\tilde{r}| < tol$. The tangent matrix of the Newton iteration has the form

$$\tilde{a} := \begin{bmatrix} \partial_{\mathbf{qq}}^2\tilde{w} & \partial_{\mathbf{qm}}^2\tilde{w} & \partial_{\mathbf{q}\gamma}^2\tilde{w} \\ \partial_{\mathbf{mq}}^2\tilde{w} & \partial_{\mathbf{mm}}^2\tilde{w} & \partial_{\mathbf{m}\gamma}^2\tilde{w} \\ \partial_{\gamma\mathbf{q}}^2\tilde{w} & \partial_{\gamma\mathbf{m}}^2\tilde{w} & \partial_{\gamma\gamma}^2\tilde{w} \end{bmatrix} = \begin{bmatrix} \rho_0\partial_{\mathbf{qq}}^2\psi' & \mathbf{1} & \mathbf{0} \\ \mathbf{1} & -\gamma\partial_{\mathbf{mm}}^2 f & -\partial_{\mathbf{m}}f \\ \mathbf{0} & -\partial_{\mathbf{m}}f & \mathbf{0} \end{bmatrix}. \tag{6.149}$$

Using the implicit function theorem, we may derive a closed-form solution of the coupled electro-mechanical tangent moduli operators defined in $(6.138)_1$

$$\mathbf{c}' := \partial_{\mathbf{f}'\mathbf{f}'}^2 w = \rho\partial_{\mathbf{f}'\mathbf{f}'}^2\psi' - s \begin{bmatrix} \rho\partial_{\mathbf{f}'\mathbf{q}}^2\psi' \\ \mathbf{0} \\ \mathbf{0} \end{bmatrix} \cdot (\tilde{a})^{-1} \cdot \begin{bmatrix} \rho\partial_{\mathbf{qf}'}^2\psi' \\ \mathbf{0} \\ \mathbf{0} \end{bmatrix} \tag{6.150}$$

in terms of a dissipative loading flag

$$s := \begin{cases} 1 & \text{for} \quad \gamma > 0, \\ 0 & \text{otherwise}. \end{cases} \tag{6.151}$$

Note that the second part of (6.150) characterizes the softening of the fully coupled electro-mechanical tangent moduli due to the evolution of the internal variables. Note also that due to the variational structure the moduli are symmetric.

A Variational Principle for Rate-Dependent Response. For rate dependent dissipative processes characterized by a reversible range a defined in (6.130) in terms of the switching function f, we may modify the variational problem (6.139) by inserting the specific dissipation function (6.134)

$$w(\mathfrak{f}') = \inf_{\dot{\mathfrak{q}}} \sup_{\mathfrak{m}} \left\{ \int_{t_n}^{t_{n+1}} \left[\frac{d}{dt}\rho\psi' + \mathfrak{m} \star \dot{\mathfrak{q}} - \frac{c}{\eta(m+1)}\langle f(\mathfrak{m})/c - 1\rangle^{m+1} \right] d\tau \right\} . \qquad (6.152)$$

For finite time increments, this principle has the algorithmic form

$$w^h(\mathfrak{f}') = \inf_{\mathfrak{q}} \sup_{\mathfrak{m}} \bar{w}(\mathfrak{f}', \mathfrak{q}, \mathfrak{m}) \qquad (6.153)$$

in terms of the approximated expression for the incremental electro-mechanical work

$$\bar{w} = \rho\psi'(\mathfrak{f}', \mathfrak{q}) - \rho\psi'(\mathfrak{f}'_n, \mathfrak{q}_n) + \mathfrak{m} \star [\mathfrak{q} - \mathfrak{q}_n] - \frac{c\Delta t}{\eta(m+1)}\langle f(\mathfrak{m})/c - 1\rangle^{m+1} . \qquad (6.154)$$

The necessary conditions of the constitutive variational problem (6.153) give the nonlinear system of equations

$$\bar{r} := \begin{bmatrix} \partial_{\mathfrak{q}}\bar{w} \\ \partial_{\mathfrak{m}}\bar{w} \end{bmatrix} = \begin{bmatrix} \rho\partial_{\mathfrak{q}}\psi' + \mathfrak{m} \\ \mathfrak{q} - \mathfrak{q}_n - \frac{\Delta t}{\eta}\langle f/c - 1\rangle^m \partial_{\mathfrak{m}}f \end{bmatrix} = \boldsymbol{0} . \qquad (6.155)$$

The first equation of the system (6.155) represents the algorithmic definition of the conjugate internal force $\mathfrak{m}$. The second equation of (6.155) is the discrete counterpart of the evolution equation (6.135). The above non-linear system (6.155) can be solved at given generalized covector $\mathfrak{f}'$ by a local Newton-type algorithm for the current variables $\bar{v} := \{\mathfrak{q}, \mathfrak{m}\}$

$$\bar{v} \Leftarrow \bar{v} - \bar{a}^{-1}\bar{r} \qquad (6.156)$$

until convergence is achieved in the sense $|\bar{r}| < tol$. The tangent matrix of the Newton iteration has the form

$$\bar{a} := \begin{bmatrix} \partial^2_{\mathfrak{qq}}\bar{w} & \partial^2_{\mathfrak{qm}}\bar{w} \\ \partial^2_{\mathfrak{mq}}\bar{w} & \partial^2_{\mathfrak{mm}}\bar{w} \end{bmatrix} = \begin{bmatrix} \rho\partial^2_{\mathfrak{qq}}\psi' & \boldsymbol{1} \\ \boldsymbol{1} & -\frac{m\Delta t}{\eta c}\langle f/c - 1\rangle^{m-1}\partial_{\mathfrak{m}}f \otimes \partial_{\mathfrak{m}}f \\ & -\frac{\Delta t}{\eta}\langle f/c - 1\rangle^m \partial^2_{\mathfrak{mm}}f \end{bmatrix} . \qquad (6.157)$$

Using the implicit function theorem, we may derive a closed-form solution of the coupled electro-mechanical tangent moduli operators defined in (6.138)

$$\mathfrak{c}' := \partial^2_{\mathfrak{f}'\mathfrak{f}'}w = \rho\partial^2_{\mathfrak{f}'\mathfrak{f}'}\psi' - \begin{bmatrix} \rho\partial^2_{\mathfrak{f}'\mathfrak{q}}\psi' \\ \boldsymbol{0} \end{bmatrix} \cdot (\bar{a})^{-1} \cdot \begin{bmatrix} \rho\partial^2_{\mathfrak{q}\mathfrak{f}'}\psi' \\ \boldsymbol{0} \end{bmatrix} . \qquad (6.158)$$

Note that the second part of (6.158) characterizes the softening of the fully coupled electro-mechanical tangent moduli due to the evolution of the internal variables. Note also that due to the variational structure the moduli are symmetric.

6.3.6. Global Variational Principle.

We start by giving a short summary of the equations describing the quasi-static electro-mechanical boundary-value-problem for small strains using a compact notation compatible with the one introduced above. The coupled boundary-value-problem is a two field problem. Usually it is described by choosing as primary variables the displacement field $\boldsymbol{u}(\boldsymbol{X}, t)$

$$\boldsymbol{u} : \begin{cases} \mathcal{B} \times [0, t] & \to & \mathbb{R}^3 \\ \\ (\boldsymbol{x}, t) & \mapsto & \boldsymbol{u}(\boldsymbol{x}, t) \end{cases} \tag{6.159}$$

and the electric potential $\phi^e(\boldsymbol{X}, t)$

$$\phi^e : \begin{cases} \mathcal{B} \times [0, t] & \to & \mathbb{R} \\ \\ (\boldsymbol{x}, t) & \mapsto & \phi^e(\boldsymbol{x}, t) \end{cases} . \tag{6.160}$$

In order to express the governing equations by using a compact notation, we introduce the generalized displacement $\mathfrak{u}'$ defined as

$$\mathfrak{u}' := [\boldsymbol{u}(\boldsymbol{x}, t), -\phi^e(\boldsymbol{x}, t)]^T . \tag{6.161}$$

As we already saw in Section 5.8, the symmetric part of the displacement gradient represents the strains

$$\boldsymbol{\varepsilon} := \text{sym}[\nabla \boldsymbol{u}(\boldsymbol{x}, t)] = \frac{1}{2} \left[\nabla \boldsymbol{u}(\boldsymbol{x}, t) + \nabla^T \boldsymbol{u}(\boldsymbol{x}, t) \right] . \tag{6.162}$$

Further in Section 4 we established that in the quasi static case the electric field has to be a curl-free field. This property is automatically satisfied if the electric field $\mathfrak{e}$ is chosen to be the gradient of the electric potential

$$\mathfrak{e} := -\nabla \phi^e(\boldsymbol{x}, t) . \tag{6.163}$$

The kinematic equations (6.162) and (6.163) can be expressed in terms of the generalized displacement $\mathfrak{u}'$ and a generalized material gradient operator $\boldsymbol{\mathcal{G}}$ as

$$\mathfrak{f}' := \boldsymbol{\mathcal{G}}[\mathfrak{u}'] , \tag{6.164}$$

with $\mathfrak{f}'$ generalized covector in $(6.117)_2$.

The key equations for the solution of the boundary-value-problem are the equilibrium equations. These are the balance of linear momentum

$$\text{div}[\boldsymbol{\sigma}] + \rho \bar{\gamma} = \boldsymbol{0} \tag{6.165}$$

and the Gauß-Law

$$\text{div}[\mathfrak{d}] - \bar{\rho}^e = 0 , \tag{6.166}$$

respectively. By using the definition of the generalized vector given in $(6.117)_1$ and the definition of a generalized divergence operator $\mathcal{D}_v$, we can recast (6.165) and (6.166) in the compact format

$$\mathcal{D}_v[\mathfrak{s}'] + \bar{\mathfrak{b}}' = \boldsymbol{0} , \tag{6.167}$$

with $\bar{\mathbf{b}}'$ array of generalized body forces

$$\bar{\mathbf{b}}' = [\rho\bar{\boldsymbol{\gamma}}, \bar{\rho}^e]^T \,. \tag{6.168}$$

Recall that the generalized vector $\mathbf{s}'$ can be determined in terms of an incremental function w as

$$\mathbf{s}' = \partial_{\mathbf{f}'} w(\mathbf{f}'; \boldsymbol{x}) \,, \tag{6.169}$$

with w defined in the Section 6.3.5. The last equation is valid for both the dissipative and non-dissipative material response. In the last case we have indeed the identification of w with the increment of the mixed energy-enthalpy function $\rho\psi'$, i.e. $w(\mathbf{f}'; \boldsymbol{x}) = (\rho\psi'(\mathbf{f}'; \boldsymbol{x}) - \rho\psi'(\mathbf{f}'_n; \boldsymbol{x}))$. Insertion of (6.164) and (6.169) into (6.167) finally yields the coupled system of quasi-static electro-mechanics

$$\mathcal{D}_v[\partial_{\mathbf{f}'} w(\boldsymbol{\mathcal{G}}[\mathbf{u}']; \boldsymbol{x})] + \bar{\mathbf{b}}' = \mathbf{0} \tag{6.170}$$

providing nine coupled scalar differential equations for the determination of the generalized displacement $\mathbf{u}'$ in the domain $\mathcal{B}$ under consideration. Those equations are in general non-linear. In order to be able to solve the system (6.170) we have to impose the boundary conditions. They read for the mechanical problem

$$\boldsymbol{u} = \bar{\boldsymbol{u}}(\boldsymbol{x}, t) \quad \text{on} \quad \partial\mathcal{B}_{\boldsymbol{u}} \qquad \text{and} \qquad \boldsymbol{\sigma}\boldsymbol{n} = \bar{\boldsymbol{t}}(\boldsymbol{x}, t) \quad \text{on} \quad \partial\mathcal{B}_{\boldsymbol{t}} \,, \tag{6.171}$$

and for the electrical problem

$$\phi^e = \bar{\phi}^e(\boldsymbol{x}, t) \quad \text{on} \quad \partial\mathcal{B}_{\phi} \qquad \text{and} \qquad \mathrm{d} \cdot \boldsymbol{n} = -\bar{\sigma}^e(\boldsymbol{x}, t) \quad \text{on} \quad \partial\mathcal{B}_{\mathrm{d}} \,. \tag{6.172}$$

Consistent with the above compact notation, we may write the boundary conditions as

$$\mathbf{u}' = \bar{\mathbf{u}}'(\boldsymbol{x}, t) \quad \text{on} \quad \partial\mathcal{B}_{\mathbf{u}'} \qquad \text{and} \qquad \mathbf{s}' \cdot \mathbf{n} = \bar{\mathbf{t}}'(\boldsymbol{x}, t) \quad \text{on} \quad \partial\mathcal{B}_{\mathbf{t}'} \,. \tag{6.173}$$

In equation (6.173) $\bar{\mathbf{u}}' := [\bar{\boldsymbol{u}}(\boldsymbol{x}, t), -\bar{\phi}^e(\boldsymbol{x}, t)]^T$ assembles the prescribed primary variables on the Dirichlet boundary $\partial\mathcal{B}_{\mathbf{u}'} := \{\partial\mathcal{B}_{\boldsymbol{u}}, \partial\mathcal{B}_{\phi}\}$. Furthermore, $\bar{\mathbf{t}}' := [\bar{\boldsymbol{t}}(\boldsymbol{x}, t), \bar{\sigma}^e(\boldsymbol{x}, t)]^T$ assembles the prescribed variables on the Neumann boundaries $\partial\mathcal{B}_{\mathbf{t}'} := \{\partial\mathcal{B}_{\boldsymbol{t}}, \partial\mathcal{B}_{\mathrm{d}}\}$. The generalized normal vector $\mathbf{n} := [\boldsymbol{n}, \boldsymbol{n}]^T$ provides the outward surface normals for each partial field of the coupled problem.

Continuous Formulation. Let us assume the existence of an incremental energy functional $I'(\mathbf{u}')$ for both generalized vectors and loads. From now on we assume that the loads do not depend on the motion of the body. It means that the directions of the loads remain parallel and their values unchanged throughout the deformation process. We say such loads are "dead".

We consider a body in static equilibrium under the action of specific "dead" loadings and boundary conditions specified in (6.173). Then the total generalized incremental energy functional $I'(\mathbf{u}')$ of the system is the difference between the internal energy $I'_{\text{int}}(\mathbf{u}')$ stored in the body and the underlying free space in the time window $[t_n, t_{n+1}]$ and the incremental work done by the external loads $I'_{\text{ext}}(\mathbf{u}')$, i.e.

$$I'(\mathbf{u}') = I'_{\text{int}}(\mathbf{u}') - I'_{\text{ext}}(\mathbf{u}') \,, \tag{6.174}$$

with

$$
\begin{aligned}
I'_{\text{int}}(\mathbf{u}') &= \int_{\mathcal{B}} w(\boldsymbol{\mathcal{G}}[\mathbf{u}']; \boldsymbol{x}) dv \\
I'_{\text{ext}}(\mathbf{u}') &= \int_{\mathcal{B}} \bar{\mathbf{b}}' \star (\mathbf{u}' - \mathbf{u}'_n) dv + \int_{\partial \mathcal{B}_{\mathbf{t}}} \bar{\mathbf{t}}' \star (\mathbf{u}' - \mathbf{u}'_n) da \, .
\end{aligned}
\tag{6.175}
$$

in terms of the generalized displacement vector defined in (6.161) and of the generalized quantities introduced above. The energy functional $I'(\mathbf{u}')$ has to be stationary with respect to generalized displacement $\mathbf{u}'$ satisfying the Dirichlet boundary conditions given in $(6.173)_1$. Thus, our main objective is to find the state of equilibrium for which the potential $I'(\mathbf{u}')$ is stationary, i.e.

$$
\mathbf{u}' = \text{Arg} \left\{ \underset{\mathbf{u}' \in \mathcal{W}}{\text{stat}} I'(\mathbf{u}') \right\} = \text{Arg} \left\{ \underset{\boldsymbol{u}}{\inf} \underset{-\phi^e}{\sup} I'(\boldsymbol{u}, -\phi^e) \right\}
\tag{6.176}
$$

for admissible generalized displacement

$$
\mathbf{u}' \in \mathcal{W} := \{ \mathbf{u}' \mid \mathbf{u}' = \bar{\mathbf{u}}'(\boldsymbol{x}, t) \quad \text{on} \quad \partial \mathcal{B}_{\mathbf{u}'} \} \, .
\tag{6.177}
$$

Note that $I'(\mathbf{u}')$ has to be minimized with respect to the mechanical primary variable $\boldsymbol{u}$ and maximized with respect to the electrical primary variable $-\phi^e$. This confers to the problem a *saddle-point character*. The stationarity position of the functional $I'(\mathbf{u}')$ is obtained by requiring the directional derivative with respect to the generalized displacement $\mathbf{u}'$ to vanish in all directions $\delta \mathbf{u}'$, i.e.

$$
\delta I'(\mathbf{u}', \delta \mathbf{u}') = \left[\frac{d}{d\epsilon} I'(\mathbf{u}' + \epsilon \delta \mathbf{u}') \right]_{\epsilon = 0} = 0 \, ,
\tag{6.178}
$$

which could be regarded as an extension of the principle of minimum potential energy of elastostatics to a stationarity principle for the fully coupled electro-mechanical problem. Equation (6.178) requires that the first variation of the functional $I'(\mathbf{u}')$, denoted with $\delta I'$, vanishes. This variation is clearly a function of both $\mathbf{u}'$ and $\delta \mathbf{u}'$. The arbitrary vector field $\delta \mathbf{u}'$ has to be consistent with the conditions imposed on the continuum body and the underlying free space. Thus, $\delta \mathbf{u}' = \boldsymbol{0}$ over $\partial \mathcal{B}_{\mathbf{u}'}$ where the generalized displacement is prescribed. Taking this constraint into account, we can write (6.178) explicitly by using the definition (6.174) and (6.175)

$$
\delta I'(\mathbf{u}', \delta \mathbf{u}') = \int_{\mathcal{B}} \left\{ \partial_{\mathsf{f}'} w \star \boldsymbol{\mathcal{G}}[\delta \mathbf{u}'] - \bar{\mathbf{b}}' \star \delta \mathbf{u}' \right\} dv - \int_{\partial \mathcal{B}_{\mathbf{t}'}} \mathbf{t}' \star \delta \mathbf{u}' da = 0 \, .
\tag{6.179}
$$

By using the Gauß theorem in terms of the generalized displacement, we get

$$
\delta I' = -\int_{\mathcal{B}} \left\{ \mathcal{D}_v[\partial_{\mathsf{f}'} w] + \bar{\mathbf{b}}' \right\} \star \delta \mathbf{u}' dv + \int_{\partial \mathcal{B}_{\mathbf{t}'}} \left\{ \partial_{\mathsf{f}'} w \cdot \mathbf{n} - \mathbf{t}' \right\} \star \delta \mathbf{u}' da = 0 \, .
\tag{6.180}
$$

Since $\delta \mathbf{u}'$ has to be arbitrary, we obtain from the necessary condition for the stationarity of the energy functional $I'(\mathbf{u}')$, the Euler-Lagrange equations associated with the variational principle (6.19)

$$
\begin{aligned}
\mathcal{D}_v[\partial_{\mathsf{f}'} w] + \bar{\mathbf{b}}' &= \boldsymbol{0} \quad \text{in} \quad \mathcal{B} \, , \\
\partial_{\mathsf{f}'} w \mathbf{n} &= \mathbf{t}' \quad \text{on} \quad \partial \mathcal{B}_{\mathbf{t}'} \, .
\end{aligned}
\tag{6.181}
$$

By including the constitutive equations (6.169), we recognize that equation $(6.181)_1$ represents the generalized balance equation (6.167) and equation $(6.181)_2$ are the generalized Neumann boundary conditions$(6.173)_2$.

Finite Element Discretization. The variational problem (6.176) is approximately solved by a finite element method. To this end, the generalized displacement and its gradients are discretized within N finite element domains $\mathcal{B}^e \subset \mathcal{B}^h$ in which the discretized solid $\mathcal{B}^h$ is decomposed, such that

$$\mathfrak{u}'^h(\boldsymbol{x}) = \mathfrak{N}'^e(\boldsymbol{x})\mathfrak{D}'^e \quad \text{and} \quad \mathcal{G}[\mathfrak{u}'^h] = \mathfrak{B}'^e(\boldsymbol{x})\mathfrak{D}'^e \quad \text{in} \quad \mathcal{B}^e \, . \tag{6.182}$$

Here, $\mathfrak{D}'^e$ is the element generalized displacement vector

$$\mathfrak{D}'^e := [\boldsymbol{d}^e, -\boldsymbol{\phi}^e]^T \tag{6.183}$$

which contains the element nodal displacements $\boldsymbol{d}^e$ and the negative electric nodal potential $-\boldsymbol{\phi}^e$ at the current time t_{n+1}. Further, $\mathfrak{N}'^e(\boldsymbol{x})$ is the matrix of element interpolation functions and $\mathfrak{B}'^e(\boldsymbol{x})$ the associated gradient matrix. After assembling the element quantities

$$\mathfrak{D}' = \mathop{\mathsf{A}}_{e=1}^{N} \mathfrak{D}'^e \quad , \quad \mathfrak{N}'(\boldsymbol{x}) = \mathop{\mathsf{A}}_{e=1}^{N} \mathfrak{N}'^e(\boldsymbol{x}) \quad , \quad \mathfrak{B}'(\boldsymbol{x}) = \mathop{\mathsf{A}}_{e=1}^{N} \mathfrak{B}'^e(\boldsymbol{x}) \, , \tag{6.184}$$

we may express the approximated generalized displacement $\mathfrak{u}'^h$ and its generalized gradient $\mathcal{G}[\mathfrak{u}'^h]$ in the discretized domain $\mathcal{B}^h$ as follows

$$\mathfrak{u}'^h(\boldsymbol{x}) = \mathfrak{N}'(\boldsymbol{x})\mathfrak{D}' \quad \text{and} \quad \mathcal{G}[\mathfrak{u}'^h] = \mathfrak{B}'(\boldsymbol{x})\mathfrak{D}' \quad \text{in} \quad \mathcal{B}^h \, . \tag{6.185}$$

With the approximation (6.185) at hand, the energy functional (6.174) appears in the approximated form

$$I'^h(\mathfrak{D}') = \int\limits_{\mathcal{B}^h} \left\{ w(\mathfrak{B}'\mathfrak{D}'; \boldsymbol{x}) - \bar{\boldsymbol{b}}' \star \mathfrak{N}'\Delta\mathfrak{D}' \right\} dv - \int\limits_{\partial\mathcal{B}^h_{\mathfrak{t}'}} \bar{\mathfrak{t}}' \star \mathfrak{N}'\Delta\mathfrak{D}' da \, , \tag{6.186}$$

with $\Delta\mathfrak{D}' = \mathfrak{D}' - \mathfrak{D}'_n$. The discrete energy functional (6.186) has to be stationary with respect to the global generalized nodal displacement $\mathfrak{D}'$ and thus we search for the global generalized nodal displacement $\mathfrak{D}'$ which satisfy the following variational principle

$$\mathfrak{D}' = \mathrm{Arg}\left\{ \mathop{\mathrm{stat}}_{\mathfrak{D}' \in \mathcal{W}^h} I'^h(\mathfrak{D}') \right\} = \mathrm{Arg}\left\{ \inf_{\boldsymbol{D}} \sup_{-\boldsymbol{\phi}} I'^h(\boldsymbol{D}, -\boldsymbol{\phi}) \right\} \tag{6.187}$$

which results to be the discrete counterpart of (6.176). Here $\boldsymbol{D} = \mathop{\mathsf{A}}_{e=1}^{N} \boldsymbol{d}^e$, $\boldsymbol{\phi} = \mathop{\mathsf{A}}_{e=1}^{N} \boldsymbol{\phi}^e$, and $\mathcal{W}^h$ is the set of admissible nodal variables which satisfy the discrete Dirichlet boundary conditions

$$\mathcal{W}^h := \left\{ \mathfrak{D}' \mid \mathfrak{D}' = \bar{\mathfrak{D}}' \quad \text{on} \quad \partial\mathcal{B}^h_{\mathfrak{u}'} \right\} \, . \tag{6.188}$$

The necessary conditions for the solution of the discrete stationary problem (6.187) are given by setting to zero the variation of $I'^h(\mathfrak{D}')$

$$I'^h_{,\mathfrak{D}'}(\mathfrak{D}') = \boldsymbol{0} \, . \tag{6.189}$$

They provide a system of non-linear equations from which the discrete generalized displacements, i.e. the mechanical nodal displacements and the electric nodal potentials, are determined. The solution vector may be obtained through an iterative method as the Newton-Raphson method, yielding the update equations

$$\mathfrak{D}' = \mathfrak{D}' - \left[I'^h_{,\mathfrak{D}'\mathfrak{D}'}(\mathfrak{D}') \right]^{-1} \left[I'^h_{,\mathfrak{D}'}(\mathfrak{D}') \right] , \tag{6.190}$$

performed by some solver of linear equations. Due to the variational structure of the coupled electro-mechanical problem, the coupled tangent $\mathfrak{K}' = I'^h_{,\mathfrak{D}'\mathfrak{D}'}$ is symmetric. The update (6.190) is performed till convergence is reached in the sense

$$\left\| I'^h_{,\mathfrak{D}'}(\mathfrak{D}') \right\| < \mathrm{tol} \,, \tag{6.191}$$

i.e. till the norm of the residuum $\mathfrak{R}' = I'^h_{,\mathfrak{D}'}$ is smaller then a certain predefined tolerance. The first and second derivatives of the discrete variational functional (6.186) give all the finite element arrays needed for the solution of the coupled electro-mechanical boundary-value-problem by means of the finite element method. These arrays are the finite element residual

$$\mathfrak{R}' := I'^h_{,\mathfrak{D}'} = \int_{\mathcal{B}^h} \left\{ \mathfrak{B}'^T \mathfrak{s}'^h - \mathfrak{N}'^T \bar{\mathfrak{b}}' \right\} dv - \int_{\partial \mathcal{B}'_{\mathfrak{t}'}} \mathfrak{N}'^T \bar{\mathfrak{t}}' da \tag{6.192}$$

and the finite element tangent matrix

$$\mathfrak{K}' := I'^h_{,\mathfrak{D}'\mathfrak{D}'} = \int_{\mathcal{B}^h} \mathfrak{B}'^T \mathfrak{c}'^h \mathfrak{B}' dv \,. \tag{6.193}$$

These arrays are expressed in terms of the first and second derivatives of the incremental functional w which gives the generalized vector $\mathfrak{s}'^h$ and moduli $\mathfrak{c}'^h$

$$\mathfrak{s}'^h := \partial_{\mathfrak{f}'^h} w(\mathfrak{B}'\mathfrak{D}'; \boldsymbol{x}) \qquad \text{and} \qquad \mathfrak{c}'^h := \partial^2_{\mathfrak{f}'^h \mathfrak{f}'^h} w(\mathfrak{B}'\mathfrak{D}'; \boldsymbol{x}) \tag{6.194}$$

of the coupled problem. Clearly, due to the variational structure of the coupled constitutive problem, the moduli $\mathfrak{c}'^h$ are symmetric. However, they are not positive definite due to the saddle-point structure of the problem. As a consequence, also the finite element tangent matrix $\mathfrak{K}'$ is not positive definite and this excludes the application of certain fast and efficient solvers for the solution of the linear iterative update (6.190).

7. Ferroelectricity at Small Strains

The final goal of this chapter is to construct a model for the dissipative ferroelectric material response at small strains. In particular we would like to build up the mixed energy-enthalpy function ψ' and the dissipation function ϕ which can be used within the incremental variational formulation proposed in Section 6.3. The small strains model will be extended in Chapter 8 to account for large deformations. The mixed energy-enthalpy function ψ' for a ferroelectric material response can be seen as a generalization of the one used to model the piezoelectric material response, see MIEHE [109] and ROSATO & MIEHE [131]. That is the reason why we consider first a model for piezoelectricity.

7.1. Functions for Piezoelectricity

Piezoelectricity at small strains are well-established in the literature. We refer to the fundamental work of VOIGT [146] in his textbook on crystal physics and the more recent comprehensive treatments JAFFE, COOK & JAFFE [70] and IKEDA [69]. A *piezoelectric material* is an electrically poled material with a macroscopic polarization whose direction remains constant in the range of the applied stress and electric field. Here, the polarization vector $\mathbb{p}^r$ describes the separation of the barycenters of negative and positive charges associated with a typical volume element, see Figure 7.1 for a visualization. The constant polarization director $\mathfrak{p} := \mathbb{p}^r / |\mathbb{p}^r|$ enters the constitutive formulation as a structural vector that characterizes a piezoelectric response typically to be transversely isotropic.

Piezoelectric materials are *non-dissipative* in nature and constitutively fully described by properly chosen *free enthalpy or Gibbs functions* $\psi^*_{pie}(\boldsymbol{\sigma}, \mathbb{e})$. The goal of this section is to construct simple functions which include in an elementary format all basic effects of electro-mechanical coupling. These functions contain a *minimum number of material parameters, each of them related to an elementary experiment.* The experiments are force driven, i.e. kinematic quantities such as strain $\boldsymbol{\varepsilon}$ and electric displacement $\mathbb{d}$ are considered to be measured in terms of prescribed forces, i.e. stresses $\boldsymbol{\sigma}$ and electric field $\mathbb{e}$. This viewpoint provides a straightforward understanding of basic coupling phenomena and allows the identification of free enthalpy functions ψ^*_{pie} based on their potential properties

$$\boldsymbol{\varepsilon} = \partial_{\boldsymbol{\sigma}} \psi^*_{pie}(\boldsymbol{\sigma}, \mathbb{e}) \qquad \text{and} \qquad \mathbb{d} = \partial_{\mathbb{e}} \psi^*_{pie}(\boldsymbol{\sigma}, \mathbb{e}). \tag{7.1}$$

An assumed decomposition into decoupled stress-induced and electric-induced contributions

$$\boldsymbol{\varepsilon} = \boldsymbol{\varepsilon}^\sigma(\boldsymbol{\sigma}) + \boldsymbol{\varepsilon}^e(\mathbb{e}) \qquad \text{and} \qquad \mathbb{d} = \mathbb{d}^e(\mathbb{e}) + \mathbb{d}^\sigma(\boldsymbol{\sigma}), \tag{7.2}$$

which is *exact for linear* constitutive response, provides a method for the construction of simple free enthalpy functions. The constitutive formulation of $\boldsymbol{\varepsilon}^\sigma(\boldsymbol{\sigma})$ and $\boldsymbol{\varepsilon}^e(\mathbb{e})$ based on kinematic observations is considered to be the most intuitive approach to the modeling of the piezoelectric coupling. From the potential relationship (7.1) one gets the Maxwell-type relationship

$$\partial_{\mathbb{e}} \boldsymbol{\varepsilon}^e(\mathbb{e}) = (\partial_{\boldsymbol{\sigma}} \mathbb{d}^\sigma(\boldsymbol{\sigma}))^T. \tag{7.3}$$

As a consequence, the formulation of $\boldsymbol{\varepsilon}^\sigma(\boldsymbol{\sigma})$, $\boldsymbol{\varepsilon}^e(\mathbb{e})$ and $\mathbb{d}^e(\mathbb{e})$ is sufficient for the contribution of the free enthalpy function $\psi^*_{pie}(\boldsymbol{\sigma}, \mathbb{e})$ by integration. The alternative mixed energy-enthalpy function $\psi'_{pie}(\boldsymbol{\varepsilon}, \mathbb{e})$ or the free energy function $\psi_{pie}(\boldsymbol{\varepsilon}, \mathbb{d})$ then follows by standard Legendre-Fenchel transformations. In this context, we outline the *necessary approximations* which provide the simple structure of constitutive functions.
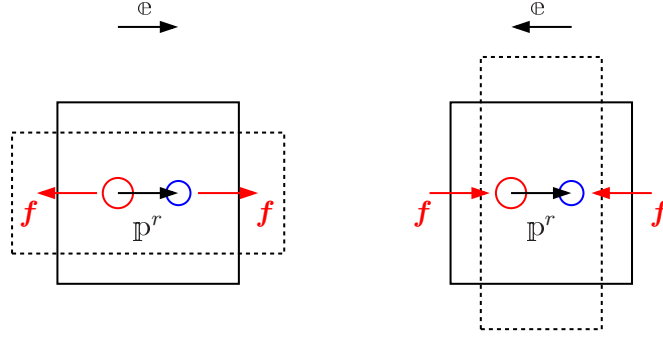
Figure 7.1: Piezoelectric effects. Consider electrically induced mechanical strain $\boldsymbol{\varepsilon}^e$ of idealized unit cubes caused by the forces $\boldsymbol{f} = q\,\mathbb{e}$ acting on the barycenters of positive and negative charges. A piezoelectric material has an a priori given polarization characterized by the polarization vector $\mathbb{p}^r$ that separates the barycenters of positive and negative charges. Then, the electric field causes a mechanical elongation or compression of the unit cube in the direction of the polarization vector, depending on the sign of the electric field. Thus, $\boldsymbol{\varepsilon}^e \sim \mathbb{e}$ is the (linear) piezoelectric coupling effect. This effect is transversely isotropic with respect to the polarization $\mathbb{p}^r$.

7.1.1. Force-Driven Modeling of Piezoelectricity

Stress-Induced Strain. Recall the standard experimental procedure for the determination of the material parameters in elasticity. *Linear-isotropic elastic response* can be based on two experimental observations associated with an *arbitrary* loading director $\boldsymbol{a}$ with $|\boldsymbol{a}| = 1$.

P1. A uniaxial stress state $\sigma_\| = \boldsymbol{\sigma} : \boldsymbol{a} \otimes \boldsymbol{a}$ produces the *axial strain*

$$\varepsilon_\|^\sigma := \boldsymbol{\varepsilon}^\sigma : (\boldsymbol{a} \otimes \boldsymbol{a}) = \frac{1}{E}\sigma_\| \tag{7.4}$$

P2. and the *lateral strain* perpendicular to the tensile axis

$$\varepsilon_\perp^\sigma := \tfrac{1}{2}\,\boldsymbol{\varepsilon}^\sigma : (\boldsymbol{1} - \boldsymbol{a} \otimes \boldsymbol{a}) = -\nu\varepsilon_\|^\sigma\,. \tag{7.5}$$

These two experiments determine the *elasticity or Young's modulus $E > 0$* and the *lateral contraction or Poisson ratio $\nu < 1/2$*. The above two elementary observations result in the standard relationship

$$\boldsymbol{\varepsilon}^\sigma(\boldsymbol{\sigma}) = \frac{1+\nu}{E}\boldsymbol{\sigma} - \frac{\nu}{E}\operatorname{tr}\boldsymbol{\sigma}\,\boldsymbol{1} \tag{7.6}$$

of isotropic, linear elasticity. Recall that $\nu = 0$ and $\nu = 1/2$ describe mechanically fully compressible and fully incompressible responses. The latter condition enforces the strain to be deviatoric, i.e. $\boldsymbol{\varepsilon}_{\nu=1/2}^\sigma = \frac{3}{2}\frac{1}{E}\operatorname{dev}[\boldsymbol{\sigma}]$. The linear relationship (7.6) can be recast in the form

$$\boldsymbol{\varepsilon}^\sigma(\boldsymbol{\sigma}) = \mathbb{C}^* : \boldsymbol{\sigma} \qquad \text{with} \qquad \mathbb{C}^* := \frac{1+\nu}{E}\mathbb{I} - \frac{\nu}{E}\boldsymbol{1} \otimes \boldsymbol{1} \tag{7.7}$$

in terms of the fourth-order *isotropic elastic compliance tensor* $\mathbb{C}^*$. Here $\mathbb{I}$ is the 4th order symmetric identity tensor.

Electric-Induced Strain. A rational method for the constitutive formulation of the electro-mechanical coupling is based on an assumption concerning the strain $\boldsymbol{\varepsilon}^e$ induced by the electric field $\mathbb{e}$, see Figure 7.2 for a schematic visualization. Assuming a *given*
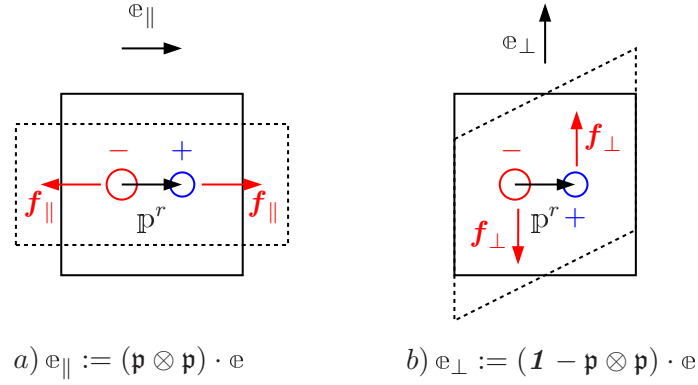
$a)\, \mathbb{e}_\parallel := (\mathfrak{p} \otimes \mathfrak{p}) \cdot \mathbb{e}$ $b)\, \mathbb{e}_\perp := (\mathbf{1} - \mathfrak{p} \otimes \mathfrak{p}) \cdot \mathbb{e}$

Figure 7.2: Piezo-electric induced mechanical deformation may be explained by the action of forces $\boldsymbol{f} = q\,\mathbb{e}$ acting on the barycenters of positive and negative charges. The electric field $\mathbb{e} = \mathbb{e}_\parallel + \mathbb{e}_\perp$ induces in an electrically poled material with poling direction $\mathbb{p}^r = |\mathbb{p}^r|\mathfrak{p}$ three deformation modes: a) axial elongation/compression $\varepsilon_\parallel \sim \mathbb{p}^r \cdot \mathbb{e}_\parallel$ and lateral contraction/extension $\varepsilon_\perp \sim -\mathbb{p}^r \cdot \mathbb{e}_\parallel$, b) shearing $\boldsymbol{\gamma} \sim \mathbb{e}_\perp$.

electric polarization $\mathbb{p}^r$ with unit director $\mathfrak{p} := \mathbb{p}^r/|\mathbb{p}^r|$, we identify in Figure 7.2 three deformation modes in a *mechanically isotropic material* induced by the two components $\mathbb{e}_\parallel := (\mathfrak{p} \otimes \mathfrak{p}) \cdot \mathbb{e}$ and $\mathbb{e}_\perp := (\mathbf{1} - \mathfrak{p} \otimes \mathfrak{p}) \cdot \mathbb{e}$ of the electric field parallel and perpendicular to the polarization direction $\mathbb{p}^r$.

P3. The first effect of electric forces acting on the material is an *axial strain* in the poling direction, which is an *elongation* or a *compression*, depending on the sign of $\mathbb{e} \cdot \mathfrak{p}$. This is modeled by the *linear* relationship

$$\varepsilon_\parallel^e := \boldsymbol{\varepsilon}^e : (\mathfrak{p} \otimes \mathfrak{p}) = \alpha_\parallel^*(\mathbb{e} \cdot \mathfrak{p}) \tag{7.8}$$

in terms of the first piezoelectric coupling parameter $\alpha_\parallel^*$, in the literature often denoted as the "d_{33}-parameter" assuming the polarization direction $\mathfrak{p}$ to coincide with the $\boldsymbol{e}_3$-director of a Cartesian frame $\{\boldsymbol{e}_i\}_{i=1,2,3}$.

P4. The second effect is a *lateral strain* in the direction perpendicular to the poling direction similar to Poisson's effort for purely mechanical response. We expect a lateral *contraction* or *extension*, depending on the sign of $\mathbb{e} \cdot \mathfrak{p}$. This is modeled by the *linear* relationship

$$\varepsilon_\perp^e := \tfrac{1}{2}\boldsymbol{\varepsilon}^e : (\mathbf{1} - \mathfrak{p} \otimes \mathfrak{p}) = \alpha_\perp^*(\mathbb{e} \cdot \mathfrak{p}) \tag{7.9}$$

with $\alpha_\perp^* := -\nu_\perp \alpha_\parallel^*$, where $\nu_\perp \leq 1/2$ may be interpreted as a Poisson-type ratio for the electric field action on the mechanically isotropic material. Hence, $\alpha_\perp^* = 0$ and $\alpha_\perp^* = -\tfrac{1}{2}\alpha_\parallel^*$ is associated with piezoelectrically fully compressible and incompressible response, respectively. The second piezoelectric coupling parameter $\alpha_\perp^*$ is in the literature often denoted as the "d_{31}-parameter".

P5. The third effect is a *shearing* in the plane spanned by the poling direction $\mathfrak{p}$ and the component $\mathbb{e}_\perp$ of the electric field perpendicular to $\mathfrak{p}$, as indicated in the Figure 7.2. We assume the linear relationship

$$\gamma_{\underline{=}}^e := 2\boldsymbol{\varepsilon}^e : \mathrm{sym}\left[\frac{\mathbb{e}_\perp}{|\mathbb{e}_\perp|} \otimes \mathfrak{p}\right] = \alpha_{\underline{=}}^*|\mathbb{e}_\perp| \tag{7.10}$$

The symmetrization of the projection tensor eliminates the rigid-body rotation of the simple shearing mode indicated in Figure 7.2. The third piezoelectric coupling parameter $\alpha_{\underline{\underline{}}}^*$ is often denoted as the "d_{15}-parameter".

Note that the polarization direction $\mathfrak{p}$ plays the role of a *given, constant structural director*, which characterizes the anisotropy of the electrically poled material. Observe furthermore that the above material response functions seem to be independent of the magnitude $|\mathbb{p}^r|$ of electric polarization. However, the three parameters $\alpha_\parallel^*$, $\alpha_\perp^*$ and $\alpha_{\underline{\underline{}}}^*$ are understood to be valid for a fixed amount $|\mathbb{p}^r| = c$. The three deformation modes outlined above induce the representation

$$
\begin{aligned}
\boldsymbol{\varepsilon}^e(\mathbb{e}; \mathfrak{p}) &= \alpha_\parallel^* (\mathbb{e} \cdot \mathfrak{p}) \mathfrak{p} \otimes \mathfrak{p} \\
&+ \alpha_\perp^* (\mathbb{e} \cdot \mathfrak{p})(\boldsymbol{1} - \mathfrak{p} \otimes \mathfrak{p}) \\
&+ \alpha_{\underline{\underline{}}}^* \overset{12}{\operatorname{sym}} [\{(\boldsymbol{1} - \mathfrak{p} \otimes \mathfrak{p}) \cdot \mathbb{e}\} \otimes \mathfrak{p}]
\end{aligned}
\tag{7.11}
$$

of the electro-mechanical coupling. Here, $\overset{12}{\operatorname{sym}}[\cdot]$ denotes symmetrization of the tensor $[\cdot]$ with respect to the first and second slot. For a piezoelectric fully incompressible response, we obtain $\boldsymbol{\varepsilon}^e(\mathbb{e}; \mathfrak{p}) = \frac{3}{2}\alpha_\parallel^*(\boldsymbol{e} \cdot \mathfrak{p}) \operatorname{dev}[\mathfrak{p} \otimes \mathfrak{p}] + \alpha_{\underline{\underline{}}}^* \operatorname{sym}[\{(\boldsymbol{1} - \mathfrak{p} \otimes \mathfrak{p}) \cdot \mathbb{e}\} \otimes \mathfrak{p}]$. For the linear assumptions made above, we may recast (7.11) in the form

$$
\boldsymbol{\varepsilon}^e(\mathbb{e}; \mathfrak{p}) = \boldsymbol{h}^*(\mathfrak{p}) \cdot \mathbb{e} \quad \text{with} \quad \boldsymbol{h}^* := \overset{12}{\operatorname{sym}}[\alpha_0^* \mathfrak{p} \otimes \mathfrak{p} \otimes \mathfrak{p} + \alpha_\perp^* \boldsymbol{1} \otimes \mathfrak{p} + \alpha_{\underline{\underline{}}}^* \mathfrak{p} \otimes \boldsymbol{1}]
\tag{7.12}
$$

where we set $\alpha_0^* := \alpha_\parallel^* - \alpha_\perp^* - \alpha_{\underline{\underline{}}}^*$. We denote $\boldsymbol{h}^*$ as the third-order *transversely isotropic piezoelectric coupling tensor*, which depends on the polarization $\mathfrak{p}$.

Stress-Induced Electric Displacement. With the electrically induced strain $\boldsymbol{\varepsilon}^e$ defined in (7.12), the stress-induced electric displacement follows from the Maxwell-type relationship (7.3) to be

$$
\mathbb{d}^\sigma(\boldsymbol{\sigma}; \mathfrak{p}) = \boldsymbol{\sigma} : \boldsymbol{h}^*(\mathfrak{p})
\tag{7.13}
$$

dual to (7.12). We get the representation of the so-called *direct piezoelectric coupling effect*

$$
\mathbb{d}^\sigma = [\,\alpha_\parallel^* \sigma_\parallel + \alpha_\perp^* (\operatorname{tr} \boldsymbol{\sigma} - \sigma_\parallel)\,]\mathfrak{p} + \alpha_{\underline{\underline{}}}^* \boldsymbol{t}_\perp
\tag{7.14}
$$

with $\sigma_\parallel := \mathfrak{p} \cdot \boldsymbol{\sigma} \cdot \mathfrak{p}$ and $\boldsymbol{t}_\perp := \boldsymbol{\sigma} \cdot \mathfrak{p} - \sigma_\parallel \mathfrak{p}$. Note in particular the simplified form for incompressible piezoelectric response $\mathbb{d}^\sigma = \frac{3}{2}\alpha_\parallel^* \{\operatorname{dev}[\boldsymbol{\sigma}] : \mathfrak{p} \otimes \mathfrak{p}\} \mathfrak{p} + \alpha_{\underline{\underline{}}}^* \boldsymbol{t}_\perp$ or $\mathbb{d}^\sigma = \frac{3}{2}\alpha_\parallel^*(\sigma_\parallel + p)\mathfrak{p} + \alpha_{\underline{\underline{}}}^* \boldsymbol{t}_\perp$, where a *pressure* $p := -\frac{3}{2}\operatorname{tr}[\boldsymbol{\sigma}] > 0$ induces an electric displacement in the direction $\mathfrak{p}$ of polarization.

Electric-Induced Electric Displacement. Finally, on the pure electric side, we have to model the electric displacement induced by the electric field. Linear-isotropic dielectric response is be based on an

P6. Experimental observation that an *electric field* $\mathbb{e}$ induces the *electric displacement*

$$
\mathbb{d}^e = \epsilon \, \mathbb{e} \, ,
\tag{7.15}
$$

where ϵ is the *dielectric permittivity*. We write this in the form

$$
\mathbb{d}^e(\mathbb{e}) = \boldsymbol{\beta}^* \cdot \mathbb{e} \quad \text{with} \quad \boldsymbol{\beta}^* := \epsilon \boldsymbol{1}
\tag{7.16}
$$

and denote $\boldsymbol{\beta}^*$ as the second-order *isotropic electric permittivity tensor*.

The six material parameters for the simple piezoelectric response with an idealized electric polarization embedded in an isotropic matrix are summarized in Table 7.1. They may be identified independently by the above described experiments P1–P6.

Table 7.1: Piezoelectric Material Parameters

No.	Parameter	Unit	Name	Eq.
1	$E > 0$	N/m^2	elasticity modulus	(7.4)
2	$\nu < \frac{1}{2}$	–	lateral elastic contraction ratio	(7.5)
3	$\alpha_\parallel^* > 0$	m/V	axial piezoelectric expansion coefficient	(7.8)
4	$\alpha_\perp^* > -\frac{1}{2}\alpha_\parallel^*$	m/V	lateral piezoelectric expansion coefficient	(7.9)
5	$\alpha_=^* > 0$	m/V	piezoelectric shearing coefficient	(7.10)
6	$\epsilon > 0$	C/(V·m)	electric permittivity	(7.15)
7	$\mathfrak{p}$	–	unit director of electric polarization	(7.8)

7.1.2. Enthalpy and Energy Function in Piezoelectricity

Free Enthalpy Function. The above outlined constitutive assumptions (7.7), (7.12) and (7.16) characterize a simple linear piezoelectric material model in terms of the six material parameters summarized in Table 7.1. Based on these expressions, we obtain an explicit form of the free enthalpy function by integration of (7.7), (7.12), and (7.16)

$$\psi_{pie}^*(\boldsymbol{\sigma}, \mathbb{e}; \mathfrak{p}) = \int_0^{\boldsymbol{\sigma}} [\,\boldsymbol{\varepsilon}^\sigma(\tilde{\boldsymbol{\sigma}}) + \boldsymbol{\varepsilon}^e(\mathbb{e}; \mathfrak{p})\,] : d\tilde{\boldsymbol{\sigma}} + \int_0^{\mathbb{e}} \mathrm{d}^e(\tilde{\mathbb{e}}) \cdot d\tilde{\mathbb{e}}\,, \tag{7.17}$$

yielding the quadratic form

$$\psi_{pie}^*(\boldsymbol{\sigma}, \mathbb{e}; \mathfrak{p}) = \tfrac{1}{2}\,\boldsymbol{\sigma} : \mathbb{C}^* : \boldsymbol{\sigma} + \boldsymbol{\sigma} : \boldsymbol{h}^*(\mathfrak{p}) \cdot \mathbb{e} + \tfrac{1}{2}\,\mathbb{e} \cdot \boldsymbol{\beta}^* \cdot \mathbb{e} \tag{7.18}$$

in terms of the three fourth-, third- and second-order structural tensors

$$\begin{aligned}
\mathbb{C}^* &:= \tfrac{1+\nu}{E}\mathbb{I} - \tfrac{\nu}{E}\boldsymbol{1} \otimes \boldsymbol{1}\,, \\
\boldsymbol{h}^* &:= \overset{12}{\mathrm{sym}}\,[\alpha_0^*\mathfrak{p} \otimes \mathfrak{p} \otimes \mathfrak{p} + \alpha_\perp^*\boldsymbol{1} \otimes \mathfrak{p} + \alpha_=^*\mathfrak{p} \otimes \boldsymbol{1}]\,, \\
\boldsymbol{\beta}^* &:= \epsilon\boldsymbol{1}
\end{aligned} \tag{7.19}$$

with $\alpha_0^* := \alpha_\parallel^* - \alpha_\perp^* - \alpha_=^*$. Note carefully that ψ_{pie}^* is a *convex function* with respect to the variables $\boldsymbol{\sigma}$ and $\mathbb{e}$. The tensors $\mathbb{C}^*$ and $\boldsymbol{\beta}^*$ are positive definite. The free enthalpy can be represented in terms of elementary trace-type invariants of the arguments $\boldsymbol{\sigma}$, $\mathbb{e}$ and $\mathfrak{p}$ in the form

$$\begin{aligned}
\psi_{pie}^*(\boldsymbol{\sigma}, \mathbb{e}; \mathfrak{p}) &= \tfrac{1+\nu}{2E}\mathrm{tr}[\boldsymbol{\sigma}^2] - \tfrac{\nu}{2E}\mathrm{tr}^2[\boldsymbol{\sigma}] + \alpha_0^*\mathrm{tr}[\boldsymbol{\sigma}(\mathfrak{p} \otimes \mathfrak{p})]\mathrm{tr}[\mathfrak{p} \otimes \mathbb{e}] \\
&+ \alpha_\perp^*\mathrm{tr}[\boldsymbol{\sigma}]\mathrm{tr}[\mathfrak{p} \otimes \mathbb{e}] + \alpha_=^*\mathrm{tr}[\boldsymbol{\sigma}(\mathfrak{p} \otimes \mathbb{e})] + \tfrac{\epsilon}{2}\mathrm{tr}[\mathbb{e} \otimes \mathbb{e}]\,.
\end{aligned} \tag{7.20}$$

The function satisfies the symmetry condition of transversely isotropic response

$$\psi_{pie}^*(\boldsymbol{Q}\boldsymbol{\sigma}\boldsymbol{Q}^T, \boldsymbol{Q}\mathbb{e}; \mathfrak{p}) = \psi_{pie}^*(\boldsymbol{\sigma}, \mathbb{e}; \mathfrak{p}) \quad \text{for all} \quad \boldsymbol{Q} \in \mathcal{G} := \{\boldsymbol{Q} \subset \mathcal{O} | \boldsymbol{Q}\mathfrak{p} = \mathfrak{p}\}\,, \tag{7.21}$$

where $\mathcal{O}$ denotes the orthogonal group. Note again that the above model assumes the purely mechanical and electric structural tensors $\mathbb{C}^*$ and $\boldsymbol{\beta}^*$ to be isotropic in order to keep number of material parameters small.

Mixed Energy-Enthalpy Function. With regard to a standard representation of the electro-mechanically coupled problem in terms of the strains $\boldsymbol{\varepsilon}$ and the electric field $\mathbb{e}$ as

Box 1: Simple Constitutive Functions for Piezoelectricity.

1. *Enthalpy Function* with the six basic material parameters defined in Table 7.1 and the definition $\alpha_0^* := \alpha_\parallel^* - \alpha_\perp^* - \alpha_=^*$

$$
\begin{aligned}
\psi_{pie}^*(\boldsymbol{\sigma}, \mathbb{e}; \mathfrak{p}) \; = & \; \tfrac{1+\nu}{2E}\mathrm{tr}[\boldsymbol{\sigma}^2] - \tfrac{\nu}{2E}\mathrm{tr}^2[\boldsymbol{\sigma}] + \alpha_0^*\mathrm{tr}[\boldsymbol{\sigma}(\mathfrak{p}\otimes\mathfrak{p})]\mathrm{tr}[\mathfrak{p}\otimes\mathbb{e}] \\
& + \; \alpha_\perp^*\mathrm{tr}[\boldsymbol{\sigma}]\mathrm{tr}[\mathfrak{p}\otimes\mathbb{e}] + \alpha_=^*\mathrm{tr}[\boldsymbol{\sigma}(\mathfrak{p}\otimes\mathbb{e})] + \tfrac{\epsilon}{2}\mathrm{tr}[\mathbb{e}\otimes\mathbb{e}] \; .
\end{aligned}
$$

2. *Mixed Energy–Enthalpy Function* with the Lame parameters $\mu := E/2(1+\nu)$ and $\lambda := E\nu/(1+\nu)(1-2\nu)$ and the modified piezoelectric coupling parameters $\alpha_0' := 2\mu\alpha_0^*$, $\alpha_\perp' := 2\mu\alpha_\perp^* + \lambda(\alpha_0^* + 3\alpha_\perp^* + \alpha_=^*)$ and $\alpha_=' := 2\mu\alpha_=^*$

$$
\begin{aligned}
\psi_{pie}'(\boldsymbol{\varepsilon}, \mathbb{e}; \mathfrak{p}) \; = & \; \mu\mathrm{tr}[\boldsymbol{\varepsilon}^2] + \tfrac{\lambda}{2}\mathrm{tr}^2[\boldsymbol{\varepsilon}] - \alpha_0'\mathrm{tr}[\boldsymbol{\varepsilon}(\mathfrak{p}\otimes\mathfrak{p})]\mathrm{tr}[\mathfrak{p}\otimes\mathbb{e}] \\
& - \; \alpha_\perp'\,\mathrm{tr}[\boldsymbol{\varepsilon}]\mathrm{tr}[\mathfrak{p}\otimes\mathbb{e}] - \alpha_='\,\mathrm{tr}[\boldsymbol{\varepsilon}(\mathfrak{p}\otimes\mathbb{e})] - \tfrac{\epsilon}{2}\mathrm{tr}[\mathbb{e}\otimes\mathbb{e}]
\end{aligned}
$$

3. *Energy Function* with the modified piezoelectric coupling parameters $\alpha_0 := \alpha_0'/\epsilon$, $\alpha_\perp := \alpha_\perp'/\epsilon$ and $\alpha_= := \alpha_='/\epsilon$

$$
\begin{aligned}
\psi_{pie}(\boldsymbol{\varepsilon}, \mathbb{d}; \mathfrak{p}) \; = & \; \mu\mathrm{tr}[\boldsymbol{\varepsilon}^2] + \tfrac{\lambda}{2}\mathrm{tr}^2[\boldsymbol{\varepsilon}] - \alpha_0\mathrm{tr}[\boldsymbol{\varepsilon}(\mathfrak{p}\otimes\mathfrak{p})]\mathrm{tr}[\mathfrak{p}\otimes\mathbb{d}] \\
& - \; \alpha_\perp\mathrm{tr}[\boldsymbol{\varepsilon}]\mathrm{tr}[\mathfrak{p}\otimes\mathbb{d}] - \alpha_=\mathrm{tr}[\boldsymbol{\varepsilon}(\mathfrak{p}\otimes\mathbb{d})] + \tfrac{1}{2\epsilon}\mathrm{tr}[\mathbb{d}\otimes\mathbb{d}]
\end{aligned}
$$

independent variables, we get from (7.18) by a partial Legendre transformation a mixed energy-enthalpy function (also called electric enthalpy function)

$$
\psi_{pie}'(\boldsymbol{\varepsilon}, \mathbb{e}; \mathfrak{p}) := \sup_{\boldsymbol{\sigma}} \left[\, \boldsymbol{\sigma} : \boldsymbol{\varepsilon} - \psi_{pie}^*(\boldsymbol{\sigma}, \mathbb{e}; \mathfrak{p}) \, \right] \; . \tag{7.22}
$$

After some algebraic manipulations, this function attains the closed form

$$
\psi_{pie}'(\boldsymbol{\varepsilon}, \mathbb{e}; \mathfrak{p}) = \tfrac{1}{2}\boldsymbol{\varepsilon} : \mathbb{C}' : \boldsymbol{\varepsilon} - \boldsymbol{\varepsilon} : \boldsymbol{h}'(\mathfrak{p}) \cdot \mathbb{e} - \tfrac{1}{2}\mathbb{e} \cdot \boldsymbol{\beta}' \cdot \mathbb{e} \tag{7.23}
$$

in terms of the structural tensors

$$
\mathbb{C}' := \mathbb{C}^{*-1} \quad , \quad \boldsymbol{h}' := \mathbb{C}^{*-1} : \boldsymbol{h}^* \quad , \quad \boldsymbol{\beta}' := \boldsymbol{\beta}^* - \boldsymbol{h}^{*T} : \mathbb{C}^{*-1} : \boldsymbol{h}^* \,. \tag{7.24}
$$

Note the negative signs in (7.23). As a result of the *partial* Legendre transformation only with respect to the first mechanical slot, the function ψ_{pie}' is *convex-concave*. The structural tensors $\mathbb{C}'$ and $\boldsymbol{\beta}'$ are positive definite. Observe furthermore, that the electric permittivity tensor $\boldsymbol{\beta}'$ becomes anisotropic due to the second term in (7.24)$_3$. However, this term is *negligible* with respect to the first term for the estimate $\mathcal{O}(\boldsymbol{h}^{*T} : \mathbb{C}^{*-1} : \boldsymbol{h}^*) = E(\alpha_\parallel^*)^2 \ll \epsilon = \mathcal{O}(\boldsymbol{\beta}^*)$. We then get the closed form

$$
\begin{aligned}
\mathbb{C}' \; &:= 2\mu\mathbb{I} + \lambda \boldsymbol{1} \otimes \boldsymbol{1} \\
\boldsymbol{h}' \; &:= \overset{12}{\mathrm{sym}}\left[\alpha_0'\mathfrak{p}\otimes\mathfrak{p}\otimes\mathfrak{p} + \alpha_\perp'\boldsymbol{1}\otimes\mathfrak{p} + \alpha_='\mathfrak{p}\otimes\boldsymbol{1}\right] \\
\boldsymbol{\beta}' \; &:= \epsilon\boldsymbol{1}
\end{aligned} \tag{7.25}
$$

with the classical Lamé parameters $\mu := E/2(1+\nu)$ and $\lambda := E\nu/(1+\nu)(1-2\nu)$ of isotropic elasticity and the modified piezoelectric coupling parameters $\alpha_0' := 2\mu\alpha_0^*$,

$\alpha'_\perp := 2\mu\alpha^*_\perp + \lambda(\alpha^*_0 + 3\alpha^*_\perp + \alpha^*_=)$, and $\alpha'_= := 2\mu\alpha^*_=$. The representation in terms of elementary trace-type invariants reads

$$\begin{aligned}\psi'_{pie}(\boldsymbol{\varepsilon}, \mathrm{e}; \mathfrak{p}) &= \mu\mathrm{tr}[\varepsilon^2] + \tfrac{\lambda}{2}\mathrm{tr}^2[\varepsilon] - \alpha'_0\mathrm{tr}[\varepsilon(\mathfrak{p}\otimes\mathfrak{p})]\mathrm{tr}[\mathfrak{p}\otimes\mathrm{e}] \\ &\quad - \alpha'_\perp\mathrm{tr}[\varepsilon]\mathrm{tr}[\mathfrak{p}\otimes\mathrm{e}] - \alpha'_=\mathrm{tr}[\varepsilon(\mathfrak{p}\otimes\mathrm{e})] - \tfrac{\epsilon}{2}\mathrm{tr}[\mathrm{e}\otimes\mathrm{e}]\end{aligned} \tag{7.26}$$

which satisfies the symmetry condition

$$\psi'_{pie}(\boldsymbol{Q}\varepsilon\boldsymbol{Q}^T, \boldsymbol{Q}\mathrm{e}; \mathfrak{p}) = \psi'_{pie}(\boldsymbol{\varepsilon}, \mathrm{e}; \mathfrak{p}) \quad \text{for all} \quad \boldsymbol{Q} \in \mathcal{G} := \{\boldsymbol{Q} \subset \mathcal{O} | \boldsymbol{Q}\mathfrak{p} = \mathfrak{p}\} \tag{7.27}$$

in analogy to (7.21). The mixed energy-enthalpy is a potential for the stresses and the electric displacement. As a consequence, (7.1) is modified to

$$\boldsymbol{\sigma} = \partial_\varepsilon\psi'_{pie}(\boldsymbol{\varepsilon}, \mathrm{e}) \quad \text{and} \quad \mathrm{d} = -\partial_\mathrm{e}\psi'_{pie}(\boldsymbol{\varepsilon}, \mathrm{e}), \tag{7.28}$$

with the decompositions

$$\boldsymbol{\sigma} = \boldsymbol{\sigma}^\varepsilon(\boldsymbol{\varepsilon}) + \boldsymbol{\sigma}^e(\mathrm{e}) \quad \text{and} \quad \mathrm{d} = \mathrm{d}^e(\mathrm{e}) + \mathrm{d}^\varepsilon(\boldsymbol{\varepsilon}) \tag{7.29}$$

and their basic representation $\boldsymbol{\sigma}^\varepsilon = \mathbb{C}' : \boldsymbol{\varepsilon}$, $\boldsymbol{\sigma}^e = -\boldsymbol{h}'(\mathfrak{p}) \cdot \mathrm{e}$ and $\mathrm{d}^e = \boldsymbol{\beta}' \cdot \mathrm{e}$. Note that $\boldsymbol{\sigma}^e$ characterizes a *stress relaxation* due to the electric-field-induced strain mode.

Free Energy Function. A further Legendre transformation converts the mixed energy-enthalpy function ψ'_{pie} defined in (7.23) to the free energy function

$$\psi_{pie}(\boldsymbol{\varepsilon}, \mathrm{d}; \mathfrak{p}) = \inf_\mathrm{e} \left[\psi'_{pie}(\boldsymbol{\varepsilon}, \mathrm{e}; \mathfrak{p}) + \mathrm{d} \cdot \mathrm{e} \right]. \tag{7.30}$$

After some algebraic manipulations, we obtain the closed form

$$\psi_{pie}(\boldsymbol{\varepsilon}, \mathrm{d}; \mathfrak{p}) = \tfrac{1}{2}\boldsymbol{\varepsilon} : \mathbb{C} : \boldsymbol{\varepsilon} - \boldsymbol{\varepsilon} : \boldsymbol{h}(\mathfrak{p}) \cdot \mathrm{d} + \tfrac{1}{2}\mathrm{d} \cdot \boldsymbol{\beta} \cdot \mathrm{d} \tag{7.31}$$

in terms of the structural tensors

$$\mathbb{C} := \mathbb{C}' + \boldsymbol{h}' \cdot \boldsymbol{\beta}'^{-1} \cdot \boldsymbol{h}'^T \quad , \quad \boldsymbol{h} := \boldsymbol{h}' \cdot \boldsymbol{\beta}'^{-1} \quad , \quad \boldsymbol{\beta} := \boldsymbol{\beta}'^{-1}. \tag{7.32}$$

Observe first that ψ_{pie} is a *convex function* with respect to the variables $\boldsymbol{\varepsilon}$ and d, because it is the *full* Legendre-Fenchel transformation of the function ψ^*_{pie} defined in (7.18). The structural tensors $\mathbb{C}$ and $\boldsymbol{\beta}$ are positive definite. Observe furthermore that the elasticity tensor $\mathbb{C}$ becomes anisotropic. However, this effect may again be *neglected* for the estimate $\mathcal{O}(\boldsymbol{h}' \cdot \boldsymbol{\beta}'^{-1} \cdot \boldsymbol{h}'^T) = (E\alpha^*_\|)^2/\epsilon \ll E = \mathcal{O}(\mathbb{C})$. We then obtain the closed form expressions

$$\begin{aligned}\mathbb{C} &:= 2\mu\mathbb{I} + \lambda\boldsymbol{1}\otimes\boldsymbol{1} \\ \boldsymbol{h} &:= \overset{12}{\mathrm{sym}}[\alpha_0\mathfrak{p}\otimes\mathfrak{p}\otimes\mathfrak{p} + \alpha_\perp\boldsymbol{1}\otimes\mathfrak{p} + \alpha_=\mathfrak{p}\otimes\boldsymbol{1}] \\ \boldsymbol{\beta} &:= \tfrac{1}{\epsilon}\boldsymbol{1}\end{aligned} \tag{7.33}$$

of the structural tensors with the modified piezoelectric coupling parameters $\alpha_0 := \alpha'_0/\epsilon$, $\alpha_\perp := \alpha'_\perp/\epsilon$ and $\alpha_= := \alpha'_=/\epsilon$. The representation in terms of elementary trace-type invariants reads

$$\begin{aligned}\psi_{pie}(\boldsymbol{\varepsilon}, \mathrm{d}; \mathfrak{p}) &= \mu\mathrm{tr}[\varepsilon^2] + \tfrac{\lambda}{2}\mathrm{tr}^2[\varepsilon] - \alpha_0\mathrm{tr}[\varepsilon(\mathfrak{p}\otimes\mathfrak{p})]\mathrm{tr}[\mathfrak{p}\otimes\mathrm{d}] \\ &\quad - \alpha_\perp\mathrm{tr}[\varepsilon]\mathrm{tr}[\mathfrak{p}\otimes\mathrm{d}] - \alpha_=\mathrm{tr}[\varepsilon(\mathfrak{p}\otimes\mathrm{d})] + \tfrac{1}{2\epsilon}\mathrm{tr}[\mathrm{d}\otimes\mathrm{d}]\end{aligned} \tag{7.34}$$

which satisfies the symmetry condition

$$\psi_{pie}(\boldsymbol{Q}\boldsymbol{\varepsilon}\boldsymbol{Q}^T, \boldsymbol{Q}\mathbb{d}; \mathfrak{p}) = \psi_{pie}(\boldsymbol{\varepsilon}, \mathbb{d}; \mathfrak{p}) \quad \text{for all} \quad \boldsymbol{Q} \in \mathcal{G} := \{\boldsymbol{Q} \subset \mathcal{O} | \boldsymbol{Q}\mathfrak{p} = \mathfrak{p}\} \qquad (7.35)$$

in analogy to (7.21) and (7.27). The free energy function is a potential for the stresses and the electric field. As a consequence of the Legendre transformation (7.1) and (7.2) are modified to

$$\boldsymbol{\sigma} = \partial_{\boldsymbol{\varepsilon}}\psi_{pie}(\boldsymbol{\varepsilon}, \mathbb{d}) \qquad \text{and} \qquad \mathbb{e} = \partial_{\mathbb{d}}\psi_{pie}(\boldsymbol{\varepsilon}, \mathbb{d}), \qquad (7.36)$$

with the decompositions

$$\boldsymbol{\sigma} = \boldsymbol{\sigma}^{\varepsilon}(\boldsymbol{\varepsilon}) + \boldsymbol{\sigma}^d(\mathbb{d}) \qquad \text{and} \qquad \mathbb{e} = \mathbb{e}^d(\mathbb{d}) + \mathbb{e}^{\varepsilon}(\boldsymbol{\varepsilon}) \qquad (7.37)$$

and their basic representation $\boldsymbol{\sigma}^{\varepsilon} = \mathbb{C} : \boldsymbol{\varepsilon}$, $\boldsymbol{\sigma}^d = -\boldsymbol{h}(\mathfrak{p}) \cdot \mathbb{d}$ and $\mathbb{e}^d = \boldsymbol{\beta} \cdot \mathbb{d}$. Note that $\boldsymbol{\sigma}^d$ is the *stress relaxation* due to an electric displacement.

A summary of the above introduced simple constitutive functions for piezoelectricity is given in Box 1.

7.2. A Model of Ferroelectric Response

7.2.1. Basic Phenomenology of a Ferroelectric Poling Process

Basic Observations. A ferroelectric material has a polycrystalline structure as visualized schematically in Figure 7.3. The polycrystalline mesostructure consists of a representative number of single crystal *grains*. These grains can be subdivided into *domains* with equal microscopic polarization. When the polycrystalline microstructure is subjected to a macroscopic electric field $\mathbb{e}$ of certain amount, the domain state changes such that the microscopic polarizations *switch* and try to become aligned to $\mathbb{e}$. Similar phenomena are also observed in ferroelectric polymers, see Chapter 2. This process is denoted as *electric poling* of the material. If the macroscopic electric field $\mathbb{e}$ is removed, the microscopic polarizations *remain* in their switched state and the overall polycrystalline aggregate has a macroscopic polarization $\mathbb{p}^r$ in a homogenized sense, as schematically visualized in Figure 7.3. The macroscopic behavior of an electrically poled ferroelectric material is then for a certain range of the electric field $\mathbb{e}$ *piezoelectric* as discussed in Section 7.1.1.

From the above consideration it becomes clear that the electric poling governed by the microscopic switching is essentially a *dissipative process*. The key dissipative feature is the remaining macro-polarization $\mathbb{p}^r$, the so-called *remanent polarization*. The process of switching needs a certain strength of the electric field $\mathbb{e}$. Below a threshold value e_c called the *coercive field strength*, micro-switching is not observed and the domain state remains unchanged. Above the coercive field strength, the domain state changes and the amount of macroscopic polarization approaches a *saturation* for increasing field strength. The saturation polarization p_s would be identical with the micro-polarization p_{micro} if all the domains were aligned to the macroscopic electric field. However, in real applications one observes $|\mathbb{p}^r| \leq p_s < p_{\text{micro}}$. If a macroscopically poled ferroelectric material is subject to an electric field oriented oppositely to the poling, it becomes poled in the opposite direction if the field strength exceeds the threshold value e_c. As a consequence, one observes for cyclic electric loading processes in the $\mathbb{d}$-$\mathbb{e}$-diagram a typical hysteresis, called the *dielectric hysteresis*. This underlines the dissipative character of the poling process. Furthermore, recall that a micro-polarization is a switching of atomic positions in an ideal crystal, accompanied by a deformation of the crystal. Thus, on the macro level a homogenized
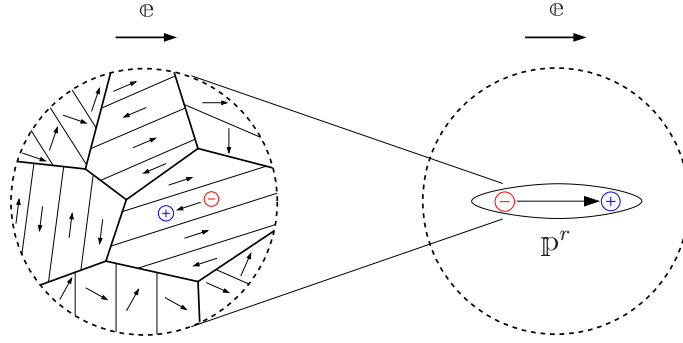
Figure 7.3: Ferroelectric effects. Ferroelectric materials are polycrystals with grains of single crystals divided into domains of equal microscopic spontaneous polarization. The domain state can be modified by a macroscopic electric field above a certain threshold value e_c such that the microscopic polarizations switch and become aligned to $\mathbb{e}$, yielding a homogenized remanent macro polarization $\mathbb{p}^r$ that remains after electric unloading. The amount of macro-polarization is limited by the spontaneous micro-polarization $|\mathbb{p}^r| \leq p_s < p_{\mathrm{micro}}$. Such a poled material then has a piezoelectric macroscopic response. The poling process is considered to be fully dissipative.

deformation of the polycrystal which remains after unloading can be noticed. This so-called *remanent strain* ε^r caused by the poling is an *elongation* of the polycrystalline aggregate in the direction $\mathbb{p}^r$ and a contraction in the direction perpendicular to $\mathbb{p}^r$, see Figure 7.4. As a consequence, one observes for cyclic electric loading processes in the ε-$\mathbb{e}$-diagram another typical hysteresis, called the *butterfly hysteresis*. Due to the saturation of the polarization $|\mathbb{p}^r| \leq p_s$, the remanent strain is also bounded by a saturation value $\|\varepsilon^r\| < \varepsilon_s$. Experiments show that the remanent strain is approximatively isochoric.

In summary, we have the following basic phenomenological effects in ferroelectric polycrystalline aggregate associated with the poling process:

- An electric field beyond the coercive field strength $|\mathbb{e}| \geq e_c$ causes a remanent macro-polarization $\mathbb{p}^r$ which remains after electric unloading.

- The amount $|\mathbb{p}^r| \leq p_s$ of polarization is bounded by saturated micro-polarizations.

- The polarization process is accompanied by a remanent strain $\varepsilon^r \sim \mathbb{p}^r \otimes \mathbb{p}^r / |\mathbb{p}^r|$ with $\mathrm{tr}[\varepsilon^r] \approx 0$, which is proportional to the remanent polarization.

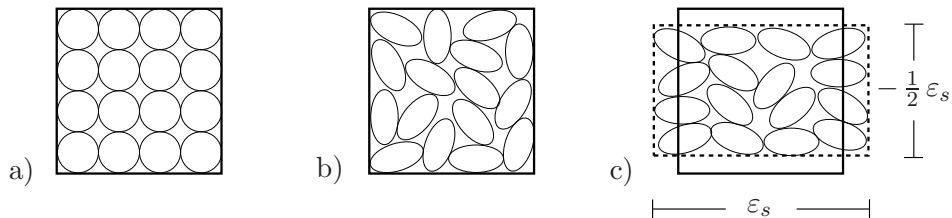- In cyclic processes driven by alternating directions of the electric field $\mathbb{e}$, typical

Figure 7.4: Deformation due to polarization. a) Cubic phase above the Curie temperature, b) random tetragonal phase below the Curie temperature, and c) aligned tetragonal phase after poling. When all the domains are switched of 90° or 180° to the direction closer to the electric field $\mathbb{e}$, an expansion equal to the saturation strain ε_s is reached in the direction parallel to $\mathbb{e}$ and due to the isochoric character of the deformation, a contraction of $-\frac{1}{2}\varepsilon_s$ is observed in the one orthogonal to $\mathbb{e}$.
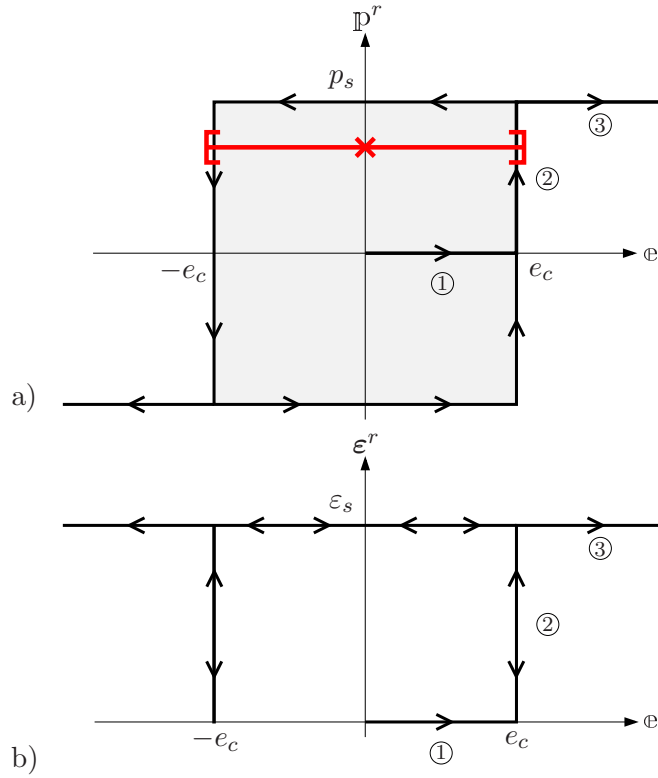
Figure 7.5: Ideal dielectric hysteresis. a) Remanent polarization and b) remanent strain induced by the polarization. Idealized process parts of poling: ① fully reversible virgin loading for $|e| < e_c$, ② full idealized switching at $|e| = e_c$ and ③ reversible response after saturated switching.

electric hystereses appear in the d-e-diagram and in the ε-e-diagram.

The macroscopic phenomenological modeling of the overall response of ferroelectric poly-crystalline aggregates needs in addition to a piezoelectric state at a given polarization p^r the *description of the dissipation process of the evolving polarization* $\dot{p}^r \neq 0$. In what follows, we focus first on an idealized modeling of this dissipative process and combine the result later with the piezoelectric energetic response.

The Fully Idealized Dielectric Hysteresis. We start with the maximal idealized description of a dielectric hysteresis visualized in Figure 7.5, where we consider monotonous and cyclic electric loading processes controlled by a prescribed electric field e. In a *monotonous electric loading process* starting from a virgin, completely unpoled material, the following three idealized steps are observed (cf. Figure 7.5):

① *Initial Range.* For a range $|e| < e_c$ below the coercive field strength e_c, no macro-polarization occurs, i.e. $p^r = 0$. Consequently no remanent strain ε^r is observed.

② *Domain Switching.* In this highly idealized picture, the switching of *all* domains takes place at the coercive field strength $|e| = e_c$ where the polarization p^r fully develops. This is accompanied by the development of a remanent strain ε^r.

③ *Saturated Range.* The poling process stops if the polarization reaches its saturation value $|p^r| = p_s$. The subsequent loading is non-dissipative.

In a *cyclic electric loading* process which alternates between fully poled states in positive and negative direction, we observe the above rectangle-shaped electric hysteresis. Thus

the idealized situation is characterized by the *reversible range of the electric field*

$$\mathcal{E} := \left\{ \mathbb{e} \in \mathbb{R}^3 \mid f(\mathbb{e}) := |\mathbb{e}| - e_c < 0 \right\} \tag{7.38}$$

in which no dissipative effect occurs. Note carefully, that the *electric field is not bounded by* $\mathcal{E}$ due to the arbitrarily large reversible post-critical range . In contrast, the *polarization is bounded by*

$$\mathcal{P} := \left\{ \mathbb{p}^r \in \mathbb{R}^3 \mid g(\mathbb{p}^r) := |\mathbb{p}^r| - p_s < 0 \right\} . \tag{7.39}$$

These two ranges are the cornerstones for the modeling of the poling process. The evolution of the polarization will takes place for an isotropic response in the direction of the electric field, i.e.

$$\dot{\mathbb{p}}^r \sim \mathbb{e} \tag{7.40}$$

and is governed by evolution laws constructed in the subsequent chapter based on standard thermodynamic arguments. Finally, the remanent strain which develops during the poling is assumed to be fully deviatoric and linearly growing with increasing amount of polarization

$$\boldsymbol{\varepsilon}^r = \frac{3}{2} \varepsilon_s \frac{|\mathbb{p}^r|}{p_s} \operatorname{dev} \left[\frac{\mathbb{p}^r}{|\mathbb{p}^r|} \otimes \frac{\mathbb{p}^r}{|\mathbb{p}^r|} \right] \tag{7.41}$$

and thus phenomena of mechanical depolarization are here neglected. Equation (7.41) will be motivated in the following subsections. The three material parameters e_c, p_s, and ε_s govern the basic characteristic of the idealized fully dissipative poling process depicted in Figure 7.5 (all the dissipative material parameters are summarized in Table 7.2).

The Regularized Dielectric Hysteresis. The above outlined modeling of the dissipative poling effort is highly idealized in particular with respect to the assumption that the domain switching takes place at the constant value $|\mathbb{e}| = e_c$ of the electric field. Experiments show that full polarization develops only for electric fields $|\mathbb{e}| > e_c$ above the coercive field strength e_c. This effect is *highly non-linear* and approaches the saturated polarization asymptotically as illustrated in Figure 7.6. As a consequence, the dissipative polarization process for monotonous electric loading reduces to the two steps:

① *Initial Range.* For a range $|\mathbb{e}| < e_c$ below the coercive field strength e_c, no macro–polarization occurs, i.e. $\mathbb{p}^r = \boldsymbol{0}$.

② *Domain Switching.* The polarization occurs for $|\mathbb{e}| > e_c$ in a nonlinear format such that it approaches asymptotically its saturation value p_s.

In a *cyclic electric loading process*, we then observe the hysteretic effects depicted in Figure 7.6, where the *center of the elastic range* is shifted by a so-called *back electric field* $\mathbb{e}^b(\mathbb{p}^r)$ that depends on the polarization $\mathbb{p}^r$. The modeling of this moving reversible range is obtained by an extension of (7.38) to

$$\mathcal{E} := \left\{ \mathbb{e} \in \mathbb{R}^3 \mid f(\mathbb{e}, \mathbb{p}^r) := |\mathbb{e} - \mathbb{e}^b(\mathbb{p}^r)| - e_c < 0 \right\} . \tag{7.42}$$

The back electric field $\mathbb{e}^b(\mathbb{p}^r)$ may assumed to be aligned to the current polarization by the functional representation

$$\mathbb{e}^b(\mathbb{p}^r) = h(|\mathbb{p}^r|) \frac{\mathbb{p}^r}{|\mathbb{p}^r|} \tag{7.43}$$

based on a scalar, monotonically increasing function $h(x)$ with the properties

$$h(x) > 0 \quad , \quad h(0) = 0 \quad , \quad \lim_{x \to p_s} h(x) = \infty , \tag{7.44}$$
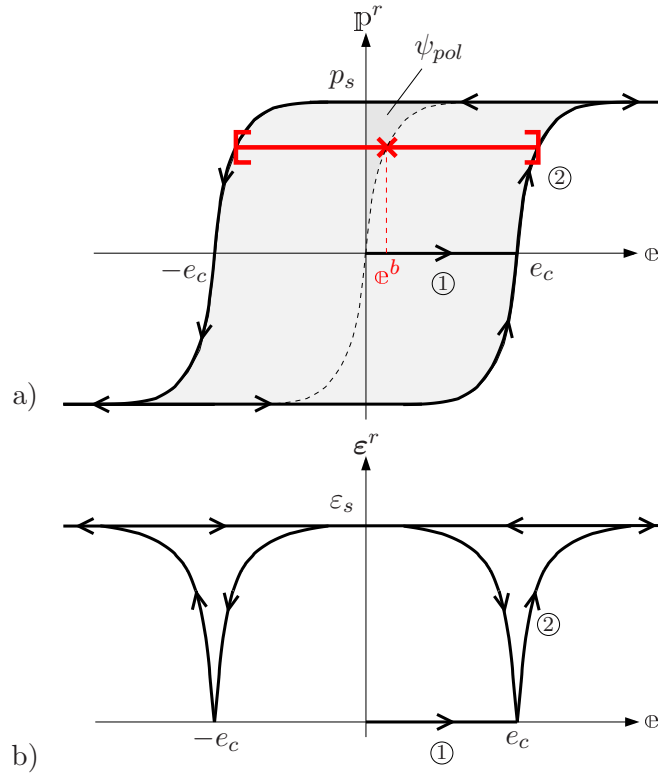
Figure 7.6: Regularized dielectric hysteresis. a) Remanent polarization and b) remanent strain induced by the polarization. Process parts of poling: ① fully reversible virgin loading for $\mathbb{e} < e_c$ and ② regularized switching at $|\mathbb{e}| > e_c$, approaching asymptotically the saturation.

providing the non-linear saturation effect visualized in Figure 7.6. Note carefully that the above made assumptions (7.42)-(7.44) ensure the bounding $\mathbb{p}^r \in \mathcal{P}$ of the polarization defined in (7.39).

From a formal viewpoint of constitutive modeling, the polarization evolves by *kinematic hardening* for cyclic electric fields $\mathbb{e}$, governed by the non-linear back-field function $\mathbb{e}^b$. Thus, (7.40), (7.41), (7.42), and (7.43) govern a regularization of the idealized model (7.38)–(7.41), which is very close to the experimentally observed phenomena. This becomes clear in Figure 7.7, where we superimposed the reversible part $\mathbb{d}^e = \epsilon \mathbb{e}$ of the electric displacement onto the remanent polarization.

7.2.2. Construction of Energy and Enthalpy Functions

We now construct based on the above outlined phenomenological assumptions suitable representations of the energy and enthalpy functions which represent the local storage mechanisms in ferroelectricity.

The Free Energy Function. The construction of the free energy function is based on the following particular assumptions which go beyond the one made in the points P1-P6 in Section 7.1.1 for the reversible piezoelectric response:

FE1. The polarization $\mathbb{p}^r$ with direction $\mathfrak{p} := \mathbb{p}^r/|\mathbb{p}^r|$ produces a remanent *axial strain* which *grows linearly* with $\mathbb{p}^r$ to the saturated value ε_s at saturated polarization
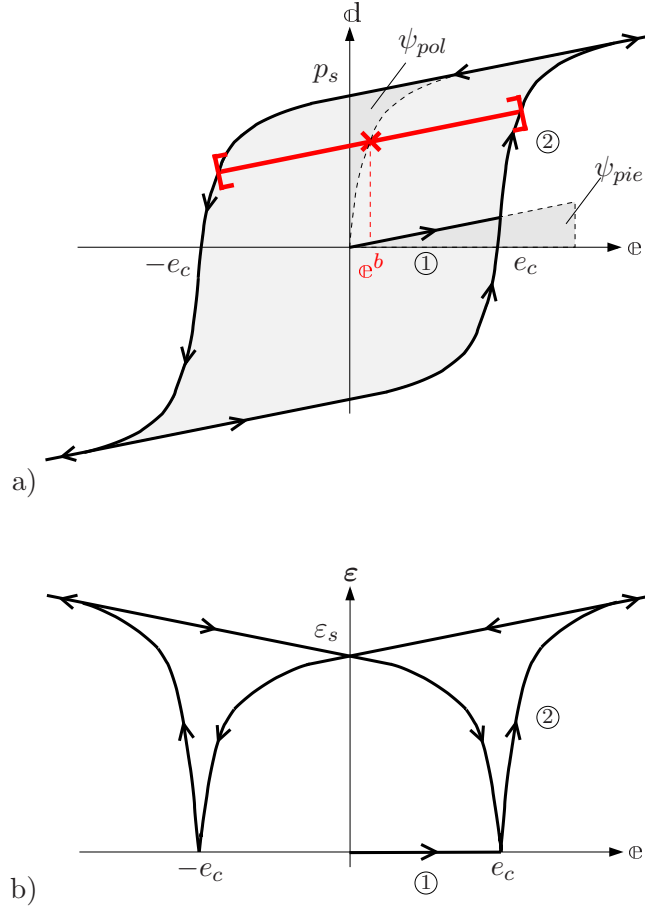
Figure 7.7: Regularized dielectric hysteresis with piezo-electric contributions. a) Electric displacement and b) normal strain in direction of the electric field. Process parts of poling: ① fully reversible virgin loading for $|e| < e_c$ and ② regularized switching at $|e| > e_c$ approaching asymptotically the saturation.

$$|\mathbb{p}^r| = p_s$$

$$\varepsilon_\parallel^r := \boldsymbol{\varepsilon}^r : (\mathfrak{p} \otimes \mathfrak{p}) = \varepsilon_s \frac{|\mathbb{p}^r|}{p_s} \,. \tag{7.45}$$

FE2. The remanent strain is *isochoric* and fully isotropic in the lateral direction, i.e.

$$2\varepsilon_\perp^r := \boldsymbol{\varepsilon}^r : (\boldsymbol{1} - \mathfrak{p} \otimes \mathfrak{p}) = -\varepsilon_\parallel^r \,. \tag{7.46}$$

These two assumptions define the remanent strain $\boldsymbol{\varepsilon}^r$ as a deviatoric function of the polarization $\mathbb{p}^r$ as already pointed out in equation (7.41), i.e. $\boldsymbol{\varepsilon}^r(\mathbb{p}^r) = \frac{3}{2}\varepsilon_s \frac{|\mathbb{p}^r|}{p_s} \,\mathrm{dev}[\mathfrak{p} \otimes \mathfrak{p}]$. With this definition of the remanent strain as a *dependent* tensor field, we proceed with the introduction of independent variables which govern the energy storage:

FE3. The strain and the electric displacement decompose additively into stress-induced, electric-field-induced and remanent contributions according to

$$\boldsymbol{\varepsilon} = \boldsymbol{\varepsilon}^\sigma + \boldsymbol{\varepsilon}^e + \boldsymbol{\varepsilon}^r(\mathbb{p}^r) \qquad \text{and} \qquad \mathbb{d} = \mathbb{d}^\sigma + \mathbb{d}^e + \mathbb{p}^r \,. \tag{7.47}$$

FE4. The stored energy decomposes into a *piezoelectric part* and a *polarization part* according to

$$\psi(\boldsymbol{\varepsilon}, \mathbb{d}, \mathbb{p}^r) = \psi_{pie}(\boldsymbol{\varepsilon} - \boldsymbol{\varepsilon}^r(\mathbb{p}^r), \mathbb{d} - \mathbb{p}^r, \mathbb{p}^r) \, + \, \psi_{pol}(\mathbb{p}^r) \,, \tag{7.48}$$

where the polarization vector $\mathbb{p}^r$ plays the role of an *internal variable.*

FE5. The piezoelectric part ψ_{pie} of the stored energy depends on the stress-induced and electric-field-induced strains and electric displacements and is assumed of the form (7.31) based on the assumptions P1–P6, however with a modified third-order coupling tensor

$$\boldsymbol{h}_{pol}(\mathbb{p}^r) := \frac{|\mathbb{p}^r|}{p_s}\boldsymbol{h}(\mathfrak{p}) \tag{7.49}$$

which *grows linearly* with the polarization in order to model a coupling which accompanies the polarization and is in particular absent for a zero macroscopic polarization, and maximum when the polarization reaches its saturation value. Thus, the parameter α_0, $\alpha_\parallel$, and $\alpha_=$ are assumed to be related to the saturated polarization state at $|\mathbb{p}^r| = p_s$.

FE6. The polarization part ψ_{pol} of the free energy is assumed to be defined by (7.43) with the *hardening function*

$$h(|\mathbb{p}^r|) = h_0|\mathbb{p}^r|/\left(1 - \frac{|\mathbb{p}^r|}{p_s}\right) , \tag{7.50}$$

satisfying the properties (7.44). Here h_0 is a material parameter governing the shape of the hysteresis curves.

With these assumptions the stored free energy of a ferroelectric material takes the form

$$\begin{aligned}
\psi(\boldsymbol{\varepsilon}, \mathbb{d}, \mathbb{p}^r) &= \tfrac{1}{2}\left[\boldsymbol{\varepsilon} - \boldsymbol{\varepsilon}^r(\mathbb{p}^r)\right] : \mathbb{C} : \left[\boldsymbol{\varepsilon} - \boldsymbol{\varepsilon}^r(\mathbb{p}^r)\right] - \left[\boldsymbol{\varepsilon} - \boldsymbol{\varepsilon}^r(\mathbb{p}^r)\right] : \frac{|\mathbb{p}^r|}{p_s}\boldsymbol{h}(\mathfrak{p}) \cdot [\mathbb{d} - \mathbb{p}^r] \\
&+ \tfrac{1}{2}[\mathbb{d} - \mathbb{p}^r] \cdot \boldsymbol{\beta} \cdot [\mathbb{d} - \mathbb{p}^r] - h_0 p_s^2 \left[\ln\left(1 - \frac{|\mathbb{p}^r|}{p_s}\right) + \frac{|\mathbb{p}^r|}{p_s}\right]
\end{aligned} \tag{7.51}$$

in terms of the structural tensors $\mathbb{C}$, $\boldsymbol{h}(\mathfrak{p})$, and $\boldsymbol{\beta}$ defined in (7.33) and the functional dependence (7.41) for the remanent strain $\boldsymbol{\varepsilon}^r(\mathbb{p}^r)$ on the polarization. The free energy ψ is a potential for the stresses $\boldsymbol{\sigma}$, the electric field $\mathbb{e}$ and the driving force $\mathbb{e}^r$ of the polarization, i.e.

$$\boldsymbol{\sigma} = \partial_{\boldsymbol{\varepsilon}}\psi(\boldsymbol{\varepsilon}, \mathbb{d}, \mathbb{p}^r) \quad , \quad \mathbb{e} = \partial_{\mathbb{d}}\psi(\boldsymbol{\varepsilon}, \mathbb{d}, \mathbb{p}^r) \quad , \quad \mathbb{e}^r = -\partial_{\mathbb{p}^r}\psi(\boldsymbol{\varepsilon}, \mathbb{d}, \mathbb{p}^r) . \tag{7.52}$$

Note that the stresses and the electric field, due to the specific form (7.48) of the free energy, are specified as follows

$$\boldsymbol{\sigma} = \partial_{\boldsymbol{\varepsilon} - \boldsymbol{\varepsilon}^r}\psi_{pie}(\boldsymbol{\varepsilon} - \boldsymbol{\varepsilon}^r(\mathbb{p}^r), \mathbb{d} - \mathbb{p}^r, \mathbb{p}^r) \quad \text{and} \quad \mathbb{e} = \partial_{\mathbb{d} - \mathbb{p}^r}\psi_{pie}(\boldsymbol{\varepsilon} - \boldsymbol{\varepsilon}^r(\mathbb{p}^r), \mathbb{d} - \mathbb{p}^r, \mathbb{p}^r) . \tag{7.53}$$

Furthermore, the thermodynamic driving force for the poling can be written in the form

$$\mathbb{e}^r = \mathbb{e}_{pie} - \mathbb{e}_{pol} \tag{7.54}$$

with the following specific *piezoenergetic contribution* and *energetic poling contribution*

$$\begin{aligned}
\mathbb{e}_{pie} &:= \mathbb{e} + \boldsymbol{\sigma} : \partial_{\mathbb{p}^r}\boldsymbol{\varepsilon}^r(\mathbb{p}^r) - \partial_{\mathbb{p}^r}\psi_{pie}(\boldsymbol{\varepsilon} - \boldsymbol{\varepsilon}^r(\mathbb{p}^r), \mathbb{d} - \mathbb{p}^r, \mathbb{p}^r) \\
\mathbb{e}_{pol} &:= \partial_{\mathbb{p}^r}\psi_{pol}(\mathbb{p}^r) ,
\end{aligned} \tag{7.55}$$

where the last is nothing but the back electric field defined in (7.43). As a consequence of the above fully coupled thermodynamic treatment, the piezoenergetic contribution $\mathbb{e}_{pie}$ of the driving force $\mathbb{e}^r$ contains mechanical-based terms. These are the second and third terms on the right hand side of $(7.55)_1$, which come from the polarization-dependent remanent strain and piezoelectric coupling term.

The Mixed Energy-Enthalpy Function. From the above free energy function we obtain by a Legendre transformation the mixed energy-enthalpy function of the ferroelectric material

$$\psi'(\boldsymbol{\varepsilon}, \mathbb{e}, \mathbb{p}^r) = \inf_{\mathbb{d}} \left[\psi(\boldsymbol{\varepsilon}, \mathbb{d}, \mathbb{p}^r) - \mathbb{e} \cdot \mathbb{d} \right] \tag{7.56}$$

which, similarly to the free energy function ψ, decomposes additively according to

$$\psi'(\boldsymbol{\varepsilon}, \mathbb{e}, \mathbb{p}^r) = \psi'_{pie}(\boldsymbol{\varepsilon} - \boldsymbol{\varepsilon}^r(\mathbb{p}^r), \mathbb{e}, \mathbb{p}^r) + \psi'_{pol}(\mathbb{e}, \mathbb{p}^r), \tag{7.57}$$

into a piezoelectric part ψ'_{pie} and a part due to the poling

$$\psi'_{pol}(\mathbb{e}, \mathbb{p}^r) = \psi_{pol}(\mathbb{p}^r) - \mathbb{e} \cdot \mathbb{p}^r . \tag{7.58}$$

Thus, the mixed energy-enthalpy function ψ' assumes the closed form representation

$$
\begin{aligned}
\psi'(\boldsymbol{\varepsilon}, \mathbb{e}, \mathbb{p}^r) = {} & \tfrac{1}{2} \left[\boldsymbol{\varepsilon} - \boldsymbol{\varepsilon}^r(\mathbb{p}^r) \right] : \mathbb{C}' : \left[\boldsymbol{\varepsilon} - \boldsymbol{\varepsilon}^r(\mathbb{p}^r) \right] - \left[\boldsymbol{\varepsilon} - \boldsymbol{\varepsilon}^r(\mathbb{p}^r) \right] : \frac{|\mathbb{p}^r|}{p_s} \boldsymbol{h}'(\mathfrak{p}) \cdot \mathbb{e} \\
& - \tfrac{1}{2} \mathbb{e} \cdot \boldsymbol{\beta}' \cdot \mathbb{e} - h_0 p_s^2 \left[\ln \left(1 - \frac{|\mathbb{p}^r|}{p_s} \right) + \frac{|\mathbb{p}^r|}{p_s} \right] - \mathbb{e} \cdot \mathbb{p}^r
\end{aligned} \tag{7.59}
$$

in terms of the constitutive tensors $\mathbb{C}'$, $\boldsymbol{h}'(\mathfrak{p})$ and $\boldsymbol{\beta}'$ defined in (7.25). The mixed energy-enthalpy function is a potential for the stresses $\boldsymbol{\sigma}$, the electric displacement $\mathbb{d}$, and the driving force $\mathbb{e}^r$ of the polarization, i.e.

$$\boldsymbol{\sigma} = \partial_{\boldsymbol{\varepsilon}} \psi'(\boldsymbol{\varepsilon}, \mathbb{e}, \mathbb{p}^r) \quad , \quad \mathbb{d} = -\partial_{\mathbb{e}} \psi'(\boldsymbol{\varepsilon}, \mathbb{e}, \mathbb{p}^r) \quad , \quad \mathbb{e}^r = -\partial_{\mathbb{p}^r} \psi'(\boldsymbol{\varepsilon}, \mathbb{e}, \mathbb{p}^r) . \tag{7.60}$$

Note that the stresses and the electric displacement appear due to the specified form (7.57) of the mixed energy-enthalpy function as

$$
\begin{aligned}
\boldsymbol{\sigma} &= \partial_{\boldsymbol{\varepsilon} - \boldsymbol{\varepsilon}^r} \psi'_{pie}(\boldsymbol{\varepsilon} - \boldsymbol{\varepsilon}^r(\mathbb{p}^r), \mathbb{e}, \mathbb{p}^r) \\
\mathbb{d} &= -\partial_{\mathbb{e}} \psi'_{pie}(\boldsymbol{\varepsilon} - \boldsymbol{\varepsilon}^r(\mathbb{p}^r), \mathbb{e}, \mathbb{p}^r) - \partial_{\mathbb{e}} \psi'_{pol}(\mathbb{e}, \mathbb{p}^r) .
\end{aligned} \tag{7.61}
$$

Furthermore, the thermodynamic driving force $\mathbb{e}^r$ of the poling appears again in the form (7.54) as the difference between the *piezoenergetic contribution*

$$\mathbb{e}_{pie} := \mathbb{e} + \boldsymbol{\sigma} : \partial_{\mathbb{p}^r} \boldsymbol{\varepsilon}^r(\mathbb{p}^r) - \partial_{\mathbb{p}^r} \psi'_{pie}(\boldsymbol{\varepsilon} - \boldsymbol{\varepsilon}^r(\mathbb{p}^r), \mathbb{e}, \mathbb{p}^r) \tag{7.62}$$

and a *energetic poling contribution* $\mathbb{e}_{pol}$, which turns out to be identical to $(7.55)_2$.

7.2.3. Construction of Dissipation Functions

What remains is the definition of a suitable dissipation function which governs the evolution of the polarization. This dissipation function is constructed starting from the above thermodynamic arguments based on standard concepts for dissipative materials. We base our subsequent formulations on the following two assumptions:

FE7. We define a *reversible range* in the space of the thermodynamic driving force $\mathbb{e}^r$ of polarization defined in (7.54) by

$$\mathcal{E} := \left\{ \mathbb{e}^r \in \mathbb{R}^3 \,|\, f(\mathbb{e}^r) := |\mathbb{e}^r|/e_c - 1 < 0 \right\} \tag{7.63}$$

in terms of the the *convex macroscopic switching function* $f : \mathbb{R}^3 \to \mathbb{R}$ for an isotropic response. The material parameter $e_c > 0$ which bounds the reversible range is the already defined *coercive field strength*.

FE8. A rate-dependent convex dissipation function can be defined in terms of the switching function f by the maximum principle

$$\phi_\eta(\dot{\mathbb{p}}^r) = \sup_{\mathbb{e}^r} \left\{ \mathbb{e}^r \cdot \dot{\mathbb{p}}^r - \frac{e_c}{\eta(1+m)} \langle f(\mathbb{e}^r) \rangle^{1+m} \right\} \qquad (7.64)$$

where $\langle x \rangle := (x + |x|)/2$ denotes the ramp function. The two material parameters $\eta > 0$ and $m > 0$ characterize the *viscosity of polarization* and the *viscosity shape*, respectively.

Note that the above definition of the dissipation function ϕ_η is a viscous regularization of a rate-independent dissipation function defined by the maximum principle

$$\phi(\dot{\mathbb{p}}^r) = \sup_{\mathbb{e}^r \in \mathcal{E}} \left\{ \mathbb{e}^r \cdot \dot{\mathbb{p}}^r \right\} . \qquad (7.65)$$

The expression (7.64) may be interpreted as a penalty-type approximative solution of the constraint maximum problem (7.65), where $1/\eta$ plays the role of a penalty parameter. However, from the physical viewpoint η is interpreted as a viscosity of the polarization. Note that the rate-independent limit is obtained for vanishing viscosity $\eta \to 0$, when the penalty parameter becomes infinitely large. Observe furthermore that the definition (7.64) of the rate-independent dissipation function can be interpreted as a Legendre transformation of the *dual dissipation function*

$$\phi_\eta^*(\mathbb{e}^r) = \frac{e_c}{\eta(1+m)} \langle f(\mathbb{e}^r) \rangle^{1+m} \qquad (7.66)$$

and the necessary condition of the maximum problem (7.64) defines the *evolution of polarization* by

$$\dot{\mathbb{p}}^r = \partial_{\mathbb{e}^r} \phi_\eta^*(\mathbb{e}^r) \qquad (7.67)$$

in terms of the thermodynamic driving force $\mathbb{e}^r$.[1] The evolution equation takes the closed-form

$$\dot{\mathbb{p}}^r = \frac{1}{\eta} \left\langle \frac{|\mathbb{e}^r|}{e_c} - 1 \right\rangle^m \frac{\mathbb{e}^r}{|\mathbb{e}^r|} . \qquad (7.70)$$

---

[1]**Smooth Dissipation Functions.** An alternative to the dissipation functions ϕ_η and ϕ_η^* defined in (7.64) and (7.66) are the smooth dual functions

$$\phi_v(\dot{\mathbb{p}}^r) = \frac{e_c}{\eta(1+1/m)} \left(\eta |\dot{\mathbb{p}}^r| \right)^{1+1/m} \qquad \text{and} \qquad \phi_v^*(\mathbb{e}^r) = \frac{e_c}{\eta(1+m)} \left(|\mathbb{e}^r|/e_c \right)^{1+m} \qquad (7.68)$$

yielding the dual dissipative response

$$\mathbb{e}^r = e_c (\eta |\dot{\mathbb{p}}^r|)^{1/m} \frac{\dot{\mathbb{p}}^r}{|\dot{\mathbb{p}}^r|} \qquad \text{and} \qquad \dot{\mathbb{p}}^r = \frac{1}{\eta} \left(\frac{|\mathbb{e}^r|}{e_c} \right)^m \frac{\mathbb{e}^r}{|\mathbb{e}^r|} \qquad (7.69)$$

without an explicit reversible range. Here, the meaning of the material parameters is quite different form those in (7.64) and (7.66). $1/\eta$ can be considered as a *reference rate* for the amount of polarization. Furthermore, the exponent m plays a much more critical role. For $m = 1$ the polarization process becomes linearly viscous in the full range of the driving force $\mathbb{e}^r$ in a sense of a Newton-law. A rate-independent response with the desired reversible range $|\mathbb{e}^r| \leq e_c$ is only approximatively approached for *very large values* of m. The limit $m \to \infty$ recovers the rate-independent response. Though the setting is attractive due to its smoothness, its numerical implementations suffers for high exponents m from bad numerical conditioning. From the numerical point of view, the functions ϕ_η and ϕ_η^* with reversible range defined in (7.64) and (7.66) are the best choice if the effect of the reversible range becomes dominant and the viscosity is restricted to a driving over-force.

Table 7.2: Ferroelectric Dissipative Material Parameters

No.	Parameter	Unit	Name	Eq.
1	$e_c > 0$	V/m	coercive electric field	(7.42)
2	$p_s > 0$	C/m^2	saturation polarization	(7.41)
3	$\varepsilon_s > 0$	–	saturation strain	(7.39)
4	$h_0 > 0$	(V·m)/C	hysteresis slop parameter	(7.50)
5	$\eta > 0$	m^2/(C·s)	viscosity of polarization	(7.64)
6	$m > 0$	–	viscosity shape exponent	(7.64)

Observe first that the polarization $\mathbb{p}^r$ evolves in the *direction* of the driving force $\mathbb{e}^r$ characterizing an isotropic macroscopic response of the polycrystalline aggregate. The *amount* $|\dot{\mathbb{p}}^r|$ of evolution is zero in the elastic range $|\mathbb{e}^r| \leq e_c$ and increases for $|\mathbb{e}^r| > e_c$ as a nonlinear function of the "*dimensionless over-force*" $|\mathbb{e}^r|/e_c - 1 > 0$ governed by the material parameters η and m. Note that $m = 1$ characterizes a dashpot-like linear Newton-law of viscosity. For $m < 1$, we have the phenomenological characteristic of a nonlinear Norton-Bailey-type creep response. The relationship between the evolution $\dot{\mathbb{p}}^r$ of polarization and the macroscopic electric field $\mathbb{e}$ becomes more clear if one inserts into (7.70) the decomposition (7.54) of the driving force $\mathbb{e}^r$ into the piezoelectric contribution $\mathbb{e}_{pie}$ and the contribution $\mathbb{e}_{pol}$ due to the polarization, i.e.

$$\dot{\mathbb{p}}^r = \frac{1}{\eta} \left\langle \frac{|\mathbb{e}_{pie} - \mathbb{e}_{pol}|}{e_c} - 1 \right\rangle^m \frac{\mathbb{e}_{pie} - \mathbb{e}_{pol}}{|\mathbb{e}_{pie} - \mathbb{e}_{pol}|} . \tag{7.71}$$

This evolution law models for $\mathbb{e}_{pie} \approx \mathbb{e}$ and the "*back electric field*" $\mathbb{e}_{pol} = [h_0|\mathbb{p}^r|/(1 - |\mathbb{p}^r|/p_s)](\mathbb{p}^r/|\mathbb{p}^r|)$ the dielectric hysteresis loops with saturation-type character such as qualitatively visualized in Figures 7.6 and 7.7 including the *viscous effects*. This evolution is in analogy to viscoplastic flow rules with nonlinear kinematic hardening in plasticity. The dissipative ferroelectric material parameters are summarized in Table 7.2.

7.3. Numerical Examples

The response of the material is assumed to be governed by the potential $w(\boldsymbol{\varepsilon}, \mathbb{e})$ having the form introduced in Section 6.3

$$w(\boldsymbol{\varepsilon}, \mathbb{e}) = \inf_{\mathbb{p}^r} \sup_{\mathbb{e}^r} \bar{w}(\boldsymbol{\varepsilon}, \mathbb{e}, \mathbb{p}^r, \mathbb{e}^r) . \tag{7.72}$$

$\bar{w}(\boldsymbol{\varepsilon}, \mathbb{e}, \mathbb{p}^r, \mathbb{e}^r)$ is the algorithmic expression of the incremental electro-mechanical work

$$\bar{w}(\boldsymbol{\varepsilon}, \mathbb{e}, \mathbb{p}^r, \mathbb{e}^r) = \psi'(\boldsymbol{\varepsilon}, \mathbb{e}, \mathbb{p}^r) - \psi'(\boldsymbol{\varepsilon}_n, \mathbb{e}_n, \mathbb{p}^r_n) + \mathbb{e}^r \cdot [\mathbb{p}^r - \mathbb{p}^r_n] - \Delta t \phi^*_\eta(\mathbb{e}^r) . \tag{7.73}$$

In (7.73) $\psi'(\boldsymbol{\varepsilon}, \mathbb{e}, \mathbb{p}^r)$ is the mixed energy-enthalpy function defined in (7.59) and $\phi^*_\eta(\mathbb{e}^r)$ the conjugate dissipation potential introduced in equation (7.66).

The enforcement of the necessary condition of the constitutive variational principle (7.72) yields the non-linear system of equations

$$\bar{\boldsymbol{r}} := \left[\begin{array}{c} \partial_{\mathbb{p}^r} \bar{w} \\ \partial_{\mathbb{e}^r} \bar{w} \end{array} \right] = \left[\begin{array}{c} \partial_{\mathbb{p}^r} \psi' + \mathbb{e}^r \\ \mathbb{p}^r - \mathbb{p}^r_n - \frac{\Delta t}{\eta} \langle \frac{|\mathbb{e}^r|}{e_c} - 1 \rangle^m \boldsymbol{n} \end{array} \right] = \boldsymbol{0} , \tag{7.74}$$

with the definition of the flow direction $\boldsymbol{n} := \mathbb{e}^r/|\mathbb{e}^r|$. The first equation in (7.74) represents the algorithmic definition of the conjugate internal force $\mathbb{e}^r$. The second equation of (7.74) gives the viscous evolution equation of the internal variable $\mathbb{p}^r$. The above non-linear system can be solved at given deformation $\boldsymbol{\varepsilon}$ and electric field $\mathbb{e}$ by a local Newton-type algorithm for the current variables $\bar{\boldsymbol{v}} := \{\mathbb{p}^r, \mathbb{e}^r\}$

$$\bar{\boldsymbol{v}} \Leftarrow \bar{\boldsymbol{v}} - \bar{\boldsymbol{a}}^{-1}\bar{\boldsymbol{r}} \tag{7.75}$$

until convergence is achieved in the sense $|\bar{\boldsymbol{r}}| < tol$. The tangent matrix of the Newton iteration has the form

$$\bar{\boldsymbol{a}} := \begin{bmatrix} \partial^2_{\mathbb{p}^r\mathbb{p}^r}\psi' & \boldsymbol{1} \\[2ex] \boldsymbol{1} & \begin{array}{c} -\frac{m\Delta t}{\eta e_c}\langle|\mathbb{e}^r|/e_c - 1\rangle^{m-1}\boldsymbol{n} \otimes \boldsymbol{n} \\ -\frac{\Delta t}{\eta}\langle|\mathbb{e}^r|/e_c - 1\rangle^m\frac{1}{|\mathbb{e}^r|}\{\boldsymbol{1} - \boldsymbol{n} \otimes \boldsymbol{n}\} \end{array} \end{bmatrix}. \tag{7.76}$$

According to (6.137) the derivatives of $w(\boldsymbol{\varepsilon}, \mathbb{e})$ with respect to the strains $\boldsymbol{\varepsilon}$ and the electric field $\mathbb{e}$, i.e. the generalized covector $\boldsymbol{f}'$, gives the stresses $\boldsymbol{\sigma}$ and electric displacement $\mathbb{d}$, i.e. the generalized vector

$$\boldsymbol{\mathfrak{s}}' := \begin{bmatrix} \boldsymbol{\sigma} \\ -\mathbb{d} \end{bmatrix} := \begin{bmatrix} \partial_{\boldsymbol{\varepsilon}}w(\boldsymbol{\varepsilon}, \mathbb{e}) \\ \partial_{\mathbb{e}}w(\boldsymbol{\varepsilon}, \mathbb{e}) \end{bmatrix} = \begin{bmatrix} \partial_{\boldsymbol{\varepsilon}}\psi' \\ \partial_{\mathbb{e}}\psi' \end{bmatrix} = \begin{bmatrix} \mathbb{C}' : \boldsymbol{\varepsilon}^e - \mathbb{e} \cdot \frac{|\mathbb{p}^r|}{p_s}\boldsymbol{h}'(\mathfrak{p}) \\ -\boldsymbol{\beta}' \cdot \mathbb{e} - \frac{|\mathbb{p}^r|}{p_s}\boldsymbol{h}'(\mathfrak{p}) : \boldsymbol{\varepsilon}^e - \mathbb{p}^r \end{bmatrix}. \tag{7.77}$$

Using the implicit function theorem we may derive a closed-form solution of the coupled electro-mechanical tangent moduli operators $\boldsymbol{\mathfrak{c}}' := \begin{bmatrix} \mathbb{C}'_{algo} & \boldsymbol{h}'_{algo} \; ; \; (\boldsymbol{h}'_{algo})^T & \boldsymbol{\beta}'_{algo} \end{bmatrix}$ with

$$\mathbb{C}'_{algo} := \partial^2_{\boldsymbol{\varepsilon}\boldsymbol{\varepsilon}}w = \partial^2_{\boldsymbol{\varepsilon}\boldsymbol{\varepsilon}}\psi' - \begin{bmatrix} \partial^2_{\boldsymbol{\varepsilon}\mathbb{p}^r}\psi' \\ \boldsymbol{0} \end{bmatrix} \cdot \bar{\boldsymbol{a}}^{-1} \cdot \begin{bmatrix} \partial^2_{\mathbb{p}^r\boldsymbol{\varepsilon}}\psi' \\ \boldsymbol{0} \end{bmatrix},$$

$$\boldsymbol{\beta}'_{algo} := \partial^2_{\mathbb{e}\mathbb{e}}w = \partial^2_{\mathbb{e}\mathbb{e}}\psi' - \begin{bmatrix} \partial^2_{\mathbb{e}\mathbb{p}^r}\psi' \\ \boldsymbol{0} \end{bmatrix} \cdot \bar{\boldsymbol{a}}^{-1} \cdot \begin{bmatrix} \partial^2_{\mathbb{p}^r\mathbb{e}}\psi' \\ \boldsymbol{0} \end{bmatrix}, \tag{7.78}$$

$$\boldsymbol{h}'_{algo} := \partial^2_{\mathbb{e}\boldsymbol{\varepsilon}}w = \partial^2_{\mathbb{e}\boldsymbol{\varepsilon}}\psi' - \begin{bmatrix} \partial^2_{\mathbb{e}\mathbb{p}^r}\psi' \\ \boldsymbol{0} \end{bmatrix} \cdot \bar{\boldsymbol{a}}^{-1} \cdot \begin{bmatrix} \partial^2_{\mathbb{p}^r\boldsymbol{\varepsilon}}\psi' \\ \boldsymbol{0} \end{bmatrix},$$

and $\partial^2_{\boldsymbol{\varepsilon}\boldsymbol{\varepsilon}}\psi' = \mathbb{C}'$, $\partial^2_{\mathbb{e}\mathbb{e}}\psi' = -\boldsymbol{\beta}'$, $\partial^2_{\mathbb{e}\boldsymbol{\varepsilon}}\psi' = -\frac{|\mathbb{p}^r|}{p_s}\boldsymbol{h}'(\mathfrak{p})$. For the considered model problem $\partial^2_{\boldsymbol{\varepsilon}\mathbb{e}^r}\bar{w} = \partial^2_{\mathbb{e}^r\boldsymbol{\varepsilon}}\bar{w} = \boldsymbol{0}$ and $\partial^2_{\mathbb{e}\mathbb{e}^r}\bar{w} = \partial^2_{\mathbb{e}^r\mathbb{e}}\bar{w} = \boldsymbol{0}$. The second terms on the right hand side of (7.78) characterize the softening of the fully coupled electro-mechanical tangent moduli due to the evolution of the internal variables. We note that due to the variational structure the moduli are symmetric.

7.3.1. Uniaxial Test with Varying Loading Frequencies

In this example, the characteristic hysteresis curves for a ferroelectric crystal is reproduced. The specimen is an homogenous quadratic piece of material with length L $=$ $10\,\text{mm}$. At the left edge the electric potential is set to zero while the other edge is exposed to a periodical electric potential $\phi^e(t)$ with the maximum value of $\phi^e_{max} = 30\,\text{kV}$. From the mechanical point of view the specimen is free to move in the horizontal direction while is constrained in the vertical movements, cf. Figure 7.8. The material parameters used are reported in Table 7.3. When the switching is initiated, i.e. the electric field ap-
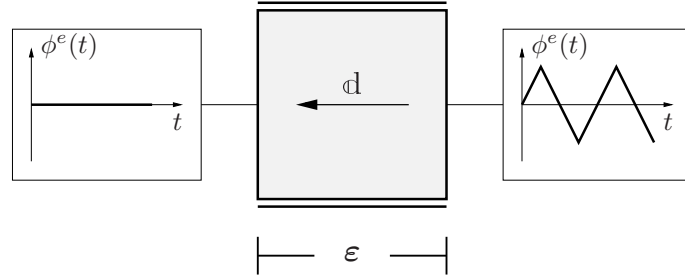
Figure 7.8: Mechanical and electrical boundary conditions for the uniaxial test. To a piece of ferroelectric material an electric potential is applied trough two electrodes along the left and right edges. The electrode on the left hand side is grounded while to the electrode on the right hand side a periodic electric potential is applied. The specimen is free to expand in the horizontal direction, but the vertical displacements are not allowed (double black lines). Under these boundary conditions an hysteretic behavior of the electric displacement d and of the total strain ε is observed.

proaches e_c, $\mathbb{p}^r$, and ε^r evolve. The hysteresis loops are given in Figure 7.9 and in order to show the time-dependent behavior of the proposed formulation, we consider varying loading frequencies, (cf. Figure 7.9). The main features of the experimental results in ZHOU, KAMLAH AND MUNZ [2001], i.e. order of remanent polarization, order of lower picks and shape of the high frequency curve, are reproduced.

7.3.2. Multiaxial Test

We now consider a numerical example reproducing the polarization rotation as occurs in the experiments of HUBER AND FLECK [64]. In these experiments a plate of PZT was first poled and the electrodes etched away. Then, specimens were cut from the poled plate and new electrodes applied to them so that an electric field could be imposed at an angle relative to the pre-existing polarization. As the electric field is increased, the remanent polarization rotates so that the angle between the polarization direction and the electric field reduces. In cases where the angle is initially obtuse, depolarization may first occur followed by repolarization parallel to the electric field. The experiments are carried out considering the same specimen as in the previous section subject to an axial

Table 7.3: Material Parameters Used for the Model Problem

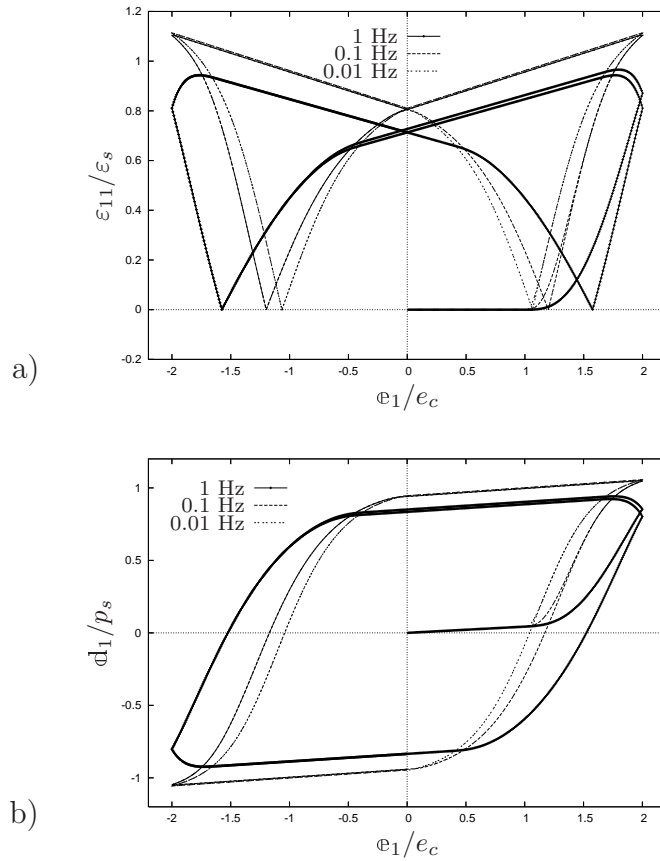| No.	Parameter	Unit	Name	Value
1	λ	N/mm^2	Lamé parameter	$76.6 \cdot 10^3$
2	μ	N/mm^2	Lamé parameter	$44.7 \cdot 10^3$
3	α'_0	N/(kV·mm)	axial piezoelectric expansion	-0.2
4	$\alpha'_\perp$	N/(kV·mm)	lateral piezoelectric expansion	-4.4
5	$\alpha'_=$	N/(kV·mm)	piezoelectric shearing	23.20
6	ϵ	mC /(kV·m)	electric permittivity	$11.2 \cdot 10^{-3}$
7	e_c	kV/mm	coercive electric field	1.0
8	p_s	C/m^2	saturation polarization	$26. \cdot 10^{-2}$
9	ε_s	−	saturation strain	10^{-3}
10	h_0	(kV·m)/C	hysteresis slope parameter	$3.8 \cdot 10^3$
11	η	mm^2/(C·s)	viscosity of polarization	10^{-2}
12	m	−	viscosity shape exponent	2

Figure 7.9: a) Numerical reproduction of the dielectric hystereses and b) butterfly curves in commercial soft PZT piezoceramic PIC151 for the loading rates of 0.01 Hz, 0.1 Hz, and 1 Hz according to ZHOU, KAMLAH AND MUNZ [156].

electric field. The material is assumed to be poled in different orientations relative to the applied electric field.

The results of the simulation are reported in Figure 7.10 which shows the change of the component of the electric displacement parallel to the direction of the applied electric field as a function of the same. Clearly, the curve for an initial angle of $180°$ is a half hysteresis loop whereas the response when the angle is initially zero is nearly linear. The latter case arises because the material is approaching lock up and the electric field is simply driving it further into this state. For angles in between, the behavior involves a gradual transition from the half hysteresis loop for an initial angle of $180°$ to linear behavior when the angle is zero. This is exactly what happens in the experiments of HUBER AND FLECK [64].

7.3.3. Square Plate with a Centered Hole

In this example a squared plate with a centered hole is used as a specimen. It has edge dimensions of $20 \times 20\,\text{mm}$ and the hole at the center has a radius of $3\,\text{mm}$ and is discretized with 800 four noded elements. The material parameters used are reported in Table 7.3. At the left and the right edge the displacements are fixed in horizontal and vertical directions. A time varying electric potential $\phi^e(t)$ and $-\phi^e(t)$ with the maximum value of $\phi^e_{max} = 20\,\text{kV}$ is applied at the left and the right edges, respectively (cf. Figure 7.11).
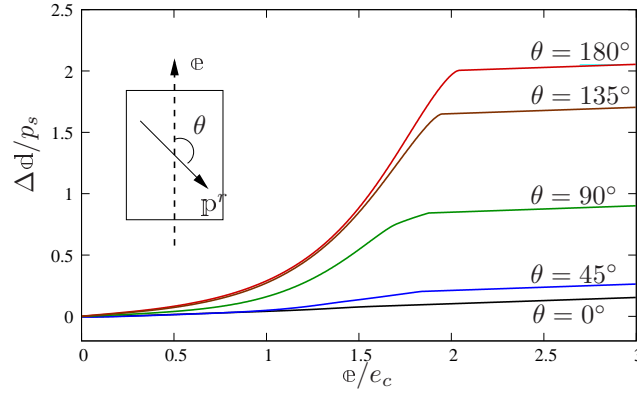
Figure 7.10: Polarization rotation curves. The component of the electric displacement parallel to the applied electric field is plotted against the electric field.

Figure 7.12 and 7.13 show the distribution of the electric potential ϕ^e and the polarization vector distribution $\mathbb{p}^r$ in the specimen in correspondence of several time steps. We can observe that to a non-uniform distribution of the potential follows a non-uniform distribution of the polarization. The polarization tries to circumvent the hole while near the edges is parallel to the vertical-edge-direction. In contrast with SCHRÖDER & RO-MANOWSKI [135] where the polarization have a fixed direction $\boldsymbol{a}$, i.e. $\mathbb{p}^r = p\boldsymbol{a}$, a non constant polarization direction is observed.

7.3.4. Multilayer Actuator

We now want to study an example of practical applications. We consider the structure shown in Figure 7.14 having the principle design of a multilayer actuator. The geometry has been chosen in adaption to the literature. Due to symmetry conditions only the shaded area is modeled and the upper electrode must not deform or rotate, but is only allowed to translate parallel to its starting position. In order to simulate a poling process the electric potential $\phi^e(t)$ is prescribed as triangular loading in the following manner: first is increased from 0 to 170 V until $t_1 = 100$ s and then reduced to zero until $t_2 = 200$ s. Thus, an electric field of approximately 3 kV/mm is reached in the region between the two electrodes, guaranteeing full poling.

In Figures 7.15a and 7.15b we reported the electric potential distribution at the instant $t_1 = 100$ s, when the highest voltage is applied, and $t_2 = 200$ s, unloading with zero applied potential, respectively. In the Figures 7.15c and 7.15d the correspondent distribution of
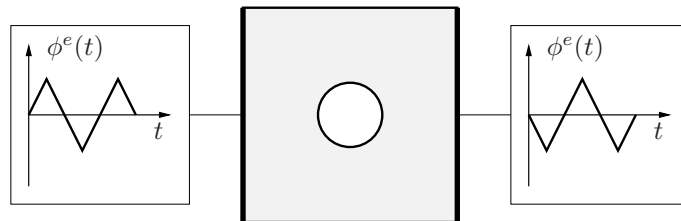

Figure 7.11: Boundary conditions for the test of the square plate with centered hole. The right and left edges of the plate are fully mechanically constraint,i.e. $\boldsymbol{u} = \boldsymbol{0}$ (bold black lines). The same edges are doted of two electrodes to wich a periodic electric potential is applied. These electrical potential are in counter phase.
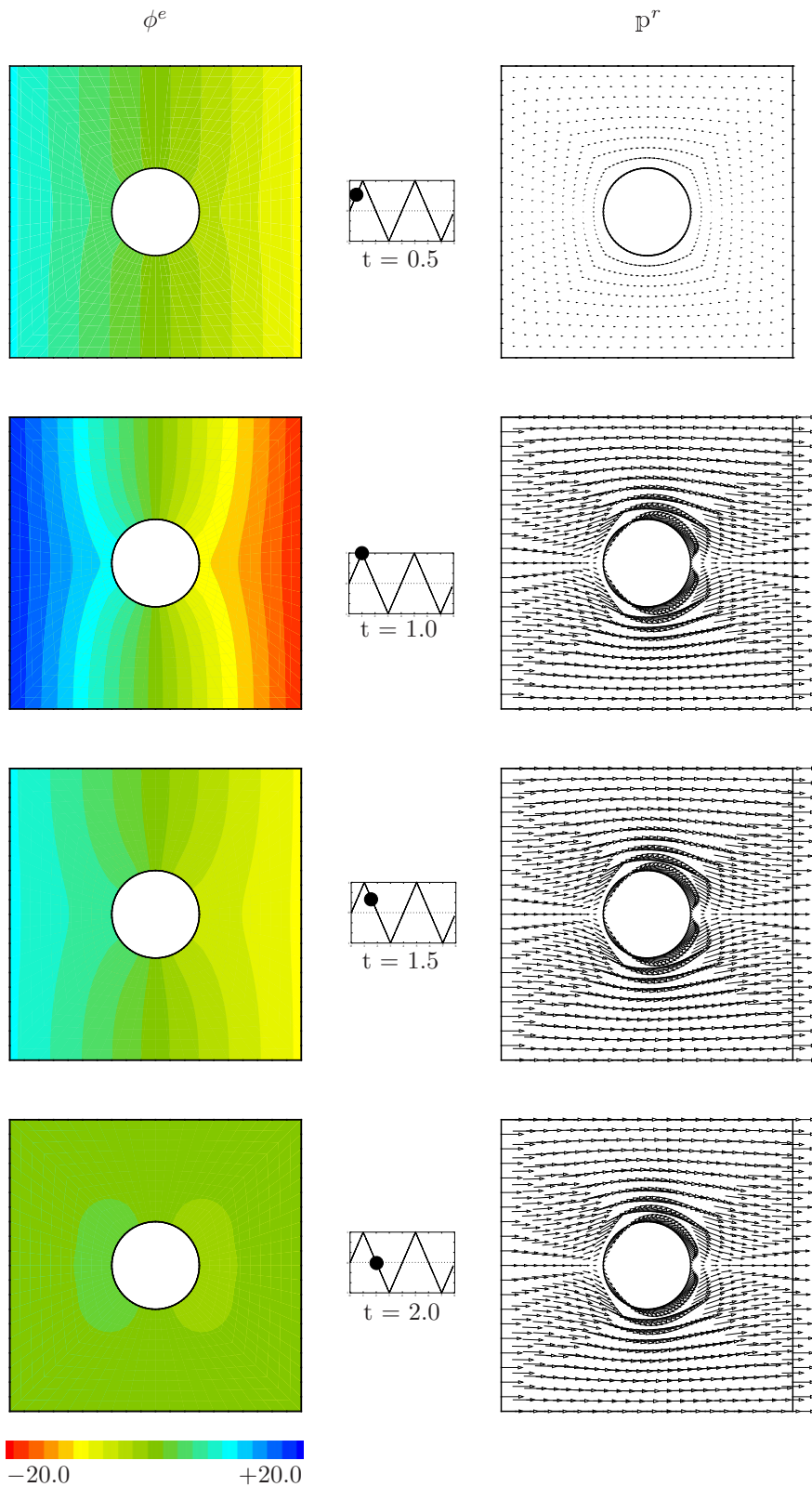
Figure 7.12: Distributions of the electric potential ϕ^e and remanent polarization $\mathbb{p}^r$ at different times.

the remanent polarization $\mathbb{p}^r$ in proximity of the electrode tip is reported. From Figures 7.15a and 7.15c we can conclude that at t_1 the region on the left of the electrode tip
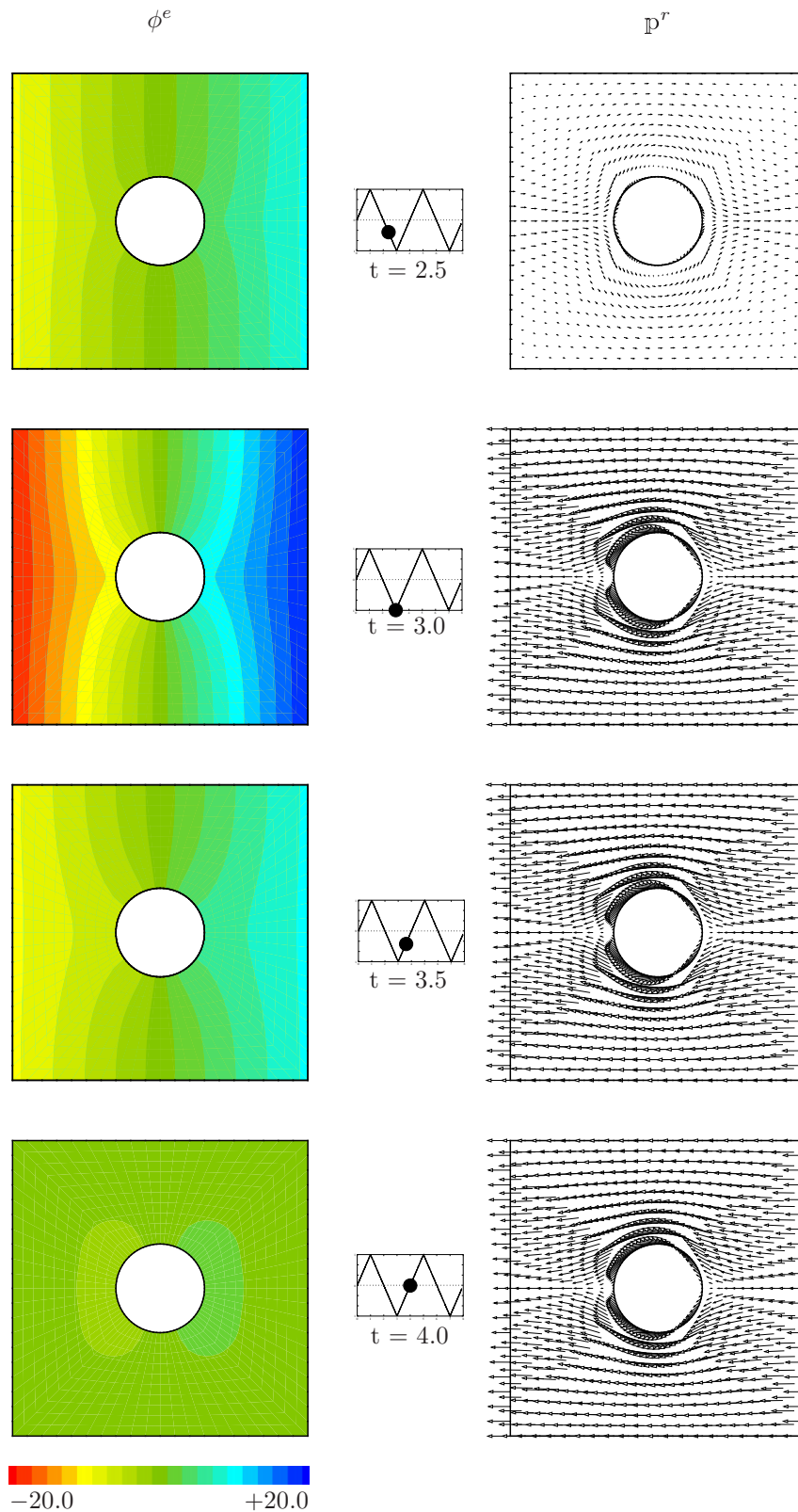
$$\phi^e \qquad\qquad\qquad \mathbb{p}^r$$

t = 2.5

t = 3.0

t = 3.5

t = 4.0

−20.0   +20.0

Figure 7.13: Distributions of the electric potential ϕ^e and remanent polarization $\mathbb{p}^r$ at different times.

is characterized by linear distribution of the electric potential between the electrodes while the region on the right of the electrode tip lies at a zero potential. The region

a)   b)
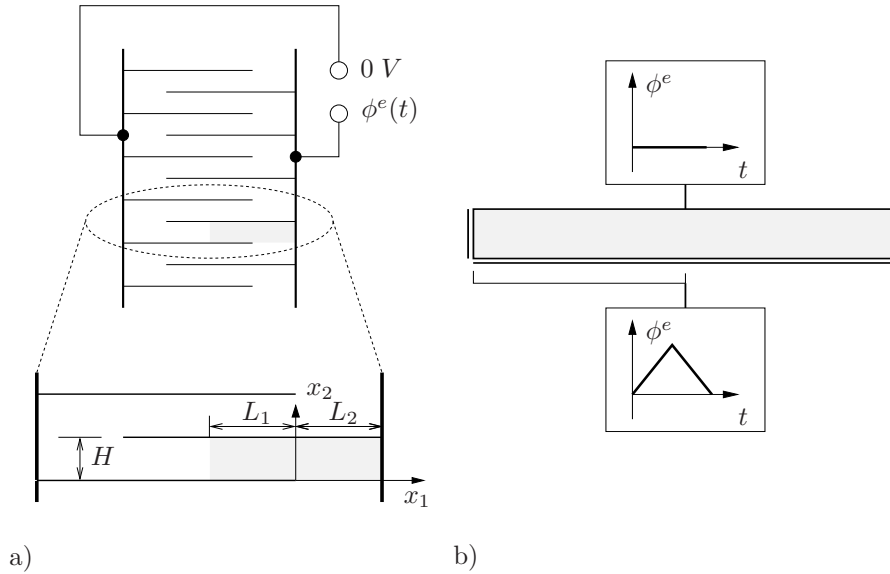
Figure 7.14: a) Principle design of a multilayer actuator: $L_1 = L_2 = 205\,\mu$m, $H = 57.5\,\mu$m. Due to symmetry properties, only the shaded area is modeled. b) Boundary conditions on the discretized shaded area. In order to simulate a poling process the electric potential $\phi^e(t)$ is prescribed as triangular loading on the lower electrode while the upper electrode is grounded. Mechanically, the modeled specimen is allowed to expand both horizontally and vertically (double bold black lines).

near the electrode tip can be considered as a transition zone. In correspondence the left region is fully poled and the right region is unpoled. Thus, the region of the electrode tip experiences a non-uniform polarization because of the transition between these two extremes. The potential at t_2 (cf. Figure 7.15b) clearly does not vanish as consequence of an inhomogeneous remanent polarization in the electrode tip region (cf. Figure 7.15d).
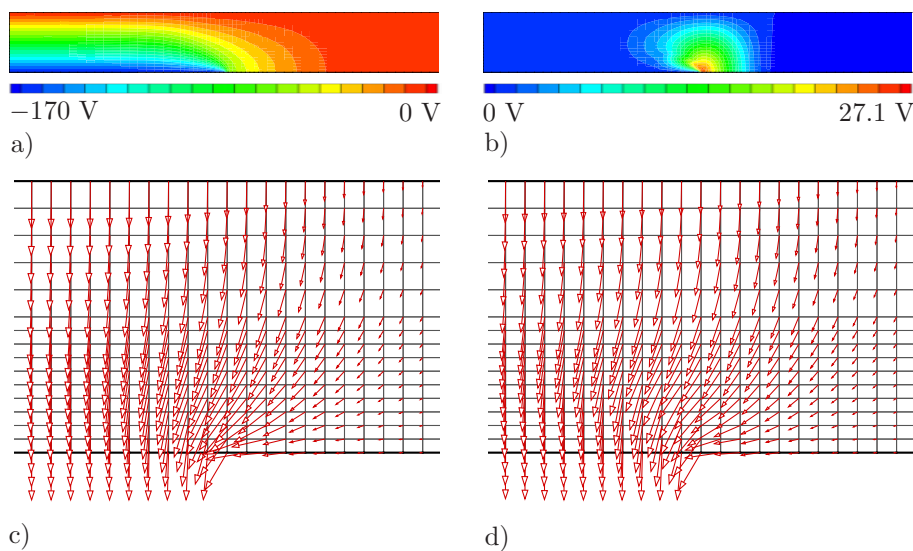
Figure 7.15: a) Electric potential ϕ^e at $t_1 = 100$ s, b) electric potential ϕ^e at $t_2 = 200$ s, c) remanent polarization $\mathbb{p}^r$ at $t_1 = 100$ s in the vicinity of the electrode tip, and d) remanent polarization $\mathbb{p}^r$ at $t_2 = 200$ s in the vicinity of the electrode tip.

8. Ferroelectricity at Large Strains

In this chapter we extend the concepts proposed in Chapter 7 in order to develop a model for the ferroelectric material response at large strains. The here constructed mixed energy-enthalpy function ψ' and the dissipation function ϕ can be used within the incremental variational formulation proposed in Chapter 6.

8.1. Piezoelectricity

In what follows, we construct a simple model for a piezoelectric material response at large strains which contains the essential electro-mechanical coupling phenomena. This serves as basis for the construction of a model describing the dissipative response of ferroelectric materials at large strains. In analogy to the small strains case we characterize the piezoelectric material response in terms of a mixed energy-enthalpy function $\psi'(\boldsymbol{F}, \mathbb{E}, \boldsymbol{\mathfrak{P}})$ depending on the deformation gradient $\boldsymbol{F}$, the Lagrangian electric field $\mathbb{E}$ and the unit director of electric polarization $\boldsymbol{\mathfrak{P}} := \mathbb{P}^r/|\mathbb{P}^r|$ in the reference configuration. Since the piezoelectric response is assumed to be fully reversible, the mixed energy-enthalpy function ψ' can be split into mechanic, electric, and coupling contributions

$$\psi'(\boldsymbol{F}, \mathbb{E}, \boldsymbol{\mathfrak{P}}) = \psi'_{mech}(\boldsymbol{F}) + \psi'_{elec}(\mathbb{E}) + \psi'_{coup}(\boldsymbol{F}, \mathbb{E}, \boldsymbol{\mathfrak{P}}). \tag{8.1}$$

In order to keep the model simple we attribute the transversely isotropic character of the piezoelectric response only to the coupling term ψ'_{coup} and assume the purely mechanical contributions, ψ'_{mech} and ψ'_{elec}, respectively, to be isotropic. Thus, only ψ'_{coup} will depend on the unit director of electric polarization $\boldsymbol{\mathfrak{P}}$.

Extending the assumptions which brought in Section 7 to the derivation of the mixed energy-enthalpy function in small strains we could specify the single terms appearing in (8.1) in the following way

$$\begin{aligned}
\psi'_{mech}(\boldsymbol{F}) &= \mu \operatorname{tr}[\boldsymbol{E}] - \mu \ln[J] + \frac{\lambda}{2} \left(\ln[J]\right)^2 \\
\psi'_{elec}(\mathbb{E}) &= -\frac{\epsilon}{2} \operatorname{tr}[\mathbb{E} \otimes \mathbb{E}] \\
\psi'_{coup}(\boldsymbol{F}, \mathbb{E}, \boldsymbol{\mathfrak{P}}) &= -\alpha'_0 \operatorname{tr}[\boldsymbol{E}(\boldsymbol{\mathfrak{P}} \otimes \boldsymbol{\mathfrak{P}})] \operatorname{tr}[\mathbb{E} \otimes \boldsymbol{\mathfrak{P}}] \\
&\quad -\alpha'_\perp \operatorname{tr}[\boldsymbol{E}] \operatorname{tr}[\mathbb{E} \otimes \boldsymbol{\mathfrak{P}}] - \alpha'_= \operatorname{tr}[\boldsymbol{E}(\mathbb{E} \otimes \boldsymbol{\mathfrak{P}})],
\end{aligned} \tag{8.2}$$

in terms of the Green-Lagrangian strain $\boldsymbol{E} := \frac{1}{2}\left(\boldsymbol{F}^T \boldsymbol{g} \boldsymbol{F} - \boldsymbol{G}\right)$ and the determinant of the deformation gradient $J := \det[\boldsymbol{F}]$. Notice that:
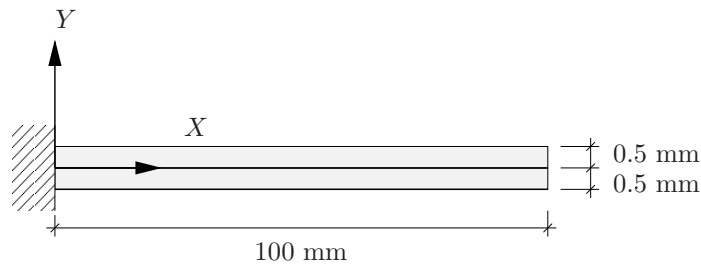

Figure 8.1: Geometrical properties of the bimorph transducer considered in the piezoelectric numerical examples. Two layers of piezoelectric polymer are glued together.

Table 8.1: Material Parameters for Piezoelectricity at Large Strains

No.	Parameter	Unit	Name	Value
1	λ	N/mm^2	Lamé parameter	$15.9 \cdot 10^3$
2	μ	N/mm^2	Lamé parameter	$10.71 \cdot 10^3$
3	α_0'	N/(kV·mm)	axial piezoelectric expansion	$4.6 \cdot 10^{-5}$
4	$\alpha_\perp'$	N/(kV·mm)	lateral piezoelectric expansion	$-8.09 \cdot 10^{-6}$
5	$\alpha_=' $	N/(kV·mm)	piezoelectric shearing	$-0.7 \cdot 10^{-2}$
6	ϵ	mC/(kV·m)	electric permittivity	$10.6 \cdot 10^{-3}$

- $(8.2)_1$ resembles a *Neo-Hookean-type* elastic response with the classical Lamé parameters λ and μ of isotropic elasticity.

- $(8.2)_2$ implies a linear-isotropic dielectric response based on the experimental observation that an electric field $\mathbb{E}$ induces an electric displacement $\mathbb{D}^e = \epsilon\mathbb{E}$ with ϵ dielectric permittivity.

- $(8.2)_3$ recovers a transversely isotropic coupled response characterized by the basic effects P3-P5 described already in Section 7. ψ_{coup}' is formulated in terms of the modified piezoelectric coupling parameters α_0', $\alpha_\perp'$ and $\alpha_='$.

With the mixed energy-enthalpy at hand we can compute the Piola-Kirchhoff stress and the electric displacement as indicated in equations $(5.85)_1$ and $(5.85)_2$, i.e. $\boldsymbol{gP} := \partial_{\boldsymbol{F}}\psi'(\boldsymbol{F}, \mathbb{E}, \boldsymbol{\mathfrak{P}})$ and $-\mathbb{D} := \partial_{\mathbb{E}}\psi'(\boldsymbol{F}, \mathbb{E}, \boldsymbol{\mathfrak{P}})$

$$
\begin{aligned}
\boldsymbol{gP} &= \mu\boldsymbol{gF}\boldsymbol{G}^{-1} - (\lambda\ln[J] - \mu)\boldsymbol{F}^{-T} - \alpha_0'\boldsymbol{gF}(\boldsymbol{\mathfrak{P}} \otimes \boldsymbol{\mathfrak{P}})\operatorname{tr}[\mathbb{E} \otimes \boldsymbol{\mathfrak{P}}] \\
&\quad -\alpha_\perp'\boldsymbol{gF}\boldsymbol{G}^{-1}\operatorname{tr}[\mathbb{E} \otimes \boldsymbol{\mathfrak{P}}] - \alpha_='\boldsymbol{gF}\operatorname{sym}[\boldsymbol{G}^{-1}\mathbb{E} \otimes \boldsymbol{\mathfrak{P}}]
\end{aligned}
\tag{8.3}
$$

$$
-\mathbb{D} = \epsilon\boldsymbol{G}^{-1}\mathbb{E} - \alpha_0'\operatorname{tr}[\boldsymbol{E}(\boldsymbol{\mathfrak{P}} \otimes \boldsymbol{\mathfrak{P}})]\boldsymbol{\mathfrak{P}} - \alpha_\perp'\operatorname{tr}[\boldsymbol{E}]\boldsymbol{\mathfrak{P}} - \alpha_='\boldsymbol{G}^{-1}\mathbb{E}\boldsymbol{\mathfrak{P}}\,.
$$

The second derivative of the mixed energy-enthalpy function ψ' delivers the tangent moduli

$$
\begin{aligned}
\mathbb{C}' &= \mu\boldsymbol{g}\bar{\otimes}\boldsymbol{G}^{-1} - (\mu - \lambda\ln[J])\mathbb{I}_{\boldsymbol{F}^{-T}} + \lambda\boldsymbol{F}^{-T} \otimes \boldsymbol{F}^{-T} \\
&\quad -\boldsymbol{g}\bar{\otimes}\left[\alpha_0'\boldsymbol{\mathfrak{P}} \otimes \boldsymbol{\mathfrak{P}} + \alpha_\perp'\boldsymbol{G}^{-1}\operatorname{tr}[\mathbb{E} \otimes \boldsymbol{\mathfrak{P}}] + \alpha_='\operatorname{sym}[\boldsymbol{G}^{-1}\mathbb{E} \otimes \boldsymbol{\mathfrak{P}}]\right] \\
\boldsymbol{h}' &= -\alpha_0'\boldsymbol{\mathfrak{P}} \otimes \boldsymbol{gF}(\boldsymbol{\mathfrak{P}} \otimes \boldsymbol{\mathfrak{P}}) - \alpha_\perp'\boldsymbol{\mathfrak{P}} \otimes \boldsymbol{gF}\boldsymbol{G}^{-1} - \alpha_='\bar{\boldsymbol{h}} \\
\boldsymbol{\beta}' &= -\epsilon\boldsymbol{G}^{-1}\,,
\end{aligned}
\tag{8.4}
$$
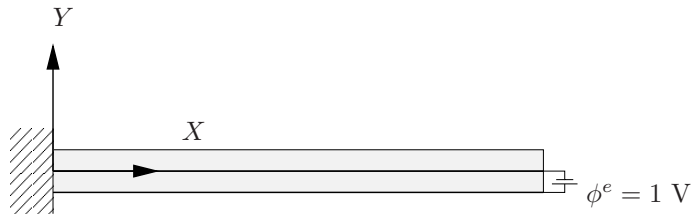
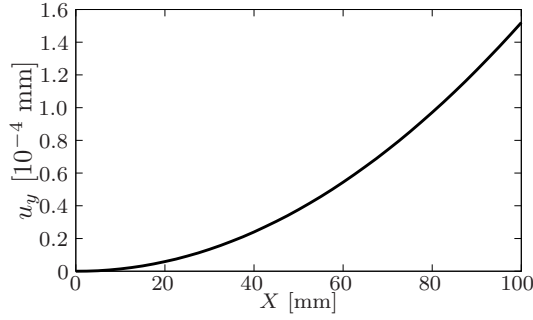**Figure 8.2:** Unit voltage applied to one layer of the bimorph transducer.

Figure 8.3: Deflection of the bimorph transducer due to an applied voltage $\phi^e = 1V$.

with $\mathbb{C}' := \partial^2_{\boldsymbol{FF}}\psi'(\boldsymbol{F}, \mathbb{E}, \boldsymbol{\mathfrak{P}})$, $\boldsymbol{h}' := \partial^2_{\boldsymbol{F}\mathbb{E}}\psi'(\boldsymbol{F}, \mathbb{E}, \boldsymbol{\mathfrak{P}})$, and $\boldsymbol{\beta}' := \partial^2_{\mathbb{E}\mathbb{E}}\psi'(\boldsymbol{F}, \mathbb{E}, \boldsymbol{\mathfrak{P}})$. In (8.4) we made use of the following operators

$$
\begin{aligned}
[(\bullet)\bar{\otimes}(\circ)]_a{}^A{}_b{}^B &= (\bullet)_{ab}(\circ)^{AB} \\
(\mathbb{I}_{\boldsymbol{F}^{-T}})_a{}^A{}_b{}^B &= (F^{-1})^A{}_b (F^{-1})^B{}_a \\
\bar{h}^I{}_m{}^M &= \tfrac{1}{2}\left((G^{-1})^{IM}(\boldsymbol{gF\mathfrak{P}})_m + (G^{-1})^{IA}F^a{}_A g_{am}\mathfrak{P}^M\right) .
\end{aligned}
\tag{8.5}
$$

The stresses $\boldsymbol{P}$ and the electric displacement $\mathbb{D}$ as well as the tangent moduli $\mathbb{C}'$, $\boldsymbol{h}'$, and $\boldsymbol{\beta}'$ can be directly used within the context of the variational formulation described in Section 6 using the identifications

$$
\boldsymbol{\mathfrak{S}}' = \begin{bmatrix} \boldsymbol{gP} \\ -\mathbb{D} \end{bmatrix} \qquad , \qquad \boldsymbol{\mathfrak{C}}' = \begin{bmatrix} \mathbb{C}' & \boldsymbol{h}' \\ \boldsymbol{h}'^T & \boldsymbol{\beta}' \end{bmatrix}
\tag{8.6}
$$

to solve electro-mechanical boundary-value-problems as done in the next subsections.

To validate the developed material formulation a number of numerical examples have been solved, see Mukherjee & Chaudhuri [114, 115]. They focus on the large deformation effects and on sensing phenomena of piezoelectric bimorphs. The specimen used therefore is a cantilever beam with length of 100 mm and height of 1 mm made up of two equal thin layers of piezoelectric polymer glued together. The left edge is fixed, the rest of the specimens boundary is unconstrained, see Figure 8.1.

The displacements $\boldsymbol{u}$ are measured in units of mm, the electric potential ϕ^e is measured in units of kV, and the electric field $\mathbb{E}$ in kV/mm, respectively. The stresses $\boldsymbol{P}$ are measured in units of N/mm^2 and the dielectric displacement $\mathbb{D}$ is measured in units of C/m^2. The chosen material parameters are reported in Table 8.1. The preferred direction is set to
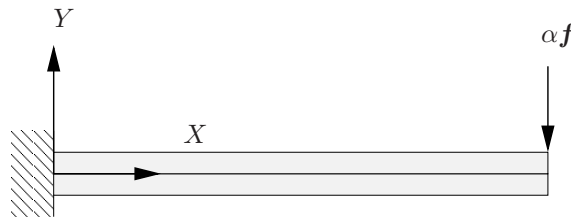

Figure 8.4: Varying transverse force applied to the bimorph transducer. For $\alpha = 1$ the maximum load of 0.5 N is reached.
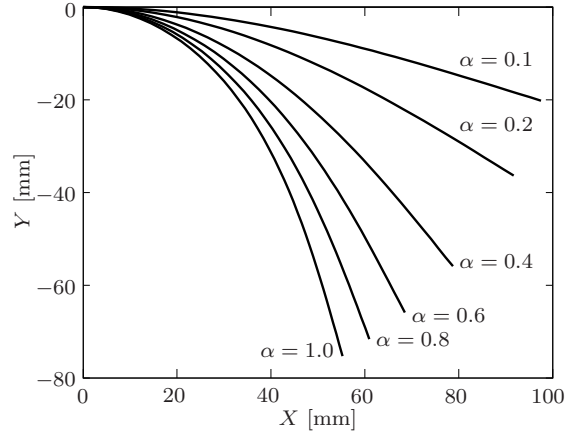
Figure 8.5: Deflected shape of the bimorph transducer under a varying transversal force αf in correspondence of various load steps α.

$\mathfrak{P} = [0, 1, 0]^T$. A shift of the measuring units is investigated to reduce the numerical difference of the material parameters from 10^{15} to 10^6, see Romanowski [130].

8.1.1. Electric Loading

In this example the cantilever bimorph is subjected to an electric potential difference $\Delta\phi^e = 1$ V, see Figure 8.2. In this case the inverse piezoelectric effect is simulated. The application of the electric field to one of the two layers will cause elongation of the same and a contraction in transverse direction. Since the other layer is not excited, its inner fiber will suffer an elongation and this will result in an overall bending motion of the actuator, see Figure 8.3. The deformation is very small by reason of the small input voltage. In the range of very small deformation a difference between linear and nonlinear analysis cannot be observed.

8.1.2. Mechanical Tip Load in Transverse Direction

In this example the direct piezoelectric effect is simulated. To examine the large deformation effect on sensed voltage of a cantilever bimorph, a varying transverse force up to 0.5 N is applied at the free end, see Figure 8.4. The potential of the inner electrode is set
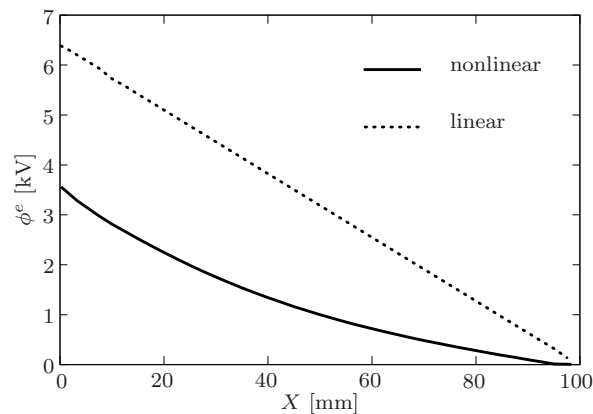

Figure 8.6: Distribution of sensed voltages along the bimorph transducer in correspondence of the maximum transverse force $\alpha|f| = 0.5N$. Comparison between the linear and nonlinear computations.
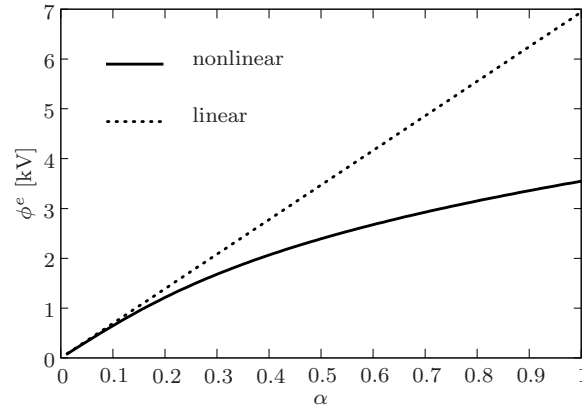
Figure 8.7: Sensed voltage at the root of bimorph transducer subject to a transversal load plotted as function of the load step $\alpha \in [0, 1]$.

to 0 V while the other to electrodes are left free. The boundary condition for the electric potential is necessary to guarantee the uniqueness of the solution because the simulation only solves for the gradient of the electric potential. Figure 8.5 shows the deflected shape at various load steps. For the maximum load, the small-strain analysis predicts a deflection of 200 mm. However, due to the stress stiffening effect in the large-strain analysis it reduces to 75 mm. From this observation it is obvious that a large-strain computation is necessary.

The distribution of the sensed voltage along the cantilever at the final load step is shown in Figure 8.6. A spatial variation of voltage can be obtained using patch sensors. In this case it is noticed that the concentration of voltage near the fixed end is very high compared to that at the free end. In comparison, the small-strain analysis predicts a linear variation of voltage. It also over-predicts the voltage to a large extent.

Figure 8.7 shows the sensor voltage at the root of the cantilever beam due to an increasing tip transverse load up to 0.5 N. The voltage sensed in the linear and the nonlinear cases have been compared. As the load grows the two graphs diverge rapidly. As a result the voltage computed by the linear analysis is significantly larger than the sensed voltage
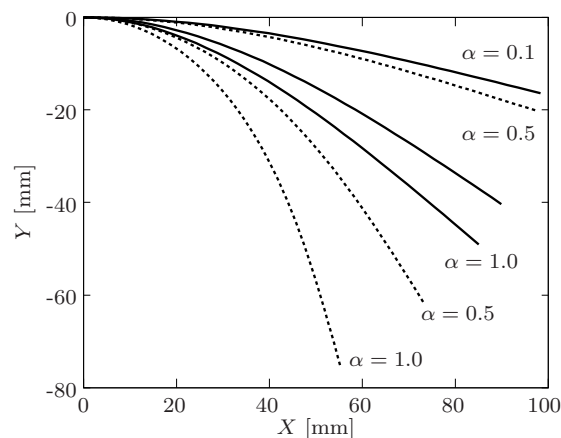

Figure 8.8: Deflected shape of the bimorph transducer under a varying transversal force $\alpha\boldsymbol{f}$ in correspondence of various load steps α. Comparison between the results obtained with (continuos lines) and without (dashed lines) a tip axial tensional load.
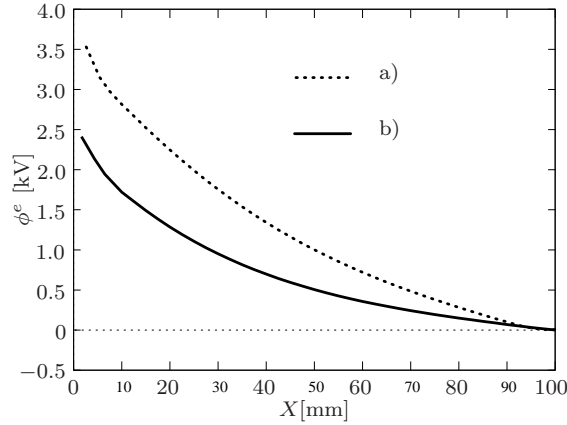
Figure 8.9: Distribution of sensed voltages along the bimorph transducer in correspondence of the final load for a) transversal load applied and b) transversal and axial load revealing the effects of stress-stiffening.

predicted through non-linear analysis.

8.1.3. Stress Stiffening due to Axial Tensional Load

In the previous example we investigated problems with purely transverse load. To study the effect of stress stiffening we add an increasing tensile tip load in axial direction of $\alpha\boldsymbol{f}$ with $|\boldsymbol{f}| = 0.5$ N. In Figure 8.8 the deflected shape for the current simulation is presented with the solid lines and the dashed lines are used for the results of the previous example. Here stress-stiffening effect occurs due to combined action of the axial and transversal loads. The deflection reduces from 75 mm to 50 mm.

The voltage distribution in the present case is also markedly different from the previous case. The axial force applied on the structure considerably reduces the voltages developed in the sensor as compared to the previous case. Figure 8.9 shows the distribution of the sensed voltages for the pure transverse and the combined load. Figure 8.10 points out the stress-stiffening for the sensed voltage over the load ratio α.
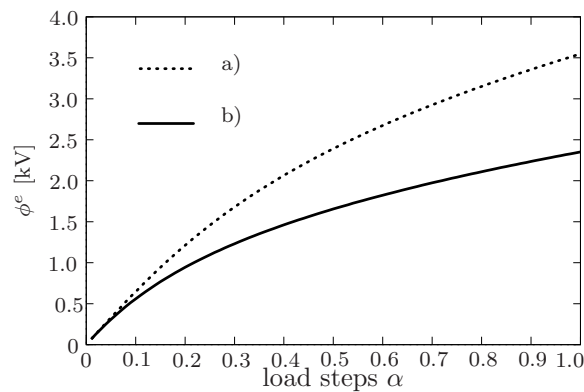

Figure 8.10: Sensed voltage at the root of bimorph transducer for increasing load of $\alpha\boldsymbol{f}$ with $|\boldsymbol{f}| = 0.5$ N. a) Single force $\alpha\boldsymbol{f}$ applied in transverse direction, b) $\alpha\boldsymbol{f}$ applied in transverse and axial direction.
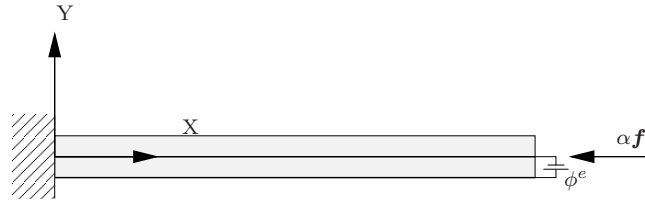
Figure 8.11: Bimorph transducer subject to an axial pressure $\alpha\boldsymbol{f}$ and to an actuation potential ϕ^e.

8.1.4. Axial Buckling Load and Actuation Voltage

In the previous examples, we presented the results for sensing in a piezoelectric bimorph. In this example, the actuation is presented. The cantilever with an axial compressive force at the tip is supplied with a voltage from an external source see Figure 8.11.

The applied voltage is varied from $0\,\mathrm{V}$ to $1.2\,\mathrm{kV}$. It is seen in Figure 8.12 that in presence of actuation voltage axial compressive force results in large transverse deformations. The transverse deformation for increasing axial load converges asymptotically to the bifurcation load of the straight column. In presence of an actuation voltage the structure does not display bifurcation and it generates a finite transverse deflection.

8.2. Modeling of Dissipative Ferroelectric Materials

In this section we will construct a model for the ferroelectric material response at large strain. This model can be seen as an enhancement of the piezoelectric material response to a dissipative ferroelectric formulation. The primary focus will be on the modeling of hysteresis phenomena in a mixed variant formulation. For this purpose, the electric displacement $\mathbb{D}$ is assumed to be additively decomposed into a reversible (elastic) $\mathbb{D}^e$ and a remanent component $\mathbb{P}^r$

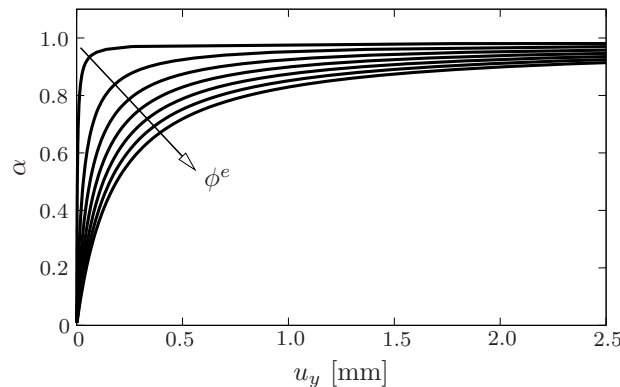$$\mathbb{D} = \mathbb{D}^e + \mathbb{P}^r \, . \tag{8.7}$$

Figure 8.12: Transverse deflection of the bimorph transducer subject to the actuation voltages of 20 V, 200 V, 400 V, 600 V, 800 V, 1000 V and 1200 V together with a tip axial force $\alpha\boldsymbol{f}$ as function of the load step α. The actuation voltage gives rice to large deformations preventing the bifurcation.
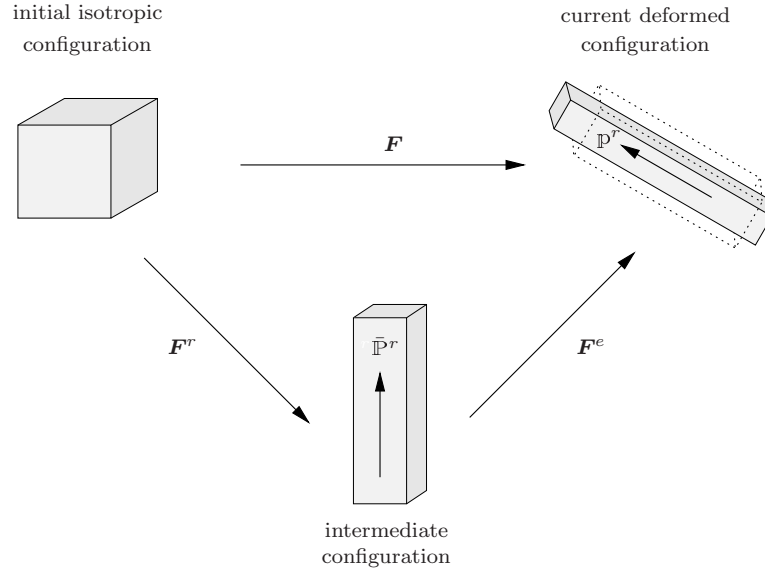
Figure 8.13: Representation of the multiplicative decomposition of the deformation gradient $\boldsymbol{F}$ into a remanent and reversible part denoted with $\boldsymbol{F}^r$ and $\boldsymbol{F}^e$, respectively. If the applied electric field $\mathbb{E}$ overcomes the coercive electric field E_c in the intermediate state we observe a remanent polarization $\bar{\mathbb{P}}^r$ which remains after unloading.

The remanent polarization $\mathbb{P}^r$ is identified as the internal variable. Its associated unit director

$$\boldsymbol{\mathfrak{P}} := \frac{\mathbb{P}^r}{|\mathbb{P}^r|} \tag{8.8}$$

defines the preferred direction of the transversely isotropic piezoelectric material response. The deformation gradient $\boldsymbol{F}$ is assumed to be multiplicatively decomposed into a reversible $\boldsymbol{F}^e$ and a remanent deformation gradient $\boldsymbol{F}^r$

$$\boldsymbol{F} = \boldsymbol{F}^e \boldsymbol{F}^r . \tag{8.9}$$

We also assume that the remanent deformation gradient $\boldsymbol{F}^r$ is only due to the remanent polarization $\mathbb{P}^r$ and we neglect stress depolarization phenomena. Under these assumptions we can give a representation of the ferroelectric material behavior. If an electric field $\mathbb{E}$ with an amount superior to the coercive electric field E_c and a deformation $\boldsymbol{F}$ are applied, we could distinguish two superimposed states of the material response. In a first state a remanent polarization $\mathbb{P}^r$ is generated, accompanied by a remanent deformation gradient $\boldsymbol{F}^r = \hat{\boldsymbol{F}}^r(\mathbb{P}^r)$. In a second step a coupled reversible response, due to the developed $\mathbb{P}^r$, is possible. In this second state the remanent polarization $\mathbb{P}^r$ can only be rigidly transformed but its amount will remain unchanged. This rigid transformation is accompanied by the reversible deformation gradient $\boldsymbol{F}^e$ and the reversible electric displacement $\mathbb{D}^e$.

In what follows, objects of the introduced intermediate configuration will be denoted by a *bar*, e.g. $\bar{\mathbb{P}}^r$. Figure 8.13 shows the initial isotropic configuration $\mathcal{B}$ which is transformed to the intermediate configuration $\bar{\mathcal{B}}$ by the mapping property of $\boldsymbol{F}^r$. In this intermediate configuration the material now possesses transversal isotropic properties characterized in terms of the remanent polarization $\bar{\mathbb{P}}^r$ or its unit director $\bar{\boldsymbol{\mathfrak{P}}}$. A further transformation with the reversible deformation gradient $\boldsymbol{F}^e$ yields the current deformed configuration $\mathcal{S}$. This last transformation may be considered as a piezoelectric transformation since the remanent polarization is not changed in amount anymore.

In order to determine $\boldsymbol{F}^r$ we assume that the remanent deformation is isochoric. Further we decompose the remanent deformation gradient $\boldsymbol{F}^r$ into a left stretch tensor $\boldsymbol{V}^r$ and a rotation tensor $\boldsymbol{R}^r$ by a left polar decomposition

$$\boldsymbol{F}^r = \boldsymbol{V}^r \boldsymbol{R}^r \,. \tag{8.10}$$

The assumption of isochoric remanent deformation implies that $\det[\boldsymbol{F}^r] = 1$ and thus $\det[\boldsymbol{V}^r] = 1$. The construction of the remanent stretch tensor $\boldsymbol{V}^r$ can be physically motivated. Being a symmetric tensor, $\boldsymbol{V}^r$ may be represented by its eigenvalues $\{\omega_i\}_{i=1,2,3}$ and the corresponding eigenvectors forming an orthonormal basis $\{\bar{\boldsymbol{N}}_i\}_{i=1,2,3}$. The spectral decomposition of $\boldsymbol{V}^r$ reads

$$\boldsymbol{V}^r = \sum_{i=1}^{3} \omega_i \bar{\boldsymbol{N}}_i \otimes \bar{\boldsymbol{N}}^i \,. \tag{8.11}$$

Notice that the $\bar{\boldsymbol{N}}_i$ are vectors and $\bar{\boldsymbol{N}}^i = \bar{\boldsymbol{G}} \bar{\boldsymbol{N}}_i$ the corresponding covectors. For a pair of equal roots, i.e. $\omega_1 \neq \omega_2 = \omega_3$ with one unique eigenvector $\bar{\boldsymbol{N}}_1$ associated with ω_1 we deduce from (8.11) the reduced representation

$$\boldsymbol{V}^r = \omega_1 \bar{\boldsymbol{N}}_1 \otimes \bar{\boldsymbol{N}}^1 + \omega_2 (\boldsymbol{1} - \bar{\boldsymbol{N}}_1 \otimes \bar{\boldsymbol{N}}^1) \,. \tag{8.12}$$

In (8.12) the eigenvector $\bar{\boldsymbol{N}}_1$ is perpendicular to a plane spanned by the mutually orthogonal eigenvectors $\bar{\boldsymbol{N}}_2$ and $\bar{\boldsymbol{N}}_3$ (GURTIN [62], HOLZAPFEL [63]).

The eigenvalue ω_2 can be determined as function of ω_1 using the isochoric constraint $\det[\boldsymbol{V}^r] = 1$. In the spectral representation the determinant is computed as $\det[\boldsymbol{V}^r] = \omega_1 \cdot \omega_2^2 = 1$ yielding $\omega_2 = 1/\sqrt{\omega_1}$. With this result at hand, $\boldsymbol{V}^r$ can be expressed in terms of the only eigenvalue ω_1 which will be denoted by ω in what follows. Further, we need to identify the unique eigenvector $\bar{\boldsymbol{N}}_1$ of $\boldsymbol{V}^r$. Therefore we have a closer look at the material response in the intermediate configuration $\bar{\mathcal{B}}$. The material response is characterized by the remanent polarization vector $\bar{\mathbb{P}}^r$ which gives rise to a transversely isotropic material behavior with preferred direction coinciding with the remanent polarization director $\bar{\boldsymbol{\mathfrak{P}}} = \bar{\mathbb{P}}^r / |\bar{\mathbb{P}}^r|$. This unit vector can be identified as the eigenvector $\bar{\boldsymbol{N}}_1$. Indeed the material experiences an expansion in the $\bar{\boldsymbol{\mathfrak{P}}}$-direction and an isotropic contraction in the directions orthogonal to $\bar{\boldsymbol{\mathfrak{P}}}$. Using these considerations, we can express $\boldsymbol{V}^r$ in terms of $\bar{\boldsymbol{\mathfrak{P}}}$ as follows

$$\boldsymbol{V}^r = \omega \bar{\boldsymbol{\mathfrak{P}}} \otimes \bar{\boldsymbol{G}} \bar{\boldsymbol{\mathfrak{P}}} + \frac{1}{\sqrt{\omega}} (\boldsymbol{1} - \bar{\boldsymbol{\mathfrak{P}}} \otimes \bar{\boldsymbol{G}} \bar{\boldsymbol{\mathfrak{P}}}) \,. \tag{8.13}$$

The eigenvalue ω is expressed in terms of a material parameter $\bar{\lambda}_s^r$ characterizing the saturation of the remanent deformation state corresponding to a saturation of the remanent polarization

$$\omega = 1 + \frac{|\bar{\mathbb{P}}^r|}{\bar{P}_s} \bar{\lambda}_s^r \,. \tag{8.14}$$

The factor $|\bar{\mathbb{P}}^r|/\bar{P}_s$ grows linearly from 0 to 1 with the remanent polarization expressing zero or maximum polarization state in terms of the saturation polarization $\bar{P}_s$.

To determine the remanent rotation $\boldsymbol{R}^r$ we observe that it is nothing but the rotation from $\boldsymbol{\mathfrak{P}}_0$ to $\bar{\boldsymbol{\mathfrak{P}}}$, i.e.

$$\bar{\boldsymbol{\mathfrak{P}}} = \boldsymbol{R}^r \boldsymbol{\mathfrak{P}}_0 \tag{8.15}$$
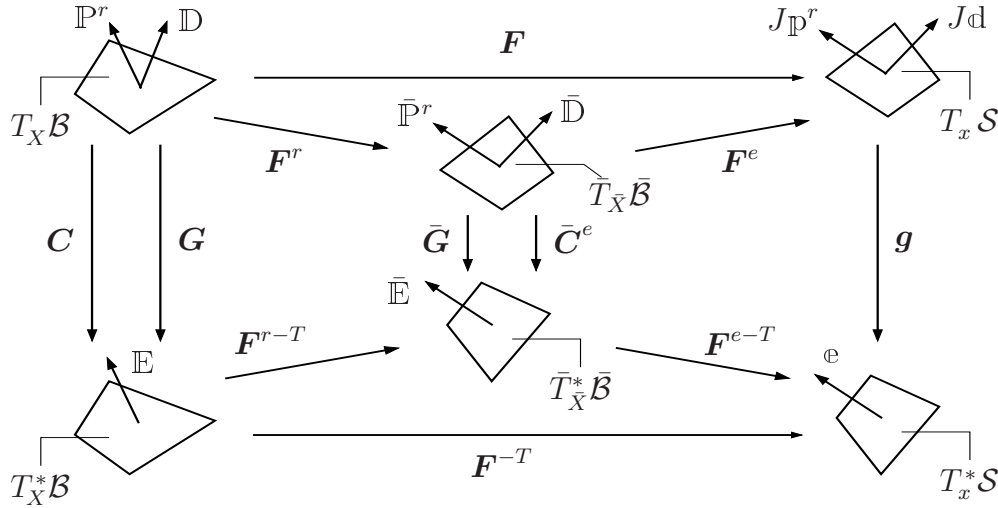
Figure 8.14: Fundamental geometric mappings in the Lagrangian, Eulerian, and intermediate configuration. Here $T_{\boldsymbol{X}}\mathcal{B}$, $\bar{T}_{\bar{\boldsymbol{X}}}\bar{\mathcal{B}}$ and $T_{\boldsymbol{x}}\mathcal{S}$ are the material, intermediate and spatial tangent spaces, while $T_{\boldsymbol{X}}^*\mathcal{B}$, $\bar{T}_{\bar{\boldsymbol{X}}}^*\bar{\mathcal{B}}$ and $T_{\boldsymbol{x}}^*\mathcal{S}$ are the corresponding cotangent spaces.

with $\boldsymbol{\mathfrak{P}}_0$ preferred direction in the initial configuration. Because of the isotropy of the initial state, $\mathbb{P}_0^r$ is a null vector and this induces $\boldsymbol{\mathfrak{P}}_0 = \boldsymbol{0}$ and consequently $\boldsymbol{R}^r = \boldsymbol{1}$. From the above argumentation it becomes evident that we need to introduce an intermediate configuration between the Lagrangian and Eulerian ones and eventually characterize the state of the materials in terms of variables belonging to this configuration. Figure 8.14 shows the geometric relations of the objects of Lagrangian, Eulerian, and the introduced intermediate configuration. In what follows the constitutive equations will be represented with respect to the intermediate setting characterized by the metric $\bar{\boldsymbol{G}}$. Its pull back to the Lagrangian configuration is denoted by $\boldsymbol{C}^r = \boldsymbol{F}^{rT}\bar{\boldsymbol{G}}\boldsymbol{F}^r$ called the remanent right Cauchy-Green tensor. The pull back of the Eulerian metric $\boldsymbol{g}$ to the intermediate configuration results in the reversible Cauchy-Green tensor $\bar{\boldsymbol{C}}^e = \boldsymbol{F}^{eT}\boldsymbol{g}\boldsymbol{F}^e$ yielding the reversible Green-Lagrange strain $\bar{\boldsymbol{E}}^e = \frac{1}{2}(\bar{\boldsymbol{C}}^e - \bar{\boldsymbol{G}})$, which is a fundamental tensor in the following modeling of the ferroelectric material response.

8.2.1. Continuous Ferroelectric Material Response

As discussed above, the material model can be expressed in terms of variables in the intermediate configuration

$$\text{State} := \{\bar{\boldsymbol{E}}^e, \bar{\mathbb{E}}, \bar{\mathbb{P}}^r\} \tag{8.16}$$

with $\bar{\mathbb{P}}^r$ taking the role of an internal variable. The macroscopic phenomenological modeling of the overall response of ferroelectric materials can be characterized by three constitutive functions: the mixed energy-enthalpy function, the dissipation function, and the hardening function. The mixed energy-enthalpy-function $\psi'_{ferro}(\bar{\boldsymbol{E}}^e, \bar{\mathbb{E}}, \bar{\mathbb{P}}^r)$ governs the local storage mechanisms in ferroelectricity, whereas the dissipation function $\phi^*(\bar{\mathbb{E}}^r)$ governs the evolution of the polarization $\bar{\mathbb{P}}^r$. The hardening function $\psi'_{pol}(|\bar{\mathbb{P}}^r|)$ characterizes on the other hand the kinematic hardening of the polarization.

Dielectric Hysteresis – Construction of the Hardening Function. We now construct a hardening function $\psi'_{pol}(|\bar{\mathbb{P}}^r|)$ based on phenomenological assumptions focusing first on an idealized modeling of the dissipative process approaching the description of a regularized material response. We start our observation with the maximal ideal-
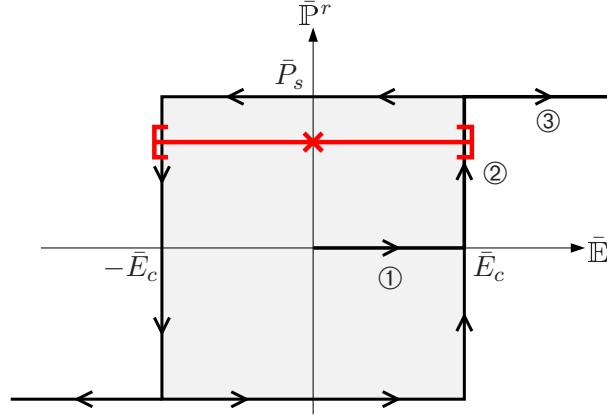
Figure 8.15: Ideal dielectric hysteresis. Remanent polarization induced by the polarization. Idealized process parts of poling: ① fully reversible virgin loading for $\bar{\mathbb{E}} < \bar{E}_c$, ② full idealized switching at $\bar{\mathbb{E}} = \bar{E}_c$ and ③ reversible response after saturated switching.

ized description of a dielectric hysteresis visualized in Figure 8.15, where we consider a monotonous electric loading process starting from a virgin, completely unpoled material, observing the following three steps (cf. Figure 8.15):

① *Initial Range.* For a range $|\bar{\mathbb{E}}| < \bar{E}_c$ below the coercive field strength $\bar{E}_c$, no macroscopic polarization occurs, i.e. $\bar{\mathbb{P}}^r = \boldsymbol{0}$.

② *Domain Switching.* In this highly idealized picture, the switching of *all* domains takes place at $\bar{E}_c$ where the polarization $\bar{\mathbb{P}}^r$ fully develops.

③ *Saturated Range.* The poling process stops if the polarization reaches its saturation value $\bar{\mathbb{P}}^r = \bar{P}_s$. The subsequent loading is non-dissipative.

In a *cyclic electric loading process* which alternates between fully poled states in positive and negative direction, we observe the above rectangle-shaped electric hysteresis. Thus the idealized situation is characterized by the *reversible range of the electric field*

$$\mathcal{E} := \{\bar{\mathbb{E}} \in \mathbb{R}^3 \mid f(\bar{\mathbb{E}}) := |\bar{\mathbb{E}}| - \bar{E}_c < 0\} \tag{8.17}$$

in which no dissipative effect occurs. Note carefully that the electric field is not bounded by $\mathcal{E}$ due to the arbitrarily large reversible saturated range ③. In contrast, the polarization is bounded by

$$\mathcal{P} := \{\bar{\mathbb{P}}^r \in \mathbb{R}^3 \mid g(\bar{\mathbb{P}}^r) := |\bar{\mathbb{P}}^r| - \bar{P}_s < 0\} . \tag{8.18}$$

These two ranges are the cornerstones for the modeling of the poling process. The evolution of the polarization will take place for an isotropic response in the direction of the electric field, e.g.

$$\dot{\bar{\mathbb{P}}}^r \sim \bar{\mathbb{E}} . \tag{8.19}$$

The above outlined modeling of the dissipative poling effort is highly idealized concerning the assumption that switching takes place at the constant value $|\bar{\mathbb{E}}| = \bar{E}_c$ of the electric field. Experiments show that full polarization develops only for electric fields $|\bar{\mathbb{E}}| > \bar{E}_c$. This effect is highly non-linear and approaches the saturation polarization asymptotically as illustrated in Figure 8.16. As a consequence, the dissipative polarization process for monotonous electric loading reduces to two steps:
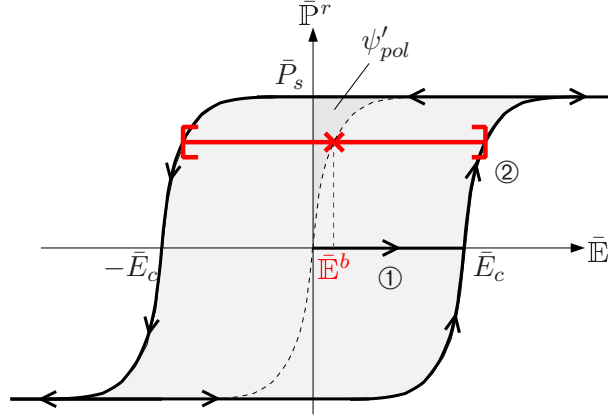
Figure 8.16: Regularized dielectric hysteresis. Remanent polarization induced by the polarization. Process parts of poling: ① fully reversible virgin loading for $\bar{\mathbb{E}} < \bar{E}_c$ and ② regularized switching at $\bar{\mathbb{E}} > \bar{E}_c$, approaching asymptotically the saturation.

① *Initial Range.* For a range $|\bar{\mathbb{E}}| < \bar{E}_c$ below the coercive field strength $\bar{E}_c$, no macroscopic polarization occurs, i.e. $\bar{\mathbb{P}}^r = \boldsymbol{0}$.

② *Domain Switching.* The polarization occurs for $|\bar{\mathbb{E}}| > \bar{E}_c$ in a nonlinear format such that it approaches asymptotically the saturation value $\bar{P}_s$.

In a cyclic electric loading process we then observe the hysteretic effect depicted in Figure 8.16, where the center of the elastic range is shifted by a so-called back electric field $\bar{\mathbb{E}}^b(\bar{\mathbb{P}}^r)$. The modeling of this moving reversible range is obtained by an extention of (8.24) to

$$\mathcal{E} := \{\bar{\mathbb{E}} \in \mathbb{R}^3 \mid f(\bar{\mathbb{E}}, \bar{\mathbb{P}}^r) := |\bar{\mathbb{E}} - \bar{\mathbb{E}}^b(\bar{\mathbb{P}}^r)| - \bar{E}_c < 0\}. \tag{8.20}$$

The back electric field $\bar{\mathbb{E}}^b(\bar{\mathbb{P}}^r)$ is assumed to be governed essentially by a scalar, monotonically increasing function $h(x)$ with the properties

$$h(x) > 0 \quad , \quad h(0) = 0 \quad , \quad \lim_{x \to \bar{P}_s} h(x) = \infty \,, \tag{8.21}$$

providing the non-linear saturation effect visualized in Figure 8.16. In analogy to the gradient character of the electric field $\mathbb{E} = -\partial_{\mathbb{D}}\psi$ the back electric field $\bar{\mathbb{E}}^b(\bar{\mathbb{P}}^r)$ is modeled as the gradient of a hardening function $\bar{\mathbb{E}}^b(\bar{\mathbb{P}}^r) = \partial_{\bar{\mathbb{P}}^r}\psi_{pol}(|\bar{\mathbb{P}}^r|)$. The specific form of $\psi_{pol}(|\bar{\mathbb{P}}^r|)$ used in the subsequent model is given by

$$\psi_{pol}(|\bar{\mathbb{P}}^r|) := -h_0\bar{P}_s^2 \left[\ln\left(1 - \frac{|\bar{\mathbb{P}}^r|}{\bar{P}_s}\right) + \frac{|\bar{\mathbb{P}}^r|}{\bar{P}_s}\right] \,, \tag{8.22}$$

whose derivative with respect to $|\bar{\mathbb{P}}^r|$ satisfies the properties (8.21). Here h_0 is a material parameter governing the shape of the hysteresis curves. The construction of an evolution law will be given in the following subsection.

Construction of a Dissipation Function. Comparably to classical plasticity models we assume that the evolution of the internal variables is governed by a dissipation function. Let us start the construction by recalling the dissipation derived in Section 5

$$\rho_0\mathscr{D}_{loc}^{red} := \mathfrak{M} \star \dot{\mathfrak{Q}} \geq 0 \quad \text{with} \quad \mathfrak{M} = -\rho_0\partial_{\mathfrak{Q}}\psi'(\boldsymbol{F}, \mathbb{E}, \mathfrak{Q}) \,. \tag{8.23}$$

In the model problem under consideration we can identify the remanent polarization as the internal variable $\mathfrak{Q} = \bar{\mathbb{P}}^r$ and the internal force as $\mathfrak{M} = \bar{\mathbb{E}}^r$. A reversible range is defined in the space of the thermodynamic driving force $\bar{\mathbb{E}}^r$ of polarization by

$$\mathcal{E} := \{\bar{\mathbb{E}}^r \in \mathbb{R}^3 \mid f(\bar{\mathbb{E}}^r) := |\bar{\mathbb{E}}^r|/\bar{E}_c - 1 < 0\} \tag{8.24}$$

in terms of the convex macroscopic switching function $f := \mathbb{R}^3 \to \mathbb{R}$. The material parameter $\bar{E}_c > 0$ which bounds the reversible range is the already defined coercive field strength.

As in classical plasticity theory, we require that the dissipation defined in (8.23) has to be maximized. This requirement is usually known as "Principle of Maximum Dissipation" (PMD in the following) and yields the definition of a rate-independent dissipation function

$$\phi(\dot{\bar{\mathbb{P}}}^r) = \sup_{\bar{\mathbb{E}}^r \in \mathcal{E}} \{\bar{\mathbb{E}}^r \cdot \dot{\bar{\mathbb{P}}}^r\} . \tag{8.25}$$

The constraint maximum problem (8.25) can be solved in an approximative way with a penalty-type method yielding a rate-dependent dissipation function

$$\phi_\eta(\dot{\bar{\mathbb{P}}}^r) = \sup_{\bar{\mathbb{E}}^r} \left\{ \bar{\mathbb{E}}^r \cdot \dot{\bar{\mathbb{P}}}^r - \frac{\bar{E}_c}{\eta(m+1)} \langle f(\bar{\mathbb{E}}^r) \rangle^{m+1} \right\} , \tag{8.26}$$

where $1/\eta$ plays the role of a penalty parameter. However, from a physical point of view η is interpreted as a viscosity of polarization. Note that the rate-independent limit is obtained for vanishing viscosity $\eta \to 0$, i.e. when the penalty parameter becomes infinitely large. Observe furthermore that (8.26) can be also seen as the Legendre-Fenchel transformation between the dissipation function $\phi(\dot{\bar{\mathbb{P}}}^r)$ and the dual dissipation function

$$\phi_\eta^*(\bar{\mathbb{E}}^r) = \frac{\bar{E}_c}{\eta(m+1)} \langle f(\bar{\mathbb{E}}^r) \rangle^{m+1} , \tag{8.27}$$

where $\langle x \rangle := \frac{1}{2}(x + |x|)$ denotes the ramp function. The two material parameters $\eta > 0$ and $m > 0$ characterize the viscosity of polarization and viscosity of shape, respectively. The necessary condition of (8.26) defines the evolution equation of polarization by

$$\dot{\bar{\mathbb{P}}}^r = \partial_{\bar{\mathbb{E}}^r} \phi_\eta^*(\bar{\mathbb{E}}^r) \tag{8.28}$$

in terms of the thermodynamic driving force $\bar{\mathbb{E}}^r$. The evolution equation of the remanent polarization takes the closed form

$$\dot{\bar{\mathbb{P}}}^r = \frac{1}{\eta} \left\langle \frac{|\bar{\mathbb{E}}^r|}{\bar{E}_c} - 1 \right\rangle^m \frac{\bar{\mathbb{E}}^r}{|\bar{\mathbb{E}}^r|} . \tag{8.29}$$

Observe that the polarization $\bar{\mathbb{P}}^r$ evolves in the direction of the driving force, characterizing an isotropic macroscopic response of the material. The amount $|\dot{\bar{\mathbb{P}}}^r|$ of evolution is zero in the elastic range $\mathcal{E}$ (8.24) and increases outside the elastic range as a nonlinear function of the "dimensionless over-force" $|\bar{\mathbb{E}}^r|/\bar{E}_c - 1 > 0$ in terms of the material parameters η and m.

Mixed Energy-Enthalpy Function. The mixed energy-enthalpy function $\psi' = \psi'_{ferro}$ is decomposed into a piezo-electric ψ'_{pie} and a polarization ψ'_{pol} contribution

$$\psi' = \psi'_{ferro} = \psi'_{pie} + \psi'_{pol}, \tag{8.30}$$

whereas the piezo-electric part ψ'_{pie} is again decomposed into a mechanical ψ'_{mech}, an electrical ψ'_{elec}, and a coupling ψ'_{coup} contribution

$$\psi'_{ferro}(\bar{\boldsymbol{E}}^e, \bar{\mathbb{E}}, \bar{\mathbb{P}}^r) = \psi'_{mech}(\bar{\boldsymbol{E}}^e, J) + \psi'_{elec}(\bar{\mathbb{E}}) + \psi'_{coup}(\bar{\boldsymbol{E}}^e, \bar{\mathbb{E}}, \bar{\mathbb{P}}^r) + \psi'_{pol}(\bar{\mathbb{E}}, \bar{\mathbb{P}}^r). \tag{8.31}$$

As described at the beginning of this section we decomposed the ferroelectric material response into an irreversible and a reversible part. The last contribution may be compared to piezo-electric material behavior when the reversible part of the deformation gradient $\boldsymbol{F}^e$ is regarded as kinematic variable and takes place between the intermediate and the Eulerian configuration. In the intermediate configuration the material possesses a remanent polarization that depends on the previous poling process but will not evolve anymore in the reversible piezoelectric process.

The modeling of the piezoelectric part of the mixed energy-enthalpy function for ferroelectricity resembles the constitutive modeling of piezoelectricity described in Section 8.1. Only the arguments in the mixed energy-enthalpy functions (8.1) and (8.2) have to be fitted to the representation in terms of variables in the intermediate configuration. Furthermore, one slight modification has to be done on the coupling part ψ'_{coup}. The amount of coupling is now dependent on the amount of developed polarization. This can be realized by simply multiplying the constitutive equation of ψ'_{coup} with the linear factor $|\bar{\mathbb{P}}^r|/\bar{P}_s$. The contributions to the mixed piezoelectric energy-enthalpy function read in particular

$$
\begin{aligned}
\psi'_{mech}(\boldsymbol{F}^e) &= \mu \operatorname{tr}[\bar{\boldsymbol{E}}^e] - \ln[J] + \frac{\lambda}{2}(\ln[J])^2 \\[2mm]
\psi'_{elec}(\bar{\mathbb{E}}) &= -\frac{\epsilon}{2}\operatorname{tr}[\bar{\mathbb{E}} \otimes \bar{\mathbb{E}}] \\[2mm]
\psi'_{coup}(\boldsymbol{F}^e, \bar{\mathbb{E}}; \bar{\boldsymbol{\mathfrak{P}}}) &= \frac{|\bar{\mathbb{P}}^r|}{\bar{P}_s}\left\{ -\alpha'_0 \operatorname{tr}[\bar{\boldsymbol{E}}^e(\bar{\boldsymbol{\mathfrak{P}}} \otimes \bar{\boldsymbol{\mathfrak{P}}})]\operatorname{tr}[\bar{\mathbb{E}} \otimes \bar{\boldsymbol{\mathfrak{P}}}] \right. \\
&\qquad \left. -\alpha'_\perp \operatorname{tr}[\bar{\boldsymbol{E}}^e]\operatorname{tr}[\bar{\mathbb{E}} \otimes \bar{\boldsymbol{\mathfrak{P}}}] - \alpha'_= \operatorname{tr}[\bar{\boldsymbol{E}}^e(\bar{\mathbb{E}} \otimes \bar{\boldsymbol{\mathfrak{P}}})] \right\}
\end{aligned} \tag{8.32}
$$

with $J := \det[\boldsymbol{F}] = \det[\boldsymbol{F}^e]$. The poling contribution to the energy-enthalpy function is defined in terms of the hardening-function ψ_{pol} as follows

$$\psi'_{pol} = \psi_{pol}(|\bar{\mathbb{P}}^r|) - \bar{\mathbb{P}}^r \cdot \bar{\mathbb{E}}. \tag{8.33}$$

8.2.2. Numerical Implementation of Ferroelectricity

The response of the material is assumed to be governed by the potential $W(\boldsymbol{F}, \mathbb{E})$ having the form introduced in Section 6.1

$$W(\boldsymbol{F}, \mathbb{E}) = \inf_{\bar{\mathbb{P}}^r} \sup_{\bar{\mathbb{E}}^r} \bar{W}(\boldsymbol{F}, \mathbb{E}, \bar{\mathbb{P}}^r, \bar{\mathbb{E}}^r). \tag{8.34}$$

$\bar{W}(\boldsymbol{F}, \mathbb{E}, \bar{\mathbb{P}}^r, \bar{\mathbb{E}}^r)$ is the algorithmic expression of the incremental electro-mechanical work

$$\bar{W}(\boldsymbol{F}, \mathbb{E}, \bar{\mathbb{P}}^r, \bar{\mathbb{E}}^r) = \rho_0 \psi'(\boldsymbol{F}, \mathbb{E}, \bar{\mathbb{P}}^r) - \rho_0 \psi'(\boldsymbol{F}_n, \mathbb{E}_n, \bar{\mathbb{P}}^r_n) + \bar{\mathbb{E}}^r \cdot [\bar{\mathbb{P}}^r - \bar{\mathbb{P}}^r_n] - \Delta t \phi^*_\eta(\bar{\mathbb{E}}^r). \tag{8.35}$$

In (8.35) $\psi'(\boldsymbol{F}, \mathbb{E}, \bar{\mathbb{P}}^r)$ is the mixed energy-enthalpy function ψ'_{ferro} defined in (8.30)-(8.33) and $\phi^*_\eta(\bar{\mathbb{E}}^r)$ the conjugate dissipation potential introduced in equation (8.27). The enforcement of the necessary condition of the constitutive variational principle (8.34) yields the non-linear system of equations

$$\bar{\boldsymbol{r}} := \begin{bmatrix} \partial_{\bar{\mathbb{P}}^r} \bar{W} \\ \partial_{\bar{\mathbb{E}}^r} \bar{W} \end{bmatrix} = \begin{bmatrix} \partial_{\bar{\mathbb{P}}^r} \psi' + \bar{\mathbb{E}}^r \\ \bar{\mathbb{P}}^r - \bar{\mathbb{P}}^r_n - \frac{\Delta t}{\eta} \left\langle \frac{|\bar{\mathbb{E}}^r|}{\bar{E}_c} - 1 \right\rangle^m \bar{\boldsymbol{N}} \end{bmatrix} = \boldsymbol{0} \qquad (8.36)$$

with the definition of the flow direction $\bar{\boldsymbol{N}} := \bar{\mathbb{E}}^r / |\bar{\mathbb{E}}^r|$. The first equation in (8.36) represents the algorithmic definition of the conjugate internal force $\bar{\mathbb{E}}^r$. The second equation of (8.36) gives the viscous evolution equation of the internal variable $\bar{\mathbb{P}}^r$. The above non-linear system can be solved at given deformation $\boldsymbol{F}$ and electric field $\mathbb{E}$ by a local Newton-type algorithm for the current variables $\bar{\boldsymbol{v}} := \{\bar{\mathbb{P}}^r, \bar{\mathbb{E}}^r\}$

$$\bar{\boldsymbol{v}} \Leftarrow \bar{\boldsymbol{v}} - \bar{\boldsymbol{a}}^{-1} \bar{\boldsymbol{r}} \qquad (8.37)$$

until convergence is achieved in the sense $|\bar{\boldsymbol{r}}| < tol$. The tangent matrix of the Newton iteration has the form

$$\bar{\boldsymbol{a}} := \begin{bmatrix} \partial^2_{\bar{\mathbb{P}}^r \bar{\mathbb{P}}^r} \psi' & \boldsymbol{1} \\ \\ \boldsymbol{1} & -\frac{m\Delta t}{\eta \bar{E}_c} \left\langle |\bar{\mathbb{E}}^r|/\bar{E}_c - 1 \right\rangle^{m-1} \bar{\boldsymbol{N}} \otimes \bar{\boldsymbol{N}} \\ & -\frac{\Delta t}{\eta} \left\langle |\bar{\mathbb{E}}^r|/\bar{E}_c - 1 \right\rangle^m \frac{1}{|\bar{\mathbb{E}}^r|} \left\{ \boldsymbol{1} - \bar{\boldsymbol{N}} \otimes \bar{\boldsymbol{N}} \right\} \end{bmatrix}. \qquad (8.38)$$

According to (6.35) the derivatives of $W(\boldsymbol{F}, \mathbb{E})$ with respect to the strains $\boldsymbol{F}$ and the electric field $\mathbb{E}$ give the stresses $\boldsymbol{gP}$ and electric displacement $\mathbb{D}$, i.e. the generalized covector $\mathfrak{S}'$

$$\mathfrak{S}' := \begin{bmatrix} \boldsymbol{gP} \\ -\mathbb{D} \end{bmatrix} := \begin{bmatrix} \partial_{\boldsymbol{F}} W(\boldsymbol{F}, \mathbb{E}) \\ \partial_{\mathbb{E}} W(\boldsymbol{F}, \mathbb{E}) \end{bmatrix} = \begin{bmatrix} \partial_{\boldsymbol{F}} \psi' \\ \partial_{\mathbb{E}} \psi' \end{bmatrix}. \qquad (8.39)$$

For the model problem under consideration, the 1st Piola-stress $\boldsymbol{P}$ and the electric displacement $\mathbb{D}$ take the specific form

$$\begin{aligned} \boldsymbol{gP} &= \mu \boldsymbol{gFC}^{r-1} + (\lambda \ln[J] - \mu) \boldsymbol{F}^{-T} - \frac{|\bar{\mathbb{P}}^r|}{\bar{P}_s} \left\{ -\alpha'_0 \boldsymbol{gF} (\mathfrak{P} \otimes \mathfrak{P}) \ \mathrm{tr}[\bar{\mathbb{E}} \otimes \bar{\mathfrak{P}}] \right. \\ &\quad \left. + \alpha'_\perp \boldsymbol{gFC}^{r-1} \mathrm{tr}[\bar{\mathbb{E}} \otimes \bar{\mathfrak{P}}] + \frac{\alpha'_=}{2} [\boldsymbol{gF}\mathfrak{P} \otimes \boldsymbol{G}^{-1}\mathbb{E} + \boldsymbol{gFG}^{-1}\mathbb{E} \otimes \mathfrak{P}] \right\}, \\ -\mathbb{D} &= -\epsilon \boldsymbol{G}^{-1} \mathbb{E} - \frac{|\bar{\mathbb{P}}^r|}{\bar{P}_s} \left\{ \alpha'_0 \mathrm{tr}[\bar{\boldsymbol{E}}^e (\bar{\mathfrak{P}} \otimes \bar{\mathfrak{P}})] \mathfrak{P} + \alpha'_\perp \mathrm{tr}[\bar{\boldsymbol{E}}^e] \mathfrak{P} \right. \\ &\quad \left. + \alpha'_= \boldsymbol{F}^{r-1} \bar{\boldsymbol{G}}^{-1} \bar{\boldsymbol{E}}^e \bar{\mathfrak{P}} \right\} - \mathbb{P}^r . \end{aligned}$$

$$(8.40)$$

Using the implicit function theorem we may derive a closed-form solution of the coupled electro-mechanical tangent moduli operators $\boldsymbol{c}' := \left[\mathbb{C}'_{algo} \quad \boldsymbol{h}'_{algo} ; \ (\boldsymbol{h}'_{algo})^T \quad \boldsymbol{\beta}'_{algo} \right]$. The single entries of $\boldsymbol{c}'$ are computed as total second derivative with respect to the deformation gradient $\boldsymbol{F}$ and the electric field $\mathbb{E}$ yielding

$$\begin{aligned} \mathbb{C}'_{algo} &:= \partial^2_{\boldsymbol{FF}} W = \partial^2_{\boldsymbol{FF}} \psi' - \begin{bmatrix} \partial^2_{\boldsymbol{F}\bar{\mathbb{P}}^r} \psi' \\ \boldsymbol{0} \end{bmatrix} \cdot \bar{\boldsymbol{a}}^{-1} \cdot \begin{bmatrix} \partial^2_{\bar{\mathbb{P}}^r \boldsymbol{F}} \psi' \\ \boldsymbol{0} \end{bmatrix}, \\ \boldsymbol{\beta}'_{algo} &:= \partial^2_{\mathbb{E}\mathbb{E}} W = \partial^2_{\mathbb{E}\mathbb{E}} \psi' - \begin{bmatrix} \partial^2_{\mathbb{E}\bar{\mathbb{P}}^r} \psi' \\ \boldsymbol{0} \end{bmatrix} \cdot \bar{\boldsymbol{a}}^{-1} \cdot \begin{bmatrix} \partial^2_{\bar{\mathbb{P}}^r \mathbb{E}} \psi' \\ \boldsymbol{0} \end{bmatrix}, \\ \boldsymbol{h}'_{algo} &:= \partial^2_{\mathbb{E}\boldsymbol{F}} W = \partial^2_{\mathbb{E}\boldsymbol{F}} \psi' - \begin{bmatrix} \partial^2_{\mathbb{E}\bar{\mathbb{P}}^r} \psi' \\ \boldsymbol{0} \end{bmatrix} \cdot \bar{\boldsymbol{a}}^{-1} \cdot \begin{bmatrix} \partial^2_{\bar{\mathbb{P}}^r \boldsymbol{F}} \psi' \\ \boldsymbol{0} \end{bmatrix}. \end{aligned} \qquad (8.41)$$

For the considered model problem $\partial^2_{\boldsymbol{F}\bar{\mathbb{E}}^r}\bar{W} = \partial^2_{\bar{\mathbb{E}}^r\boldsymbol{F}}\bar{W} = \boldsymbol{0}$ and $\partial^2_{\mathbb{E}\bar{\mathbb{E}}^r}\bar{W} = \partial^2_{\bar{\mathbb{E}}^r\mathbb{E}}\bar{W} = \boldsymbol{0}$. Note that the second terms on the right hand side of (8.41) characterize the softening of the fully coupled electro-mechanical tangent moduli due to the evolution of the internal variables. We note that due to the variational structure the moduli are symmetric. The fully coupled electro-mechanical reversible tangent moduli are obtained as second derivative of the mixed energy-enthalpy function ψ' with respect to the deformation gradient $\boldsymbol{F}$ and the electric field $\mathbb{E}$, i.e. $\mathbb{C}' = \partial^2_{\boldsymbol{F}\boldsymbol{F}}\psi'$, $\boldsymbol{\beta}' = \partial^2_{\mathbb{E}\mathbb{E}}\psi'$, and $\boldsymbol{h}'(\mathfrak{p}) = \partial^2_{\mathbb{E}\boldsymbol{F}}\psi'$. Using the mixed energy-enthalpy function defined above in (8.30)-(8.33) they take the specific form

$$
\begin{aligned}
\mathbb{C}' &= \mu\boldsymbol{g}\overline{\otimes}\boldsymbol{C}^{r-1} - (\lambda\ln[J] - \mu)\boldsymbol{F}^{-1}\widetilde{\otimes}\boldsymbol{F}^{-1} + \lambda\boldsymbol{F}^{-T}\otimes\boldsymbol{F}^{-T} \\
&\quad -\frac{|\bar{\mathbb{P}}^r|}{\bar{P}_s}\left\{-\alpha'_0\boldsymbol{g}\overline{\otimes}(\mathfrak{P}\otimes\mathfrak{P})\operatorname{tr}[\bar{\mathbb{E}}\otimes\bar{\mathfrak{P}}] + \alpha'_\perp\boldsymbol{g}\overline{\otimes}\boldsymbol{C}^{r-1}\operatorname{tr}[\bar{\mathbb{E}}\otimes\bar{\mathfrak{P}}]\right. \\
&\quad \left. +\frac{\alpha'_=}{2}[\boldsymbol{g}\overline{\otimes}(\mathfrak{P}\otimes(\boldsymbol{G}^{-1}\mathbb{E})) + (\boldsymbol{G}^{-1}\mathbb{E})\otimes\mathfrak{P})]\right\}, \\
\boldsymbol{h}' &= -\frac{|\bar{\mathbb{P}}^r|}{\bar{P}_s}\left\{\alpha'_0\mathfrak{P}\otimes\boldsymbol{g}\boldsymbol{F}(\mathfrak{P}\otimes\mathfrak{P}) + \alpha'_\perp\mathfrak{P}\otimes\boldsymbol{g}\boldsymbol{F}\boldsymbol{C}^{r-1} + \frac{\alpha'_=}{2}\widetilde{h}\right\}, \\
\boldsymbol{\beta}' &= -\epsilon\boldsymbol{G}^{-1}.
\end{aligned}
\tag{8.42}
$$

In (8.42) we made use of the operators

$$
[(\bullet)\overline{\otimes}(\circ)]_a{}^A{}_b{}^B = (\bullet)_{ab}(\circ)^{AB} \quad \text{and} \quad [\boldsymbol{F}^{-1}\widetilde{\otimes}\boldsymbol{F}^{-1}]_a{}^A{}_b{}^B = F^{-1A}{}_b F^{-1B}{}_a
\tag{8.43}
$$

together with the definition

$$
\widetilde{\boldsymbol{h}} = \widetilde{h}^I{}_m{}^M = C^{r-1MI}(g_{ml}F^l{}_L\mathfrak{P}^L) + (C^{r-1})^{LI}g_{lm}F^l{}_L\mathfrak{P}^M.
\tag{8.44}
$$

In order to have a quick and robust implementation different types of simplifications of the model problem can be considered. The easiest one consists in making the following assumption concerning the remanent deformation gradient which is approximated with the remanent deformation gradient at time $t = t_n$

$$
\boldsymbol{F}^r \approx \boldsymbol{R}^r\boldsymbol{V}^r(\bar{\mathbb{P}}^r_n) := \boldsymbol{F}^r_n
\tag{8.45}
$$

yielding to a simplified expression for the remanent Cauchy-Green Tensor $\boldsymbol{C}^r$ and of the reversible Green-Lagrange strain $\bar{\boldsymbol{E}}^e$ which now only depend on the internal variable $\bar{\mathbb{P}}^r_n$ at time t_n

$$
\begin{aligned}
\boldsymbol{C}^r &\approx \boldsymbol{F}^{rT}_n\bar{\boldsymbol{G}}\boldsymbol{F}^r_n := \boldsymbol{C}^r_n \\
\bar{\boldsymbol{E}}^e &= \tfrac{1}{2}\left(\boldsymbol{F}^{eT}\boldsymbol{g}\boldsymbol{F}^e - \bar{\boldsymbol{G}}\right) \approx \tfrac{1}{2}\left(\boldsymbol{F}^{rT}_n\boldsymbol{F}^T\boldsymbol{g}\boldsymbol{F}\boldsymbol{F}^r_n - \bar{\boldsymbol{G}}\right).
\end{aligned}
\tag{8.46}
$$

Further, the explicit linear dependence of the coupling term in the mixed energy-enthalpy function with respect to the normalized amount of the polarization $|\bar{\mathbb{P}}^r|/\bar{P}_s$ is simplified by considering a proportionality with respect to the normalized amount of the polarization $|\bar{\mathbb{P}}^r_n|/\bar{P}_s$ at time t_n. Finally, the polarization director $\mathfrak{P}$ in the coupling term of the mixed energy-enthalpy function is replaced with its value $\bar{\mathfrak{P}}_n = \bar{\mathbb{P}}^r_n/|\bar{\mathbb{P}}^r_n|$ at time t_n. Including these assumptions, the free energy reads

$$
\begin{aligned}
\psi'_{ferro} &\approx \mu\operatorname{tr}[\bar{\boldsymbol{E}}^e] - \mu\ln[J] + \frac{\lambda}{2}(\ln[J])^2 - \frac{\epsilon}{2}\operatorname{tr}[\bar{\mathbb{E}}\otimes\bar{\mathbb{E}}] \\
&\quad -\frac{|\bar{\mathbb{P}}^r_n|}{\bar{P}_s}\left\{\alpha'_0\operatorname{tr}[\bar{\boldsymbol{E}}^e(\bar{\mathfrak{P}}_n\otimes\bar{\mathfrak{P}}_n)]\operatorname{tr}[\bar{\mathbb{E}}\otimes\bar{\mathfrak{P}}_n] + \alpha'_\perp\operatorname{tr}[\bar{\boldsymbol{E}}^e]\operatorname{tr}[\bar{\mathbb{E}}\otimes\bar{\mathfrak{P}}_n]\right. \\
&\quad \left. +\alpha'_=\operatorname{tr}[\bar{\boldsymbol{E}}^e(\bar{\mathbb{E}}\otimes\bar{\mathfrak{P}}_n)]\right\} + \psi_{pol}(|\bar{\mathbb{P}}^r|) - \bar{\mathbb{P}}^r\cdot\bar{\mathbb{E}}.
\end{aligned}
\tag{8.47}
$$

These assumptions simplify the dependency of the internal force $\bar{\mathbb{E}}^r$ which will be influenced only by the electric field and the hardening function ψ_{pol}. The stresses and dielectric displacement then read

$$
\begin{aligned}
\boldsymbol{gP} \;=\;& \mu \boldsymbol{gF}\boldsymbol{C}^{r-1} + (\lambda \ln[J] - \mu)\boldsymbol{F}^{-T} - \frac{|\bar{\mathbb{P}}^r_n|}{\bar{P}_s}\Big\{ \alpha'_0 \boldsymbol{gF}(\boldsymbol{\mathfrak{P}}_n \otimes \boldsymbol{\mathfrak{P}}_n) \ \mathrm{tr}[\bar{\mathbb{E}} \otimes \bar{\boldsymbol{\mathfrak{P}}}_n] \\
& + \alpha'_\perp \boldsymbol{gF}\boldsymbol{C}^{r-1} \,\mathrm{tr}[\bar{\mathbb{E}} \otimes \bar{\boldsymbol{\mathfrak{P}}}_n] + \frac{\alpha'_=}{2}[\boldsymbol{gF}\boldsymbol{\mathfrak{P}}_n \otimes \boldsymbol{G}^{-1}\mathbb{E} + \boldsymbol{gF}\boldsymbol{G}^{-1}\mathbb{E} \otimes \boldsymbol{\mathfrak{P}}_n] \Big\} \\
-\mathbb{D} \;=\;& -\epsilon \boldsymbol{G}^{-1}\mathbb{E} - \frac{|\bar{\mathbb{P}}^r_n|}{\bar{P}_s}\Big\{ \alpha'_0 \,\mathrm{tr}[\bar{\boldsymbol{E}}^e(\bar{\boldsymbol{\mathfrak{P}}}_n \otimes \bar{\boldsymbol{\mathfrak{P}}}_n)]\boldsymbol{\mathfrak{P}}_n + \alpha'_\perp \,\mathrm{tr}[\bar{\boldsymbol{E}}^e]\boldsymbol{\mathfrak{P}}_n \\
& + \alpha'_= \boldsymbol{F}^{r-1}\bar{\boldsymbol{G}}^{-1}\bar{\boldsymbol{E}}^e\boldsymbol{\mathfrak{P}}_n \Big\} - \mathbb{P}^r \; .
\end{aligned}
$$

$$\tag{8.48}$$

The derivatives appearing in (8.41) have the following expression

$$
\begin{aligned}
\partial_{\bar{\mathbb{P}}^r}\psi' \;&=\; -\bar{\mathbb{E}} + (\partial_{|\bar{\mathbb{P}}^r|}\psi_{pol})\boldsymbol{G}\bar{\boldsymbol{\mathfrak{P}}} \;, \\
\partial^2_{\mathbb{P}^r\boldsymbol{F}}\psi' \;&=\; \partial^2_{\boldsymbol{F}\bar{\mathbb{P}}^r}\psi' = \boldsymbol{0} \;, \\
\partial^2_{\bar{\mathbb{P}}^r\bar{\mathbb{P}}^r}\psi' \;&=\; (\partial_{|\bar{\mathbb{P}}^r|}\psi_{pol})\frac{1}{|\mathbb{P}^r|}(\boldsymbol{G} - \boldsymbol{G}\bar{\boldsymbol{\mathfrak{P}}} \otimes \boldsymbol{G}\bar{\boldsymbol{\mathfrak{P}}}) + (\partial^2_{|\bar{\mathbb{P}}^r||\bar{\mathbb{P}}^r|}\psi_{pol})\bar{\boldsymbol{\mathfrak{P}}} \otimes \bar{\boldsymbol{\mathfrak{P}}} \;, \\
\partial^2_{\bar{\mathbb{P}}^r\mathbb{E}}\psi' \;&=\; \partial^2_{\mathbb{E}\bar{\mathbb{P}}^r}\psi' = -\boldsymbol{F}^{r-T} \;.
\end{aligned}
$$

$$\tag{8.49}$$

The reversible part of the moduli in (8.41) is obtained by replacing $\boldsymbol{\mathfrak{P}}$ with $\boldsymbol{\mathfrak{P}}_n$ and $\boldsymbol{C}^r$ with $\boldsymbol{C}^r_n$ in the equation (8.42)

$$
\begin{aligned}
\mathbb{C}' \;=\;& \mu \boldsymbol{g}\overline{\otimes}\boldsymbol{C}^{r-1}_n - (\lambda \ln[J] - \mu)\boldsymbol{F}^{-1}\widetilde{\otimes}\boldsymbol{F}^{-1} + \lambda \boldsymbol{F}^{-T} \otimes \boldsymbol{F}^{-T} \\
& -\frac{|\bar{\mathbb{P}}^r|}{\bar{P}_s}\Big\{ -\alpha'_0 \boldsymbol{g}\overline{\otimes}(\boldsymbol{\mathfrak{P}}_n \otimes \boldsymbol{\mathfrak{P}}_n)\,\mathrm{tr}[\bar{\mathbb{E}} \otimes \bar{\boldsymbol{\mathfrak{P}}}_n] + \alpha'_\perp \boldsymbol{g}\overline{\otimes}\boldsymbol{C}^{r-1}_n \,\mathrm{tr}[\bar{\mathbb{E}} \otimes \bar{\boldsymbol{\mathfrak{P}}}_n] \\
& + \frac{\alpha'_=}{2}[\boldsymbol{g}\overline{\otimes}(\boldsymbol{\mathfrak{P}}_n \otimes (\boldsymbol{G}^{-1}\mathbb{E}) + (\boldsymbol{G}^{-1}\mathbb{E}) \otimes \boldsymbol{\mathfrak{P}}_n)] \Big\} \;, \\
\boldsymbol{h}' \;=\;& -\frac{|\bar{\mathbb{P}}^r|}{\bar{P}_s}\Big\{ \alpha'_0 \boldsymbol{\mathfrak{P}}_n \otimes \boldsymbol{gF}(\boldsymbol{\mathfrak{P}}_n \otimes \boldsymbol{\mathfrak{P}}_n) + \alpha'_\perp \boldsymbol{\mathfrak{P}}_n \otimes \boldsymbol{gF}\boldsymbol{C}^r_n + \frac{\alpha'_=}{2}\widetilde{\boldsymbol{h}}(\boldsymbol{\mathfrak{P}}_n) \Big\} \;, \\
\boldsymbol{\beta}' \;=\;& -\epsilon \boldsymbol{G}^{-1} \;.
\end{aligned}
$$

$$\tag{8.50}$$

8.3. Numerical Examples

In this section we test the newly proposed material model of ferroelectricity at large strains with representative numerical examples. We first reproduce some of the tests regarding piezoceramics which were already computed by using the proposed model for the ferroelectric material response at small strains in order to check that the same results are obtained. To show the potentialities of the proposed formulation we consider afterwards typical applications of ferroelectric polymers which show large deformations.

8.3.1. Uniaxial Test with Varying Loading Frequencies

In this example, the characteristic hysteresis curves for a ferroelectric crystal is reproduced. The specimen is a homogenous quadratic piece of material with length L = 10 mm. At the left edge the electric potential is set to zero, while the other edge is exposed to a periodical electric potential $\phi^e(t)$ with the maximum value of $\phi^e_{max} = 20$ kV. From the
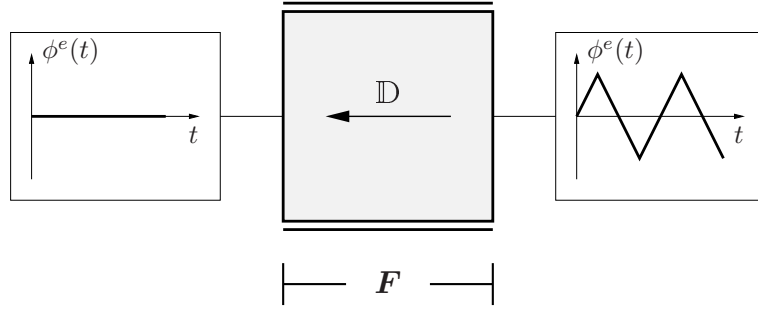
Figure 8.17: Mechanical and electrical boundary conditions for the uniaxial test. To a piece of ferroelectric material an electric potential is applied trough two electrodes along the left and right edges. The electrode on the left hand side is grounded while to the electrode on the right hand side a periodic electric potential is applied. The specimen is free to expand in the horizontal direction, but the vertical displacements are not allowed (double black lines). Under these boundary conditions an hysteretic behavior of the electric displacement $\mathbb{D}$ and of the total deformation $\boldsymbol{F}$ is observed.

mechanical point of view the specimen is free to move in the horizontal direction while is constrained in the vertical movements, cf. Figure 8.17. The material parameters used are reported in Table 8.2.

When the switching is initiated, i.e. the electric field approaches the coercive value, $\bar{\mathbb{P}}^r$ and $\boldsymbol{F}^r$ evolve. The hysteresis loops are given in Figure 8.18 and in order to show the time dependent behavior of the proposed formulation we consider varying loading frequencies. The main features of the experimental results in ZHOU, KAMLAH AND MUNZ [156], i.e. order of remanent polarization, order of lower picks, and shape of the high frequency curve are reproduced.

8.3.2. Multiaxial Test

We now consider a numerical example reproducing the polarization rotation as occurs in the experiments of HUBER & FLECK [64]. In these experiments a plate of PZT was first poled and the electrodes etched away. Then, specimens were cut from the poled plate

Table 8.2: Piecoceramic Material Parameters

| No.	Parameter	Unit	Name	Value
1	λ	N/mm^2	Lamé parameter	$76.6 \cdot 10^3$
2	μ	N/mm^2	Lamé parameter	$44.7 \cdot 10^3$
3	α_0'	N/(kV·mm)	axial piezoelectric expansion	-0.2
4	$\alpha_\perp'$	N/(kV·mm)	lateral piezoelectric expansion	-4.4
5	$\alpha_='$	N/(kV·mm)	piezoelectric shearing	23.20
6	ϵ	mC/(kV·m)	electric permittivity	$11.2 \cdot 10^{-3}$
7	$\bar{E}_c$	kV/mm	coercive electric field	1.0
8	$\bar{P}_s$	C/m^2	saturation polarization	$26. \cdot 10^{-2}$
9	$\bar{\lambda}_s^r$	–	saturation strain	10^{-3}
10	h_0	(kV·m)/C	hysteresis slope parameter	$3.8 \cdot 10^3$
11	η	mm^2/(C·s)	viscosity of polarization	10^{-2}
12	m	–	viscosity shape exponent	2
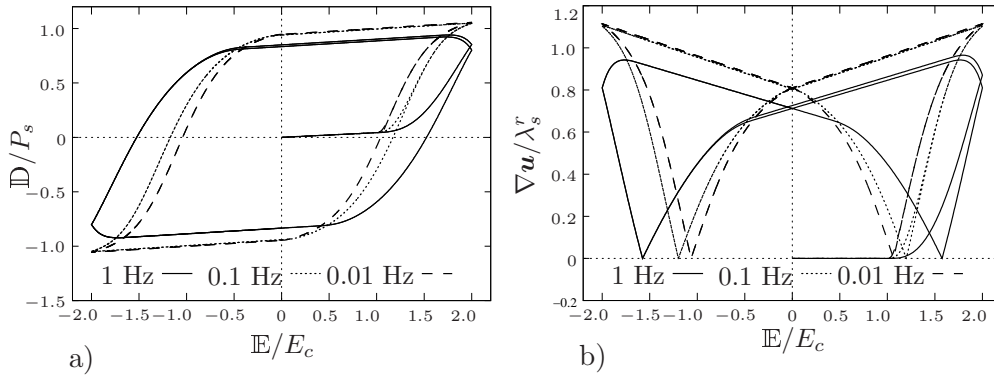
Figure 8.18: a) Numerical reproduction of the dielectric hystereses and b) butterfly curves for loading rates of 0.01, 0.1 and 1 Hz.

and new electrodes applied to them so that an electric field could be imposed at an angle relative to the pre-existing polarization. As the electric field is increased the remanent polarization rotates so that the angle between the polarization direction and the electric field reduces. In cases where the angle is initially obtuse, depolarization may first occur followed by re-polarization parallel to the electric field. The experiments are carried out considering the same specimen as in the previous section subjected to an axial electric field. The material is assumed to be poled in different orientations relative to the applied electric field.

The results of the simulation are reported in Figure 8.19 which shows the change of the component of the electric displacement parallel to the direction of the applied electric field as a function of the applied electric field. Clearly, the curve for an initial angle of 180° is a half hysteresis loop whereas the response when the angle is initially zero is nearly linear. The latter case arises because the material is approaching lock up and the electric field is simply driving it further into this state. For angles in between, the behavior involves a gradual transition from the half hysteresis loop for an initial angle of 180° to linear behavior when the angle is zero. This is exactly what happens in the experiments of HUBER & FLECK [64].
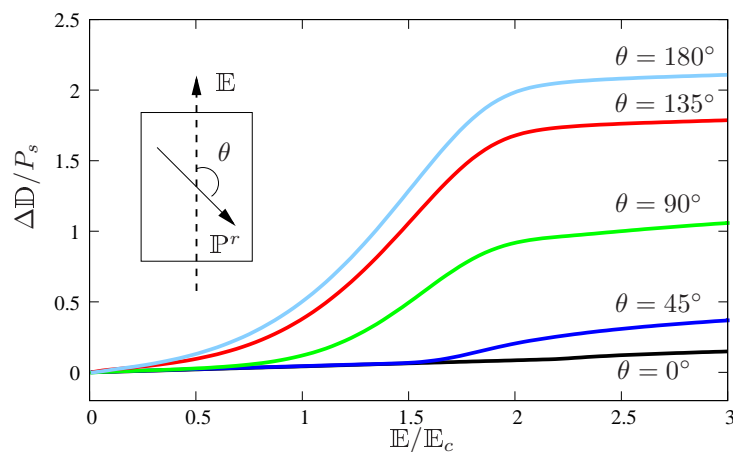

Figure 8.19: Polarization rotation curves. The component of the electric displacement parallel to the applied electric field is plotted against the electric field.
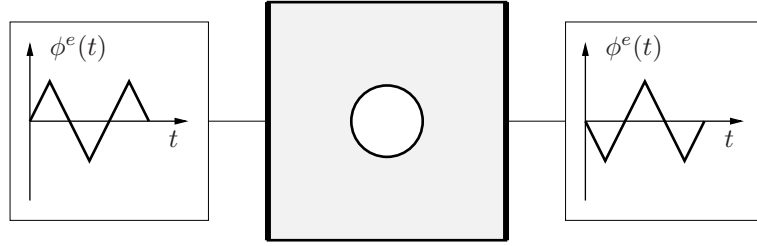
Figure 8.20: Boundary conditions for the test of the square plate with centered hole. The right and left edges of the plate are fully mechanically constraint, i.e. $\boldsymbol{u} = \boldsymbol{0}$ (bold black lines). The same edges are doted of two electrodes to wich a periodic electric potential is applied. These electrical potential are in counter phase.

8.3.3. Square Plate with a Centered Hole

In this example, a squared plate with a centered hole is used as a specimen. It has edge dimensions of 20×20 mm and the hole at the center has a radius of mm and is discretized with 800 four noded elements. The material parameters used are reported in Table 8.2. At the upper and the lower edge, the displacements are fixed in horizontal and vertical directions. A time varying electric potential $\phi^e(t)$ and $-\phi^e(t)$ with the maximum value of $\phi^e_{max} = 20$ kV is applied at the upper and bottom edge, respectively (cf. Figure 8.20). Figure 8.21 and 8.22 show the distribution of the electric potential ϕ^e and the polarization vector distribution $\bar{\mathbb{P}}^r$ in the specimen in correspondence of several time steps. We can observe that to a non-uniform distribution of the potential follows a non-uniform distribution of the polarization. The polarization tries to circumvent the hole while near the edges is parallel to the vertical-edge-direction.

8.3.4. Multilayer Actuator

We now want to study an example of practical application. We consider the structure shown in Figure 8.23 having the principle design of a multilayer actuator. The geometry has been chosen in adaption to the literature, cf. KAMLAH [73]. Due to symmetry conditions only the shaded area is modeled and the upper electrode must not deform or rotate, but is only allowed to translate parallel to its starting position. In order to simulate a poling process, the electric potential $\phi^e(t)$ is prescribed as triangular loading in the following manner: first it is increased from 0 to 170 V until $t_1 = 100$ s and then reduced to zero until $t_2 = 200$ s. Thus, an electric field of approximately 3 kV/mm is reached in the region between the two electrodes, guaranteeing full poling.

In Figure 8.24a and 8.24b, we reported the electric potential distribution at the instant $t_1 = 100$ s, when the highest voltage is applied, and $t_2 = 200$ s, unloading with zero applied potential, respectively. In Figure 8.24c and 8.24d the correspondent distribution of the remanent polarization $\bar{\mathbb{P}}^r$ in proximity of the electrode tip is reported. From Figure 8.24a and 8.24c we can conclude that at t_1 the region on the left of the electrode tip is characterized by linear distribution of the electric potential between the electrodes, while the region on the right hand side of the electrode tip lies at a zero potential. The region near the electrode tip can be considered as a transition zone. In correspondence, the left region is fully poled and the right region is unpoled. Thus, the region of the electrode tip experiences a non-uniform polarization because of the transition between these two extremes. The potential at t_2 (cf. Figure 8.24b) clearly does not vanish as consequence of
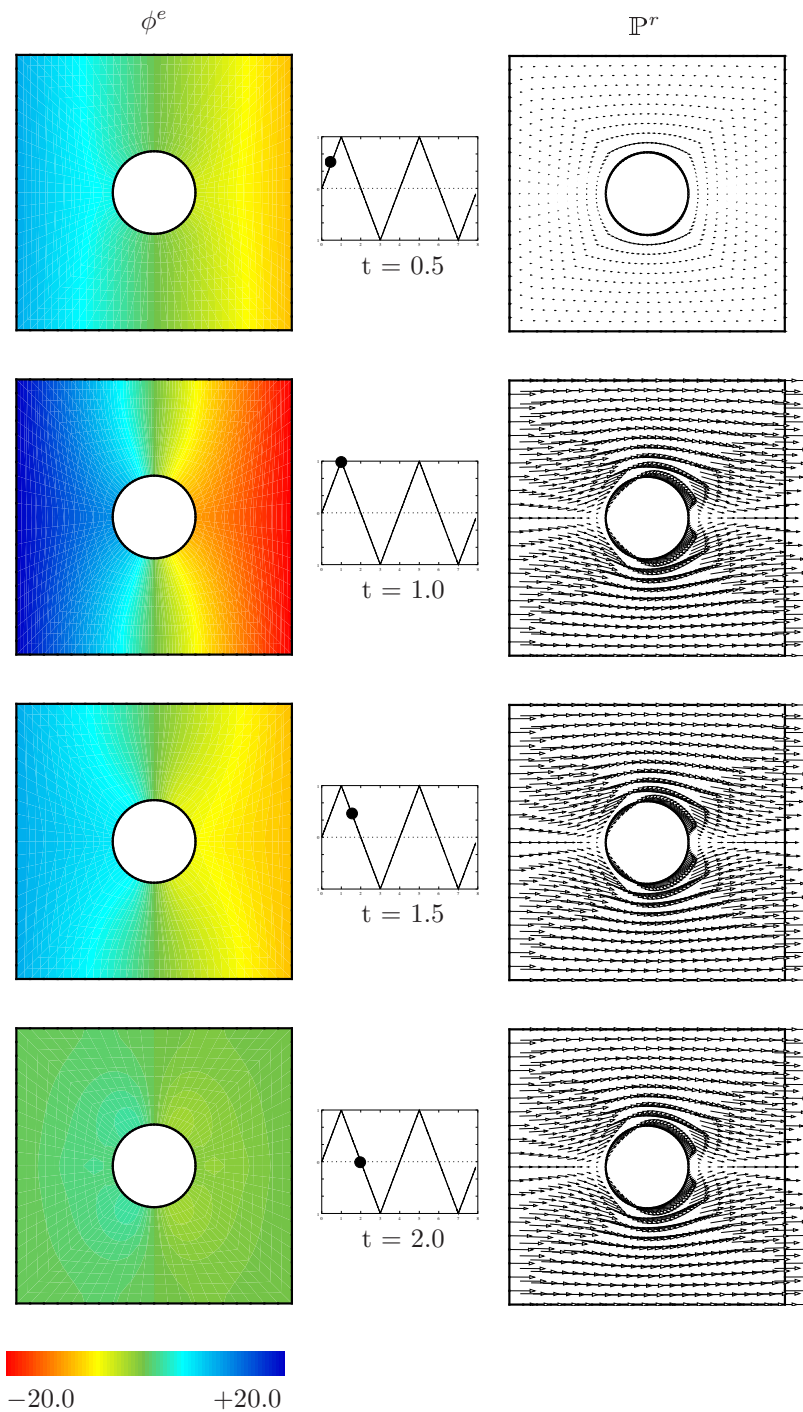
Figure 8.21: Distributions of the electric potential ϕ^e and remanent polarization $\mathbb{P}^r$ at different times.

an inhomogeneous remanent polarization in the electrode tip region (cf. Figure 8.24d).

Figure 8.25 shows the results of the 3D computation, where the specimen described in the previous was extruded in $\boldsymbol{e}_3$ direction to a thickness of 60 mm. The boundary conditions of the 2D example are incorporated, the bottom left edge is only allowed to expand in the $\boldsymbol{e}_3$ direction. The results obtained are in agreement with the 2D computation. The polarization develops uniformly in the thickness direction of the specimen in the region between the electrodes not closed to the electrode-tip, is zero in the region far away from
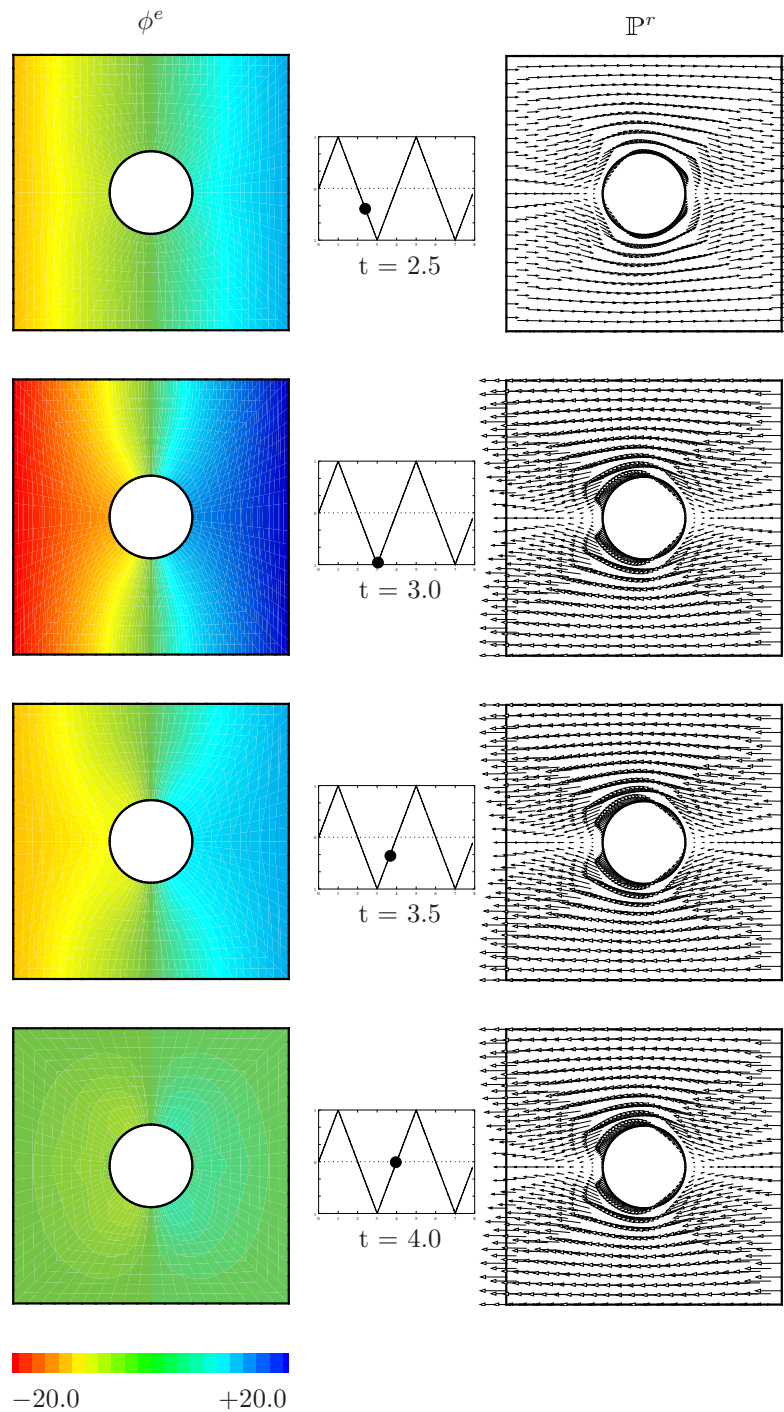
Figure 8.22: Distributions of the electric potential ϕ^e and remanent polarization $\mathbb{P}^r$ at different times.

the electrode-tip where no electric potential is applied, and is non-uniformly distributed around the electrode-tip.

8.3.5. Polymers in an Undrawn State

In the previous examples, we investigated the modeling of dissipative materials that show hystereses found in ferroelectric crystals. In the following we focus on the modeling of the hysteretic behavior of ferroelectric polymers. To this end we adapt the homogeneous
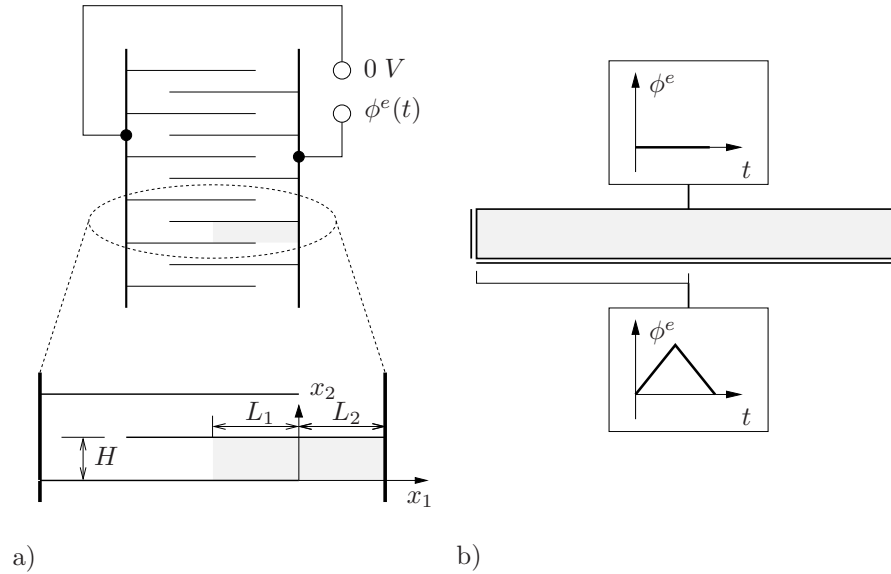
Figure 8.23: a) Principle design of a multilayer actuator: $L_1 = L_2 = 205\,\mu$m, $H = 57.5\,\mu$m. Due to symmetry properties, only the shaded area is modeled. b) Boundary conditions on the discretized shaded area. In order to simulate a poling process, the electric potential $\phi^e(t)$ is prescribed as triangular loading on the lower electrode while the upper electrode is grounded. Mechanically, the modeled specimen is allowed to expand both horizontally and vertically (double bold black lines).

quadratic specimen used in the previous subsection (cf. Figure 8.17) with length $L = 10$ mm. At the left edge the electric potential is set to zero, while the other edge is exposed to a periodic electric potential $\phi^e(t)$ with the maximum value of $\phi^e_{max} = 300$ kV ensuring an electric field $\mathbb{E} = 3\bar{E}_c$. The aim is to reproduce the hysteresis curves for VDF-TrFE copolymers shown in Figure 2.18. The developed material parameters for VDF-TrFE copolymers are given in Table 8.3 and are derived from MUKHERJEE & CHAUDHURI
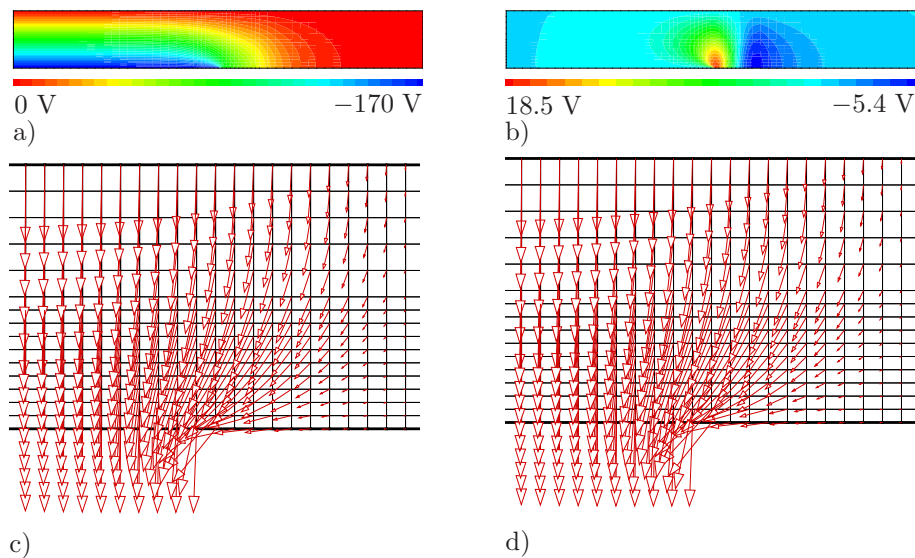

Figure 8.24: a) Electric potential ϕ^e at $t_1 = 100$ s, b) electric potential ϕ^e at $t_2 = 200$ s, c) remanent polarization $\mathbb{P}^r$ at $t_1 = 100$ s in the vicinity of the electrode tip, and d) remanent polarization $\mathbb{P}^r$ at $t_2 = 200$ s in the vicinity of the electrode tip.
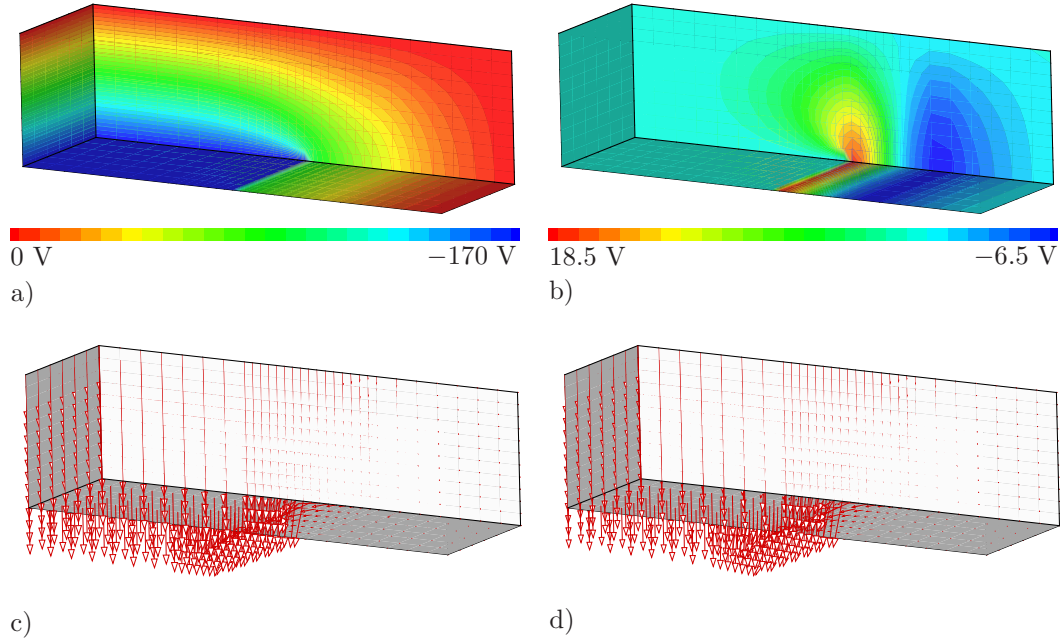
0 V   −170 V   18.5 V   −6.5 V
a)   b)

c)   d)

Figure 8.25: a) Electric potential ϕ^e at $t_1 = 100$ s, b) electric potential ϕ^e at $t_2 = 200$ s, c) remanent polarization $\mathbb{P}^r$ at $t_1 = 100$ s, and d) remanent polarization $\mathbb{P}^r$ at $t_1 = 200$ s.

[114], FURUKAWA & SEO [54], and ZHANG, BHARTI AND ZHAO [153]. The hysteresis curves generated with this set of material parameters are shown in Figure 8.26a and 8.26b. The $\boldsymbol{F}$-$\mathbb{E}$-hysteresis has two sharp picks at $\mathbb{E} = \boldsymbol{0}$. As we already mentioned in Section 2, homopolymer and copolymer of VDF become thicker when their polarization reverses and thinner when the absolute value of the electric displacement is maximum. As shown in Figure 2.18, this is opposite to the case for ferroelectric PZT which becomes thinner when the polarization reverses.

Table 8.3: Material Parameters for Undrawn Polymers

| No.	Parameter	Unit	Name	Value
1	λ	N/mm^2	Lamé parameter	$1.59 \cdot 10^2$
2	μ	N/mm^2	Lamé parameter	$1.0705 \cdot 10^2$
3	α'_0	N/(kV·mm)	axial piezoelectric expansion	$4.6 \cdot 10^{-5}$
4	$\alpha'_\perp$	N/(kV·mm)	lateral piezoelectric expansion	$-8.09 \cdot 10^{-6}$
5	$\alpha'_=$	N/(kV·mm)	piezoelectric shearing	$-0.7 \cdot 10^{-2}$
6	ϵ	mC/(kV·m)	electric permittivity	$10.62 \cdot 10^{-3}$
7	$\bar{E}_c$	kV/mm	coercive electric field	45.0
8	$\bar{P}_s$	C/m^2	saturation polarization	$8.0 \cdot 10^{-2}$
9	$\bar{\lambda}_s^r$	–	saturation strain	$-3.0 \cdot 10^{-3}$
10	h_0	(kV·m)/C	hysteresis slope parameter	16.67
11	η	mm^2/(C·s)	viscosity of polarization	1.0
12	m	–	viscosity shape exponent	2
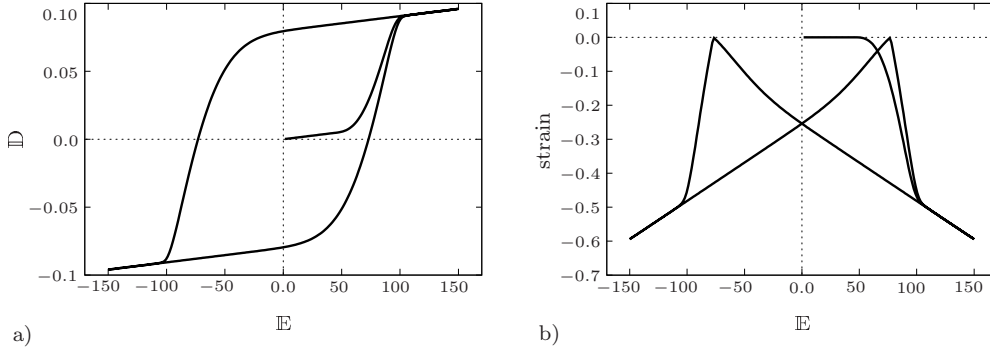
Figure 8.26: a) Dielectric hysteresis and b) butterfly curve of an homogeneous specimen of VDF-TrFE copolymer.

8.3.6. Polymers in a Modified Material State

As reported in Section 2, large hystereses are not desirable for some practical applications and there exist some techniques to modify the material response of polymers rendering the hystereses thinner. The existence of hystereses in ferroelectric materials is due to the energy barrier when switching from one polarization direction to another when the material transforms from one phase to another. This phase transformation can be facilitated and exceptionally large electrostrictive strain can be achieved reducing the size of all-trans conformation by introducing defects. One possible approach to achieve this is through a high-energy radiation. The aim of this section is to reproduce the thin hysteresis curves presented in Figure 8.27. The considerable differences between the two material states are the very thin hysteresis and butterfly loop and the enormous strain response at equal electric loading. To this end a new set of material parameters is identified as reported in Table 8.4.

Again, the specimen described in the previous subsection is used with the same boundary-conditions and electric potentials. The results are plotted in Figure 8.27a and Figure 8.27b comparing the two sets of material parameters. The black curves repeat the results achieved in the previous calculations whereas the red ones depict the present calculations.

Table 8.4: Material Parameters for Irradiated Polymers

| No.	Parameter	Unit	Name	Value
1	λ	N/mm^2	Lamé parameter	$1.59 \cdot 10^2$
2	μ	N/mm^2	Lamé parameter	$1.0705 \cdot 10^2$
3	α'_0	N/(kV·mm)	axial piezoelectric expansion	$4.6 \cdot 10^{-4}$
4	$\alpha'_\perp$	N/(kV·mm)	lateral piezoelectric expansion	$-8.09 \cdot 10^{-6}$
5	$\alpha'_=$	N/(kV·mm)	piezoelectric shearing	$-2.7 \cdot 10^{-1}$
6	ϵ	mC/(kV·m)	electric permittivity	$10.62 \cdot 10^{-3}$
7	$\bar{E}_c$	kV/mm	coercive electric field	4.0
8	$\bar{P}_s$	C/m^2	saturation polarization	$5.0 \cdot 10^{-2}$
9	$\bar{\lambda}_s^r$	–	saturation strain	$-1.0 \cdot 10^{-2}$
10	h_0	(kV·m)/C	hysteresis slope parameter	10
11	η	mm^2/(C·s)	viscosity of polarization	1.0
12	m	–	viscosity shape exponent	2
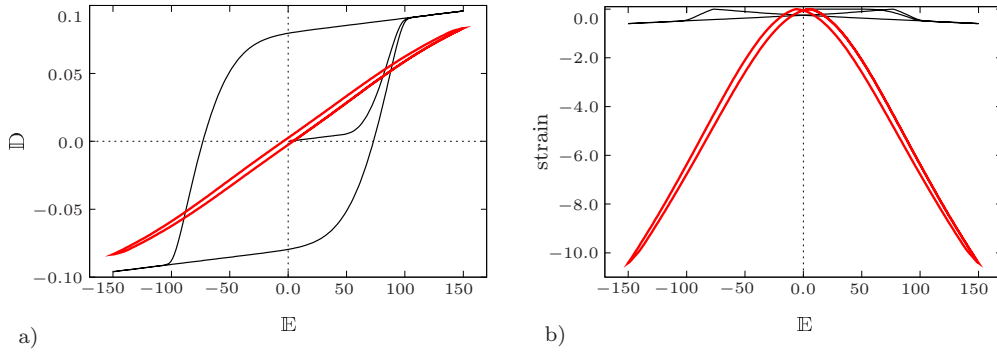
Figure 8.27: a) Dielectric hysteresis and b) butterfly curve of an homogeneous specimen of VDF-TrFE copolymer in undrawn state (black lines) and irradiated state (red lines).

We can observe a good qualitative agreement with the experimental data reported in Section 2.

To validate the developed material formulation and material parameters a boundary-value-problem showing large deformations has to be solved. Therefore, we analyze a finger-actuator consisting of two sheets of electroded polymer films glued together. The length of the specimen is equal to 100 mm and its width is equal to 1 mm. In the following examples, only one sheet is electrically active, see Figure 8.28. The electric field applied to one of the two films will cause the elongation of the same. Since the other layer is not activated, its inner fiber will suffer an elongation and this will result in an overall bending motion of the actuator. The motion will be upward or downward (a finger-like motion) according to the activated layer. In the considered case the displacement of the left edge is fixed in one direction, the bottom left corner is fixed in both directions implying a homogeneous deformation at the fixed end. A time varying electric potential $\phi^e(t)$ with the maximum value of $\phi^e_{max} = 70$ kV is applied at the bottom line ensuring a electric field $\mathbb{E} = 3\bar{E}_c$ guaranteeing full poling.

The hysteresis curves for strain and dielectric displacements over the electric field of a point near the outward surface of the active layer are shown in Figure 8.29. The green curves represent the results of calculation for polymers in the natural material state using the first set of material parameters reported in Table 8.3. The red curves depict the outcome of calculation for irradiated polymers where the second set of material parameters (cf. Table 8.4) is used. Figures 8.30 and 8.31 show the bending motion of the polymer-film
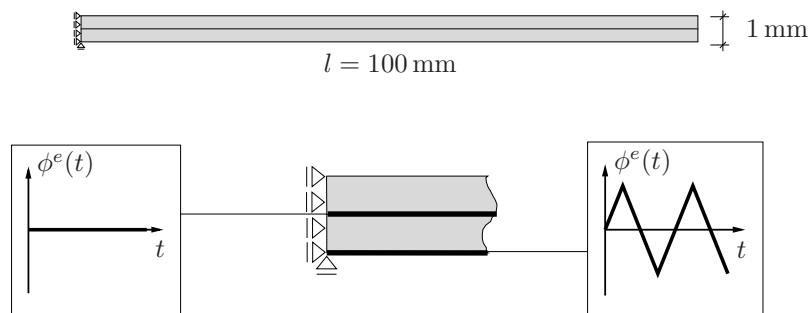

Figure 8.28: Top pannel: geometry of the finger actuator. Bottom pannel: mechanical and electrical boundary condition for the films integrated in the finger actuator.
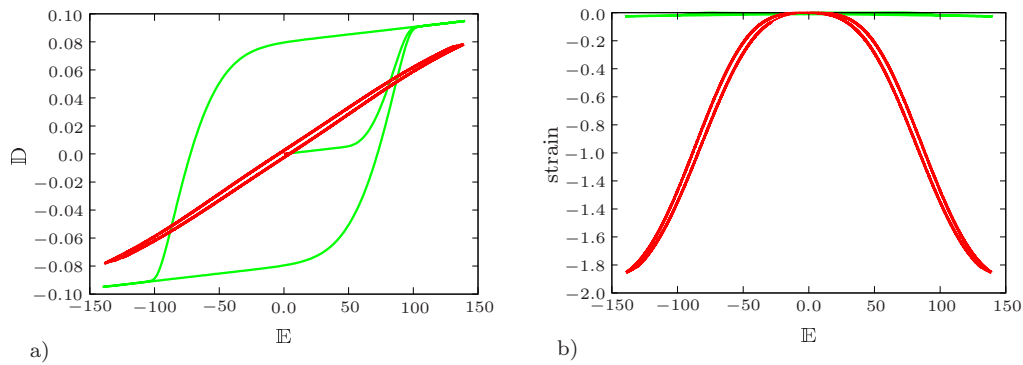
Figure 8.29: a) Dielectric hysteresis and b) butterfly curve measured on the film specimen for an operating voltage of 70 kV. The geen curves represent the results of calculation with material parameters for polymers in the natural material state, the red curves depict the outcome of calculation with material parameters describing modified polymers.

as well as the remanent polarization vector for both sets of material parameters at several time steps. The enormous difference in the deformation has to be noticed. While the calculations for polymers in a natural state yield a low bending motion, the results for modified polymers describe almost a circle.
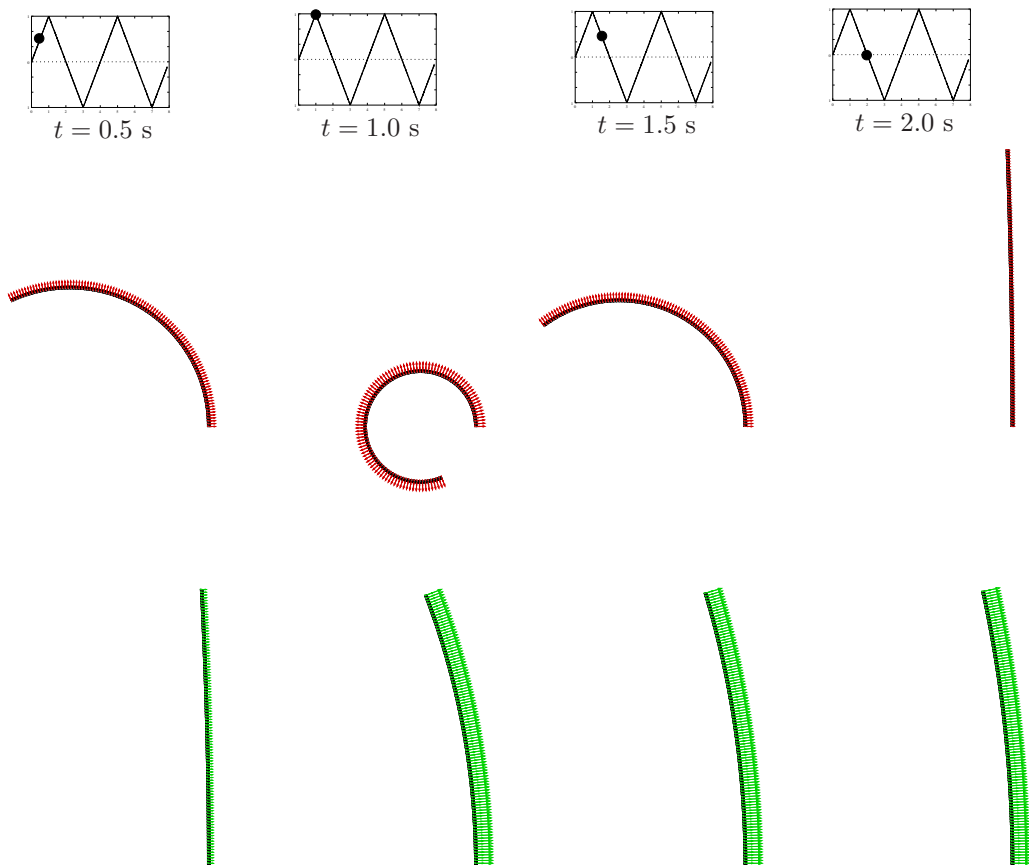

$t = 0.5$ s $t = 1.0$ s $t = 1.5$ s $t = 2.0$ s

Figure 8.30: Distribution of remanent polarzation $\mathbb{P}^r$ and deformed configuratio at different times for a finger-actuator. Comparison between the response of an irradiated polymer (red arrows) and the response of an undrawn polymer (green arrows).
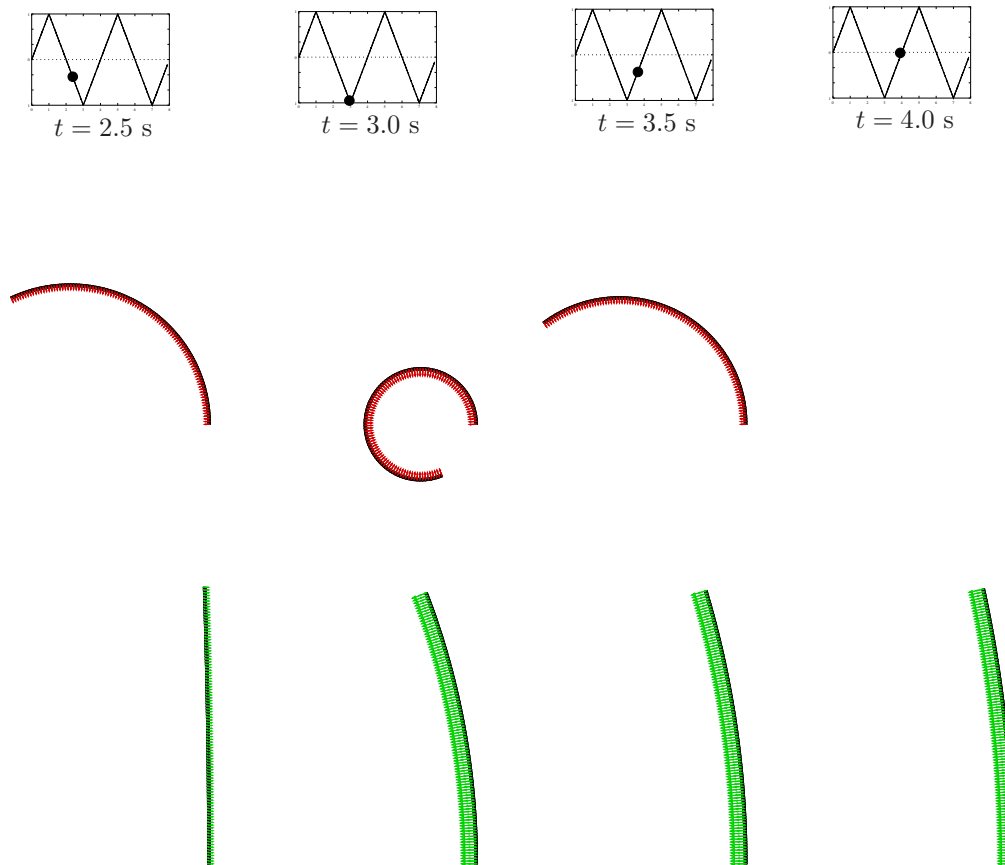
Figure 8.31: Distribution of remanent polarzation $\mathbb{P}^r$ and deformed configuratio at different times for a finger-actuator. Comparison between the response of an irradiated polymer (red arrows) and the response of an undrawn polymer (green arrows).

The same finger actuator with dimensions length 100 mm, width 20 mm, and thickness 1 mm is also simulated in a 3D fashion. Homogeneous boundary conditions ensure a uniform
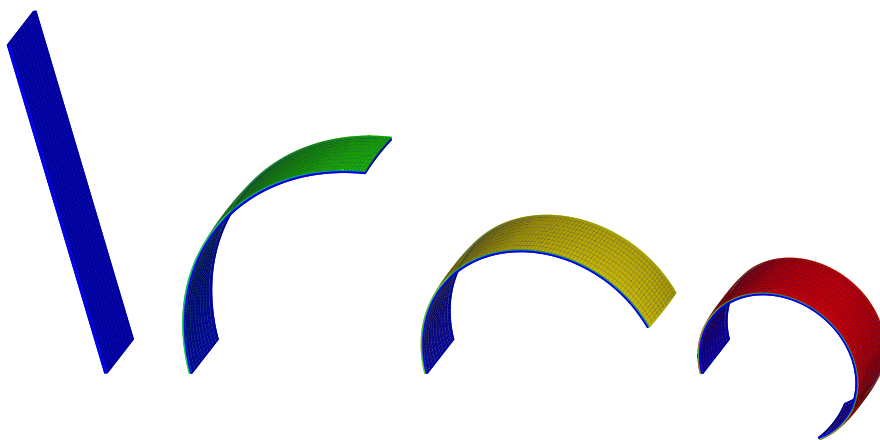

Figure 8.32: Bending motion of a finger-actuator at several time steps. The actuating potential is increased linearly up to a maximum value of $\phi^e_{max} = 70$ kV.
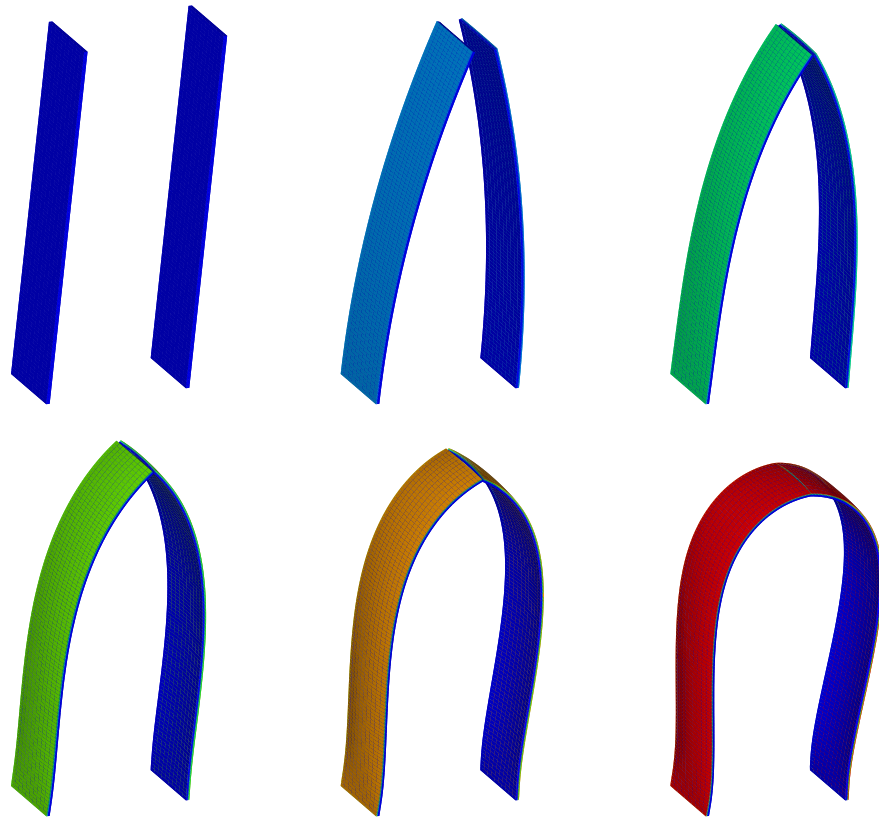
Figure 8.33: Grip actuator designed with two finger actuators disposed parallel to each other at a certain distance. The consequent evolution of the deformation is shown.
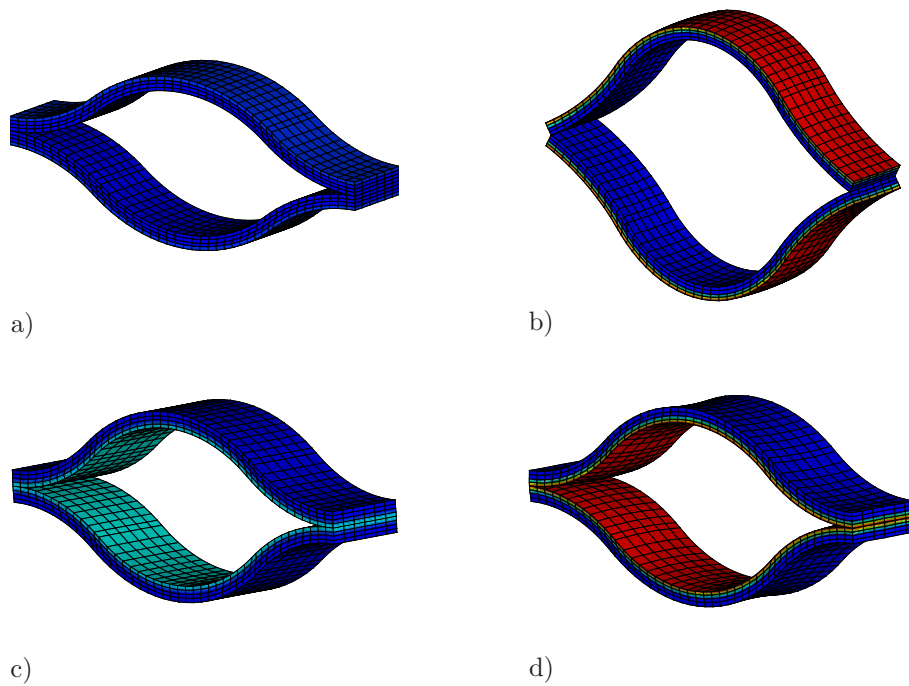

a)

b)

c)

d)

Figure 8.34: Different deformation stages of a bimorph double-S-shaped-actuator. a) Undeformed configuration, b) deformed shape when the external layers are active, c) deformed shape when the internal layers are active, and d) deformed shape when the internal layers are active and the contact renders the system stiffer.

development of the polarization and of the deformation. A linear increasing electric potential $\phi^e(t)$ with the maximum value of $\phi^e_{max} = 70$ kV is applied at the left outward surface. In Figure 8.32 one can see the bending motion of a finger actuator at different time steps. Afterwards, a configuration with two finger-actuators disposed parallel to each other at a certain distance in order to grip objects is considered. In this case, the two finger-actuators touch each other after a certain deformation. The consequent evolution of the deformation is analyzed in Figure 8.33. The deformation of the polymer film can be used in many other different ways to produce actuation. Another possible configuration is the bimorph double-S-shaped-actuator. Here, two sheets of electroded polymer films are glued together and form a double-S-shape. If the external layers are active, the curvature of the actuator can be accentuated (see Figure 8.34a and 8.34b) and otherwise diminished if the internal layers are active (see Figure 8.34c and 8.34d). The configuration in which the curvature is diminished turns out to be stiffer with respect to the previous one. The reason of such a behavior is the occurring contact between the upper and lower part of the actuator. As the contact evolves the curvature after diminishing starts to increase again as shown in Figure 8.34d.

9. Conclusion

This work was concerned with aspects of the formulation and numerical implementation of dissipative electro-mechanics at large strains. At first, the principal equations of non-linear continuum mechanics and electrostatics were separately described. The description of the electrostatic boundary-value-problem was done by using an approach similar to the one used for the non-linear continuum mechanics to get a better understanding through proper analogies. Particular emphasis was given to the geometric nature of the two problems which allowed the differentiation between geometric and physical dual quantities.

Thereafter, the continuum mechanics and electrostatic equations were properly combined to account for a fully coupled, dissipative, and geometrically non-linear electro-mechanical boundary value problem. The point of departure was a merging of the two set of equations with a proper modification of the mechanical set in order to incorporate the effect of body force, couple and energy supply due to the interaction of the electrostatic field with the body under consideration. The set of electro-mechanical equations was afterwards modified in terms of a total stress, sum of the mechanical and of the Maxwell stress, and a total energy, sum of the energy stored in the body and the electrostatic energy stored in the underlying free space. This proper modification brought a clear understanding of the fields characterizing the electro-mechanical boundary-value-problem.

The core of this work was the development of a variational formulation for a generic dissipative electro-mechanical response. At first, a purely local constitutive modeling was treated. An incremental constitutive variational principle in terms of the energy storage and of the dissipation functional was proposed to describe the local material response when advancing the electro-mechanical loading process in a discrete time interval. Secondly, the global treatment of the electro-mechanical boundary-value-problem was taken under consideration. The variational approach was taken as the cornerstone for the development of the finite element methodology. The discretization of the two-field problem appeared, as a natural consequence of the proposed incremental variational principle, in a symmetric and very compact format.

As case of studies for the proposed variational formulation, the ferroelectric dissipative material response was taken under consideration. Particular attention was paid on the construction of the storage and dissipation functionals, in order to built up a micro-mechanically motivated phenomenological model, and on the fundamental kinematic assumptions. The performance of the proposed methods was demonstrated by means of a spectrum of benchmark problems showing eventually large deformations.

The proposed incremental variational approach is a very robust tool. It allows a very compact treatment of the coupled dissipative electro-mechanical boundary-value-problem and an easier overall understanding. It is not only confined to the treatment of phenomenological ferroelectricty. With the proper extensions other case of studies could be considered. Few examples are electro-mechanical phase field modeling, electro-mechanical fracture, viscous dissipative material response of electro-active-polymers. Further, a straight forward extension to magneto-mechanical coupled problems could be considered, since the underlying differential equations have an almost identical structure.

References

[1] ALLIK, H.; HUGHES, T. J. R. [1970]: *Finite element method for piezoelectric vibration.* International Journal for Numerical Methods in Engineering, 2: 151–157.

[2] ALLOCK, H. R.; LAMPE, F. W. [1981]: *Contemporary polymer chemistry.* Prentice-Hall, Englewood Cliffs, NJ.

[3] ARLT, G. [1990]: *Twinning in ferroelectric and ferroelastic ceramics: stress relief.* Journal of Material Science, 25: 2655–2666.

[4] AROCKIARAJAN, A.; DELIBAS, B.; MENZEL, A.; SEEMANN, W. [2006]: *Studies on rate-dependent switching effects of piezoelectric materials using a finite element model.* Computational Materials Science, 37: 306–317.

[5] BAR-COHEN, Y. (Editor) [2004]: *Electroactive polymer (EAP) actuators as artificial muscles - reality, potential and challenges.* SPIE Press.

[6] BASSIOUNY, E.; GHALEB, A. F.; MAUGIN, G. A. [1988]: *Thermodynamical formulation for coupled electromechanical hysteresis effects. I. Basic equations.* International Journal of Engineering Science, 26: 1279–1295.

[7] BASSIOUNY, E.; GHALEB, A. F.; MAUGIN, G. A. [1988]: *Thermodynamical formulation for coupled electromechanical hysteresis effects. II. Poling of ceramics.* International Journal of Engineering Science, 26: 1297–1306.

[8] BASSIOUNY, E.; MAUGIN, G. A. [1989]: *Thermodynamical formulation for coupled electromechanical hysteresis effects. III. Parameter identification.* International Journal of Engineering Science, 27: 975–987.

[9] BASSIOUNY, E.; MAUGIN, G. A. [1989]: *Thermodynamical formulation for coupled electromechanical hysteresis effects. IV. Combined electromechanical loading.* International Journal of Engineering Science, 27: 989–1000.

[10] BELOV, Y. A.; KREHER, S. W. [2005]: *Viscoplastic models for ferroelectric ceramics.* Journal of Computers and Structures, 25: 2567–2571.

[11] BENJEDDOU, A. [2000]: *Advances in piezoelectric finite element modeling of adaptive structural elements: a survey.* Journal of Computers and Structures, 76: 347–363.

[12] BIOT, M. A. [1965]: *Mechanics of incremental deformations.* John Wiley & Sons Inc., New York.

[13] BRIGADNOV, A. L.; DORFMANN, A. [2003]: *Mathematical modeling of magneto-sensitive elastomers.* International Journal of Solids and Structures, 40: 4659–4674.

[14] BRIGADNOV, A. L.; DORFMANN, A. [2005]: *Mathematical modelling of magnetorheological fluids.* Continuum Mechanics and Thermodynamics, 17: 29–42.

[15] BROADHURST, M.; DAVIS, G.; McKINNEY, J.; COLLINS, R. [1978]: *Piezoelectricity and pyroelectricity in polyvinylidene fluoride - A model.* Journal of Applied Physics, 49: 4992–4997.

[16] BROADHURST, M. G.; DAVIS, G. T.; DEREGGI, A. S.; ROTH, S. C.; COLLINS, R. E. [1982]: *Pyroelectricity and charge transport in a copolymer of Vinylidene Fluoride and Tetrafluoroethylene.* Polymer, 23: 22–28.

[17] BUSTAMANTE, R.; DORFMANN, A.; OGDEN, R. W. [2006]: *Universal relations in isotropic nonlinear magnetoelasticity.* Quarterly Journal of Mechanics and Applied Mathematics, 59: 435–450.

[18] BUSTAMANTE, R.; DORFMANN, A.; OGDEN, R. W. [2007]: *A nonlinear magnetoelastic tube under extension and inflation in an axial magnetic field: numerical solution.* Journal of Engineering Mathematics, 59: 139–153.

[19] BUSTAMANTE, R.; DORFMANN, A.; OGDEN, R. W. [2008]: *Nonlinear electroelastostatics: A variational framework.* Zeitschrift für angewandte Mathematik und Physik ZAMP, 60: 154–177.

[20] BUSTAMANTE, R.; DORFMANN, A.; OGDEN, R. W. [2009]: *On electric body forces and Maxwell stresses in nonlinearly electroelastic solids.* International Journal of Engineering Science, in press.

[21] BUSTAMANTE, R.; OGDEN, R. W. [2006]: *Universal relations for nonlinear electroelastic solids.* Acta Mechanica, 182: 125–140.

[22] BUTZ, A. [2006]: *Nichtlineare Formulierung piezoelektrischer 3d-Stabstrukturen - Theorie und Finite-Element-Modellierung.* Ph.D. Thesis, Universität Fridericiana Karlsruhe (TH).

[23] BUTZ, A.; KLINKEL, S. [2005]: *A finite element formulation for the nonlinear analysis of piezoelectric three-dimensional beam structures.* Proceedings in Applied Mathematics and Mechanics, 5: 383–384.

[24] CARSTENSENS, C.; HACKL, K.; MIELKE, A. [2002]: *Non-convex potentials and microstructures in finite-strain plasticity.* Proceedings of the Royal Society London A, 458: 299–317.

[25] CHADWICK, P. [1999]: *Continuum mechanics.* Dover Publications, Inc., Mineola.

[26] CHENG, Z.; BHARTI, V.; XU, T.; XU, H.; MAI, T.; ZHANG, Q. [2001]: *Electrostrictive Poly(Vinylidene Fluoride-Trifluoroethylene) copolymers.* Sensors and Actuators A, 90: 138–147.

[27] CHEN, P. [1980]: *Three dimensional dynamic electromechanical constitutive relations for ferroelectric materials.* International Journal of Solids and Structures, 16: 1059–1068.

[28] CHEN, P.; MONTGOMERY, S. [1980]: *A macroscopic theory for the existence of the hysteresis and butterfly loops in ferroelectricity.* Ferroelectrics, 27: 199–208.

[29] CHEN, P.; TUCKER, T. [1981]: *One dimensional polar mechanical and dielectric responses of the ferroelectric ceramic PZT 65/35 due to domain switching.* International Journal of Engineering Science, 19: 147–158.

[30] CHEN, W.; LYNCH, S. C. [1998]: *A micro-electro-mechanical model for polarization switching of ferroelectric materials.* Acta Materialia, 46: 5303–5311.

[31] COCKS, C. F. A.; MCMEEKING, R. M. [1999]: *A phenomenological constitutive law for the behaviour of ferroelectric ceramics.* Ferroelectrics, 228: 219–228.

[32] COLEMAN, B. D.; GURTIN, M. E. [1967]: *Thermodynamics with internal state variables.* The Journal of Chemical Physics, 47: 597–613.

[33] COLEMAN, B. D.; NOLL, W. [1963]: *The thermodynamics of elastic materials with Heat Conduction and Viscosity.* Archive for Rational Mechanics and Analysis, 13: 167–178.

[34] DAVIS, G. T. In WONG, C. P. (Editor): *Polymers for electronic and photonic applications.* Academic Press, Boston.

[35] DESIMONE, A.; JAMES, R. D. [2002]: *A constrained theory of magnetoelasticity.* Journal of the Mechanics and Physics of Solids, 50: 283–320.

[36] DESIMONE, A.; PODIO-GUIDUGLI, P. [1996]: *On the continuum theory of deformable ferromagnetic solids.* Archive for Rational Mechanics and Analysis, 136: 201–233.

[37] DORFMANN, A.; OGDEN, R. W. [2003]: *Magnetoelastic modelling of elastomers.* European Journal of Mechanics A/Solids, 22: 497–507.

[38] DORFMANN, A.; OGDEN, R. W. [2004]: *Nonlinear magnetoelastic deformations.* Journal of Applied Mathematics and Mechanics, 57: 599–622.

[39] DORFMANN, A.; OGDEN, R. W. [2004]: *Nonlinear magnetoelastic deformations of elastomers.* Acta Mechanica, 167: 13–28.

[40] DORFMANN, A.; OGDEN, R. W. [2005]: *Nonlinear electroelasticity.* Acta Mechanica, 174: 167–183.

[41] DORFMANN, A.; OGDEN, R. W. [2005]: *Some problems in nonlinear magnetoelasticity.* Zeitschrift für angewandte Mathematik und Physik, 56: 718–745.

[42] DORFMANN, A.; OGDEN, R. W.; SACCOMANDI, G. [2004]: *Universal relations for non-linear magnetoelastic solids.* International Journal of Non-Linear Mechanics, 39: 1699–1708.

[43] DORFMANN, A.; OGDEN, R. W.; SACCOMANDI, G. [2005]: *The effect of rotation on the nonlinear magnetoelastic response of a circular cylindrical tube.* International Journal of Solids and Structures, 42: 3700–3715.

[44] DOYLE, T. C.; ERICKSEN, J. L. [1956]: *Nonlinear elasticity.* In Dryden, H. L.; Kármán, T. von (Editors): Advances in Applied Mechanics, Vol. 4, pp. 53–116. Academic Press, New York.

[45] ELHADROUZ, M.; ZINEB, B. T.; PATOOR, E. [2004]: *Phenomenological modelling of the non-linear behavior of ferroelectric materials.* Journal of Physics. IV France, 115: 67–72.

[46] ELHADROUZ, M.; ZINEB, B. T.; PATOOR, E. [2005]: *Constitutive law for ferroelastic and ferroelectric piezoceramics.* Journal of Intelligent Material Systems and Structures, 16: 221–236.

[47] ERINGEN, A. C. [1962]: *Nonlinear theory of continuous media.* McGraw-Hill Book Company, Inc., New York.

[48] ERINGEN, A. C.; MAUGIN, G. [1990]: *Electrodynamics of continua. Vol. 1: Foundations and solid media.* Springer–Verlag, - Edition.

[49] ERINGEN, A. C.; MAUGIN, G. A. [1990]: *Electrodynamics of continua. Vol. 2: Fluid and complex media.* Springer–Verlag, - Edition.

[50] FLEURY, P.; MATHIEU, J. P. [1970]: *Electrostatica, corrente continua, magnetismo.* Zanichelli vol. 6.

[51] FUKADA, E.; NISHIYAMA, K. [1972]: *Piezoelectric properties in polarized Poly(Vinyl Fluoride).* Japanese Journal of Applied Physics, 11: 36–40.

[52] FUKADA, E.; SAKURAI, T. [1971]: *Piezoelectricity in polarized Poly(Vinylidene Fluoride) films.* Polymer Journal, 2: 656–662.

[53] FURUKAWA, T. [1989]: *Ferroelectric properties of Vinylidene Fluoride copolymers.* Phase Transitions, 18: 143–211.

[54] FURUKAWA, T.; SEO, N. [1990]: *Electrostriction as the origin of piezoelectricity in ferroelectric polymers.* Japanese Journal of Applied Physics, 29: 675–680.

[55] GAUDENZI, P.; BATHE, K. [1995]: *An iterative finite element procedure for the analysis of piezoelectric continua.* Journal of Intelligent Material Systems and Structures, 6: 266–273.

[56] GERMAIN, P. [1973]: *Cours de mécanique des milieux continus.* Masson et Cie, Paris.

[57] GROOT, S. R. DE; MAZUR, P. [1984]: *Non-equilibrium thermodynamics.* Dover Publications, Inc., Mineola.

[58] HALLIDAY, D.; RESNICK, R.; KRANE, K. S. [1992]: *Physics.* John Wiley & Sons Inc., New York, 4th Edition.

[59] HALPEN, B.; NGUYEN, Q. S. [1975]: *Sur les matéraux standard généralisés.* Journal de Mécanique, 14: 39–63.

[60] HAUPT, P. [1999]: *Continuum mechanics and theory of materials.* Springer-Verlag, Berlin, Heidelberg, 2. Edition.

[61] HIGASHIHATA, Y.; SAKO, J.; YAGI, T. [1981]: *Piezoelectricity of Vinylidene Fluoride-Trifluoroethylene copolymers.* Ferroelectrics, 32: 85–92.

[62] HOLZAPFEL, G. A. [1981]: *An introduction to continuum mechanics.* Academic Press.

[63] HOLZAPFEL, G. A. [2000]: *Nonlinear solid mechanics.* John Wiley & Sons, Chichester, New York.

[64] HUBER, E. E.; FLECK, A. N. [2001]: *Multi-axial electrical switching of a ferroelectric: theory versus experiment.* Journal of Mechanics and Physics of Solids, 49: 785–811.

[65] HUBER, J. E. [2005]: *Micromechanical modeling of ferroelectrics.* Current Opinion in Solid State and Materials Science, 9: 100–106.

[66] HUBER, J. E.; FLECK, N. A.; LANDIS, C. M.; MCMEEKING, R. M. [1999]: *A constitutive model for ferroelectric polycrystals.* Journal of Mechanics and Physics of Solids, 47: 1663–1697.

[67] HUTTER, K.; VEN, A. A. F. VAN DE ; URESCU, A. [2006]: *Electromagnetic field matter interactions in thermoelastic solids and viscous fluids.* Springer–Verlag.

[68] HWANG, S. C.; LYNCH, S. C.; MCMEEKING, R. M. [1995]: *Ferroelectric/ferroelastic interactions and a polarization switching model.* Acta Metallurgica Materialia, 43: 2073–2084.

[69] IKEDA, T. [1990]: *Fundamentals of piezoelectricity.* Oxford University Press.

[70] JAFFE, B.; COOK, W. R.; JAFFE, H. [1971]: *Piezoelectric ceramics.* Academic Press, London New York.

[71] JAMES, R. D. [2002]: *Configurational forces in magnetism with application to the dynamics of a small-scale ferromagnetic shape memory cantilever.* Continuum Mechanics and Thermodynamics, 14: 55–86.

[72] JAMES, R. D.; KINDERLEHRER, D. [1993]: *Theory of magnetostriction with applications to $Tb_x Dy_{1-x} Fe_2$.* Philosophical Magazine B, 68: 237–274.

[73] KAMLAH, M. [2001]: *Ferroelectric and ferroelastic piezoceramics- modelling of electromechanical hysteresis phenomena.* Continuum Mechanics and Thermodynamics, 13: 219–268.

[74] KAMLAH, M.; BÖHLE, U. [2001]: *Finite element analysis of piezoceramic components taking into account ferroelectric hysteresis behavior.* International Journal of Solids and Structures, 38: 605–633.

[75] KAMLAH, M.; LISKOWSKY, C. A.; MCMEEKING, R. M.; BALKE, H. [2005]: *Finite element simulation of a polycrystalline ferroelectric based on a multidomain single crystal switching model.* International Journal of Solids and Structures, 42: 2949–2964.

[76] KAMLAH, M.; TSAKMAKIS, C. [1999]: *Phenomenological modeling of the nonlinear electro-mechanical coupling in ferroelectrics.* International Journal of Solids and Structures, 36: 669–695.

[77] KAMLAH, M.; WANG, Z. [2003]: *A thermodynamically and microscopically motivated constitute model for piezoceramics.* Computational Materials Science, 28: 409–418.

[78] KANKANALA, S. V.; TRIANTAFYLLIDIS, N. [2004]: *On finitely strained magnetorheological elastomers.* Journal of the Mechanics and Physics of Solids, 52: 2869–2908.

[79] KAWAI, H. [1969]: *The piezoelectricity of Poly (Vinylidene Fluoride).* Japanese Journal of Applied Physics, 8: 975–976.

[80] KEPLER, R. G.; ANDERSON, R. A. [1992]: *Ferroelectric polymers.* Advances in physics, 41 no: 1: 1–57.

[81] K., GHANDI; W., H. N. [1997]: *A hybrid finite-element model for phase transition in nonlinear electro-mechanically coupled material.* In *In Smart Structures and Materials 1997: Mathematics and Control in Smart Structures, Proceedings of SPIE*, Vol. 3039 of *Varadan VV, Chandra J, (eds).*, pp. 97–112.

[82] KIMURA, K.; OHIGASHI, H. [1986]: *Polarization behavior in Vinylidene Fluoride-Trifluroethylene copolymer thin films.* Japanese Journal of Applied Physics, 25: 383–387.

[83] KLINKEL, S. [2006]: *A phenomenological constitutive model for ferroelastic and ferroelectric hysteresis effects in ferroelectric ceramics.* International Journal of Solids and Structures, 43: 7197–7222.

[84] KLINKEL, S. [2007]: *Nichtlineare Modellierung ferroelektrischer Keramiken und piezoelektrischer Strukturen-Analyse und Finite-Elemente-Formulierung.* Habilitation, Universität Karlsruhe.

[85] KLINKEL, S.; WAGNER, W. [2005]: *A geometrically non-linear piezoelectric solid shell element based on a mixed multi-field variational formulation.* International Journal for Numerical Methods in Engineering, 65: 349–382.

[86] KLINKEL, S.; WAGNER, W. [2008]: *A piezoelectric solid shell element based on a mixed variational formulation for geometrically linear and nonlinear applications.* Computers and Structures, 86: 38–46.

[87] KOVETZ, A. [2000]: *Electromagnetic theory.* Oxford University Press.

[88] LANDAU, L. D.; LIFSCHITZ, E. M. [1960]: *Electrodynamics of continuous media.* Pergamon Press, Oxford.

[89] LANDAU, L. D.; LIFSCHITZ, E. M. [1967]: *Elektrodynamik der Kontinua.* In *Lehrbuch der Theoretischen Physik*, Vol. 8. Akademie-Verlag.

[90] LANDIS, C. M. [2002]: *A new finite element formulation for electromechanical boundary value problems.* International Journal for Numerical Methods in Engineering, 55: 613–628.

[91] LANDIS, C. M. [2002]: *Uncoupled, asymptotic mode III and mode E crack tip solutions in non-linear ferroelectric materials.* Engineering Fracture Mechanics, 69: 13–23.

[92] LANDIS, C. M. [2004]: *Non-linear constitutive modelling of ferroelectrics.* Current Opinion in Solid State and Materials Science, 8: 59–69.

[93] LINES, M. E.; GLASS, A. M. [1977]: *Principles and applications of ferroelectrics and related materials.* Clarendon Press, London.

[94] LOVINGER, A. J. [1981]: *Unit cell of the γ phase of Poly(Vinylidene Fluride).* Macromolecules, 14: 322–325.

[95] LOVINGER, A. J. [1982]: *Poly(Vinylidene Fluoride).* In BASSET, ED. D. C. (Editor): *Developments in crystalline polymers-I.* Applied Science Publisher, London and New Jersey.

[96] LOVINGER, A. J. [1985]: *Polymorphic transformations in ferroelectric copolymers of Vinylidene Fluoride induced by electron irradiation.* Macromolecules, 18: 910–918.

[97] LYNCH, C. S. [1996]: *The effect of uniaxial stress on the electro-mechanical response of 8/65/35 PLZT.* Acta Materialia, 44 No. 10: 4137–4148.

[98] MARSDEN, J. E.; HUGHES, T. J. R. [1983]: *Mathematical foundations of elasticity.* Dover Publications, Inc., Mineola.

[99] MAUGIN, G. A. [1988]: *Continuum mechanics of electromagnetic solids.* Elsevier.

[100] MAUGIN, G. A. [1992]: *The thermomechanics of plasticity and fracture.* Cambridge University Press, Cambridge.

[101] MAUGIN, G. A. [1998]: *The thermomechanics of nonlinear irreversible behaviors. An introduction.* World Scientific Publishing Co. Pte. Ltd.

[102] McMeeking, R. M.; Landis, C. M. [2002]: *A Phenomenological multi-axial constitutive law for switching in polycrystalline ferroelectric ceramics.* International Journal of Engineering Science, 40: 1553–1577.

[103] McMeeking, R. M.; Landis, C. M. [2005]: *Electrostatic forces and stored energy for deformable dielectric materials.* Journal of Applied Physics, 72: 581–590.

[104] McMeeking, R. M.; Landis, C. M.; Jimenez, S. M. A. [2007]: *A principle of virtual work for combined electrostatic and mechanical loading of materials.* International Journal of Non-Linear Mechanics, 42: 831–838.

[105] Miehe, C. [1998]: *A Constitutive frame of elastoplasticity at large strains based on the notion of a plastic metric.* International Journal of Solids and Structures, 35: 3859–3897.

[106] Miehe, C. [1998]: *A formulation of finite elastoplasticity based on dual co- and contra-variant eigenvector triads normalized with respect to a plastic metric.* Computer Methods in Applied Mechanics and Engineering, 159: 223–260.

[107] Miehe, C. [2001]: *Geometrical methods of nonlinear continuum thermomechanics.* Lecture Notes, University of Stuttgart.

[108] Miehe, C. [2002]: *Strain-driven homogenization of inelastic microstructures and composites based on an incremental variational formulation.* International Journal for Numerical Methods in Engineering, 55: 1285–1322.

[109] Miehe, C. [2009]: *Variational principles and stability in electro-magneto-mechanics.* To appear in Journal of the Mechanics and Physics of Solids.

[110] Miehe, C.; Schotte, J.; Lambrecht, M. [2002]: *Homogenization of inelastic solid materials at finite strains based on incremental minimization principles. Application to the texture analysis of polycrystals.* Journal of the Mechanics and Physics of Solids, 50: 2123–2167.

[111] Mielke, A.; Timofte, M. A. [2006]: *An energetic material model for time-dependent ferroelectric behavior: existence and uniqueness.* Mathematical Methods in the Applied Sciences, 29: 1393–1410.

[112] Mielke, A.; Timofte, M. A. [2006]: *Modeling and analytical study for ferroelectric materials.* Mechanics of Advanced Materials and Structures, 13: 457–462.

[113] Moulson, A. J.; Herbert, J. M. [1990]: *Electroceramics materials, properties, applications.* Chapman and Hall, London et al.

[114] Mukherjee, A.; Chaudhuri, A. S. [2002]: *Piezolaminated beams with large deformations.* International Journal of Solids and Structures, 39: 4567–4582.

[115] Mukherjee, A.; Chaudhuri, A. S. [2005]: *Nonlinear dynamic response of piezolaminated smart beams.* Computers and Structures, 83: 1298–1304.

[116] Murayama, N.; Nakamura, K.; Obara, H.; Segawa, M. [1976]: *The strong piezoelectricity in Polyvinylidene Fluoride.* Ultrasonics, 14: 15–24.

[117] Nguyen, Q. S. [2000]: *Stability and nonlinear solid mechanics.* John Wiley & Sons Inc., New York.

[118] Nowacki, W. [1979]: *Foundations of linear piezoelectricity.* In *Parkus, H. (ed.) Electromagnetic interactions in elastic solids.* Springer.

[119] OGDEN, R. W. [1984]: *Non-linear elastic deformations.* Dover Publications, Inc., Mineola.

[120] ORTIZ, M.; REPETTO, E. A. [1999]: *Nonconvex energy minimization and dislocation structure in ductile single crystals.* Journal of the Mechanics and Physics of Solids, 47: 397–462.

[121] ORTIZ, M.; STAINIER, L. [1999]: *The variational formulation of viscoplastic constitutive updates.* Computer Methods in Applied Mechanics and Engineering, 171: 419–444.

[122] PAO, Y.-H. [1978]: *Electromagnetic forces in deformable continua.* In NEMAT-NASSER, S. (Editor): *Mechanics today*, Vol. 4, Chapter 4, pp. 209–305. Pergamon Press, New York. Published on behalf of the American Academy of Mechanics.

[123] PAO, Y.-H.; HUTTER, K. [1974]: *A dynamic theory for magnetizable elastic solids with thermal and electrical conduction.* Journal of Elasticity, 4: 89–114.

[124] PAO, Y.-H.; HUTTER, K. [1975]: *Electrodynamics for moving elastic solids and viscous fluids.* Proceedings of the IEEE, 63: 1011–1021.

[125] PENFIELD, P.; HAUS, H. [1967]: *Electrodynamics of moving media.* MIT Press, Cambridge.

[126] PHELAN, R. J.; MAHLER, R. J.; COOK, A. R. [1971]: *High D* pyroelectric polyvinylfluoride detectors.* Applied Physic Letters, 19: 337.

[127] POHL, R. W. [1928]: *Elementi teorico-pratici di elettrofisica moderna.* Hoepli.

[128] PREISACH, E. [1935]: *Über die magnetische Nachwirkung.* Zeitschrift für Physik, 94: 277–302.

[129] ROCKAFELLAR, R. T. [2003]: *A general correspondence between dual minimax problems and convex programs.* Pacific Journal of Mathematics, 25: 597–611.

[130] ROMANOWSKI, H. [2006]: *Kontinuumsmechanische Modellierung ferroelektrischer Materialien in Rahmen der Invariantheorie.* Ph.D. Thesis, Universität Duisburg-Essen.

[131] ROSATO, D.; MIEHE, C. [2009]: *Rate-dependent incremental variational formulation of ferroelectricity.* To appear in International Journal of Solids and Structures.

[132] SCHELKUNOFF, S. A. [1963]: *Electromagnetic fields.* Blaisdell.

[133] SCHRADE, D.; MÜLLER, R.; GROSS, D. [2007]: *Domain evolution in ferroelectric materials: A continuum phase field model and finite element implementation.* Computational Methods in Applied Mechanics and Engineering, 196: 4365–4374.

[134] SCHRÖDER, J.; GROSS, D. [2004]: *Invariant formulation of the electromechanical enthalpy function of transversely isotropic piezoelectric materials.* Archive of Applied Mechanics, 73: 533–552.

[135] SCHRÖDER, J.; ROMANOWSKI, H. [2005]: *A thermodynamically consistent mesoscopic model for transversely isotropic ferroelectric ceramics in a coordinate-invariant setting.* Archive of Applied Mechanics, 74: 863–877.

[136] SEMENOV, A. S.; KESSLER, H.; LISKOWSKY, A.; BALKE, H. [2006]: *On a vector potential formulation for 3D electromechanical finite element analysis.* Communication in Numerical Methods in Engineering, 22: 357–375.

[137] Simo, J. C.; Hughes, T. J. R. [1998]: *Computational inelasticity.* Springer-Verlag, New York.

[138] Smith, R. C. [2005]: *Smart material systems.* SIAM, Philadelphia.

[139] Steigmann, D. J. [2004]: *Equilibrium theory for magnetic elastomers and magnetoelastic membranes.* International Journal of Non-Linear Mechanics, 39: 1193–1216.

[140] Stratton, J. A. [2007]: *Electromagnetic theory.* John Wiley & Sons, Hoboken, New Jersey.

[141] Su, Y.; Landis, C. M. [2007]: *Continuum thermodynamics of ferroelectric domain evolution: Theory, finite element implementation, and application to domain wall pinning.* Journal of the Mechanics and Physics of Solids, 55: 280–305.

[142] Tonti, E. [2001]: *Formulazione finita dell'elettromagnetismo.* Lecture Notes, University of Trieste.

[143] Truesdell, C.; Noll, W. [1965]: *The non-linear field theories of mechanics.* In Flügge, S. (Editor): *Encyclopedia of physics*, Vol. III/3. Springer–Verlag, Berlin.

[144] Truesdell, C.; Toupin, R. [1960]: *The classical field theories.* In Flügge, S. (Editor): *Encyclopedia of physics*, Vol. III/1. Springer, Berlin, Heidelberg, New York.

[145] Viehland, D.; Chen, Y. H. [2000]: *Random-field model for ferroelectric domain dynamics and polarization reversal.* Journal of Applied Physics, 88: 6696–6707.

[146] Voigt, W. (Editor) [1928]: *Lehrbuch der Kristallphysik.* Teubner-Verlag, Leipzig/Berlin.

[147] Vu, D. K.; Steinmann, P. [2007]: *Nonlinear electro- and magneto-elastostatics: Material and spatial settings.* International Journal of Solids and Structures, 44: 7891–7905.

[148] Vu, D. K.; Steinmann, P. [2007]: *Theoretical and numerical aspects of the material and spatial settings in nonlinear electro-elastostatics.* International Journal of Fracture, 147: 109–116.

[149] Vu, D. K.; Steinmann, P.; Possart, G. [2007]: *Numerical modelling of nonlinear electroelasticity.* International Journal for Numerical Methods in Engineering, 70: 685–704.

[150] Wang, T. T.; Herbert, J. M.; Glass, A. M. [1988]: *The applications of ferroelectric polymers.* Chapman and Hall, New York.

[151] Weber, M. A.; Kamlah, M.; Munz, D. [2000]: *Experimente zum Zeitverhalten von Piezokeramiken.* Technical Report FZKA 6465, Forschungszentrum Karlsruhe, Institut für Material Forschung.

[152] Xu, B. X.; Schrade, D.; Müller, R.; Gross, D. [2009]: *Micromechanical analysis of ferroelectric structures by a phase field method.* Computational Materials Science, 45: 832–836.

[153] Zhang, Q.; Bharti, V.; Zhao, X. [1998]: *Giant electrostriction and relaxor ferroelectric behavior in electron-irradiated Poly(Vinylidene Fluoride-Trifluoroethylene) copolymer.* Science, 280: 2101–2104.

[154] ZHANG, W.; BHATTACHARYA, K. [2005]: *A computational model of ferroelectric domains. Part I: Model formulation and domain switching.* Acta Materialia, 53: 185–198.

[155] ZHANG, W.; BHATTACHARYA, K. [2005]: *A computational model of ferroelectric domains. Part II: Grain boundaries and defect pinning.* Acta Materialia, 53: 199–209.

[156] ZHOU, D.; KAMLAH, M.; MUNZ, D. [2001]: *Rate dependence of soft PZT ceramics under electric field loading.* Proceedings of the SPIE, 4333: 64–70.

[157] ZIEGLER, H.; WEHRLI, C. [1987]: *The derivation of constitutive relations from the energy and the dissipation function.* In WU, TH. Y.; HUTCHINSON, J. (Editors): *Advances in applied mechanics*, Vol. 4. Academic Press Inc.

Curriculum Vitae

Personal Data

Name	Daniele Rosato
Date of Birth	April 10, 1977
Place of Birth	Mesagne(Br), Italy
Parents	Romeo Rosato and Angela Calcagni in Rosato
Siblings	Giovanni Carlo Rosato and Angelo Rosato
Marital Status	Married to Sylwia Rosato
Nationality	Italian

School Education

1983-1988	Scuola Elementare "Giovanni XXIII" Primary School Mesagne (Br), Italy
1988-1991	Scuola Media "Aldo Moro" Secondary School Mesagne (Br), Italy
1991-1996	Liceo Scientifico Statale "F. Muscogiuri" High School Mesagne (Br), Italy

University Education

1996-2002	Master Degree in Electrical Engineering, Politecnico di Bari, Bari, Italy
2003-2005	M.Sc. in Computational Mechanics of Materials and Structures (COMMAS), University of Stuttgart

Professional Occupation

2001-2003	Research activity at the computational laboratory "Max Planck Institute", Leipzig, Germany
2005-2009	Research Associate and COMMAS Course Director Institute of Applied Mechanics, Civil Engineering, University of Stuttgart

In dieser Schriftenreihe bisher erschienene Berichte:

I-1(1996) *Theoretische und algorithmische Konzepte zur phänomenologischen Beschreibung anisotropen Materialverhaltens*, J. Schröder, Dissertation, 1996.

I-2(1996) *Zur Theorie und Numerik finiter elastoplastischer Deformationen von Schalentragwerken*, B. Seifert, Dissertation, 1996.

I-3(1996) *Zur Modellierung des künstlichen Infrarot-Dichroismus in Poymerfolien bei großen Verformungen*, J. Buhler, Dissertation, 1996.

I-4(1998) *Verfahren zur Ermittlung der Erdbebenlasten mit Berücksichtigung des stochastischen Charakters des Bebens*, S. Zhang, Dissertation, 1998.

I-5(1998) *Zur Beschreibung finiter Deformationen von Polymeren: Experimente, Modellbildung, Parameteridentikation und Finite-Elemente- Formulierung*, J. Keck, Dissertation, 1998.

I-6(1999) *Berechnungsverfahren instationär erregter Systeme im Frequenzbereich*, A. Jaworek, Dissertation, 1999.

I-7(2000) *Homogenisierungsmethoden der nichtlinearen Kontinuumsmechanik unter Beachtung von Stabilitätsproblemen*, J. Schröder, Habilitation, 2000.

I-8(2002) *Theorie und Numerik von Materialinstäbilitaten elastoplastischer Festkörper auf der Grundlage inkrementeller Variationsformulierungen*, M. Lambrecht, Dissertation, 2002.

I-9(2002) *Mikromechanisch motivierte Modelle zur Beschreibung finiter Deformationen gummiartiger Polymere: physikalische Modellbildung und numerische Simulation*, F. Lulei, Dissertation, 2002.

I-10(2003) *Adaptive Finite-Elemente-Berechnungen der nichtlinearen Festkörpermechanik bei kleinen und großen Verzerrungen*, A. Koch, Dissertation, 2003.

I-11(2003) *Theorie und Numerik der Parameteridentikation von Materialmodellen der finiten Elastizität und Inelastizität auf der Grundlage optischer Feldmeßmethoden*, G. Scheday, Dissertation, 2003.

I-12(2004) *Approaches to the Description of Anisotropic Material Behaviour at Finite Elastic and Plastic Deformations, Theory and Numerics*, N. Apel, Dissertation, 2004.

I-13(2004) *Temperaturabhängige Beschreibung visko-elasto-plastischer Deformationen kurzglasfaserverstärkter Thermoplaste: Modellbildung, Numerik und Experimente*, S. Rieger, Dissertation, 2004.

I-14(2005) *Zur Parameteridentikation komplexer Materialmodelle auf der Basis realer und virtueller Testdaten*, A. Rieger, Dissertation, 2005.

I-15(2005) *Viskoelastisches Verhalten von Elastomeren bei finiten Verzerrungen: Experimente, Modellierung und Simulationen*, H. Zecha, Dissertation, 2005.

I-16(2005) *Mehrskalenmodelle in der Festkörpermechanik und Kopplung von Mehrgitter-methoden mit Homogenisierungsverfahren*, C.G. Bayreuther, Dissertation, 2005.

I-17(2005) *Static and Dynamic Homogenization Analyses of Discrete Granular and Atomistic Structures on Different Time and Length Scales*, J. Dettmar, Dissertation, 2005.

I-18(2006) *Incompatibility and Instability Based Size Effects in Crystals and Composites at Finite Elastoplastic Strains*, M. Becker, Dissertation, 2006.

I-19(2007) *Aspects of Energy Minimization in Solid Mechanics: Evolution of Inelastic Microstructures and Crack Propagation*, E. Gürses, Dissertation, 2007.

I-20(2007) *Micro-Macro Approaches to Rubbery and Glassy Polymers: Predictive Micromechanically-Based Models and Simulations*, S. Göktepe, Dissertation, 2007.

I-21(2008) *Material Forces in Finite Inelasticity and Structural Dynamics: Topology Optimization, Mesh Refinement and Fracture*, D. Zimmermann, Dissertation, 2008.

I-22(2010) *Thermoviscoplasticity of Glassy Polymers: Experimental Characterization, Parameter Identification and Model Validation*, J. Méndez Diez, Dissertation, 2010.

I-23(2010) *On the Formulation and Numerical Implementation of Dissipative Electro–Mechanics at Large Strains*, Daniele Rosato, Dissertation, 2010.